MIT Libraries | DSpace@MIT

MIT Open Access Articles

Interactions of Water with Mineral Dust Aerosol: Water Adsorption, Hygroscopicity, Cloud Condensation, and Ice Nucleation

Massachusetts Institute of Technology

1 **Interactions of Water with Mineral Dust Aerosol: Water Adsorption,**

2 **Hygroscopicity, and Cloud Condensation and Ice Nucleation Activities**

3 M. J. Tang[1], D. J. Cziczo[2], V. H. Grassian[1,*]

4 1 Department of Chemistry, University of Iowa, Iowa City, IA 52242, USA

5 2 Department of Earth, Atmospheric and Planetary Sciences and Civil and Environmental

6 Engineering, Massachusetts Institute of Technology, Cambridge, MA 02139, USA

7

8 **Abstract:** Mineral dust aerosol is one of the major types of aerosol present in the troposphere. The

9 molecular level interactions of water vapor with mineral dust are of global significance.

10 Hygroscopicity, light scattering and absorption, heterogneous reactivity and the ability to form

11 clouds are all related to water-dust interactions. In this review article, experimental techniques to

12 probe water interactions with dust and theoretical frameworks to understand these interactions are

13 discussed. A comprehensive overview of laboratory studies of water adsorption, hygroscopicity,

14 and cloud condensation nucleation and ice nucleation activity of fresh and atmspherically aged

15 mineral dust particles is provided. Finally, we relate laboratory studies and theoretical simulations

16 that provide fundamental insights into these processes on the molecular level with field

17 measurements that illustrate the atmospheric significance of these processes. Overall, the details

18 of water interactions with mineral dust are covered from multiple perspectives in this review article.

CONTENTS

91

1 Introduction

1.1 Significance of mineral dust aerosol in the atmosphere

Atmospheric aerosols are ubiquitous in the atmosphere and consist of solid and liquid particles that range in size from a few nanometers to tens of micrometers. In addition to their impacts on air quality, human health, and visibility,[1,2] these particles can alter the energy balance of the earth by scattering and absorbing solar and terrestrial radiation and by influencing the formation and properties of clouds.[3,4] The lack of a complete understanding of the role of aerosols (and thus clouds) on the climate system becomes a bottleneck for reliable and accurate projections of climate change.[5] Mineral dust aerosol is one of the main types of aerosol in the troposphere. Mineral dust particles are mainly emitted from arid and semi-arid regions (e.g., Saharan and Gobi Deserts),[6,7] with an annual flux of ~2000 Tg yr^{-1}.[8,9] It is estimated that natural dust sources account for 75% of the emission and anthropogenic sources account for the other 25%.[10] One outstanding issue is the abundance of relatively bare mineral dust emitted from arid regions versus internally mixed "fertile soil dust" containing both mineral and organic components. Forster et al.[11] suggested the latter contributed 0-20% of the global mineral dust budget, while a more recent satellite-based study [10] coupled to land usage maps suggested ~25%. After being lifted into the troposphere, mineral dust particles have lifetimes of up to several days [9] and can be transported over thousands of kilometres.[12-18]

Table 1. Average emission fluxes and atmospheric loadings of different types of aerosol particles in the troposphere, as estimated by models participating in the aerosol model intercomparison initiative (AeroCom).[8]

aerosol type	emission (Tg yr^{-1})	atmospheric loading (Tg)
mineral dust	1840	19.2
sea spray	16600	7.52

4

sulfate	179	1.99
primary organic matter	96.6	1.7
black carbon	11.9	0.24

113

114 The average emission fluxes and atmospheric abundances of different types of tropospheric

115 aerosol particles, as estimated by models participating in the aerosol model intercomparison

116 initiative (AeroCom),[8] are provided in Table 1. While the emission of mineral dust is the second

117 largest in the troposphere, with sea spray being the largest, it is the most abundant type of aerosol

118 particle by mass with an estimated average atmospheric loading of 19.2 Tg,[8] as much of sea spray

119 particles have diameters larger than 10 μm and thus are quickly removed from the atmosphere

120 through deposition.[19] A substantial fraction of mineral dust particles also have large diameters and

121 thus are quickly removed by dry deposition after they are entrained into the atmosphere.[9] Dust

122 emissions are closely linked to hydrological cycles, and climate variability can change dust

123 emissions, leading to further feedbacks on the climate system.[10,20-28]

124

125 Because of the overall loading and lifetime in the atmosphere, mineral dust can impact the Earth's

126 atmosphere and climate in a number of ways. Mineral dust particles can both scatter and absorb

127 solar and terrestrial radiations, thus having direct radiative effects.[29-43] [44]Optical scattering and

128 absorption by mineral dust particles can further change the photolysis rates and thus influence

129 photochemical cycles in the troposphere.[45] Mineral dust particles can also have indirect impact on

130 radiative forcing by acting as cloud condensation nuclei (CCN) to form liquid cloud droplets [46-55]

131 and ice nuclei (IN) to form ice clouds.[56-73] In fact, mineral dust particles may be the dominant IN

132 in the troposphere [74,75] and therefore have a significant impact on the Earth's radiative budget,[76-79]

133 precipitation, and the hydrological cycle.[58,80-83] Additionally, deposited mineral dust particles can

134 be a major contributor of several important elements, including Fe,[84-87] P,[88-91] and Cu,[92,93]

especially into open ocean waters [88,94-97] and the Amazon,[98,99] and therefore have strong effects on biogeochemical cycles and the Earth's climate system.[100-103]

Mineral dust aerosol also influences air quality,[104-106] visibility,[107] and public health in dust-impacted regions.[12,20,104,108-119] For example, clear enhanced effects of particulate matter on respiratory and cerebrovascular diseases were observed during Saharan dust outbreaks in Roma, Italy.[120] A recent modeling study [108] estimated that the fraction of cardiopulmonary deaths caused by mineral dust aerosol is about 1.8% globally, and in countries most affected by dust storms it is up to 15-50%.

The mineralogy of dust particles is very complex, showing large variation with their sources and atmospheric transport processes.[121-130] Different minerals can have very different physical and chemical properties, such as heterogeneous reactivity, refractive index, CCN and IN activity, and therefore have different impacts on atmospheric chemistry, cloud formation, and climate. For example, it has been shown that the kinetics of N_2O_5 uptake onto mineral dust particles vary over almost two orders of magnitude for different minerals,[131-139] and the ice nucleation activity of different minerals can differ by several orders of magnitude.[140,141] It is also suggested that the iron solubility in dust particles is strongly dependent on the mineloragy.[142-144] Mineral dust particles in the troposphere consist of a variety of minerals that can be externally and internally mixed.[145-149] The emission fluxes and atmospheric abundance of the most abundant minerals, estimated by a recent modeling study,[150] are shown in Table 2.

Table 2. Emission fluxes and atmospheric loadings of different mineral phases, estimated by a recent study [150] using the Community Atmosphere Model.

mineral	flux (Tg yr^{-1})	atmospheric loadings (Tg)

quartz	568.9	4.1
illite	370.1	4.2
montmorillonite	246.2	2.8
feldspar	205	1.4
kaolinite	192.3	2.2
calcite	145.1	1.3
hematite	24	0.2
gypsum	15.3	0.1

159

160 Less abundant minerals have not been included in most modeling studies; however, the impact of

161 a mineral in the troposphere is not necessarily proportional to its abundance. For example, the

162 mass fractions of TiO_2 in mineral dust particles are typically a few percents or less,[32,151-153] but its

163 semiconductor properties make it very important in heterogeneous photochemical reactions which

164 may play an important role in the formation or removal of reactive trace gases in the

165 troposphere.[154-156] Saharan dust particles only contain 0.09% phosphorus on average, though the

166 deposition of mineral dust particles from the Sahara desert is a major source of phosphorus for

167 oceans.[97] It has also been suggested that transition metals of trace amounts contained by mineral

168 dust particles (and probably also anthropogenic particles) may significantly enhance the

169 multiphase oxidation of SO_2.[157] Furthermore, the complexity of mineral dust particles can be

170 significantly increased due to their transformations resulting from chemical processing during

171 transport.[158-162]

172

173 In addition, a few minerals with high refractive indexes (such as TiO_2 and Al_2O_3),[138,139,163-165] have

174 recently been proposed as alternative particles to be injected into the stratosphere to scatter more

175 solar radiation back into space, as a geoengineering method [166] to counteract global warming due

176 to increasing levels of greenhouse gases. For example, it is estimated that in order to achieve the

7

177   same scattering effect, the use of TiO_2 for stratospheric particle injection requires a factor of ~3

178   less in mass than that of H_2SO_4 aerosols which are present as a natural aerosol in the

179   stratosphere.[163]

180   **1.2 Overview of the interaction of water with mineral dust aerosol: adsorption,**

181   **hygroscopic growth, and cloud condensation and ice nucleation**

182   Water is ubiquitous in the troposphere and can exist in the gas, liquid, and solid states. The amount

183   of water vapor contained by air is usually described by relative humidity (RH), typically in %,

184   which is defined as the ratio of its partial pressure to the saturated vapor pressure at the same

185   temperature (T) multiplied by 100, as shown in Eq. (1):

186    $$RH = 100 \times \frac{P(water)}{P_s(water)} \quad (1),$$

187   where P(water) is the partial pressure of water vapor and P_s(water) is the saturated vapor pressure

188   of water. Under sub-saturation conditions, i.e. RH is lower than 100%, some water vapor will

189   partition onto/into mineral dust particles. The amount of water associated with particles, in

190   equilibrium with water vapor in the gas phase, depends on RH, T, and the type of dust particles.

191   The partitioning of water between the gas and particle phase, is called water adsorption in surface

192   science and hygroscopicity in aerosol science. Hygroscopicity is in fact a general term which

193   describes the ability to absorb or release water as a function of water activity and how a substance

194   can attract and hold water molecules from the surrounding environment. In aerosol science, it

195   usually refers to the change in diameter, volume, or mass of particles when exposed to water vapor.

196   Different theories are used to describe water adsorption versus hygroscopicity which differ in

197   fundamental underlying assumptions to describe water partitioning between gas and particle

198   phases under sub-saturation conditions, as discussed in more detail in Section 3.

199

200 When RH is larger than 100%, i.e. under super-saturation conditions, dust aerosol particles can be

201 activated to cloud droplets (a process called cloud condensation nucleation).[167] At a given super-

202 saturation, the ability of a particle to be activated to a cloud droplet depends on the particles

203 diameter [168,169] and also its CCN activity, which is determined by its chemical composition and

204 mixing state.[170] When T is less than 273 K, mineral dust particles might be activated to form ice

205 particles (ice nucleation) if the relative humidity to ice (RHi, defined as the ratio of the partial

206 pressure of water vapor to the saturated pressure of ice at the same temperature) is larger than

207 100%.[167] In this article RH and RHi are referred to relative humidity with respect to liquid water

208 and ice, respectively.

209

210 What makes water uptake properties of mineral dust more complicated is that, as well known,

211 during transport mineral dust particles react with a wide range of trace gases in the

212 troposphere.[156,161,171-187] These heterogeneous reactions involve gas-solid interactions. If mineral

213 dust particles are activated to cloud droplets, multiphase reactions can occur in these aqueous cloud

214 droplets.[157,162,188-191] Heterogeneous and multiphase reactions can directly and indirectly change

215 the concentrations of several important trace gases,[161,172,192-198] such as NOx, O_3 and OH radicals,

216 thus imposing significant impacts on tropospheric chemistry. Furthermore, these reactions also

217 lead to a change in surface and sometimes even the bulk chemical composition of mineral dust

218 particles,[126,158,199-210] thereby modifying their interactions with water, including surface

219 adsorption,[211,212] hygroscopicity,[213-215] and cloud condensation nucleation [216-218] and ice nucleation

220 activity.[219-221]

221

222 The change in the interaction with water can in turn further influence the reactivity of mineral dust

223 particles towards reactive trace gases. The change in composition and hygroscopicity of dust

224 particles may influence both their refractive index [222] and optical diameters, and the change in

CCN and IN activity can results in the change in the probability of wet deposition,[223,224] thereby impacting their atmospheric lifetime.[224] In addition, heterogeneous chemistry can modify the solubility and/or bio-availability of elements within individual mineral dust particles.[84,88,96,225] The complex interactions of mineral dust particles with reactive trace gases and water, and their impacts on cloud formation, are depicted in Figure 1.

R1: chemical aging
R2: hygroscopic growth
R3: cloud activation
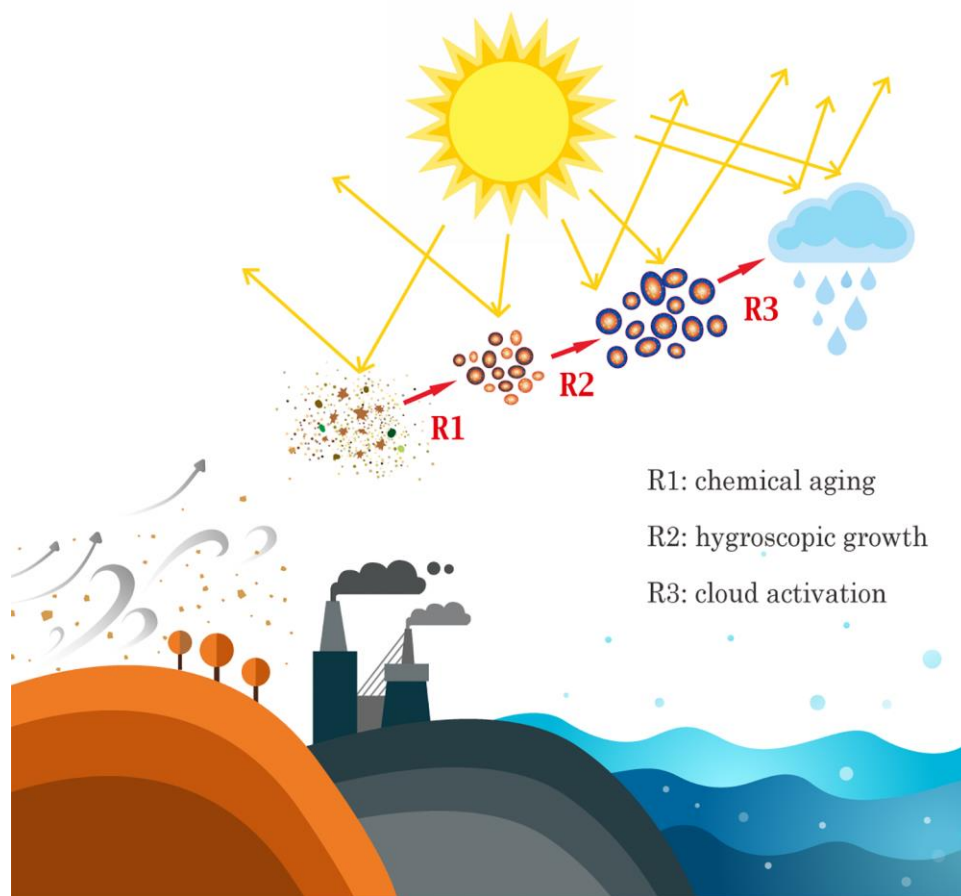
Figure 1. A schematic diagram of the interactions of mineral dust aerosol particles with reactive trace gases and water and their impacts on cloud formation and radiative balance. R1) chemical transformation/aging of mineral dust aerosol particles due to reactions with reactive trace gases; R2) enhanced hygroscopic growth of aged mineral dust aerosol particles; and R3) activation of mineral dust particles to cloud droplets and ice particles.

238   It is important to note that heterogeneous chemistry and photochemistry of mineral dust particles

239   in the atmosphere have been summarized in several comprehensive review papers.[161,171,172] It has

240   been widely recognized that water adsorbed by mineral dust plays a central role in determining the

241   heterogeneous reactivity and photoreactivity towards reactive trace gases in the

242   atmosphere.[137,199,226-228] In particular, a recent review paper [229] described in detail how surface

243   adsorbed water can play a myriad of roles in the surface chemistry and can either enhance or

244   suppress the reactivity of mineral dust particles towards reactive trace gases. For example, Figure

245   2 shows the dependence of the uptake coefficient of N_2O_5, $\gamma(N_2O_5)$, on RH (and thus surface

246   adsorbed water) for different mineral dust particles. Even for the same trace gas, the influence of

247   RH on the uptake kinetics can be very different for different minerals, highlighting the importance

248   of accurate determination of water adsorption as a function of RH for a variety of different minerals

249   that make up dust in the atmosphere. Adsorbed water can also change the reaction products and

250   the partitioning of reaction products among different phases.[229]
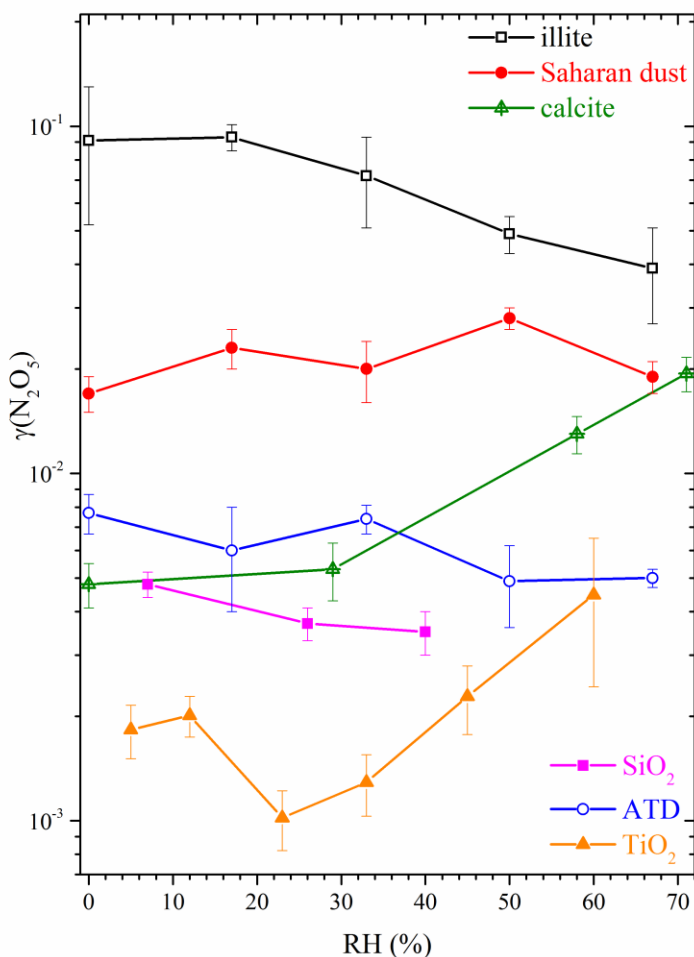
Figure 2. Dependence of $\gamma(N_2O_5)$ on RH for different mineral dust particles. Sources of data: illite,[137] Saharan dust,[136] calcite,[135] SiO$_2$,[139] Arizona Test Dust (ATD),[137] and TiO$_2$.[138]

However, the interactions of mineral dust particles with water vapor at temperatures higher than that for ice nucleation has hitherto not been reviewed in the context of atmospheric chemistry and climate, despite that in the last two decades a large number of studies have been published by both the surface science and aerosol science communities. We note that a recent review paper has discussed the multi-faceted roles of surface adsorbed water in heterogeneous reactions of mineral dust particles.[229] Therefore, in this article, we undertake a comprehensive review of the interactions of water with mineral dust particles. Following the Introduction section, we summarize and discuss experimental techniques used to study water adsorption properties, hygroscopicity, and CCN

12

263   activity of mineral dust particles (Section 2). In Section 3, we introduce and discuss theories used

264   in this review to describe water adsorption in surface science and hygroscopicity and CCN activity

265   in aerosol science, and we also describe guidelines used to compare experimental data reported in

266   these previous studies. Following this, laboratory studies of water adsorption properties,

267   hygroscopicity, and CCN activity of different mineral dust particles are reviewed in Section 4, in

268   which the effects of chemical aging processes on water interaction are also discussed. We focus

269   on mineral particles and surfaces which are of direct relevance for atmospheric chemistry and

270   microphysics of aerosols and clouds. Therefore, water adsorption on single crystal surfaces,[230-236]

271   although relevant, is not discussed in too much detail in this review. In this section, we also discuss

272   some theoretical studies to illustrate how these studies can provide insight into the fundamental

273   mechanisms of water adsorption on mineral surface on the molecular and sub-molecular levels. In

274   addition, at the end of this section we also summarize results from field measurements which

275   provide evidence that the hygroscopicity of mineral dust particles can be significantly modified

276   due to heterogeneous reactions and cloud processing. Although ice nucleation activity of mineral

277   dust particles has been reviewed in a few excellent recent papers,[140,237-239] these papers are mainly

278   focused on fresh mineral dust particles and only one review article [238] has briefly summarized ice

279   nucleation activity of aged mineral dust particles. Increasing number of laboratory studies suggest

280   that chemical aging processes can significantly change the ice nucleation activity of mineral dust

281   particles. Thus in Section 5, recent work on the effects of chemical aging on the ice nucleation

282   activity of dust particles is reviewed. Finally, in Section 6 we outline several key questions from a

283   physical chemistry view which preclude us from a better understanding of the interactions of

284   mineral dust aerosol particles with water vapor (including water adsorption, hygroscopicity, and

285   CCN and IN activities), and discuss how these challenges can be addressed through future research.

2 An overview of sample preparation methods and experimental techniques

Experimental techniques which have been used to investigate water adsorption properties, hygroscopicity, and CCN activity of mineral dust particles are briefly summarized here. Instead of providing a comprehensive discussion of each techniques, we introduce the basic principles and key features, and refer interested readers to the relevant literature for further details. These techniques can be classified into three groups which are discussed in Sections 2.2-2.4, according to the way particles under investigation exist: 1) particle ensembles or single particles deposited on a substrate; 2) levitated single particles; and 3) an ensemble of particles as an aerosol. A quick overview of these techniques is provided in Table 3 along with their key measurement features. A variety of sample preparation methods have been used in previous studies, and it has been suggested that experimental results may vary with sample preparation methods. Therefore, we first briefly discuss the effects of different particle preparation/generation methods in Section 2.1. In this review paper, we focus on techniques which have been used to quantitatively determine the amount of water adsorbed by mineral dust particles of direct atmospheric relevance. In addition, there have been a large number of studies on water adsorption on single crystals of minerals, for example, $CaCO_3$,[211] α-Al_2O_3,[230,240] TiO_2,[231,232,241], and α-Fe_2O_3.[242] Although surfaces of these single crystals may not completely resemble the complexity of mineral dust particles in the troposphere, studies using well-defined single crystal surfaces can provide a wealth of fundamental information and insights into water adsorption mechanisms and intermolecular interactions between water molecules and water molecules with surface atoms. Techniques used to study the ice nucleation activity have been discussed recently [140,238,239] and thus are not covered here.

Note that one shortcoming of many laboratory studies is that overly simplistic dust samples, when compared to the complex internal mixtures found in the atmosphere,[243,244] [158] are often utilized. For example, atmospheric mineral dust is often associate with surface coatings due to

14

311 heterogeneous reactions with reactive trace gases,[158,161,202,245] but laboratory studies most often

312 consider unprocessed particles which may be only representative of mineral dust particles freshly

313 emitted into the troposphere.

314

315 **Table 3.** Summary of representative literature on different experimental techniques which have been used

316 to measure water adsorption, hygroscopicity, and CCN activity of mineral dust particles.

techniques	references	main features
QCM	Navea et al., 2010 [246]	Change in particle mass at different RH is quantified by the frequency change of the quartz crystal.
TGA	Gustafsson et al., 2005 [247]	Change in particle mass at different RH is directly measured.
PSA	Ma et al., 2010 [248]	Change in partial pressure of water vapor due to surface adsorption is measured.
ATR-FTIR	Schuttlefield et al., 2007 [249]	IR absorption of surface adsorbed water is measured and can be converted to the amount of adsorbed water.
transmission FTIR	Goodman et al., 2001 [250]	
DRIFTS	Gustafsson et al., 2005 [247]	
AP-XPS	Ketteler et al., 2007 [241]	Chemically specific and quantitative measurements of water and other species adsorbed on the surface can be achieved.
EDB	Pope et al., 2010 [251]	Relative change in mass of a single particle at different RH is determined from the change of the DC voltage used to balance the gravitational force.
optical levitation	Tong et al., 2011 [252]	Particle size change of a single particle at different RH is determined by light scattering.
H-TDMA	Herich et al., 2009 [49]	Mobility diameter change at different RH is measured.
aerosol optical extinction	Attwood and Greenslade, 2011 [253]	Change in aerosol optical extinction properties at different RH is measured, e.g., using an AE-CRD.
aerosol optical scattering	Li-Jones et al., 1998 [254]	Change in aerosol optical scattering properties at different RH is measured, e.g., using a nephelometer.

aerosol optical adsorption	Utry et al., 2015 [255]	Change in aerosol optical scattering properties at different RH is measured, e.g., using a photoacoustic absorption spectrometer.
CCNc	Sullivan et al., 2010 [256]	Concentrations of aerosol particles activated to cloud droplets at a certain super-saturation are measured.

QCM: quartz crystal microbalance. TGA: thermogravimetric analyser. PSA: physisorption analyser. ATR-FTIR: attenuated total reflection Fourier transform infrared spectroscopy. DRIFTS: diffuse reflectance Fourier transform spectroscopy. AP-XPS: atmospheric pressure X-Ray photoelectron spectroscopy. EDB: electrodynamic balance. H-TDMA: hygroscopicity tandem differential mobility analyser. CCNc: cloud condensation nuclei counter.

2.1 Methods used for sample preparation

There are two common methods used to generate mineral dust aerosols: i) wet generation: aerosol particles were generated by atomizing the suspension of mineral dust powders in water;[139,256,257] ii) dry generation: mineral dust particles are directly dispersed and entrained into the air, typically by using a high-speed air jet.[136,258-260] Commercial instruments, such as rotating brusher generators [134,136] and fluidized beds,[220,261] are also available for dry generation of dust aerosol particles. Recent studies have shown that mineral dust particles generated by these two methods can have distinctive hygroscopicity and CCN activities,[49,217,262,263] with wet-generated aerosol particles having higher hygroscopicity and CCN activities. The change of hygroscopicity and CCN activities of dust particles after wet-generation can be due to a couple of reasons: 1) soluble impurities contained by the dust particles are enriched in generated aerosol particles by wet-generation, and 2) some components contained by dust particles may undergo chemical reaction in the water suspension. For example, Sullivan et al.[256] suggest that the formation of $Ca(HCO_3)_2$, due to the reaction of $CaCO_3$ with H_2O and CO_2, causes wet-generated $CaCO_3$ particles to have higher CCN activity than dry-generated $CaCO_3$. This conclusion is further supported by Zhao et al.,[264] who have demonstrated that $Ca(HCO_3)_2$ particles are more hygroscopic than $CaCO_3$

338   particles. We expect that similar phenomena may occur for clay mineral but less likely for

339   relatively inert minerals such as SiO_2.

340

341   Compared to wet generation, dry generation produces dust aerosol particles which may better

342   resemble the composition and thus the hygroscopicity of original powders used to generate those

343   aerosol particles. On the other hand, dust aerosol particles can be activated to cloud droplets and

344   undergo cloud processing several times during their residence in the troposphere,[48,162,223,265-267] and

345   dust aerosol particles produced by wet generation might better resemble the properties of dust

346   particles which were activated cloud droplets. Thus, to summarize, dry and wet generation

347   methods have been shown to produce aerosol particles with different hygroscopicity and CCN

348   activity. Nevertheless, currently it is not clear which method may generate aerosol particles which

349   better resemble dust particles in the troposphere. This is because nascent dust or cloud activated

350   dust may be very different and therefore may best described by dry generation and wet generation

351   techniques, respectively.

352

353   To investigate water adsorption on mineral dust particles deposited on a substrate, typically a slurry

354   of dust particles in water is deposited on the supporting substrate, leading to the formation of a

355   relatively uniform dry film after the evaporation of water.[268] Alternatively, other solvents, such as

356   methanol or ethanol, can be used instead of water.[196] In some studies [269,270] dry powders of dust

357   were also directly placed on a substrate, without using any solvents. Whether a solvent is used

358   during deposition of dust particles on a substrate may influence the measured water adsorption and

359   hygroscopicity of dust particles; however, to date this has not been systematically examined.

2.2 Mineral dust particles supported on substrates

2.2.1 Mass measurements of adsorbed water as a function of water vapor pressure

The mass of a particle ensemble can be measured at different RH (in %) to investigate the amount of adsorbed water by using several techniques. For examples, in a quartz crystal microbalance (QCM) experiment, the measured frequency of the quartz crystal reflects the mass of particles loaded on it.[249,271] The frequency change, Δf (Hz), is directly related to the change in mass, Δm, according to the Sauerbrey equation:[246,249,272]

$$\Delta f = -C_f \Delta m \qquad (2),$$

where C_f is the constant sensitivity factor for the specific QCM and can be experimentally calibrated. Usually a slurry of dust particles in water (or other solvents, e.g., methanol) was sprayed onto the quartz crystal and then dried to form a thin film on the quartz crystal.[246,273]
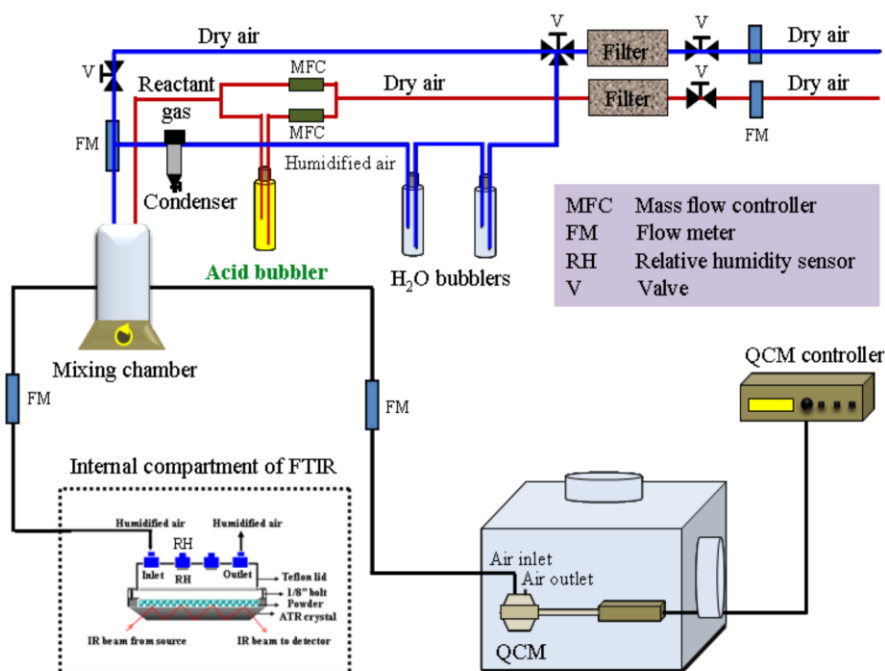
Figure 3. A schematic diagram of ATR-FTIR spectroscopy and quartz crystal microbalance (QCM). Although these measurements are integrated in time and the gas phases above the samples are at the same relative humidity, it should be noted that the ATR-FTIR cell and the QCM cell both have separate thin film samples. Reprinted with permission from ref 274. Copyright 2012 American Chemical Society.

376

377 A schematic diagram of a typical QCM set-up,[274] is shown in Figure 3. The change in frequency

378 of the quartz crystal (and thus the change in particle mass) measured at different RH, can be used

379 to determine the amount of adsorbed water. Figure 4 shows the frequency change of a QCM (upper

380 panel) and water adsorption isotherm (lower panel) for SiO_2 particles.[273]
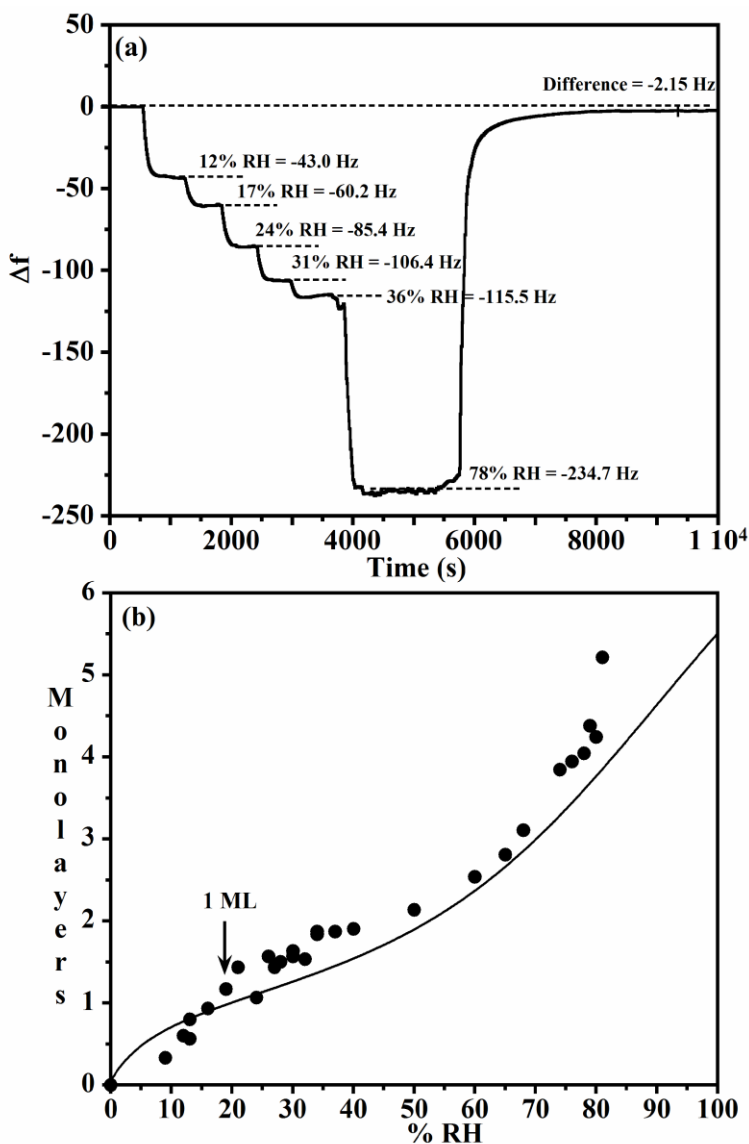
381

382 **Figure 4.** Water adsorption on SiO_2 at different RH as measured by QCM. (a) Change in frequency of the

383 quartz crystal at different RH; b) the number of adsorbed water layers on the surface at different RH, and

384 the curve is the modified three-parameter BET fit reported by Goodman et al.[250] Reprinted with permission

385 from ref 273. Copyright 2007 Society for Applied Spectroscopy.

386

387 Thermogravimetric analysers can also be used to investigate water adsorption on mineral dust

388 particles. For example, a Mettlet-Toledo TGA/SDTA851e thermogravimetric analyzer (Mettler-

389 Toledo, USA) with a mass measurement accuracy of ± 1 μg, was used to measure the amount of

390 water adsorbed on $CaCO_3$ and Arizona Test Dust particles.[247]

391

392 In addition, the amount of surface adsorbed water can also be quantified by measuring the change

393 of water vapor pressure in the gas phase due to adsorption onto the surface, using a physisorption

394 analyser (PSA).[212,248] The change in partial pressure of water vapor due to adsorption on mineral

395 dust particles can be measured to determine the water adsorption isotherm, in a similar way to the

396 BET surface area measurement using N_2. For example, a commercial physisorption analyser,

397 AUTOSORB (Quantachrome, USA), was modified and used to investigate the hygroscopicity of

398 fresh and aged Al_2O_3 and $CaCO_3$ particles.[212,248]

399

400 These experimental techniques provide direct quantification of water adsorbed by mineral dust

401 particles. Water may also adsorb on the apparatus wall and cause artifacts, and this effect can be

402 subtracted by blank experiments in which no particles are used.

403 **2.2.2 FTIR measurements of water uptake**

404 Water adsorbed on mineral dust surface at different RH can be monitored by Fourier transform

405 infrared spectroscopy (FTIR), including transmission FTIR,[250] diffuse reflectance Fourier

406 transform spectroscopy (DRIFTS),[247] and attenuated total reflection Fourier transform infrared

407 spectroscopy (ATR-FTIR).[273] As shown in Figure 5, surface adsorbed water has two distinctive

408 IR absorption peaks in the region extending from 1500 to 4000 cm^{-1}, one near 3400 cm^{-1} due to

409 the O-H stretching mode and the other near 1645 cm^{-1} due to H_2O bending mode.[250,273,275]
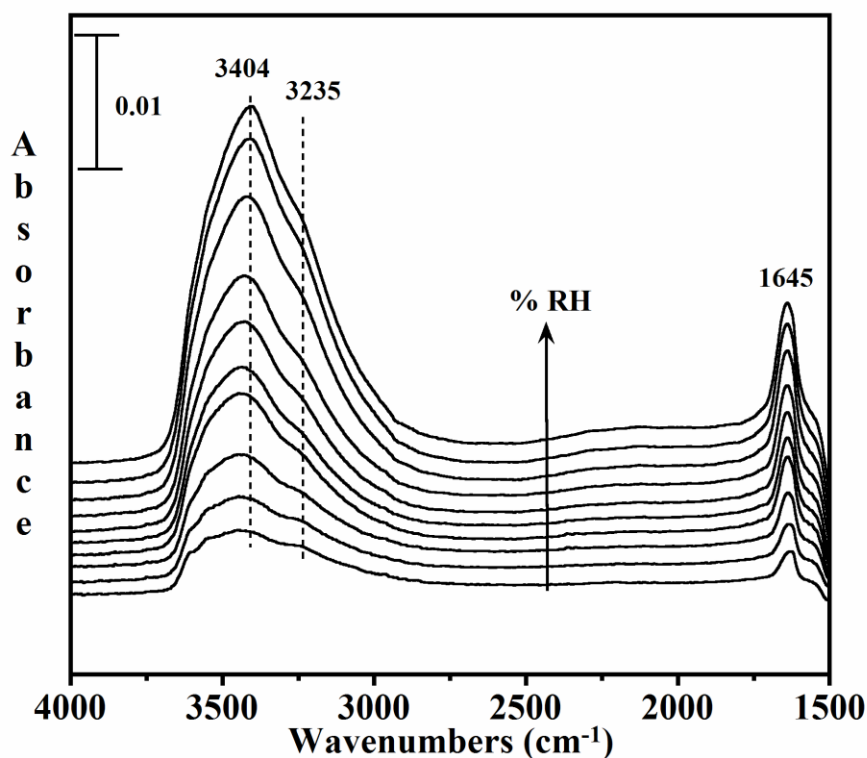
Figure 5. ATR-FTIR spectra following the water uptake on 19.2 mg of SiO_2 at different RHs (5, 8, 13, 20, 27, 37, 47, 66, 74, and 78%). Reprinted with permission from ref 273. Copyright 2007 Society for Applied Spectroscopy.

Since surface hydroxyl groups can also contribute to the O-H stretching mode, it is better to use the H_2O bending mode to analyze molecularly adsorbed water on the surface. The integrated IR absorption can be used to quantify the amount of surface-adsorbed water, using a modified Lambert-Beer law and assuming that the IR absorption cross section of surface-adsorbed water is equal to that of liquid water.[211,240]

2.2.3 Surface analysis techniques used for water uptake measurements

Surface techniques can be very valuable in studying water adsorption and hygroscopicity of mineral dust particle. Some surface techniques are able to provide information on both chemical composition and morphology of the surface under investigation, though absolute quantification of

424   the amount of water associated with the surface may be non-trivial. Here we provide several

425   examples to demonstrate how different surface techniques can be used to understand water

426   adsorption and hygroscopicity of fresh and aged mineral dust particles. In addition to the

427   techniques mentioned in this section, there are many other surface techniques which have been

428   used to study water adsorption on single crystals including scanning probe techniques such as

429   scanning tunneling microscopy (STM).[232,276-278]

430

431   The transformation of solid $CaCO_3$ particles to aqueous droplets, due to the reaction with HNO_3,

432   has been observed in the laboratory for the first time by Krueger et al.,[279] using Scanning Electron

433   Microscopy (SEM) and Energy Dispersive X-ray analysis (EDX). Two years later the atmospheric

434   significance of this finding was supported by a field study,[245] which showed that dust particles

435   collected in Israel have been substantially processed in the atmosphere and could exist in aqueous

436   state even at very low RH (9-11%). Transmission Electron Microscopy can also be used to monitor

437   the morphology change of mineral dust particles. For example, using TEM, Matsuki et al.[159] found

438   that some of the Asian dust particles collected in Beijing are spherical, due to internal mixing with

439   nitrate and sulfate. Liu et al.[215] used a micro-Raman spectrometry to investigate the hygroscopicity

440   of $CaCO_3$ particles after exposure to NO_2. They [215] found that after the reaction, irregular $CaCO_3$

441   particles are converted to spherical droplets at 37% RH and the internally mixed $CaCO_3/Ca(NO_3)_2$

442   particles have the same phase transition properties as pure $Ca(NO_3)_2$ particles.

443

444   Traditionally, X-Ray photoelectron spectroscopy (XPS) is a technique applied to surfaces in ultra-

445   high vacuum, limiting its application under atmospheric relevant conditions (i.e. with pressures

446   close to 1 bar). Over the past decade, advances in atmospheric pressure XPS (AP-XPS) makes it a

447   very promising method to investigate the interaction of gases, including water vapor, with mineral

448   dust particles, because of its chemically specific and quantitative nature.[280-284] Using this technique,

449   Ketteler et al.[241] measured the amounts of adsorbed water and surface OH groups on $TiO_2(110)$

450   surface over a very large RH range, from $<1\times10^{-4}$ to almost 100%. In addition, they [241] found that

451   AP-XPS can also differentiate the oxygen species (lattice O, OH, and H_2O) on the surface by their

452   difference in O1s binding energies, providing very useful information on mechanisms of water

453   adsorption on the mineral surface. In another study,[242] the coverages of surface-adsorbed water

454   and OH groups on single crystal $\alpha\text{-}Fe_2O_3(0001)$ surface were measured as a function of RH, as

455   shown in Figure 6. Though AP-XPS has shown large potential to quantify the amount of adsorbed

456   water and to explore the adsorption mechanisms on a molecular and/or atomic level, to our

457   knowledge AP-XPS has not been used to investigate the interaction of water vapor with clay

458   mineral or authentic dust particles.
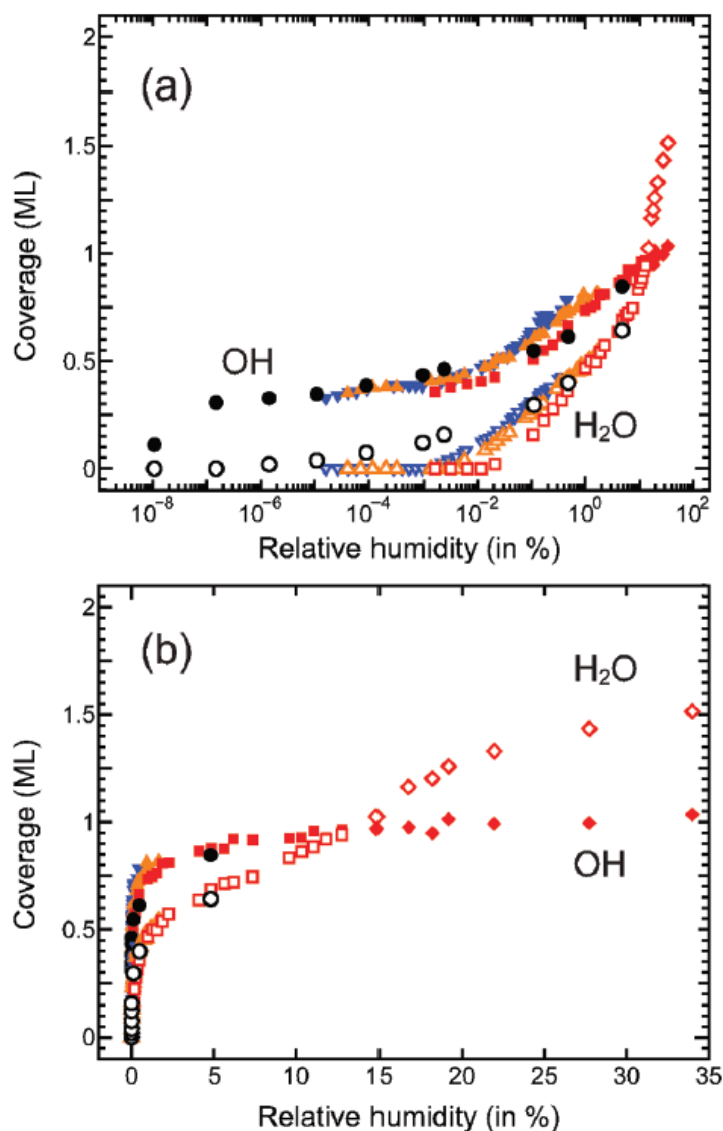
459

460 **Figure 6.** Coverages of surface OH groups (filled symbols) and molecularly adsorbed H_2O (open symbols)

461 on α-Fe_2O_3(0001) surface as a function of RH. RH is plotted on a logarithmic scale in (a) and a linear scale

462 in (b). Measurements were carried out at different experimental conditions: black circles, varying P(water)

463 with a constant temperature of 295 K; blue triangles, varying temperature with a constant P(water) of 0.02

464 Torr; orange triangles, varying temperature with a constant P(water) of 0.1 Torr; red squares, varying

465 temperature with a constant P(water) of 1 Torr; red diamonds, P(water) in the range of 1.0-2.0 Torr and

466 temperature in the range of 277-280 K. Reprinted with permission from ref 242. Copyright 2010 American

467 Chemical Society.

468

469 Surface vibrational spectroscopy, such as sum frequency generation (SFG), is a nonlinear and

470 interface-specific technique to investigate the structure and dynamics of the interface.[285-287] SFG

471 has been widely used to study the liquid water-air interface under environmental conditions, and

472 have contributed to the elucidation of environmental interfacial processes at the molecular

473 level.[234,288] Several studies also utilized SFG to investigate water adsorption on minerals, including

474 Al_2O_3 and SiO_2. For example, Ma et al.[289] suggested that at 35% RH, α-Al_2O_3(0001) surface can

475 be described as a H-bonding network formed by molecularly adsorbed water and surface hydroxyl

476 groups H-bonded to the adsorbed water. A further study by Liu et al.[290] found that for SiO_2 at 54%

477 RH, isolated silanol OH groups were in fact the major surface species and molecularly adsorbed

478 water only covered a limited fraction of the surface. SFG can provide invaluable insights into the

479 mechanisms of water adsorption on mineral dust particles, though absolute quantification of the

480 adsorbed water is non-trivial.

481

482 Many surface spectroscopic methods, such as FTIR, Raman, and SFG, as discussed above,

483 typically provide the average information of the surface under investigation. Atomic force

484 microscopy is a technique which can provide spatial resolution down to sub-nanometres under

485 atmospheric relevant conditions.[291-294] If complemented with spectroscopic measurements, it could

486 help elucidate the mechanisms of water adsorption on mineral dust surface.[229]

487

488 Knudsen cell reactors are widely utilized to study the heterogeneous reactions of mineral dust

489 particles with atmospheric reactive trace gases.[151,184,295-297] They have also been used to investigate

490 the interaction of water vapor with mineral dust.[298,299] Because a Knudsen cell reactor is typically

491 operated in the molecular flow regime (with a total pressure of less than 1 mTorr), the partial

492 pressure of water vapor (and thus the RH) used in these experiments is very low. Therefore, these

493 studies are less relevant for atmospheric chemistry and climate, though they can provide valuable

494 insights into the mechanisms of water adsorption on mineral dust. Molecular beam scattering

495 techniques have been used to explore how gas molecules interact with surfaces of atmospheric

496 chemistry interest,[236,300-305] and if applied to study mineral dust surface, can potentially help us

497 understand the fundamental dynamics and kinetics of water adsorption.

498 **2.3 Levitated single particle measurements**

499 Levitation of single particles avoids potential effects due to interaction of different particles and

500 those due to contact with the substrate used to support particles. A few particle levitation

501 techniques, such as the electrodynamic balance (EDB) and optical levitation, have been widely

502 used to study the hygroscopicity of aerosol particles.[306] Acoustic levitation is limited to particles

503 with sizes of larger than 20 μm, which are less relevant for atmospheric aerosols; therefore, this

504 technique is not further described here.[306] In an EDB a combination of AC and DC electric fields

505 is used to trap and levitate a charged particle,[307] with typical sizes of 5 to 50 μm.[306] The mass of

506 the particle is proportional to the balancing DC voltage, and the relative change of the particle

507 mass at different RH, usually compared to that at 0% RH, is determined from the change of the

508 DC voltage used to balance the gravitational force.[251,307] Though this technique seems to be a

509 suitable technique to study the hygroscopic growth of mineral dust particles, to our knowledge it

510 has not been applied to mineral dust particles yet.

511

512 Optical levitation methods, e.g., optical tweezers, can routinely trap and levitate aqueous (and thus

513 spherical) particles of 1-10 μm,[252,306,308-310] limiting their applications to mineral dust particles.

514 However, recent advances show that spherical and quasi-spherical solid particles can also be

515 trapped for many hours.[139,252,311] The size of a particle which is optically levitated can be estimated

516 from the measured intensity of scattered light as a function of scattering angle, i.e. the phase

517 function. Very accurate size measurements have been achieved by using optical tweezers. For

518 example, a precision of better than 1 nm for measuring the diameter of micrometer sized droplets

519   has been reported, with simultaneous measurements of complex refractive indexes.[312,313] However,

520   most of the sizing techniques based on light scattering are strictly applicable to spherical particles

521   and thus may not be suitable for mineral dust particles which are typically non-spherical.

522

523   An advantage of these levitation techniques is that, in addition to online measurements of particle

524   mass/size, several non-intrusive techniques, such as Raman spectroscopy [139,314] and fluorescence

525   spectroscopy,[315] can be used to measure the particle composition change simultaneously.

526   Therefore, these techniques have a large potential to investigate the change of both chemical

527   composition and hygroscopicity of single mineral dust particles due to heterogeneous reactions as

528   a function of time.

529   **2.4 Aerosol measurements**

530   **2.4.1 Hygroscopic tandem differential mobility analyzer measurements**

531   Hygroscopicity-tandem differential mobility analyzers (H-TMDA) have been widely used to

532   investigate the hygroscopicity of aerosol particles. Comprehensive discussions of this technique

533   have been provided elsewhere,[316-319] and only a brief description is given here. In a typical H-

534   TDMA set-up, a dry aerosol flow is passed through a bipolar charger and then into the first

535   differential mobility analyzer (DMA) which is used to produce a quasi-momodisperse aerosol flow

536   based on mobility diameters. These size-selected particles are then humidified to a certain RH and

537   then enter the second DMA coupled to a condensation nuclei counter (CPC) to measure the size

538   distribution of the humidified aerosol particles. The change in aerosol particle diameters before

539   and after humidification can be used to derive the hygroscopic growth factors.

540

541   H-TDMA has been widely used to measure the hygroscopicity of mineral dust aerosol

542   particles.[49,247,260,320] However, there are a few issues related to its application to mineral dust

543   particles: 1) dust particles are non-spherical in general, and thus it is non-trivial to interpret the

27

544　H-TDMA measurements; 2) the hygroscopicity of dust particles is relatively low, and the mobility

545　diameter change before and after humidification may not be significant; and 3) restructuring of

546　clay minerals may occur during humidification/dehumidification. Very recently Ardon-Dryer et

547　al.[321] used several different techniques to measure the size distribution of size-selected mineral

548　dust aerosol particles using a DMA, and concluded that mobility size selection using a DMA

549　usually does not yield mineral dust particles with desired physical sizes. Similar findings were also

550　reported by Veghte and Freedman.[322]

551　**2.4.2 Optical properties**

552　Water adsorption by mineral dust aerosol particles may lead to change in their size (and probably

553　also refractive indices), thus modifying the optical properties. The change in optical properties of

554　aerosol particles, in principle, can then be used to derive their hygroscopicity.[323] A variety of in-situ

555　instruments are readily available to measure aerosol optical extinction,[324,325] scattering,[254,326-328]

556　and absorption.[255,329] For example, light extinction properties at 532 nm were measured at different

557　RH using a Cavity Ring-Down spectroscopy, to investigate the hygroscopicity of several clay and

558　clay/salt aerosol particles.[253] However, it is non-trivial to convert change in optical diameter at

559　different RH to hygroscopicity for mineral dust aerosol particles, again due to the non-sphericity

560　of dust particles.

561　**2.4.3 Cloud condensation nuclei activity**

562　Under super-saturation (i.e. RH larger than 100%) aerosol particles can be activated to cloud

563　droplets, and the number concentration of activated particles at a given super-saturation can be

564　measured by using cloud condensation nuclei counters (CCNc). If such an instrument is coupled

565　to a CPC in parallel, the activation fraction, defined as the ratio of the concentration of activated

566　particles to the total particle number concentration, can then be determined. The most widely used

567　cloud condensation nuclei counters are commercialized by Droplet Measurement Technologies

568　(Boulder, CO, USA), based on the original design by Roberts and Nenes.[330]

569

570 Details on the principle, operation, and calibration of this instrument are provided elsewhere.[330-

571 333] A typical schematic diagram of the experimental set-up used by Kumar et al.[262] to measure the

572 CCN activity of aerosol particles is shown in Figure 7. A dry aerosol flow is delivered through an

573 aerosol neutralizer and then into a DMA to produce a quasi-monodisperse aerosol particles. After

574 that, the aerosol flow is split: one flow is delivered into a CPC to measure the total particle number

575 concentration, and the other flow is delivered into a CCNc to measure the concentration of particles

576 activated to cloud droplets under a given super-saturation ratio (SS).

577
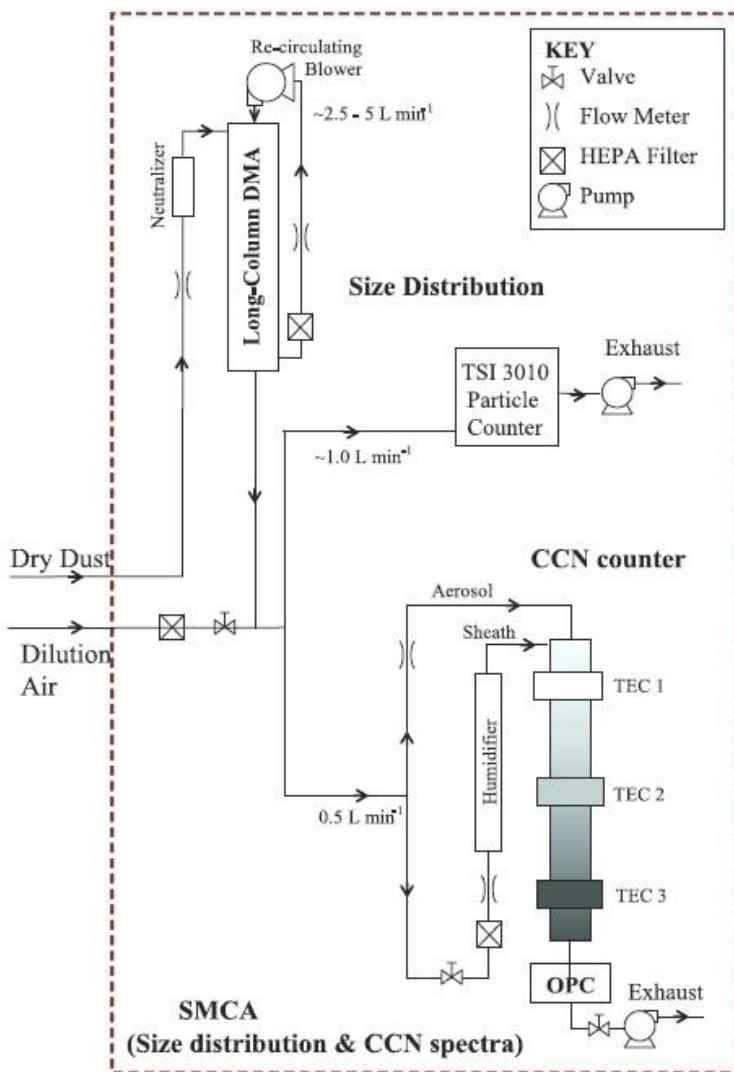
578

579   **Figure 7.** A schematic diagram of an experimental set-up used to determine the CCN activity of (mineral

580   dust) aerosol particles. Reprinted with permission from ref 262. Copyright 2011 Copernicus Publications.

581

582   There are usually two modes to operate a CCN counter: i) measuring the activation fraction as a

583   function of super-saturation ratio for a given dry particle diameter to determine the critical super-

584   saturation under which 50% of the aerosol particles are activated; ii) measuring the activation

585   fraction as a function of the dry particle diameter under a given super-saturation to determine the

586   critical dry diameter at which 50% of the aerosol particle are activated. This information can then

587   be used to derive the cloud condensation nucleation activity of aerosol particles. This technique

588   has been widely used to measure the cloud condensation nucleation activities of fresh and aged

589   mineral dust particles,[46,49,256,257,259,262] significantly improving our understanding of the role of dust

590   particles in the formation of clouds in the troposphere. Different theories used to describe the CCN

591   activity, and the relation between hygroscopic growth under sub-saturation conditions and CCN

592   activity under super-saturation conditions, are further discussed in more detail in Section 3.

593   **2.5 Discussion**

594   As summarized in this section, a wide range of techniques, based on different measurement

595   principles, have been developed to study water adsorption, hygroscopicity, and CCN activity of

596   mineral dust particles. Experimental techniques used to investigate the hygroscopic growth of

597   mineral dust aerosol particles are based on measurements of changes in diameter at different RH.

598   For examples, H-TDMA measures the change in mobility diameter and AE-CRD measures the

599   change in optical extinction properties which can then be related to particle size using Mie theory

600   which assumes particles are spherical. Since mineral dust particles are typically non-spherical, it

601   is non-trivial to quantify the absolute amount of water associated with aerosol particles at a given

602   RH, though they can provide other important information, such as the dependence of particle

603   mobility and optical properties on RH. Aerosol particle mass analyzers (usually referred to as APM

604 or PMA) have been widely used to classify aerosol particles based on their mass.[334-338] In principle,

605 two APM and one CPC can be combined to measure changes in the aerosol particle mass as a

606 function as RH, in a similar way as a H-TDMA system is constructed. In brief, dry dust aerosol

607 particles with the same mass is selected by the first APM; after that, the aerosol flow will be

608 humidified to a given RH, and the mass distribution of the humidified dust aerosol particles will

609 be measured by the second APM coupled to a CPC. This instrument has promising potential to

610 quantitatively determine the mass change of mineral dust particles as a function of RH.

611

612 Diameter changes of single particles trapped by optical levitation techniques at different RH are

613 usually determined by light scattering. The non-sphericity of mineral dust particles can render the

614 data interpretation difficult. Relative mass changes of single particles levitated in an EDB can be

615 directly measured, regardless of the particle shape. EDB has been used to determine the amount

616 of water adsorbed by pollen particles which are also non-spherical,[339] and therefore can also be

617 used to study water adsorption by mineral dust particles. Nevertheless, it is still unclear if the EDB

618 is sensitive enough to detect small mass changes of dust particle due to water adsorption.

619

620 FTIR based techniques have been widely used to monitor adsorbed water by mineral dust particles

621 supported on substrates.[250,268,269] Although in principle adsorbed water can be quantified by its IR

622 absorption bands, this types of analysis typically requires several assumptions which may

623 introduce uncertainties in quantification.[249] In this aspect, techniques which can directly quantify

624 changes in dust particle mass [247,249,271] or water vapor pressure,[212,248] due to the interaction of water

625 vapor with mineral dust, show their advantages. For techniques which use particles supported on

626 substrates, particles are usually not size-selected and therefore it is difficult to investigate the size

627 dependence of the amount of water associated with particles (for the same mass of dry materials,

628 surface adsorption theories indicate that the amount of adsorbed water increases with decreasing

31

629   particle diameter while the hygroscopic growth theory implies that it is size-independent, as

630   discussed in detail in Section 3). Many surface science techniques, though they may not

631   quantitatively measure adosrbed water, can nevertheless provide valuable information about

632   chemical composition, morphology, and adsorption mechanisms on the fundamental level, with

633   some examples given in Section 2.2.3.

634

635   For CCN activity measurements, it is critical to accurately determine the dry particle diameters.

636   Typically a DMA is used to classify aerosol particles based on their mobility. The mobility

637   diameter is not necessarily equivalent to the geometrical diameter for dust particles, due to their

638   non-sphericity. This has also been supported by experimental work,[321,322] showing that mobility

639   size selection using a DMA usually does not generate mineral dust particles with desired physical

640   sizes. Additionally, after passing through the aerosol neutralizer, dry-generated dust aerosol

641   particles may consist of a substantial fraction of multiply charged particls which in fact have larger

642   diameters and can be activated to cloud droplets at lower supersaturation, compared to single

643   charged particles. Both factors can lead to biases in the reported CCN activity,[259] and therefore

644   charge and shape corrections should be applied in determining the CCN activity of mineral dust

645   particles.

646   **3 Introduction of different theories**

647   Several different theories have been developed to describe the partitioning of water between the

648   gas phase and mineral dust particles under both sub- and super-saturation conditions with respect

649   to liquid water. Most widely used theories are introduced in this section. These theories can be

650   generally classified to two groups, with one originating from surface science and surface chemistry

651   and the other one developed for atmospheric aerosol science.

3.1 Theories and models used to describe sub-saturation conditions

Several different models are available to describe the amount of the absorbate adsorbed at different partial pressures.[340-342] In this review, water is the adsorbate and it partial pressure is expressed as RH instead, and mineral dust particles (or their surfaces) are the adsorbents. Among adsorption models, the Langmuir adsorption isotherm model [341-343] is the first and probably the most widely used adsorption theory, but its application is limited to adsorption below one monolayer. Therefore, it is not suitable to describe water adsorption on mineral dust particles at high RH and thus no further discussion on the Langmuir adsorption isotherm is provided here.

3.1.1 Brunauer-Emmet-Teller adsorption isotherm model

The Brunauer-Emmett-Teller (BET) adsorption isotherm [341,342,344] can be used to describe water adsorption for mineral dust particles:[250]

$$\theta = \frac{c \cdot RH}{(1-RH)(1-RH+c \cdot RH)} \qquad (3),$$

where θ is the surface coverage of adsorbed water, and c is a constant related to the enthalpy of desorption, $\Delta_{des}H^o$ (kJ K^{-1}):

$$c = \exp[(\Delta_{des}H^o - \Delta_{vap}H^o)/RT] \qquad (4),$$

where R is the gas constant (8.314 J mol^{-1} K^{-1}), T is the temperature (K), and $\Delta_{vap}H^o$ is the standard enthalpy of water evaporation (kJ K^{-1}). For the adsorption of water on mineral dust, c is usually found to be >1, suggesting that $\Delta_{des}H^o$ is larger than $\Delta_{vap}H^o$.[250]

It has been found that in many cases that the BET equation, Eq. (3), may overestimate the surface coverage of adsorbed water (θ) at high RH. Therefore, by introducing the third parameter, n, a modified three-parameter BET equation has been proposed to describe the water adsorption on mineral particles:[345]

$$\theta = \frac{c \cdot RH}{(1-RH)} \cdot \frac{1-(n+1) \cdot RH^n + n \cdot RH^{n+1}}{1+(c-1) \cdot RH - c \cdot RH^{n+1}} \qquad (5).$$

676   Goodman et al.[250] found that the three-parameter BET equation could fit fairly well the water

677   adsorption on several different mineral dust particles for RH ranging from ~0% to >90%. They [250]

678   also described in details how to derive c and n from experimentally measured θ as a function of

679   RH, using Eq. (5). Ma et al.[269] also suggsted that the three-parameter BET equations can fit well

680   water adsorption on five different oxides which they investigated, as shown in Figure 8.
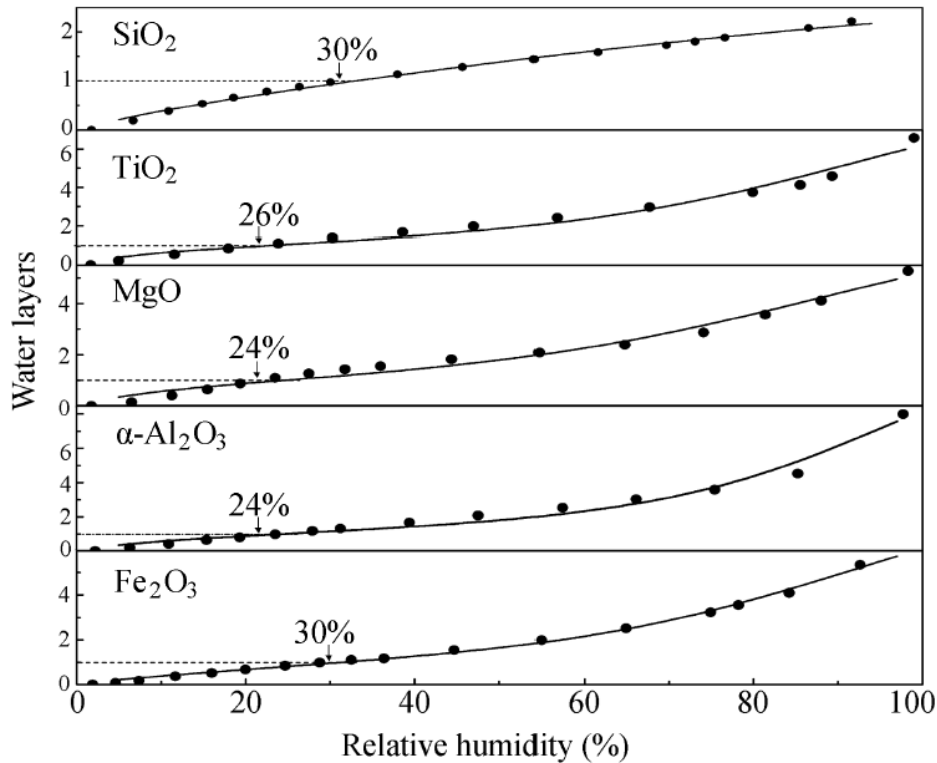
681

682   **Figure 8.** Water adsorption on SiO_2, TiO_2, MgO, α-Al_2O_3, and Fe_2O_3 as a function of RH at 30 °C. Cirlces

683   represent experimental data and curves represent corresponding fitted three-parameter BET isotherms.

684   Relative humidities under which a monolayer of adsorbed water is formed are given in the figure for each

685   minerals. Reprinted with permission from ref 269. Copyright 2011 Elsevier.

686   **3.1.2 Freundlich adsorption isotherm model**

687   The Freundlich adsorption isotherm expresses the mass ratio of the adsorbed water to the dry

688   mineral dust particles as a function of partial pressure or RH:[346,347]

689     $\dfrac{m(water)}{m(mineral)} = A_F \cdot \sqrt[B_F]{RH}$ (6),

34

690   where m(water) and m(mineral) are the mass of adsorbed water and dry mineral dust particles, and

691   A_F and B_F are the empirical Freundlich constants which represent the adsorption capacity and

692   strength, respectively.[268] Eq. (6) can be rearranged to

693    $$\ln \frac{m(water)}{m(mineral)} = \ln A_F + \frac{\ln(RH)}{B_F} \qquad (7),$$

694   Therefore, simple linear regression of the natural logarithm of the mass ratio (of adsorbed water

695   to dry dust particles) versus the natural logarithm of RH can be used to derive A_F and B_F.
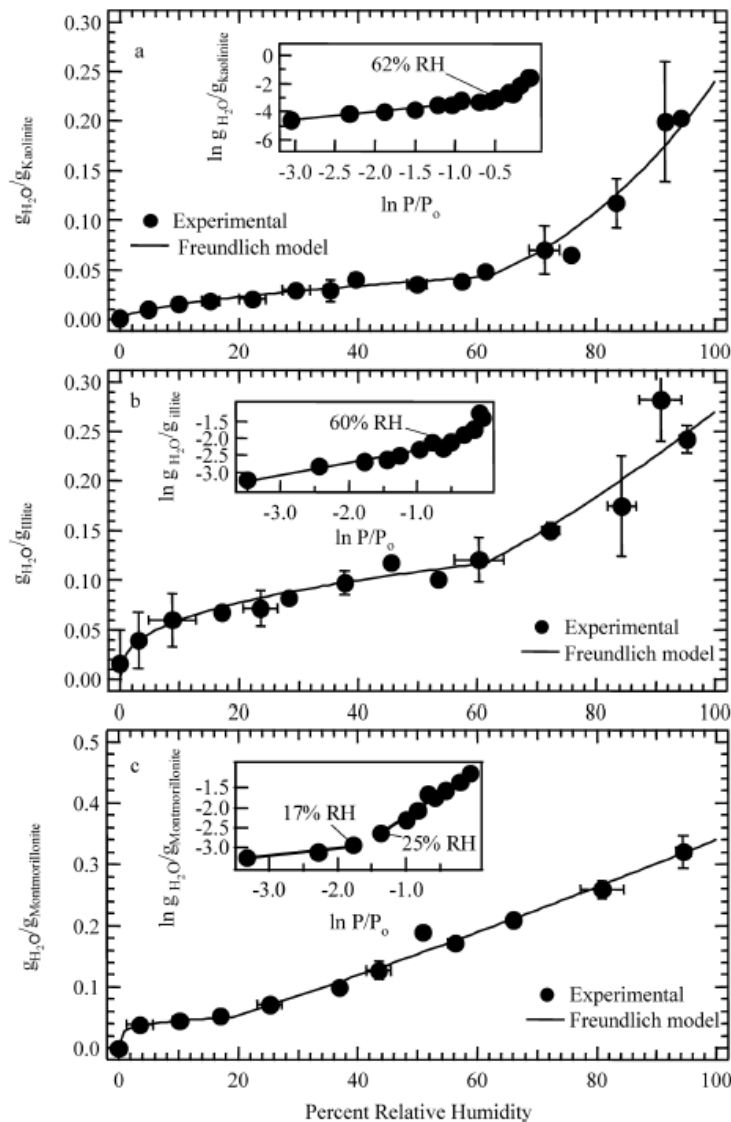
696

697   **Figure 9.** Measured and modeled water adsorption (represented by the mass ratio of adsorbed water to dry

698   mineral) at 298 K as a function of RH on (a) kaolinite, (b) illite, and (c) montmorillonite. The insets

699   represent the data fitted to the linear form of the Freundlich adsorption isotherm, i.e. Eq. (7). Reprinted with

700   permission from ref 268. Copyright 2011 American Chemical Society.

701

702   Hatch et al.[268] measured water adsorption on illite, kaolinite, and montmorillorite particles, and

703   fitted these experimenrtal results using the Freundlich adsorption isotherm, as shown in Figure 9.

704   It was suggested that compared to the two-parameter BET adsorption isotherm, the Freundlich

705   adsorption isotherm can better describe water adsorption by these three clay minerals they

706   investigated.[268]

3.1.3 Frenkel-Halsey-Hill adsorption isotherm model

708   The Frenkel-Halsey-Hill (FHH) isotherm uses a two-parameter equation to describe RH as a

709   function of surface coverage of adsorbed water, θ:

710    $$RH = \exp(-A_{FHH} \cdot \theta^{-B_{FHH}}) \quad (8),$$

711   where A_{FHH} and B_{FHH} are empirical parameters.[341,348] A_{FHH} describes interactions between the

712   surface and first adsorbed water layer and interactions between adjacent adsorbed water molecules.

713   Therefore, it governs the overall extent of water coverage, and higher A_{FHH} values suggest that

714   more water may be adsorbed. B_{FHH} describes interactions between the surface and subsequent

715   adsorbed water layers. Smaller B_{FHH} values mean that attractive forces function over a longer

716   distance from the particle surface. As a result, B_{FHH} significantly influences the shape of the

717   adsorption isotherm, especially at high RH. Consequently, CCN activation described by the FHH

718   activation theory is predominantly determined by the magnitude of B_{FHH},[47,52] and this will be

719   further discussed in Section 3.2.2.

720

721   Eq. (8) can be rearranged to

722    $$\ln[-\ln(RH)] = \ln A_{FHH} - B_{FHH} \cdot \ln(\theta) \quad (9).$$

723   As shown in Eq. (9), A_{FHH} and B_{FHH} can be derived from linear regression of ln[-ln(RH)] versus

724   ln(θ). We can also describe the surface coverage of adsorbed water as a function of RH by

725   rearranging Eq. (9):

726     $\theta = \sqrt[B_{FHH}]{\dfrac{A_{FHH}}{-\ln(RH)}}$ (10).

3.1.4 Hygroscopic growth theory

728   The change of the diameter of a particle at elevated RH due to adsorption of water, called

729   hygroscopic growth in aerosol science, can be described by the single hygroscopicity parameter,

730   κ:[169]

731     $RH = \dfrac{GF^3-1}{GF^3-(1-\kappa)} \exp(\dfrac{A_{Kelvin}}{D_{d\cdot GF}})$ (11),

732     $A_{Kelvin} = \dfrac{4\sigma M_w}{RT\rho_w}$ (12),

733   where GF is the growth factor, defined as the ratio of the diameter of a particle at a given RH to

734   that of the dry particle (D_d).[169] The second term in the right part of Eq. (11), $\exp(A_{Kelvin}/D_d \cdot GF)$, is

735   due to the Kelvin effect, referring to the increase of vapor pressure on a curved surface of the

736   particle, relative to that for a flat surface. A_{Kelvin} is a constant which describes the Kelvin effect,

737   depending on the surface tension (σ), density (ρ_w) and molar mass (M_w) of water, and temperature.

738   A_{Kelvin} is equal to 2.1×10^{-9} m for a surface tension of 0.072 J m^{-2} (pure water) and temperature of

739   298.15 K.[217]

740

741   The Kelvin effect becomes negligible for large particles, and in this case Eq. (11) can be simplified

742   to

743     $RH = \dfrac{GF^3-1}{GF^3-(1-\kappa)}$ (13).

744   Eq. (13) can then be rearranged to express GF as a function of RH:

745     $GF = \sqrt[3]{1 + \kappa \cdot \dfrac{RH}{1-RH}}$ (14).

746   Calculations show that the difference between calculated GF at 90% using Eq. (11) (i.e. taking

747   into account the Kelvin effect) and that using Eq. (14) (i.e. neglecting the Kelvin effect) is

748   negligible for particles with dry diameters larger than 100 nm. As a result, in this review for

749   simplicity, Eq. (14) is used to calculate hygroscopic growth factors and thus also amounts of

750   adsorbed water at different RH for mineral dust particles.

751   The surface coverage, θ, can be expressed as the change of particle diameters:[47,349]

752    $$\theta = \frac{D - D_d}{2 D_w} = \frac{GF - 1}{2} \cdot \frac{D_d}{D_w} \qquad (15).$$

753   where D_d and D are the diameters of the dry particle and the wet particle. D_w is the average diameter

754   of a water molecule adsorbed on the particle surface. D_w is sometimes assumed to be 0.275

755   nm,[47,349] meaning that a water molecule adsorbed on mineral dust surface occupies an area of

756   5.9×10^{-16} cm^2. Al-Abadleh et al.[211] assumes that the hydroxylated $CaCO_3$ surface can

757   accommodate 1×10^{15} water molecules per cm^2, i.e. a water molecule adsorbed on the surface

758   occupies an area of 1×10^{-15} cm^2 (or 0.1 nm^2), corresponding to D_w of 0.36 nm. In this paper, the

759   diameter of one water molecule adsorbed on a mineral dust particle is always assumed to be

760   0.36 nm.

761   **3.1.5 Discussion**

762   There is a fundamental difference between adsorption theories originating from surface science

763   and hygroscopicity theories used to describe the interaction of water vapor with mineral particles

764   under sub-saturation conditions. All adsorption theories assume that at given RH and T, the amount

765   of water adsorbed by mineral particles is proportional to the total surface area; therefore, for the

766   same amount (mass or volume) of dry material, the amount of water adsorbed by mineral particles

767   increase with decreasing average particle diameter. On the other hand, hygroscopicity theories

768   assume that the amount of water is proportional to the volume of solute, and thus for the same

769   amount of dry material, the amount of water associated with mineral dust is independent of particle

770   diameter, if the Kelvin effect is negligible. This difference can make direct comparison of some

771   experimental measurements difficult, and this issue will be discussed further in Section 3.3.

772   **3.2 Theories and models used to describe super-saturation conditions**

773   **3.2.1 κ-Köhler activation theory**

774   The saturation ratio of water vapor, S, in equilibrium with an aqueous droplet, can be describe by

775   the Köhler theory,[350] which takes into account the effects of both water activity and surface

776   curvature:

777    $S = a_w \cdot \exp(\frac{A_\kappa}{D})$ (16),

778   where a_w is the water activity, and D is the droplet diameter, and A_{Kelvin} is defined in Eq. (12). In

779   fact the definition of S is the same as RH, as shown in Eq. (1). However, to keep consistent with

780   conventional terminology, S is used for super-saturation conditions and RH is used for sub-

781   saturation conditions. The single hygroscopicity parameter, κ, links water activity (a_w), the volume

782   of the dry particle (V_s), and the volume of water (V_w):[169,351]

783    $\frac{1}{a_w} = 1 + \kappa \frac{V_s}{V_w}$ (17),

784   As shown by Petters and Kreidenweis (2007),[169] inserting Eq. (17) into Eq. (16) and converting

785   volumes to corresponding diameters can yield the "κ-Köhler theory" equation:

786    $S(D) = \frac{D^3 - D_d^3}{D^3 - (1-\kappa) \cdot D_d^3} \cdot \exp(\frac{A_\kappa}{D})$ (18).

787

788   The critical saturation for a dry particle, S_c, is defined as the saturation above which the particle is

789   activated to a cloud droplet. The critical super-saturation, s_c, which is equal to S_c-1, is more widely

790   used in describing cloud condensation nucleation. For a particle with given dry diameter and

791   hygroscopicity, S_c (and thus s_c) can be calculated from the maximum of the κ-Köhler curve, i.e.

792   Eq. (18). Three κ-Köhler curves, for particles with a dry diameter of 50 nm and different

793   hygroscopicity, are plotted in Figure 10 as examples. The maxima of s, i.e., s_c, are 0.47%, 1.03%,

794 and 2.46% for 50 nm particles with κ values of 0.5, 0.1, and 0.01, respectively. If the

795 supersaturation ratio in the ambient air is larger than the s_c for a given particle, this particle will be

796 activated to a cloud droplet.
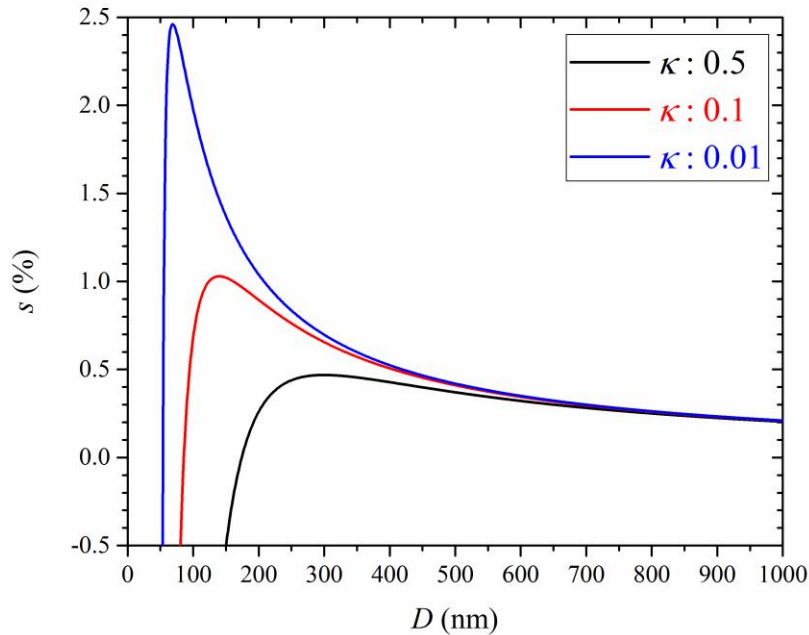
797

798 **Figure 10.** Calculated super-saturations as a function of the diameter of aqueous particles with a dry

799 diameter of 50 nm and different hygroscopicity (κ is equal to 0.5, 0.1, and 0.01, respectively), using Eq.

800 (18). Note that super-saturation (s) instead of saturation (S), is plotted.

801

802 The same procedure can be applied to a wide range of D_d and κ to calculate corresponding s_c, and

803 a look-up table for s_c as a function of D_d and κ can then be produced. The critical super-saturation,

804 s_c, for momodisperse aerosol particles with a dry diameter of D_d, or alternatively the critical

805 diameter of polydisperse aerosol particles for a gievn super-saturation, can be measured using the

806 procedure described in Section 2.3.3. Corresponding κ values can then be derived from s_c and D_d,

807 using the look-up table.

40

3.2.2 Frenkel-Halsey-Hill adsorption activation theory

The FHH adsorption activation theory [349] describes the activity of adsorbed water on the surface of insoluble particles:

$$a_w = \exp[-A_{FHH} \cdot \theta^{-B_{FHH}}] \qquad (19),$$

where θ is the surface coverage of water, and A_{FHH} and B_{FHH} are empirical parameters which are described in Eq. (8). Inserting Eq. (19) into Eq. (16) gives

$$S = \exp[-A_{FHH} \cdot \theta^{-B_{FHH}}] \cdot \exp(\frac{A_\kappa}{D_d}) \qquad (20).$$

A_{FHH} and B_{FHH} can be derived from to the fit to the s_c-D_d data, as detailed by Kumar et al.[52]

A_{FFH} and B_{FHH} vary with different compounds. Typically, A_{FHH} ranges from 0.1 to 3.0, and B_{FHH} ranges from 0.5 to 3.0.[349] If the dry diameter, A_{FHH} and B_{FHH} are known for a particle, the critical super-saturation can be calculated from the maximum of its FHH adsorption activation curve. Three FHH curves for B_{FHH} values of 0.7, 0.8, and 0.9 (all with an A_{FHH} value of 0.3) are shown in Figure 11, and have s_c values of ~0.26%, ~0.62%, and ~0.89%, respectively. If the supersaturation ratio in the ambient air is larger than the s_c for a given particle, this particle will be activated to a cloud droplet.

If B_{FHH} is small enough, the activation curve may never reach a maximum but instead asymptotes to a negative value, $-s_\infty$. Two FHH curves with B_{FHH} values of 0.5 and 0.6 (and A_{FHH} is 0.3 for both cases), are shown in Figure 11 for illustration. The asymptotic value of s at very large D_p determines if this particle will be activated:[47] if it is smaller than 0, the particle can be spontaneously activated at RH less than 100%; otherwise, the particle will never be activated (i.e. always in stable equilibrium with the environment). However, such observations have not been reported yet, shedding doubt on its atmospheric relevance.
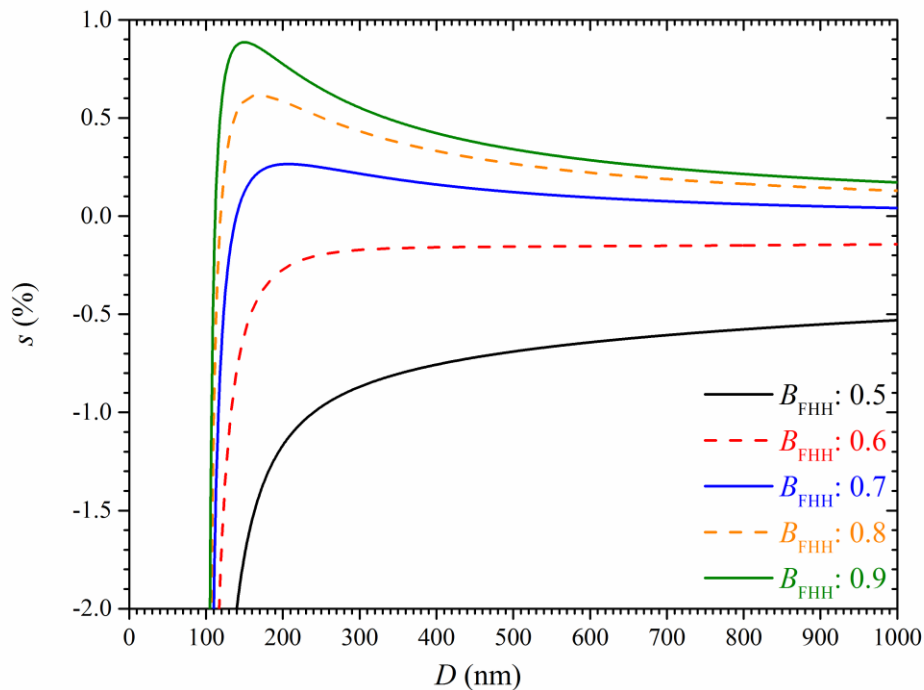
Figure 11. Calculated super-saturations as a function of the diameter of a wet particle, here for a dry diameter of 100 nm, using Eq. (20). A_{FHH} is assumed to be 0.3, and B_{FHH} are assumed to be 0.5, 0.6, 0.7, 0.8, and 0.9, respectively. Note that super-saturation (s) instead of saturation (S), is plotted.

The two empirical FHH parameters, A_{FHH} and B_{FHH}, can be determined by measuring the surface coverage (θ) of adsorbed water as a function of RH under sub-saturation conditions, as discussed in Section 3.1.3. Alternatively, they can also be determined by measuring critical super-saturation as a function of particle diameter under super-saturation conditions.[262,263]

Activity of adsorbed water can also be described by other water adsorption isotherms (e.g., the BET adsorption isotherm), and corresponding adsorption activation theories, analogous to Eq. (20), can be subsequently derived. For example, the BET adsorption activation theory has been developed and applied to describe cloud activation of black carbon particles.[352] To our knowledge, this theory has not been used to describe cloud activation of mineral dust particles, and therefore it is not discussed further in this review.

848 **3.2.3 Discussion**

849 It has been shown that both κ-Köhler and FHH theories are superior to the original Köhler theory,

850 at the expense of increased complexity, since they can account for the hygroscopic content of

851 mineral dust.[47,52,217] Differences do exist between these two methods. As noted by Kumar et al,[47,52]

852 using FHH theory changes the maximum super-saturations and cloud droplet number with respect

853 to aerosol variations, compared to the κ-Köhler theory. This is because when compared to the κ-

854 Köhler theory, the FHH activation theory requires less water uptake to reach a critical diameter.

855 This is further illustrated by Figure 12, displaying the κ-Köhler and FHH activation curves for a

856 particles with a dry diameter of 100 nm. Both theories suggest that the particle will be activated at

857 a super-saturation of ~0.88%. However, the predicted wet particle diameters when super-saturation

858 is equal to sc are different, with 150 nm predicted by the FHH activation theory and 174 nm

859 predicted by the κ-Köhler theory. As a result, compared to the κ-Köhler theory, the FHH activation

860 theory requires less water uptake for the particle to be activated.

861

862 In addition, the two theories suggest different dependence of s_c on D_d, as shown in Figure 12. Both

863 theories suggest that a particle with a dry diameter of 100 nm has the same s_c. Compared to the κ-

864 Köhler theory, the FHH activation theory predicts that particles with $D_d <100$ nm will be activated

865 at smaller s_c while they have larger s_c for $D_d >100$ nm.

866
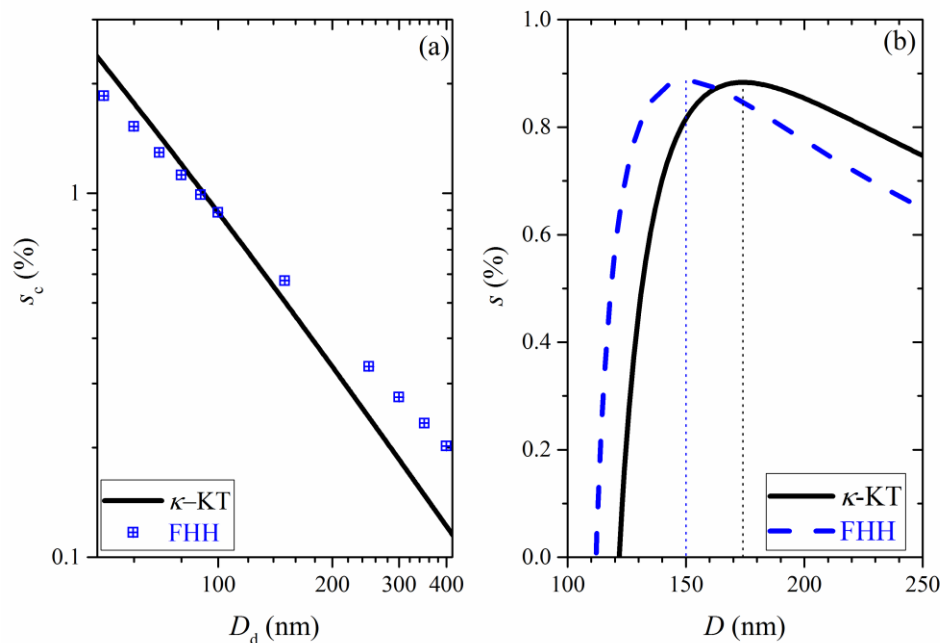
Figure 12. Comparison of κ-Köhler ($\kappa = 0.014$) and FHH ($A_{FHH} = 0.3$, $B_{FHH} = 0.9$) activation theories. Values of κ, A_{FHH}, and B_{FHH} are chosen in such a way that both theories predict that a particle with a dry diameter (D_d) of 100 nm will have a s_c of ~0.88%. (a) Predicted sc as a function of D_d by κ-Köhler (solid black curve) and FHH (blue squares) activation theories. (b) Calculated activation curves for a particle with a dry diameter of 100 nm by κ-Köhler (solid black curve) and FHH (dashed blue curve) activation theories.

A recent study suggests that the κ-Köhler activation theory provides a better fit to laboratory data with slightly less complexity of calculation.[259] Nevertheless, it still remains under debate which theory can better describe the activation of cloud droplets by mineral dust particles.

3.3 Suggested guidelines used for data comparison

The amounts of water adsorbed or condensed on mineral dust particles are reported in different ways. The following guidelines are used to compare available data for each type of mineral particles:

44

881   i) Under super-saturation conditions the single hygroscopic parameter, κ, is usually reported. Using

882   Eq. (14), reported κ values can be converted to the hygroscopic growth factors, which are directly

883   measured by H-TDMA under sub-saturation conditions.

884

885   ii) The change in particle diameters due to hygroscopic growth, calculated from measured κ values

886   or directly measured by H-TDMA, can be converted to the surface coverage (θ) of adsorbed water,

887   using Eq. (15). Usage of Eq. (15) requires the knowledge of dry particle diameter. In this review,

888   three different dry particle diameters, i.e. 500, 1000, and 2000 nm, are used when we convert

889   hygroscopic growth factors to surface coverages, θ, using Eq. (15). The dry particle diameter (D_d)

890   and the hygroscopic growth factor at a given RH can be used to calculate the wet particle diameter

891   (D) at this RH, and the number of monolayers (i.e. surface coverage) of adsorbed water is

892   approximately equal to $(D_d\text{-}D)/D_w$, where D_w is the average diameter of the adsorbed water

893   molecules. We choose these three diameters because they may reasonably represent the size range

894   of tropospheric dust particles after long range transport. According to Eq. (15), the calculated θ is

895   proportional to the dry particle diameter used in the calculation. Therefore, large uncertianties may

896   occur when converting hygroscopic growth factors to θ, making data comparison difficult. For

897   example, for the same hygroscopic growth factor, the calculated θ using a dry particle diameter of

898   1000 nm will be twice as large as that using a dry particle diameter of 500 nm. In some CCN

899   activity measurements the two FHH parameters (instead of κ values) are reported;[262,263] in this case,

900   the surface coverage of adsorbed water at different RH can be directly calculated using Eq. (10).

901

902   iii) If the mass ratio of adsorbed water to dry mineral particle is reported, the surface coverage (θ)

903   of adsorbed water can then be calculated by

904    $\theta = \frac{m(water)}{m(mineral)} \cdot \frac{N_A \cdot A(water)}{M(water) \cdot A_{BET}}$ (21),

905 where m(water) and m(mineral) are the masses (g) of adsorbed water and dry mineral, M_m(water)

906 is the molar mass of water (g mol^{-1}), N_A is the Avogadro constant (6.02×10^{23} mol^{-1}), A(water) is

907 the average surface area of one adsorbed water molecule (1×10^{-15} cm^2), and A_{BET} is the BET area

908 (cm^2 g^{-1}) of the mineral.

909

910 It should be emphasized that large uncertainties may occur when we convert reported data in other

911 units to θ. The largest uncertainties may come from i) converting hygroscopic growth factors,

912 either directly measured by using H-TDMA or calculated from κ values determined by CCN

913 activity measurements, to surface coverages of adsorbed water, and ii) the nonsphericity (and

914 probably also porosity) of mineral particles. In this review it is always assumed that the mass-,

915 volume-, and surface area-equivalent diameters are equal to mobility diameters. However, this is

916 a clear oversimplification and will inherently yield some uncertainty for mineral dust particles

917 which are typically non-spherical.[353]

4 Water adsorption properties, hygroscopicity, and CCN activity of fresh and aged mineral dust particles

920 In this section, the interaction of water vapor with different components of mineral dust particles

921 under both sub-saturation and super-saturation conditions are reviewed. Mineral dust particles

922 covered in this section include calcium carbonate (CaCO$_3$, usually in the form of calcite), Arizona

923 Test Dust, illite, kaolinite, montmorillonite, quartz, several metal oxides (TiO$_2$, Al$_2$O$_3$, and Fe$_2$O$_3$),

924 and authentic desert dust samples. Laboratory studies on the effects of atmospheric aging through

925 heterogeneous processes are also reviewed. We also discuss some theoretical studies on water

926 adsorption on mineral dust surfaces. After that, we summarize some field measurements that have

927 provided evidence that chemical transformation in the atmosphere could change the interaction of

928 mineral dust particles with water vapor. A brief summary is then provided to conclude this section.

4.1 Calcium carbonate

With respect to the interaction with water vapor, calcium carbonate ($CaCO_3$), usually in the form of calcite, is the most widely investigated component of mineral dust particles. We first review the interactions of water vapor with fresh $CaCO_3$, and then discuss the effects of chemical aging on these interactions.

4.1.1 Fresh CaCO₃ particles

As shown in Table 4, the interaction of fresh $CaCO_3$ particles with water vapor has been investigated under both sub-saturation and super-saturation conditions by a number of studies.

Table 4. Water adsorption, hygroscopicity, and CCN activity of fresh $CaCO_3$ particles: summary of previous studies.

references	techniques	aerosol generation method
Al-Hosney et al., 2005 [354]	ATR-FTIR	not applicable
Gustafsson et al., 2005 [247]	DRIFTS, TGA, and H-TDMA	wet generation
Gibson et al., 2006 [355]	H-TDMA and CCNc	wet generation
Gibson et al., 2007 [257]	CCNc	wet generation
Schuttlefield, 2008 [356]	QCM	not applicable
Hatch et al., 2008 [216]	QCM and CCNc	wet generation
Sullivan et al., 2010 [256]	CCNc	wet and dry generation
Zhao et al., 2010 [264]	H-TDMA and CCNc	see text for details
Kumar et al., 2011 [262]	CCNc	dry generation
Kumar et al., 2011 [263]	CCNc	wet generation
Gierlus et al., 2012 [218]	CCNc	wet generation
Ma et al., 2012 [212]	PSA	not applicable
Tang et al., 2015 [357]	CCNc	dry generation

941   Al-Hosney et al.[354] investigated water adsorption on $CaCO_3$ particles at different RH, using ATR-

942   FTIR, and observed that the bending (ca. 1646 cm^{-1}) and stretching (3000-3700 cm^{-1}) modes of

943   adsorbed water both increase with RH. However, absolute amounts of adsorbed water was not

944   reported.[354] DRIFTS was used by Gustafsson et al.[247] to study the water adsorption on $CaCO_3$

945   particles (BET surface area: 17.8 m^2 g^{-1}), and they found that 1 and 4.5 monolayers of adsorbed

946   water is formed at ~55% and 80% RH, respectively. The same study [247] also measured the

947   hygroscopic growth of wet-generated $CaCO_3$ particles at different RH using a H-TDMA, and

948   suggested that the relative change of mobility diameters can be described by the following equation:

949      $\frac{D}{D_0} = (1 - RH)^{-0.073}$ (22).

950   It should be noted that $CaCO_3$ aerosol particles used by Gustafsson et al.[247] are polydisperse, with

951   a first mode at 40 nm and a second mode at 250 nm. Gibson et al.[355] also used a H-TDMA to

952   measure the hygroscopic growth of 100 nm wet-generated $CaCO_3$ particles, and found that the

953   hygroscopic growth factor can be described by an average value of 1.00±0.02 over the entire RH

954   range (0-85%), i.e. the hygroscopic growth of $CaCO_3$ particles is not significant within the

955   experimental uncertainties.

956

957   Ma et al.[212] measured the amount of water adsorbed on $CaCO_3$ (BET area: 0.6 m^2 g^{-1}) at 278 K

958   using a physisorption analyser. They [212] reported that there is one monolayer of adsorbed water

959   formed on the surface at 52% RH, increasing to ~2 layers at 90% RH and ~7 layers at 95% RH.

960   Hatch et al.[216] showed that the mass of adsorbed water on $CaCO_3$ particles (BET surface area: 10.1

961   m^2 g^{-1}) is equal to ~8% of the mass of dry $CaCO_3$ particles at 78% RH, corresponding to

962   approximately 3 monolayers of water. The amount of water adsorbed on $CaCO_3$ particles at

963   different RH was also measured by Schuttlefield et al.,[356] using a QCM.

964

965 Wet-generated $CaCO_3$ particles were reported to have κ values of ~0.043 by Gibson et al.,[355]

966 0.0110±0.0015 by Gibson et al.,[257] ~0.005 by Hatch et al.,[216] and 0.0070±0.0017 by Gierlus et

967 al.[218] from CCN activity measurements. The CCN activity of dry generated $CaCO_3$ particles was

968 studied by Sullivan et al.[217] and Tang et al.,[357] with reported κ values of 0.0008-0.0018 [217] and

969 0.001-0.003.[357] Zhao et al.[264] developed a novel method to produce dry $CaCO_3$ particles, by

970 transforming $Ca(HCO_3)_2$ aerosol particles to $CaCO_3$ particles via thermal decomposition in a tube

971 furnace. They reported a mobility diameter growth factor of 1.01 at 95% RH (corresponding to κ

972 values of 0.0016±0.004) using a H-TDMA and κ values of 0.0019±0.0007 using a CCNc.[264]

973 Kumar et al.[262] also investigated the CCN activity of dry-generated $CaCO_3$ aerosol particles, and

974 they suggested the activation of $CaCO_3$ particles can be better described by the FHH activation

975 theory, with A_{FHH} of 3.00±0.04 and B_{FHH} of 1.30±0.03.

976

977 As summarized above, the CCN activities of $CaCO_3$ aerosol particles were measured by several

978 previous studies. For dry generated $CaCO_3$ particles, different studies reported very similar CCN

979 activities, with measured κ values of ~0.002.[256,264,357] The CCN activity of wet generated $CaCO_3$

980 aerosol particles is significantly higher.[216,218,257,355] The difference in the measured CCN activities

981 of dry and wet generated $CaCO_3$ particles has been investigated,[256,262,263] and it has been concluded

982 that wet generation of $CaCO_3$ aerosol particles will lead to higher CCN activities.

983

984 Using the data comparison guideline discussed in Section 3.3, a κ value of 0.002 means that the

985 hygroscopic growth factors are 1.003, 1.006, and 1.013 at RH of 80%, 90%, and 95%. This shows

986 excellent agreement with H-TDMA measured hygroscopic growth factors reported by the two

987 previous studies (1.00±0.01 for RH <85% [355] and 1.01 at 95% RH [264]).

988
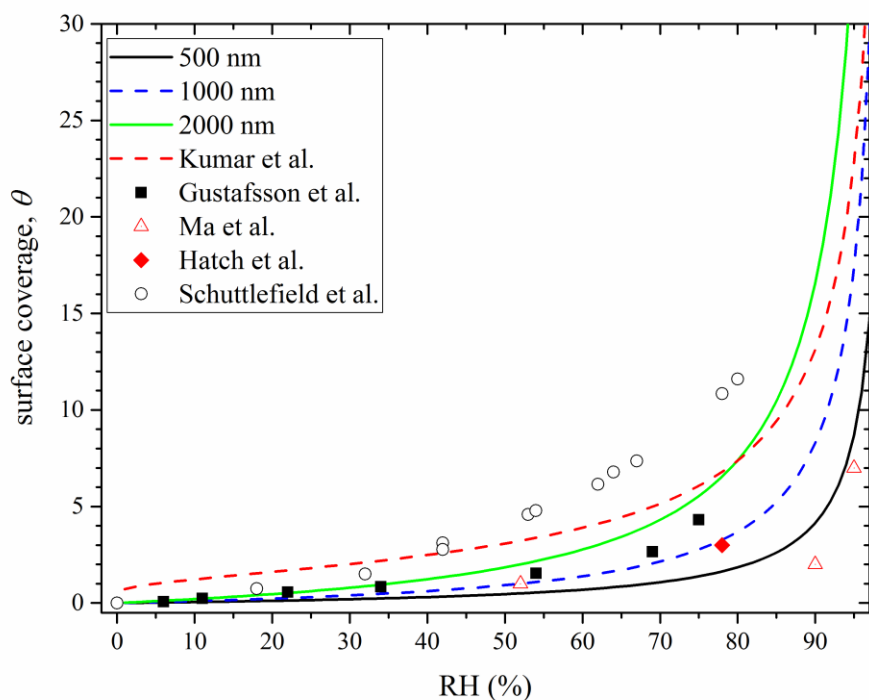
Figure 13. Comparison of measured surface coverages (θ) of adsorbed water on $CaCO_3$ particles reported by previous studies. Squares: Gustafsson et al.;[247] diamonds: Hatch et al.;[216] circles: Schuttlefield et al.;[356] triangles: Ma et al.;[212] dashed red curve: calculated using the two FHH parameters reported by Kumar et al.[262] In addition, an avearge κ values of 0.002 is used to calculated θ using Eq. (14-15) with assumed dry particle diameters of 500 (solid black curve), 1000 (dashed green curve), and 2000 nm (solid green curve).

Surface coverages of adsorbed water, measured by the four previous studies using particles deposited on some substrates,[212,216,247,356] are plotted in Figure 13 for comparison. Reasonably good agreement is found between these four different studies, as shown in Figure 13. However, discrepancies do also occur. For example, Gustafsson et al.[247] and Schuttlefield et al.[356] suggested that 4.5 and ~12 monolayers, respectively, of adsorbed water are formed at 80% RH, while Ma et al.[212] found that only ~2 monolayers of adsorbed water are formed at ~90% RH. Surface coverages of adsorbed water can be calculated using the two FHH parameters reported by Kumar et al.[262] As shown by the dashed red curve in Figure 13, the calculated θ fall into the range of those measured using particles deposited on substrates. We further calculate θ using an average κ value of 0.002

50

1004   for CaCO$_3$, with assumed dry particle diameters of 500, 1000, and 2000 nm, respectively. The

1005   calculated θ are within the same order of magnitude as those directly measured. Considering

1006   measurement uncertainties and more importantly, uncertainties related to assumptions used in

1007   converting reported κ values into surface coverage (as discussed in Section 3.3), these studies show

1008   reasonably good agreement.

1009

1010   There are also a few studies which may not be directly relevant for atmospheric interest but can

1011   provide fundamental insight into the mechanisms of water adsorption on CaCO$_3$. For example,

1012   Neagle and Rochester [358] measured the mass of calcite samples at different temperatures and found

1013   that a cumulative loss of particle mass by 5.2% when increasing temperature from 273 K to 873

1014   K. Synchrotron X-ray reflectivity was used to measure the thickness of water adsorbed on single

1015   crystal CaCO$_3$ surface (1014) at different RH by Bohr et al.,[359] and they found that the adsorbed

1016   water was constant in thickness (1.55±0.1 nm) while RH was varied from <4% to 90%. The result

1017   reported by Bohr et al.[359] appears to disagree with several other studies which suggest that the

1018   amount of adsorbed water on CaCO$_3$ significantly increases with RH. The discrepancy may be due

1019   to the fact that much less defect sites were present on the single crystals used by Bohr et al.[359]

1020

1021   Most of the aforementioned studies on water adsorption by CaCO$_3$ used techniques which provide

1022   information on the average ensemble for the surfaces under investigation, AFM can achieve spatial

1023   resolution down to sub-nanometer. AFM has been widely used to study calcite surfaces in dry and

1024   humid environments,[292,360-362] revealing that calcite surface is very dynamic and complex in the

1025   presence of water vapor. More recently, alternating current AFM height images combined with

1026   force measurements and phase imaging were used by Baltrusaitis and Grassian [291] to examine

1027   surface structure and chemistry of calcite (1014) surface at 70% for a total period of ~ 3h and at

1028   278 and 296 K. They [291] found that calcite surfaces under ambient conditions are complex and

1029 inhomogeneous in terms of surface composition and phases, containing regions with very different

1030 water contents. Therefore, the heterogeneous reactivity of the surface will also be spatially

1031 controlled and inhomogeneous,[291] though this complication has not been considered or understood.

1032 **4.1.2 Effect of chemical aging**

1033 As summarized in Table 5, a number of previous laboratory studies have examined the change in

1034 water adsorption, hygroscopicity, and CCN activity of $CaCO_3$ particles, using different

1035 experimental techniques and methods to produce aged dust particles.

1036   **Table 5.** Laboratory studies on the effects of chemical aging processes on water adsorption, hygroscopicity, CCN activity of $CaCO_3$ particles:

1037   summary of previous studies

references	techniques	particle aging methods	major findings
Krueger et al., 2003 [214]	SEM-EDX	Particles deposited on supporting substrates were exposed to $HNO_3(g)$ at different RH.	Exposure to 26 ppbv HNO_3 at (41±1)% RH only for 1 hour will change irregular $CaCO_3$ particles to spherical aqueous droplets.
Al-Abadleh et al., 2003 [363]	FTIR	$CaCO_3$ single crystals were exposed to $HNO_3(g)$ at different RH.	$CaCO_3(104)$ and $CaCO_3(110)$ surfaces exposed to 100 mTorr HNO_3 at 23% RH have similar deliquescence relative humidities as amorphous $Ca(NO_3)_2$ particles.
Gibson et al., 2007 [257]	CCNc	Internally mixed $CaCO_3/Ca(NO_3)_2$ aerosol particles were generated by atomizing $CaCO_3/Ca(NO_3)_2/H_2O$ mixture.	Internally mixed $CaCO_3/Ca(NO_3)_2$ particles show much higher CCN activities than $CaCO_3$ particles, and the enhancement increases with the ratio of $Ca(NO_3)_2$ to $CaCO_3$ in the particles.
Hatch et al., 2008 [216]	QCM and CCNc	Aged $CaCO_3$ particles were generated by atomizing $CaCO_3/H_2O$ mixtures containing humic acid sodium salt or fulvic acid.	$CaCO_3$ particles internally mixed with humic acid sodium salt and Suwannee River fulvic acid adsorb significantly larger amounts of water, compared to fresh $CaCO_3$ particles.
Liu et al., 2008 [215]	micro Raman spectrometry	$CaCO_3$ particles on supporting surface were exposed to NO_2 at different RH.	After exposure to 100 ppmv NO_2 for 50 min at 37% RH, $CaCO_3$ particles have much higher hygroscopicity compared to fresh particles, and they exhibit the same phase transition behavior as pure $Ca(NO_3)_2$ particles.
Sullivan et al., 2009 [258]	CCNc	Monodisperse $CaCO_3$ aerosol particles were exposed to gaseous HNO_3 in an aerosol flow tube at different RH.	Exposure to HNO_3 can increase the CCN activity of $CaCO_3$ particles from $\kappa = \sim 0.002$ to $\kappa = \sim 0.1$ very quickly. A comparison of different calcium-containing minerals shows a range of CCN activities.

Gierlus et al., 2012 [218]	CCNc	Internally mixed $CaCO_3$ particles were generated by atomizing $CaCO_3/H_2C_2O_4/H_2O$ mixture.	Internally mixed $CaCO_3/CaC_2O_4$ particles only have slightly higher CCN activity, compared to fresh $CaCO_3$ particles.
Ma et al., 2012 [212]	PSA	$CaCO_3$ particles on supporting surface were exposed to gaseous CH_3COOH at different RH.	Reaction with CH_3COOH can significantly enhance the amount of water adsorbed by $CaCO_3$ particles.
Tang et al., 2015 [357]	CCNc	Monodisperse $CaCO_3$ aerosol particles were exposed to N_2O_5 in an aerosol flow tube at 0% RH.	Exposure of $CaCO_3$ aerosol particles to N_2O_5 (~550 to 15000 ppbv·s) at 0% RH increases their κ values from 0.001-0.003 to 0.02-0.04.

1038

1039

1040   Phase transformation of solid dust particles to liquid droplets, i.e. significant change in

1041   hygroscopicity, due to heterogeneous chemistry, was first reported by Krueger et al.,[214] using

1042   Scanning Electron Microscopy. It is found that exposure to 26 ppbv HNO_3 at (41 ± 1)% RH only

1043   for 1 hour will change irregular $CaCO_3$ particles to spherical aqueous droplets.[214] Similar phase

1044   change of $CaCO_3$ particles was also observed at (17 ± 1)% RH after exposed to HNO_3 of the same

1045   concentration, though it only occurred after much longer exposure time.[214] Energy Dispersive X-

1046   Ray (EDX) analysis reveals that the observed phase change of aged $CaCO_3$ particles is caused by

1047   the formation of $Ca(NO_3)_2$ (R1),[199] which has a much higher hygroscopicity than $CaCO_3$.

1048 $CaCO_3(s) + 2HNO_3(g) \rightarrow Ca(NO_3)_2(l) + H_2O(l) + CO_2(g)$ (R1)
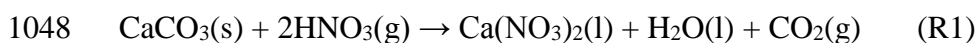
1049

1050   This innovative discovery has been supported by many following studies, which have provided

1051   further insights and more quantitative results. For example, Al-Abadleh et al.[211] found that after

1052   exposure to 100 mTorr HNO_3 at 23% RH and 295 K, the amount of adsorbed water by $CaCO_3$

1053   single crystals (104 and 110 surface planes) is significantly increased, due to the formation of

1054 $Ca(NO_3)_2$ on the surface. Aged $CaCO_3(104)$ and $CaCO_3(110)$ surfaces have deliquescence relative

1055   humidities (DRH) of (9 ± 2)% and (13 ± 5)% at 295 K,[211] similar to that for amorphous $Ca(NO_3)_2$

1056   particles.[364]

1057   In addition to HNO_3, uptake of NO_2 [201,365] and N_2O_5 [131,136,139] also lead to the formation of nitrate

1058   on dust particles. Using micro-Raman spectrometry, Liu et al.[215] found that after exposure to 100

1059   ppmv NO_2 for 50 min at 37% RH, fresh $CaCO_3$ particles were converted to internally mixed

1060 $CaCO_3/Ca(NO_3)_2$ particles with much higher hygroscopicity. This study further showed those

1061   internally mixed $CaCO_3/Ca(NO_3)_2$ particles, though still containing $CaCO_3$ inclusion, exhibit the

1062   same phase transition behavior as pure $Ca(NO_3)_2$ particles.[215]

1063

1064   Heterogeneous reactions of $CaCO_3$ particles with other acidic trace gases, in addition to nitrogen

1065   oxides, can also lead to the increase in hygroscopicity. For example, Hatch et al.[216] used a QCM

1066   to measure the amount of water adsorbed on fresh $CaCO_3$ and $CaCO_3$ particles mixed with humic

1067   acid sodium salt (NaHA) and Suwannee River fulvic acid (SRFA) at different RH. As shown in

1068   Figure 14, compared to fresh $CaCO_3$, the amount of water is significantly increased for $CaCO_3$

1069   particles internally mixed with NaHa or SRFA.[216]
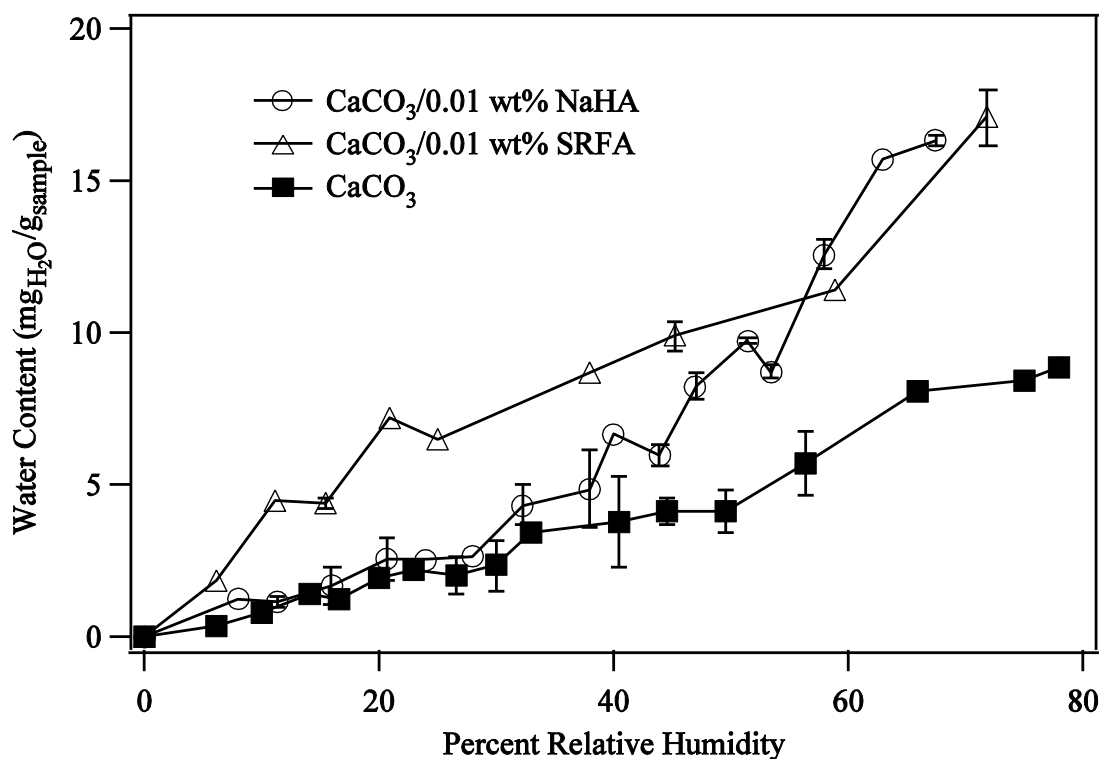
1070

1071   **Figure 14**. Amounts of water adsorbed on fresh $CaCO_3$ particles and $CaCO_3$ mixed with humic acid sodium

1072   salt (NaHA) and Suwannee River fulvic acid (SRFA) at different RH. Reprinted with permission from ref

1073   216. Copyright 2008 Elsevier.

1074

1075   Ma et al.[212] observed that at 90% RH, while fresh $CaCO_3$ particles only contain 0.1% water,

1076   internally mixed $CaCO_3/Ca(CH_3COO)_2$ particles formed in the reaction of $CaCO_3$ with acetic acid

1077   at 50% RH contains ~70% water. They found that these internally mixed $CaCO_3/Ca(CH_3COO)_2$

1078   particles have almost the same DRH as pure $Ca(CH_3COO)_2$ particles.[212] Exposure to acetic acid at

1079   0% RH also enhances the ability of $CaCO_3$ to adsorb water, though the increase is smaller

1080   compared to that at 50% RH.[212]

1081

1082   As discussed previously, several studies suggest that the CCN activity of fresh $CaCO_3$ particles is

1083   very low, with κ values of <0.005.[217,264,357] Thermodynamic theories predict that the formation of

1084   more hygroscopic materials through atmospheric aging processes on $CaCO_3$ particles will increase

1085   their CCN activities.[366,367] Indeed the CCN activities of several pure Ca-containing compounds

1086   that could be formed in the atmospheric transformation of $CaCO_3$ particles, are found to have

1087   higher κ values. For example, the κ values are ~0.5 for $Ca(NO_3)_2$ and $CaCl_2$,[217,357] similar to that

1088   for $(NH_4)_2SO_4$, and 0.05 for CaC_2O_4.[217]

1089

1090   The CCN activities of fresh $CaCO_3$ and internally mixed particles, generated by atomization, have

1091   been measured to mimic the effect of chemical aging on the CCN activities of $CaCO_3$

1092   particles.[218,257] For example, internally mixed $CaCO_3/Ca(NO_3)_2$ particles show much higher CCN

1093   activities than $CaCO_3$ particles, and the enhancement of CCN activities increases with the mass

1094   ratio of $Ca(NO_3)_2$ to $CaCO_3$ in the aqueous mixtures which were atomized to produce aerosol

1095   particles.[257] On the other hand, another study [218] found that internally mixed $CaCO_3/CaC_2O_4$

1096   aerosol particles have κ values of 0.0090±0.0019, only slightly higher than 0.0070±0.0017 for

1097   fresh $CaCO_3$ aerosol particles generated using a similar method. For a particle with a dry diameter

1098   of 200 nm, κ values of 0.0070 and 0.0090 correspond to s_c of 0.442% and 0.402%, respectively.

1099   The smaller enhancement in CCN activity of $CaCO_3/CaC_2O_4$ particles, compared to fresh $CaCO_3$

1100   particles, may be explained by relative low CCN activity of CaC_2O_4 particles, with κ values of

1101   ~0.05.[217] In addition, mixing humic acid sodium salt (NaHA) and fulvic acid can substantially

1102   increase the CCN activities of $CaCO_3$ particles and therefore reduce the critical super-saturation

1103   required to activate these particles to cloud droplets.[216] It has been reported that for 235 nm

1104   particles, the critical super-saturation is 0.39% for fresh $CaCO_3$, 0.35% for $CaCO_3$ mixed with 0.01

1105   wt.% NaHA, and 0.32% for $CaCO_3$ mixed with 0.05 wt.% NaHA.[216] Similar but smaller effects

1106   have also been observed for $CaCO_3$ particles mixed with fulvic acid.[216]

1107

1108   CCN activity of $CaCO_3$ aerosol particles before and after exposure to reactive trace gases has been

1109   measured by a few studies to better mimic the effects of atmospheric aging processes. For

1110   examples, Sullivan et al.[258] exposed $CaCO_3$ particles to HNO_3 in the aerosol flow tube and then

1111   measured the CCN activities of reacted particles. In this study [258] HNO_3 concentration, RH and

1112   exposure time were varied. As shown in Figure 15, they found [258] that the CCN activity of reacted

1113 $CaCO_3$ particles was significantly enhanced.
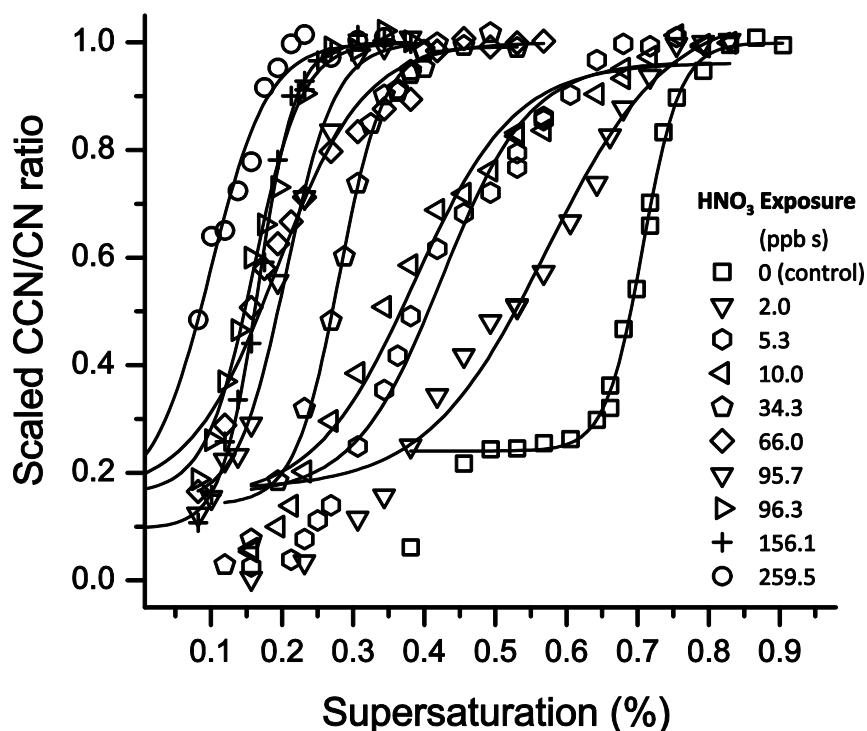
1114

1115   **Figure 15**. CCN activation curves of fresh and aged (exposure to HNO_3 at 50% RH) $CaCO_3$ aerosol

1116   particles with initial mobility diameters of 200 nm. Reprinted with permission from ref 258. Copyright

1117   2009 the PCCP Owner Societies.

1118

1119   It is clear that heterogeneous reactions can significantly change the CCN activity of $CaCO_3$

1120   particles. However, its relevance for cloud formation depends on how fast these changes occur in

1121   the troposphere. This important question has just started to be explored. For example, Sullivan et

1122   al.[258] investigated the CCN activity of aged particles as a function of HNO_3 exposure, and

1123   suggested that the κ values of $CaCO_3$ particles increase with HNO_3 exposure at three different RHs,

1124   as shown in Figure 16. Interestingly no RH dependence is found, though the uptake of HNO_3 by

1125 $CaCO_3$ particles is enhanced at higher RH.[199,227] It is further concluded by Sullivan et al.[258] that

1126   fresh $CaCO_3$ particles will be rapidly converted to aged particles with κ values of >0.1 within 4 h

1127   for 10 pptv HNO_3 and within 3 min for 1 ppbv HNO_3. HNO_3 in the troposphere can reach up to

1128   several ppbv,[368-370] suggesting that $CaCO_3$ particles can be converted to hygroscopic particles soon

1129   after they are emitted into the troposphere.

1130

59
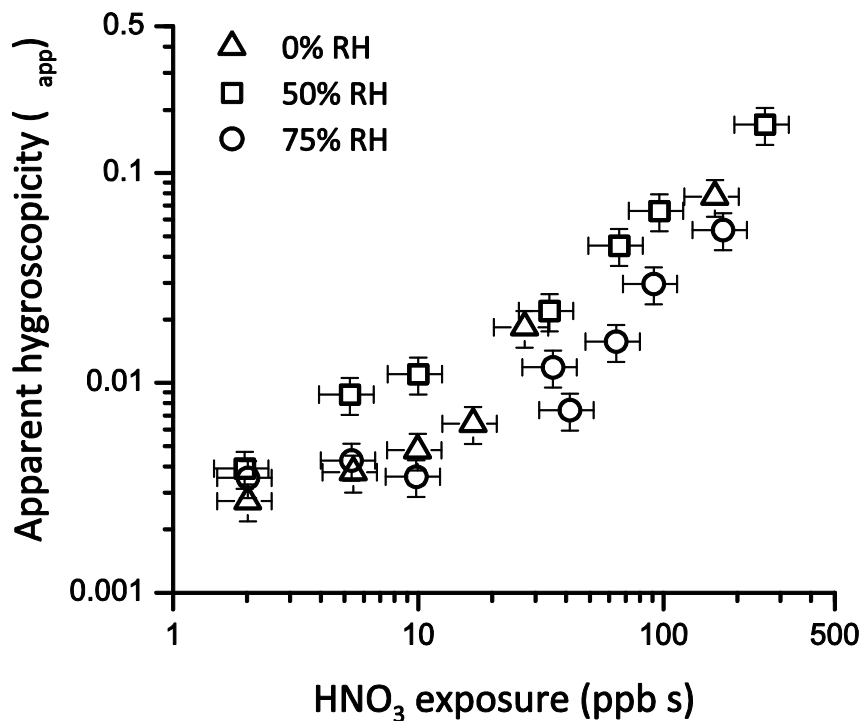
1131 **Figure 16**. Measured CCN activities (represented by κ values) of aged $CaCO_3$ particles (due to the reaction

1132 with HNO_3) as a function of nitric acid exposure at 0%, 50%, and 70% RH. Reprinted with permission from

1133 ref 258. Copyright 2009 the PCCP Owner Societies.

1134

1135 N_2O_5 concentrations up to several ppbv have been reported,[371-374] and its reaction with $CaCO_3$ (R2)

1136 could lead to the formation of nitrate in particles. In a very recent study, Tang et al.[357] found that

1137 CCN activity of $CaCO_3$ particles which had been exposed to N_2O_5 at 0% RH in an aerosol flow

1138 tube was enhanced, with κ increased from 0.001-0.003 to 0.02-0.04. It was also found that variation

1139 of N_2O_5 exposure from ~550 to 15000 ppbv·s did not lead to change in the CCN activity of aged

1140 $CaCO_3$ particles,[357] probably because at 0% RH $CaCO_3$ may be quickly saturated with respect to

1141 reaction with N_2O_5.

1142 $CaCO_3(s) + N_2O_5(g) \rightarrow Ca(NO_3)_2(l) + H_2O(l) + CO_2(g)$ (R2)
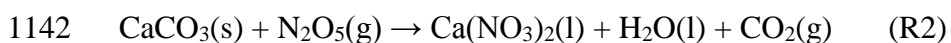
1143 **4.2 Arizona Test Dust**

1144 Arizona Test Dust (ATD) is in fact one type of authentic dust samples. It is often used as a test

1145 dust and a number of previous studies have investigated water adsorption, hygroscopicity and CCN

1146 activity of both fresh and aged ATD, as listed in Table 6. Therefore, it is separately discussed here

1147 in Section 4.2, instead of being included Section 4.8 together with other authentic dust samples.

1148 **4.2.1 Fresh ATD particles**

1149 Based on their DRIFTS measurement, Gustafsson et al.[247] suggested that ~2.5 and ~4 monolayers

1150 of adsorbed water are formed on ATD particles at ~70% and ~80% RH, respectively, though the

1151 BET surface area of their ATD samples was not clearly stated. Gustafsson et al.[247] also measured

1152 the hygroscopic growth of wet-generated ATD aerosol particles which have the first mode at 56

1153 nm and the second mode at 250 nm, and suggested that the hygroscopic growth factors of ATD

1154 particles at different RH can be described by the following equation:

1155 $\frac{D}{D_0} = (1 - RH)^{-0.036}$ (23)

1156

Table 6. Water adsorption, hygroscopicity, and CCN activity of fresh Arizona Test Dust (ATD) particles:

1158 summary of previous studies.

references	techniques	aerosol generation method
Gustafsson et al., 2005 [247]	DRIFTS, TGA, and H-TDMA	wet generation
Vlasenko et al., 2005 [260]	H-TDMA	dry generation
Koehler et al., 2009 [46]	H-TDMA and CCNc	dry and wet generation
Herich et al., 2009 [49]	H-TDMA and CCNc	dry and wet generation
Navea et al., 2010 [246]	ATR-FTIR and QCM	not applicable
Sullivan et al., 2010 [261]	CCNc	dry generation
Sullivan et al., 2010 [375]	CCNc	dry generation
Kumar et al., 2011 [262]	CCNc	dry generation
Kumar et al., 2011 [263]	CCNc	wet generation
Yamashita et al., 2011[376]	CCNc	dry generation
Garimella et al., 2014 [259]	CCNc	dry generation

1159

1160 Navea et al.[246] investigated water adsorption on ATD particles using ATR-FTIR and QCM, and

1161 reported the mass ratio of adsorbed water to dry particles from 0-70% RH. Vlasenko et al.[260] used

1162 a H-TDMA to study the hygroscopic growth of ATD aerosol particles, and found that the

1163 hygroscopic growth factors of monodisperse particles with mobility diameters of 55, 100, 250, and

1164 400 nm are all <1.01 for RH up to 90%. Koehler et al.[46] measured the hygroscopic growth and

1165 CCN activity of dry- and wet-generated ATD aerosol particles. The H-TDMA measurements show

1166 both dry and wet generated ATD particles have a growth factor of 1.09 at 90% RH, corresponding

1167 to a κ value of 0.03.[46] The CCN activity measurements suggest that while the dry generated ATD

1168 particles have κ values of ~0.025, the CCN activity of wet generated ATD particles is much higher,

1169 with κ values of 0.35.[46] This may indicate that compared to dry generation, wet generation can

1170 lead to significant increase of CCN activities of mineral dust particles, as suggested by several

61

1171   other studies.[49,256,263] Therefore, the CCN activity of wet generated ATD particles reported by

1172   Koehler et al.[46] is not included for further discussion.

1173

1174   The interaction of water vapor with dry and wet generated ATD particles was also studied by

1175   Herich et al.[49] under both sub- and super-saturation conditions, using H-TDMA and CCNc,

1176   respectively. They also found that wet-generated ATD particles show significantly higher CCN

1177   activities, due to effects introduced by redistribution of soluble materials among the particles.[49]

1178   The κ value derived from the CCN activity measurement is 0.003.[49] The κ value derived from H-

1179   TDMA measurement appears to be slightly lower than that from CCN activity measurement;

1180   however, the difference may not be significant due to the large uncertainty associated with the

1181   measured growth factors.[49] The CCN activity of dry generated ATD particles was also investigated

1182   by several other studies, with reported κ values being 0.0041,[259] 0.002,[261] 0.0042,[375] and 0.017,[376]

1183   respectively. Kumar et al.[262] investigated the CCN activity of dry generated ATD aerosol particles

1184   and interpreted their results using the FHH activation theory, with A_{FFH} of 2.96±0.03 and B_{FHH} of

1185   1.28±0.03. In another study, Kumar et al.[263] also investigated the CCN activity of wet-generated

1186   ATD aerosol particles, and concluded that compared to dry generation, wet-generation will

1187   significantly increase the CCN activity of ATD particles.
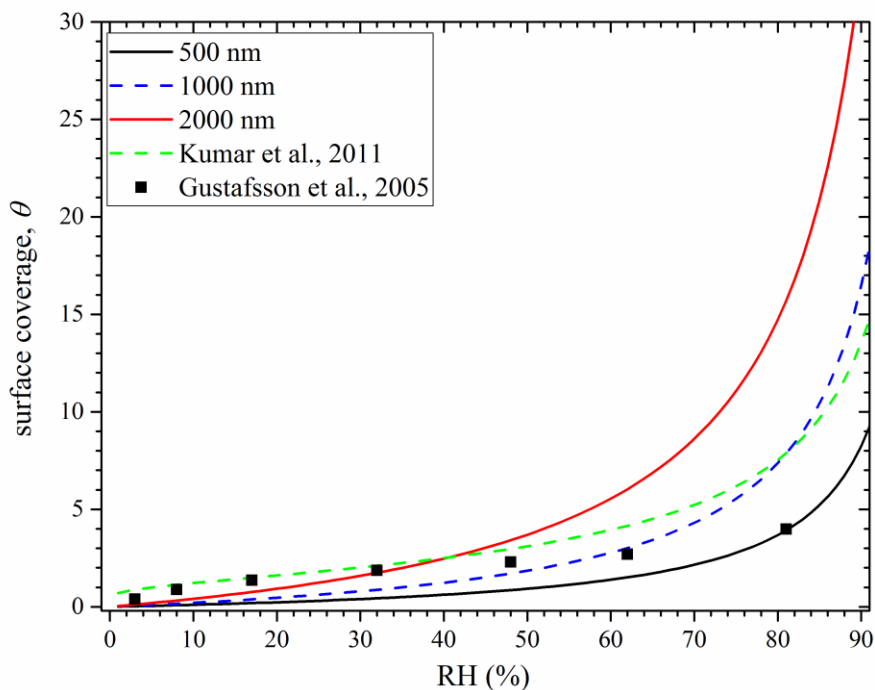
1188

Figure 17. Comparison of measured and calculated surface coverages (θ) of adsorbed water on ATD particles. Black squares: measured by Gustafsson et al;[247] solid black curve: calculated using an average κ value of 0.004 [259,375] and an assumed diameter of 500 nm; dashed blue curve: calculated using a κ value of 0.004 [259,375] and an assumed diameter of 1000 nm; solid red curve: calculated using a κ value of 0.004 [259,375] and an assumed diameter of 2000 nm; dashed green curve: calculated using the two FHH parameters reported by Kumar et al.[262]

Surface coverages of adsorbed water on ATD particles reported by Gustafsson et al.[247] are plotted in Figure 17 together with those calculated using the two FHH parameters derived by Kumar et al.[262] from their CCN activity measurement. In addition, the surface coverages of adsorbed water are also calculated using an average κ value of 0.004 [259,375] for particles with diameters of 500, 1000, and 2000 nm, respectively. As shown in Figure 17, considering the experimental uncertainties and errors in extrapolating measurements done under super-saturation conditions to sub-saturation conditions, these studies show fairly good agreement, though some discrepancies also occur.
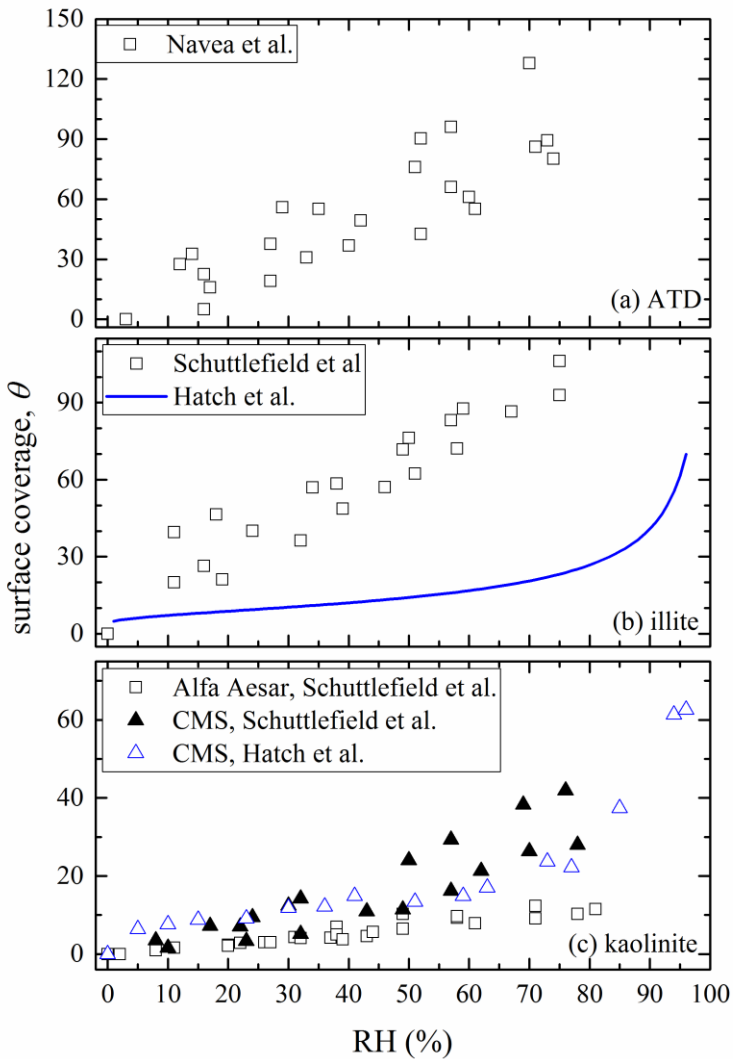
Figure 18. Surface coverage of adsorbed water on ATD (a), illite (b), and kaolinite (c), reported by Navea et al.,[246] Schuttlefield et al,[249] and Hatch et al.[268,348] Alfa Aesar indicates that particles are provided by Alfa Aesar, and CMS indicates that particles are provided by Clay Mineral Society (CMS).

The results reported by Navea et al.,[246] directly measured by using particles deposited a substrate, are shown in Figure 18a. Compared to those plotted in Figure 17, the surface coverages of adsorbed water measured by Navea et al.[246] are significantly higher. Navea et al.[246] deposited a water slurry of ATD particles on the quartz crystal surface in their QCM to form a dry dust film after the evaporation of water. When being mixed with water, clay minerals contained by ATD particles may undergo interaction with liquid water and therefore change their physicochemical properties,

64

a phenomena known as swelling for some clay minerals.[377] This may begin to explain the relative large difference between Navea et al.[246] and those shown in Figure 17. This may also be due to possible chemical reactions of ATD particles (or some of their components) in the aqueous mixture, leading to compositional changes. However, further studies are needed to explain and resolve this discrepancy.

4.2.2 Effect of chemical aging

The change of hygroscopicity of ATD particles due to heterogeneous reactions has been explored by a few studies. For example, Vlasenko et al.[213] measured the hygroscopic growth of ATD particles after being exposed to HNO_3 (3×10^{13} molecule cm^{-3}, i.e. ~1.2 ppmv) for 3 min at different RH in an aerosol flow tube. As shown in Figure 19, the change in hygroscopicity was negligible for exposure at 30% RH; however, the hygroscopic growth factor at ~85% RH increased from <1.02 to ~1.08 after exposure to the same amount of HNO_3 at 85% RH.[213]
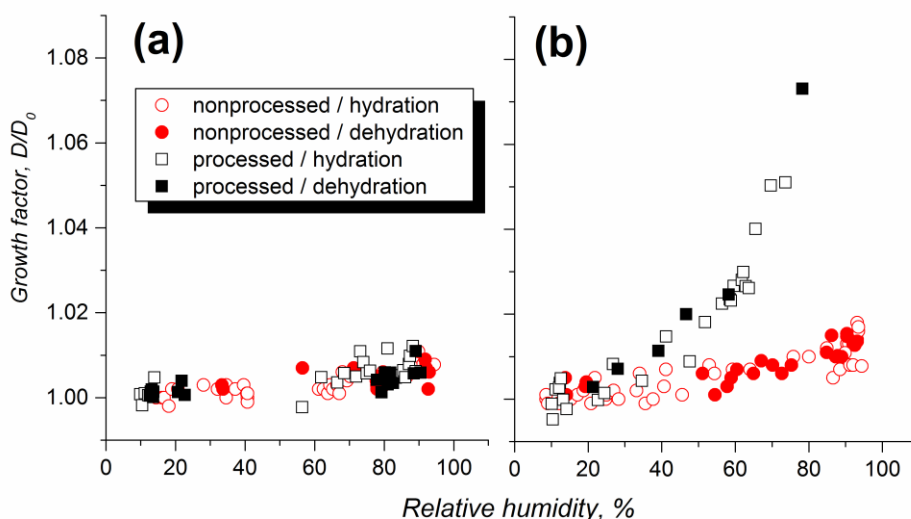
Figure 19. Hygroscopic growth of ATD particles with initial mobility diameters of 100 nm before (red circles) and after (black squares) reaction with HNO_3 of 3×10^{13} molecule cm^{-3} at RH of (a) 30% and (b) 85%. Reprinted with permission from ref 213. Copyright 2006 Copernicus Publications.

1232 It is also found that exposure to HNO_3 [375] and H_2SO_4 [261] vapor could significantly increase the

1233 CCN activity of ATD aerosol particles. In another study, Keskinen et al.[378] suggested that

1234 secondary organic coatings which are formed from α-pinene ozonolysis can also significantly

1235 enhance the CCN activity of ATD particles.

1236 **4.3 Illite**

1237 Illite is the most abundant clay in mineral dust particles,[150] and its interaction with water vapour

1238 has been investigated by several studies. Table 7 summarizes previous studies which have

1239 investigated water adsorption, hygroscopicity, and CCN activity of illite particles. The interaction

1240 of water vapor with illite particles was investigated by Schuttlefield et al.[249] using ATR-FTIR and

1241 QCM, and the amount of water adsorbed by illite was quantified at different RH. Hatch et al.[268]

1242 studied water adsorption on illite particles using ATF-FTIR. They found that the two-parameter

1243 BET adsorption isotherm failed to describe the experimental data at higher RH while the Feundlich

1244 adsorption model could fit the data over the entire RH range.[268] In a following study, Hatch et

1245 al.[348] also used the FHH adsorption isotherm to fit their data, with A_{FFH} and B_{FHH} equal to 75±17

1246 and 1.77±0.11.

1247

1248 **Table 7.** Water adsorption, hygroscopicity, and CCN activity of fresh illite: summary of previous studies.

references	techniques (and aerosol generation method, if applicable)
Schuttlefield et al., 2007 [249]	ATR-FTIR and QCM
Herich et al., 2009 [49]	H-TDMA and CCNc (dry and wet generation)
Attwood and Greenslade, 2011[253]	AE-CRD (wet generation)
Hatch et al., 2011 [268]	ATR-FTIR
Kumar et al., 2011 [262]	CCNc (dry generation)
Kumar et al., 2011 [263]	CCNc (wet generation)
Garimella et al., 2014 [253]	CCNc (dry generation)
Hatch et al., 2014 [348]	ATR-FTIR

1249

1250   Attwood and Greenslade [253] measured the optical extinction of wet-generated illite aerosol

1251   particles at 532 nm and at different RH to study their hygroscopicity. The hygroscopic growth

1252   factors were found to be 0.90, 0.93, and 1.06 at RH of 50%, 68%, and 90%, respectively.[253] It

1253   should be pointed out that the hygroscopic growth reported by Attwood and Greenslade [253] is based

1254   on the measured optical extinction coefficients. Hygroscopic growth factors smaller than 1, which

1255   have also been reported for ATD particles using H-TDMA,[46,260] can be due to change in particle

1256   morphology and even restructure of particles during humidification.[46,253,260] Since it is difficult to

1257   convert change in optical extinction cross sections at different RH to the amount of adsorbed water,

1258   the result reported by Attwood and Greenslade [253] is not included in further discussion.

1259

1260   Herich et al.[49] produced illite aerosol particles using both dry and wet generation methods, and

1261   measured the hygroscopicity and CCN activity of generated illite aerosol particles using H-TDMA

1262   and CCNc, respectively. They [49] found that wet-generated illite particles are more CCN active than

1263   those generated by dry dispersion, and that the dry-generated illite particles has κ values of 0.002-

1264   0.003. Kumar et al.[262,263] also investigated the CCN activity of dry- and wet-generated illite aerosol

1265   particles, and suggested that the FHH activation theory could better describe CCN activation of

1266   illite particles. A_{FHH} and B_{FHH} were reported to be 1.02±0.38 and 1.12±0.04 for dry-generated illite

1267   particles,[262] and 3.00 and 1.27 for wet-generated illite particles.[263] Recently Garimella et al.[259] also

1268   studied the CCN activity of dry-generated illite particles, and they suggested that the κ-Köhler

1269   activation theory could adequately describe the CCN activation of illite particles, with an average

1270 κ value of 0.0072.
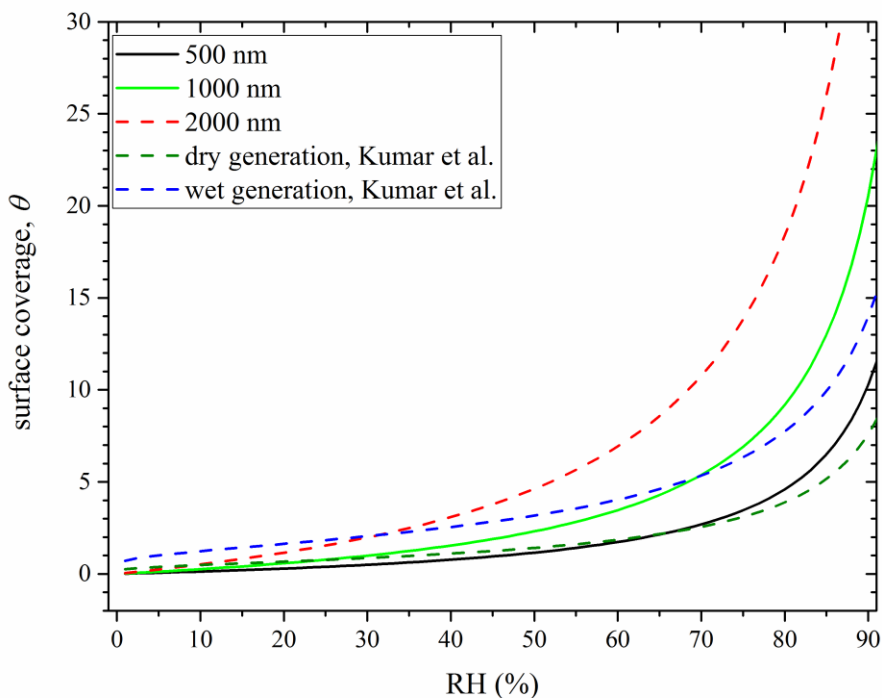
1271

Figure 20. Comparison of calculated surface coverages (θ) of adsorbed water on illite particles. Surface

coverages of adsorbed water are calculated using an average κ value of 0.005 and different dry particle

diameters of 500 (solid black curve), 1000 (solid green curve), and 2000 nm (dashed red curve), and using

A_{FHH} and B_{FHH} for dry- (dashed olive curve) and wet-generated (dashed blue curve) illite aerosol particles

reported by Kumar et al.[262,263]

1277

A_{FFH} and B_{FHH} parameters for dry- and wet-generated illite particles, derived by Kumar et al.[262,263]

from their CCN activity measurements, are used to calculate surface coverages of adsorbed water

under sub-saturation conditions. κ values for dry-generated illite aerosol particles were reported to

be 0.002-0.003 by Herich et al.[49] and 0.0072 by Garimella et al.[259] An average κ value of 0.005 is

then used here to calculate surface coverage of adsorbed water under sub-saturation conditions for

particles with uniform diameters of 500, 1000, and 2000 nm. All the calculated results are shown

in Figure 20, exhibiting relatively good agreement in general.

1285

1286   Schuttlefield et al.[249] and Hatch et al.[268,348] experimentally measured water adsorption under sub-

1287   saturation conditions on illite particles which were deposited on supporting substrates, and their

1288   results are displayed in Figure 18b. Comparison of results shown in Figure 20 to those in Figure

1289   18b suggests that surface coverages of adsorbed water reported by Schuttlefield et al.[249] and Hatch

1290   et al.[268,348] are both significantly higher than those using aerosol particles, including those reported

1291   by Kumar et al.[263] who generated aerosol particles by atomizing illite/water mixture. Therefore,

1292   the difference between studies using particles deposited on substrates and those using aerosol

1293   particles cannot be fully explained by the potential change in particle properties due to the

1294   interaction of clay with liquid water during the sample preparation stage. Clay minerals are

1295   inherently complex with variability between samples. Variability in clay minerals are due to

1296   differences in metal cations present and potentially contamination with other clay components (e.g.

1297   montmorillonite) can potentially cause the observed difference. Considering the abundance of illite

1298   in tropospheric mineral dust particles, more studies are required to better understand its interaction

1299   of water vapor.

1300   **4.4 Kaolinite**

1301   Previous studies which reported water adsorption, hygroscopicity, and CCN activities of fresh

1302   kaolinite are summarized in Table 8. ATR-FTIR and QCM were used by Schuttlefield et al.[249] to

1303   investigate water adsorption on kaolinite particles at different RH. Two different kaolinite samples

1304   were used,[249] with one purchased from Alfa Aesar and the other one provided by the Source Clay

1305   Repository (Clay Mineral Society). Hatch et al.[268] also investigated water adsorption on Clay

1306   Mineral Society kaolinite using ATR-FTIR, and suggested that the Freundlich adsorption isotherm

1307   can better describe their experimental data, compared to the two-parameter BET adsorption

1308   isotherm. Recently Hung et al.[270] used a physisorption analyser to study water adsorption on

1309   kaolinite provided by Fluka.

1310

Table 8. Water adsorption, hygroscopicity, and CCN activity of fresh kaolinite: summary of previous studies.

references	techniques (and aerosol generation method, if applicable)
Schuttlefield et al., 2007 [249]	ATR-FTIR and QCM
Gibson et al., 2007 [257]	CCNc (wet generation)
Herich et al., 2009 [49]	H-TDMA and CCNc (dry and wet generation)
Hatch et al., 2011 [268]	ATR-FTIR
Attwood and Greenslade, 2011[253]	AE-CRD (wet generation)
Kumar et al., 2011 [263]	CCNc (wet generation)
Hung et al., 2015 [270]	PSA

Optical extinction coefficients were measured at 532 nm using Cavity Ring-Down spectroscopy to determine the hygroscopic growth of Clay Mineral Society kaolinite particles at different RH.[253] The hygroscopic growth factors, relative to the diameter at <10% RH, were measured to be 0.90±0.08, 0.79±0.11 and 0.80±0.17 at RH of 50%, 68%, and 90%, respectively.[253] Hygroscopic growth factors significantly smaller than 1 suggest that restructure of mineral dust particles may occur during humidification, and also make it difficult to derive the amount of adsorbed water from optical extinction measurements. It should be noted that potential restructure of dust particles can also affect H-TDMA measurements. For example, hygroscopic growth factors of ATD particles, as measured by H-TDMA, were reported to be slightly smaller than 1 at some RH.[46,260]

CCN activity of wet-generated Clay Mineral Society kaolinite aerosol particles were studied by Gibson et al.,[257] and the critical super-saturation was measured to be 0.44±0.02 for 200 nm dry particles, corresponding to a κ value of 0.0071. Herich et al.[49] used H-TDMA and CCNc to study the hygroscopicity and CCN activity of kaolinite particles, provided by Fluka and Clay Mineral Society. In the study by Herich et al.,[49] aerosol particles were produced by both dry and wet

1329   generation, and wet generation was found to increase the CCN activity of kaolinite particles. The

1330   CCN activity of dry-generated kaolinite particles is quite low, with average κ values of ~0.001.[49]

1331   By comparison, another study by Kumar et al.[263] found that wet-generated kaolinite aerosol

1332   particles exhibited a κ values of 0.45 which is only slightly lower than that for ammonia sulfate,

1333   highlighting that dry and wet generation methods can lead to considerable difference in the CCN

1334   activities of resulting dust aerosol particles.
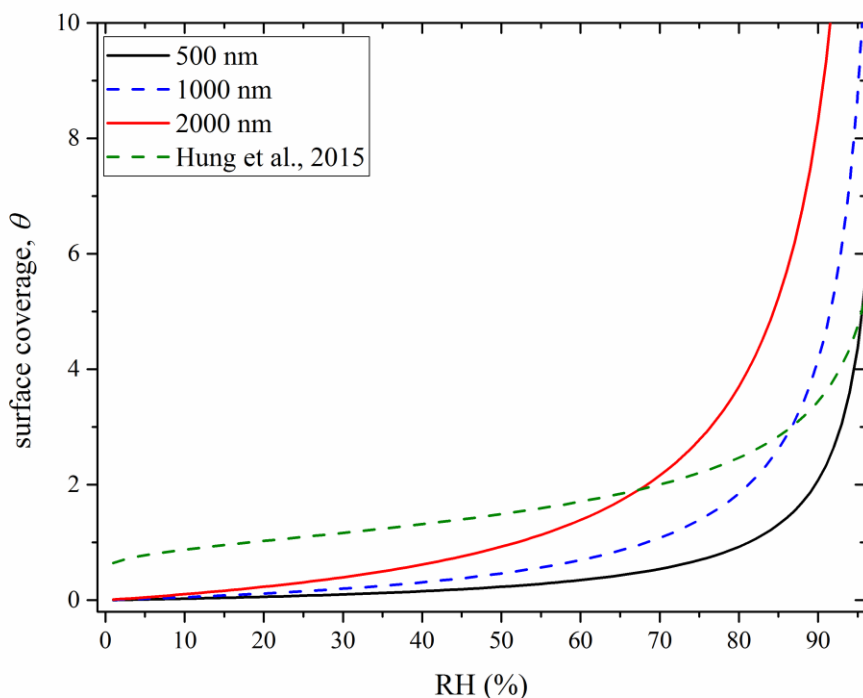
1335

1336   **Figure 21**. Comparison of surface coverage (θ) of adsorbed water on kaolinite particles experimentally

1337   measured by Hung et al.[270] (dashed olive curve) and those calculated using a κ value of 0.001 reported by

1338   Herich et al.[49] and assumed particle diameters of 500 (solid black curve), 1000 (dashed blue curve), and

1339   2000 nm (solid red curve).

1340

1341   Surface coverages of adsorbed water on kaolinite particles experimentally by Hung et al.[270] are plotted in

1342   Figure 21 together with those calculated using a κ value of 0.001 reported by Herich et al.[49] and assumed

1343   particle diameters of 500, 1000, and 2000 nm. As shown in Figure 21, reasonably good agreement is found,

1344   considering the uncertainties (as discussed in Section 3.3) when using the κ value to calculate surface

1345   coverages of adsorbed water.

1346

1347   Experimentally determined surface coverages of adsorbed water on kaolinite particles by Schuttlefield et

1348   al.[249] and Hatch et al.[268] are shown in Figure 18c. Several conclusions can be drawn when comparing these

1349   two studies.[249,268] First of all, Schuttlefield et al.[249] and Hatch et al.[268] used very similar techniques to

1350   measure the amounts of water adsorbed by kaolinite particles from the same source (provided by Clay

1351   Mineral Society), and their results agree quite well with each other, as shown in Figure 18c. Second,

1352   Schuttlefield et al.[249] measured water adsorption on two different kaolinite samples, and significant

1353   difference between these two samples was found. This may suggest the same type of dust particles from

1354   different sources, because of variability within sources, could have very different ability to uptake water

1355   vapor.

1356

1357   Surface coverages of adorbed water on kaolinite particles measured by Schuttlefield et al.[249] and Hatch et

1358   al.,[268] as shown in Figure 18c, are significantly higher than those (as shown Figure 21) directly measured

1359   by Hung et al.[270] and those calculated using the κ value reported by Herich et al.[49] We note that Schuttlefield

1360   et al.,[249] Hatch et al.[268], and Hung et al.[270] all deposited kaolinite particles on supporting substrates. The

1361   observed large discrepancy between the first two studies[249,268] and that by Hung et al.[270] is somehow

1362   unexpected. A potential explanation is that the two studies by Schuttlefield et al.[249] and Hatch et al.[268] placed

1363   particles onto the supporting substrates via depositing water slurry onto them, probably leading to swelling

1364   and changes in the properties of kaolinite particles, while dry kaolinite powders were directly placed onto

1365   the supporting substrate by Hung et al.[270]

1366

1367   Internally mixed kaolinite/ammonia sulfate particles, generated by atomizing kaolinite-ammonia

1368   sulfate-water mixture, were found to have higher CCN activity compared to fresh kaolinite

1369   particles.[257] The internally mixed kaolinite-ammonia sulfate particles have κ values of ~0.017 and

1370   ~0.038, increasing with the mass ratio of ammonia sulfate to kaolinite in the aqueous mixtures

72

1371 which were atomized to produce aerosol particles.[257] Although this study [257] may not mimic actual

1372 atmospheric aging processes very well, it does suggest that the CCN activity of kaolinite particles

1373 can be substantially enhanced if being mixed more soluble compounds due to heterogeneous

1374 reactions and/or cloud processing.

1375 **4.5 Montmorillonite**

1376 As summarized in Table 9, water adsorption, hygroscopicity, and CCN activity of montmorillonite

1377 particles have been investigated by several studies in the last 2-3 decades. For example, Hall and

1378 Astill [379] used a vacuum microbalance to measure the mass of montmorillorite particles at different

1379 RH (up to 70%) and at different temperature (25-75 $^{\circ}$C). Four homoionic (Ca^{2+}, Li^+, Na^+, and K^+)

1380 exchanged forms of Clay Mineral Society montmorillorite (SWy-1) were studied.[379] Water

1381 adsorption by Na-exchanged montmorillorite was also investigated at different RH and 25 $^{\circ}$C by

1382 Cases et al.,[380] using a microbalance. An environmental infrared microbalance was deployed by

1383 Xu et al.[381] to investigate water adsorption on Na-, Li-, Ca-, and Mg-exchanged forms of two

1384 montmorillonite samples (SWy-1 and SAz-1) provided by Clay mineral Society. Gas

1385 chromatography was used by Zent et al.[382] to study water uptake on Na-montmorillorite (Swy-1)

1386 at different RH and at 211 and 273 K.

1387

1388 **Table 9.** Water adsorption, hygroscopicity, and CCN activity of fresh montmorillonite: summary of

1389 previous studies.

references	techniques (and aerosol generation method, if applicable)
Hall and Astill, 1989 [379]	vacuum microbalance
Cases et al., 1992 [380]	microbalance
Xu et al., 2000 [381]	environmental infrared microbalance
Zent et al., 2001 [382]	gas chromatography
Frinak et al., 2005 [383]	Transmission FTIR

Schuttlefield et al., 2007 [249]	ATR-FTIR and QCM
Herich et al., 2009 [49]	H-TDMA and CCNc (dry and wet generation)
Attwood and Greenslade, 2011[253]	AE-CRD (wet generation)
Hatch et al., 2011 [268]	ATR-FTIR
Kumar et al., 2011 [262]	CCNc (dry generation)
Kumar et al., 2011	CCNc (wet generation)
Hatch et al., 2014 [348]	ATR-FTIR
Garimella et al., 2014 [259]	CCNc (dry and wet generation)
Hung et al., 2015 [270]	PSA

1390

1391   More recently, Frinak et al.[383] used transmission FTIR to determine the amount of water adsorbed

1392   on montmorillonite (SWy-2) provided by Clay Mineral Society as a function of temperature (212-

1393   231 K) and RH. They found that water uptake by montmorillonite is almost as large as ammonia

1394   sulfate.[383] It was further suggested by Frinak et al.[383] that though water adsorption on

1395   montmorillonite depended strongly on RH, no strong dependence on temperature (212-231 K) was

1396   observed.

1397

1398   Frinak et al.[383] also compared their measurement to those reported in previous studies.[379-382] As

1399   shown in Figure 22, except that reported by Zent et al.,[382] all the other studies in general show

1400   good agreement. A close look reveals that the amount of adsorbed water measured by Cases et

1401   al.[380] at RH<30% may be lower than those reported by Hall and Astill,[379] Xu et al.,[381] and Frinak

1402   et al.[383]
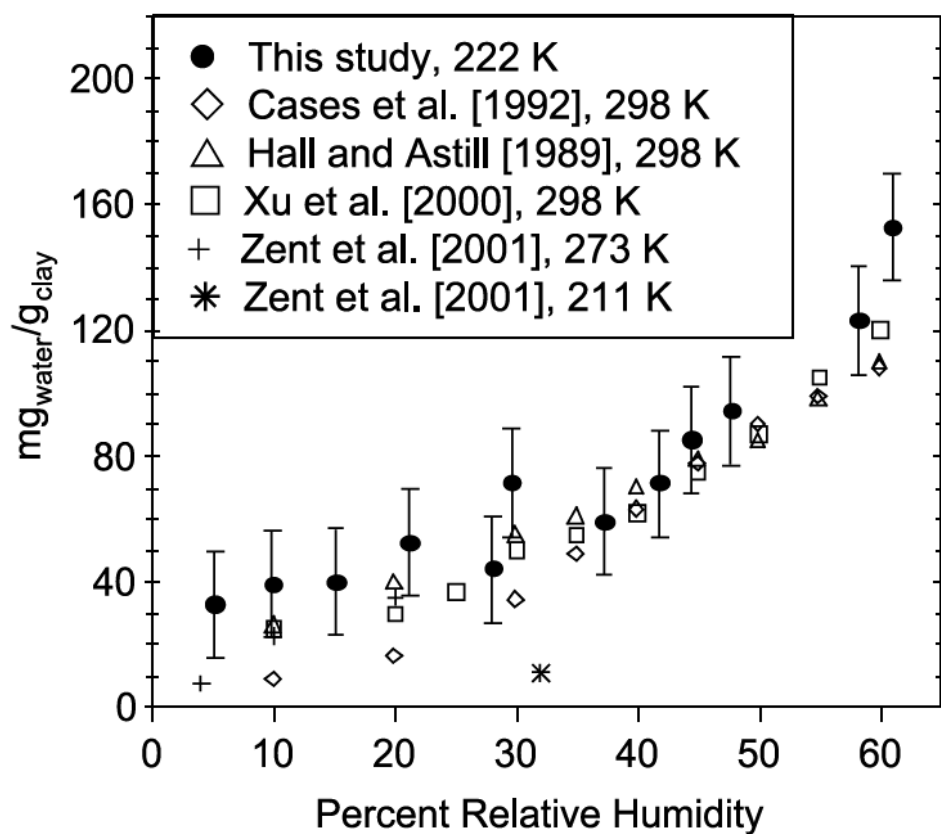
Figure 22. Comparison of amounts of water adsorbed on SWy-2 (montmorillorite from Clay Mineral Society) measured by studies before 2006. Reprinted with permission from ref 383. Copyright 2005 John Wiley & Sons, Inc.

Water adsorption on three different montmorillonite samples (one from Alfa Aesar, the other two from Clay Mineral Society: SWy-2 and SAz-1) was investigated by Schuttlefield et al.[249] using ATR-FTIR and QCM. The amount of water adsorbed by montmorillorite was quantified at room temperature and at different RH, using QCM.[249] As shown in Figure 23a, montmorillorite particles from various sources exhibit different ability to adsorb water. At the same RH, the amount of water adsorbed by SAz-1 is much larger than those by the other two montmorillorite samples, and Alfa Aesar montmorillorite adsorbs the least amount of water.
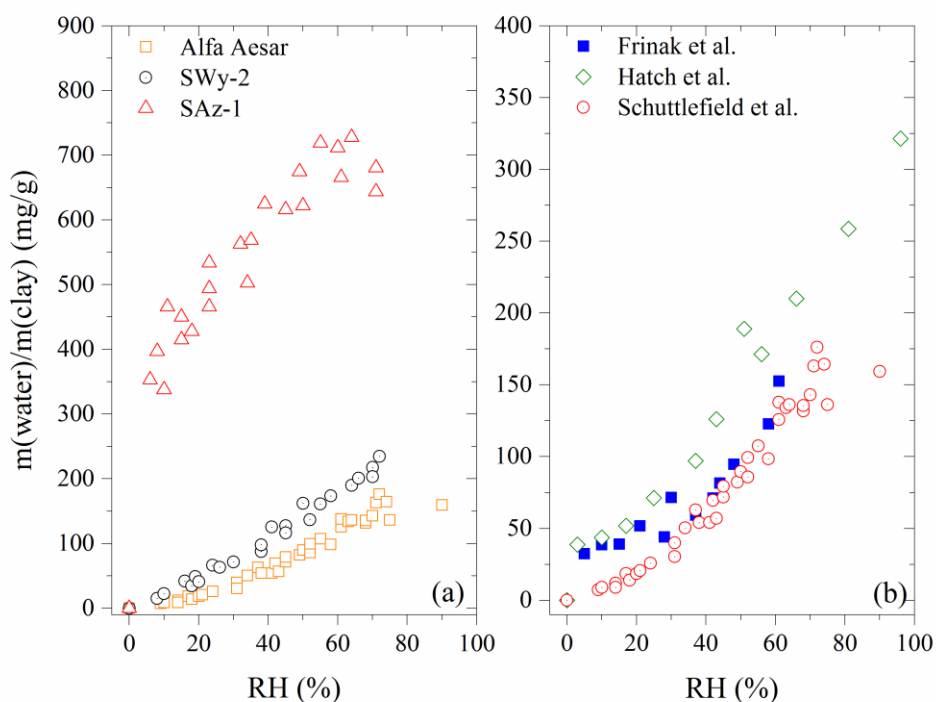
Figure 23. (a) Water adsorption on three different montmorillorite samples as a function of RH, measured by Schuttlefield et al.[249] at room temperature. Squares: Alfa Aesar montmorillorite; circles: SWy-2 provided by Clay Mineral Society; triangles: SAz-1 provide by Clay Mineral Society. (b) Water adsorption on SWy-2 montmorillorite as a function of RH measured three different studies. Squares: measured by Frinak et al.[383] at 222 K; diamonds: measured by Hatch et al.[268] at room temperature; circles: measured by Schuttlefield et al.[249] at room temperature.

ATR-FTIR was used by Hatch et al.[268] to determine the amount of water adsorbed on Clay Mineral Society montmorillorite (SWy-2) particles at room temperature and at different RH, and the experimental result was fitted by the FHH adsorption isotherm with A_{FHH} and B_{FHH} equal to 98±22 and 1.79±0.11.[348] The mass ratios of adsorbed water to dry SWy-2, as a function of RH, measured by Frinak et al.[383] at 222 K and by Schuttlefield et al.,[249] and Hatch et al.[268] at room temperature, are plotted in Figure 23b for comparison. Results reported by studies [379-382] prior to Frinak et al.[383] are already shown in Figure 22, and therefore they are not included in Figure 23b. Considering the experimental uncertainties, all the three studies show very good agreement, even though Frinak et

1432 al.[383] carried out the measurement at 222 K and the other two studies [249,268] were conducted at

1433 room temperature. Considering earlier measurements which are plotted in Figure 22, one could

1434 conclude that most of the available studies [249,268,379-381,383] in which samples were supported on

1435 substrates reported similar water adsorption for SWy-2 montmorillorite, although different

1436 experimental techniques were used to quantify the amount of adsorbed water.

1437

1438 Optical extinction of wet-generated Clay Mineral Society montmorillorite particles at 532 nm was

1439 measured at room temperature and at different RH by Attwood and Greenslade [253] to study their

1440 hygroscopic growth, using Cavity Ring-Down spectroscopy. Their reported hygroscopic growth

1441 factors are 1.03 at 50% RH, 1.18% at 68% RH, and 1.4 at 90%, respectively.[253] As discussed in

1442 Sections 4.3 and 4.4, their reported hygroscopic growth factors are <1 for illite and kaolinite,[253]

1443 likely due to restructure of clay particles at elevated RH. Restructure of montmorillorite particles

1444 may also occur during humidification. In addition, since montmorillorite particles are non-

1445 spherical, it is non-trivial to convert change in optical properties at different RH to the amount of

1446 adsorbed water by the particles. Therefore, the result reported by Attwood and Greenslade [253] for

1447 montmorillorite is not included in comparison. Using the same experimental method, in a

1448 following study Attwood and Greenslade [384] found that internal mixing with montmorillorite

1449 would decrease the deliquescence RH of both ammonia sulfate and sodium chloride.

1450

1451 Using H-TDMA and CCNc, Herich et al.[49] studied the hygroscopicity and CCN activity of

1452 montmorillorite particles provided Aldrich and Clay Mineral Society. Aerosol particles were

1453 produced by both dry- and wet-generation.[49] Wet generation was found to increase the CCN

1454 activity of montmorillonite particles, compared to dry generation.[49] The single hygroscopicity

1455 parameter, κ, was determined to be ~0.003 for dry-generated montmorillorite particles and close

1456 to 0.02 for wet-generated particles.[49] The CCN activation of dry-generated Na-montmorillorite

1457   provided by Clay Mineral Society was investigated by Garimella et al.,[259] with κ reported to be

1458   0.0088.

1459

1460   Kumar et al.[262,263] investigated the CCN activity of dry and wet-generated Na- and Ca-

1461   montmorillonite aerosol particles, and suggested that the FHH adsorption activation theory could

1462   better describe the CCN activation of montmorillonite aerosol particles. Reported A_{FHH} and B_{FHH}

1463   are 1.23±0.31 and 1.08±0.03 for dry-generated Na-montmorillonite,[262] 2.06±0.72 and 1.23±0.04

1464   for dry-generated Ca-montmorillonite,[262], 0.87 and 1.00 for wet-generated Na-montmorillonite,[263]

1465   and 1.09 and 1.04 for wet-generated Ca-montmorillonite,[263] respectively.
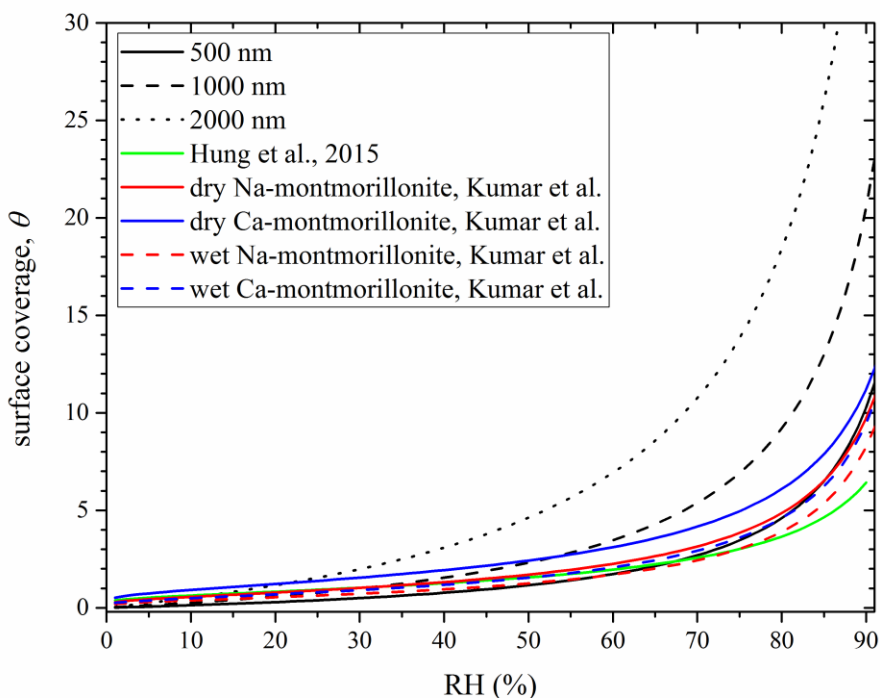
1466

1467   **Figure 24.** Comparison of surface coverages of adsorbed water on montmorillorite measured by Hung et

1468   al.[270] (solid green curve) with those extrapolated from CCN activity measurements. Surface coverages of

1469   adsorbed water are also calculated using an average κ of 0.005 [49,259] and assumed dry particle diameters of

1470   500 (solid black curve), 1000 (dashed black curve), and 2000 nm (dotted black curve), respectively. In

1471   addition, θ are calculated using A_{FHH} and B_{FHH} values reported by Kumar et al.[262,263] Red curves: calculated

1472   using A_{FHH} and B_{FHH} parameters for dry- (solid) and wet-generated (dashed) Na-montmorillorite; blue

1473   curves: calculated using A_{FHH} and B_{FHH} parameters for dry- (solid) and wet-generated (dashed) Ca-

1474   montmorillorite.

1475

1476   Recently Hung et al.[270] measured water adsorption on kaolinite K10 powders (provided by Sigma

1477   Aldrich) at 28 °C and at different RH, using a PSA. For comparison, the measurements[49,259,262,263]

1478   in which the CCN activity of aerosol particles were investigated are extrapolated to sub-saturation

1479   conditions and plotted in Figure 24 together with the surface coverage of adsorbed water directly

1480   measured Hung et al.[270] As shown in Figure 24, reasonably good agreement is found, though large

1481   errors can occur in these extrapolations, as discussed in Section 3.2.

1482

1483   However, differences can be found when comparing studies plotted in Figures 22-23, to those

1484   shown in Figure 24. For example, Schuttlefield et al.[249] suggested that at around 70% RH,

1485   approximately 50-60 and 200 monolayers of adsorbed water were formed on SWy-2 and SAz-1

1486   kaolinite particles, compared to approximately 10 or less monolayers at the same RH for studies

1487   shown in Figure 24. It should be noted that the surface coverage is calculated by dividing the total

1488   amount of adsorbed water by the BET surface area of particles under investigation. The reasons

1489   for such relatively large discrepancies are complicated and unclear at this stage. For example, the

1490   difference between using particles supported on substrates and aerosol particles cannot explain the

1491   discrepancies alone, because Hung et al.[270] also studied particles deposited on a substrate but

1492   reported similar results to those using aerosol particles.[49,259,262,263] This can not be explained by

1493   clay swelling effects alone which may play a role in several studies, for example, by Frinak et

1494   al.,[383] Schuttlefield et al.,[249] and Hatch et al.[268] This is because the calculated surface coverages of

1495   adsorbed water from the CCN activity measurement of wet-generated particles by Kumar et al.[263]

1496   are not very different from those for dry-generated particles,[262] as shown in Figure 24. In addition,

1497   such discrepancies cannot be only due to the usage of different types of montmorillorite particles,

1498 because studies [49,259,262,263,270] included in Figure 24 used montmorillorite from various sources but

1499 still showed reasonably good agreement. Careful and systematical measurements in future can help

1500 resolve these discrepancies and better understand the interaction of montmorillorite with water

1501 vapor.

1502 **4.6 Quartz**

1503 Table 10 provides a summary of previous studies in which water adsorption, hygroscopicity, and

1504 CCN activity of SiO_2, TiO_2, Al_2O_3, and Fe_2O_3 were determined. Section 4.6 discusses previous

1505 studies on SiO_2, while those for TiO_2, Al_2O_3, and Fe_2O_3 are reviewed in Section 4.7.

1506

1507 **Table 10.** Water adsorption, hygroscopicity, and CCN activity of fresh SiO_2, TiO_2, Al_2O_3, and Fe_2O_3:

1508 summary of previous studies.

mineral	References	techniques
SiO_2	Goodman et al., 2001 [250]	Transmission FTIR
	Schuttlefield et al., 2007 [273]	ATR-FTIR and QCM
	Ma et al., 2010 [269]	DRIFTS
	Keskinen et al., 2011 [320]	H-TDMA (wet generation)
	Kumar et al., 2011 [262]	CCNc (dry generation)
	Dalirian et al., 2015 [385]	CCNc (wet generation)
TiO_2	Goodman et al., 2001 [250]	Transmission FTIR
	Ketteler et al., 2007 [241]	AP-XPS
	Ma et al., 2010 [269]	DRIFTS
Al_2O_3	Goodman et al., 2001 [250]	Transmission FTIR
	Al-Abadleh and Grassian, 2003 [240]	Transmission FTIR
	Schuttlefield et al., 2007 [249]	ATR-FTIR and QCM
	Ma et al., 2010 [269]	DRIFTS
	Ma et al., 2012 [212]	PSA
Fe_2O_3	Goodman et al., 2001 [250]	Transmission FTIR

1509

1510   Water adsorbed on SiO_2 particles was measured using transmission FTIR, and its surface coverage

1511   at different RH was fitted by a modified three-parameter BET equation with n equal to 10 and c

1512   equal to 13.1.[250] Schuttlefield et al.[273] investigated water adsorption on SiO_2 particles by coupling

1513   ATR-FTIR with QCM in tandem. In another study, DRIFTS was used by Ma et al.[269] to investigate

1514   the interaction of water vapor with SiO_2 surface at different RH, and the result was also fitted with

1515   a modified three-parameter BET equation with n equal to 3.8 and c equal to 4.8.

1516

1517   H-TDMA was used to study the hygroscopic growth of spherical SiO_2 aerosol particles of 8-10

1518   nm,[320] and it is suggested that the water adsorption on SiO_2 particles can be described by the FHH

1519   adsorption isotherm, with A_{FHH} and B_{FHH} equal to 4.82 and 2.16. It is also suggested that compact

1520   agglomerate particles which contain a few primary spherical particles could adsorb ~1.5 times

1521   more water at the same RH, compared to small spherical particles.[320] This may probably result

1522   from the capillary effects of these small cavities between primary small particles in the

1523   agglomerate.[320]

1524

1525   Kumar et al.[262] investigated the CCN activity of SiO_2 aerosol particles under super-saturation

1526   conditions. Their measurements were interpretted using the FHH adsorption activation theory,

1527   with A_{FHH} and B_{FHH} equal to 2.96 and 1.36, respectively.[262] The CCN activity of SiO_2 aerosol

1528   particles were also investigated by Dalirian et al.,[385] and they suggested that the activation of SiO_2

1529   particles can be described by the FHH activation theory with A_{FHH} and B_{FHH} equal to 2.50 and 1.62,

1530   respectively.
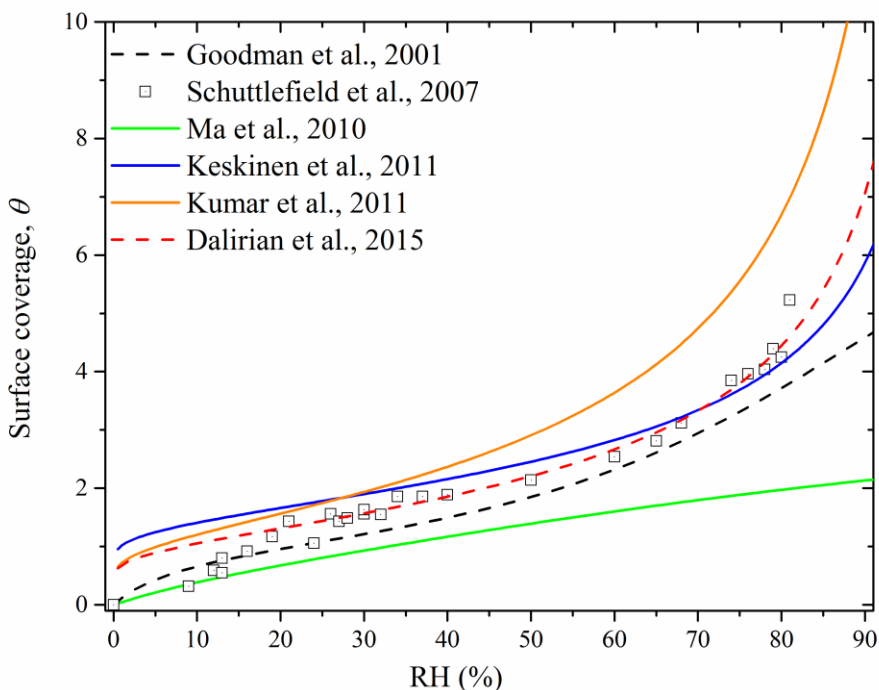
Figure 25. Comparison of surface coverage of adsorbed water on SiO_2 particles reported by Goodman et al.[250] (black dashed curve), Schuttlefield et al.[273] (squares), Ma et al.[269] (green solid curve), Keskinen et al.[320] (blue solid curve), Kumar et al.[262] (orange solid curve) and Dalirian et al.[385] (red dashed curve).

Water adsorption on SiO_2 particles, as measured by previous studies under sub-saturation conditions [250,269,273,320] or calculated using the two FHH parameters derived from CCN activation measurements under super-saturation conditions,[262,385] is plotted in Figure 25 for comparison. In general good agreement is found, though different experimental techniques and different SiO_2 samples were used. Significant discrepancies also exist. For example, the surface coverages of adsorbed water reported by Ma et al.[269] are always lower than those reported by other studies, and the discrepancy becomes more evident for RH >50%. In addition, for RH >50%, the difference between the calculated surface coverages of adsorbed water using the two FHH parameters reported by Kumar et al.[262] and those reported by Goodman et al.,[250] Schuttlefield et al.,[273] Keskinen et al.[320] and Dalirian et al.[385] appears to increase with RH.
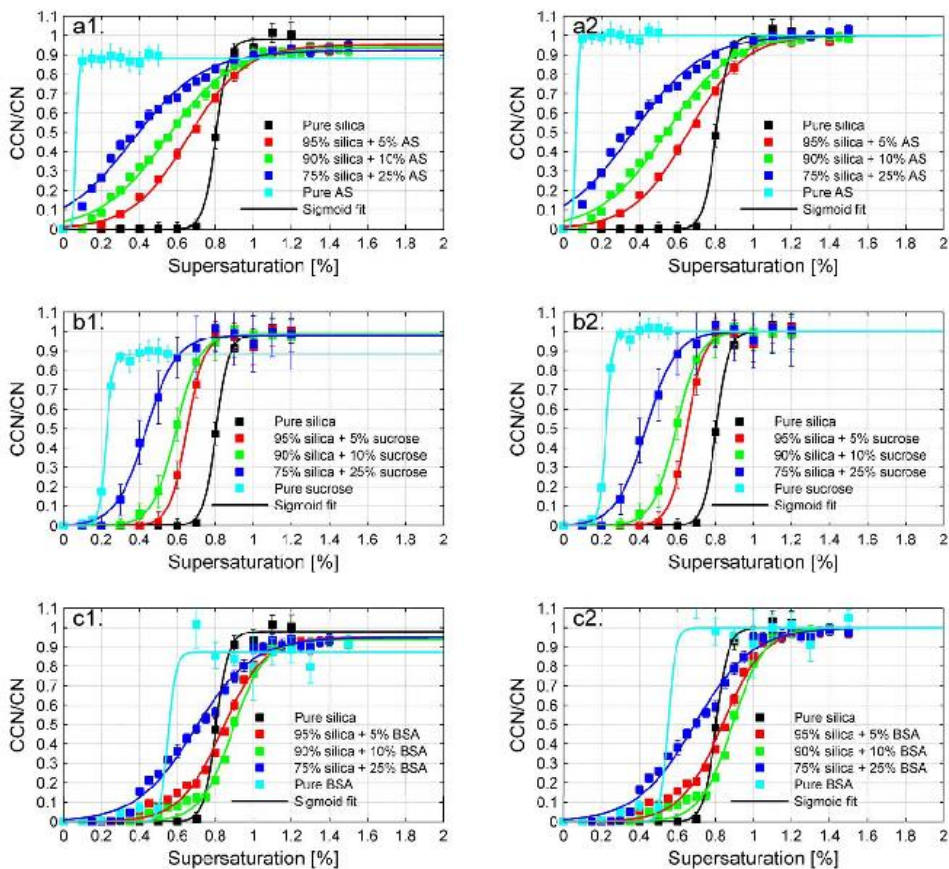
Figure 26. CCN activation curves for 150 nm pure SiO_2 particles and SiO_2 particles mixed with (a1-a2) ammonia sulfate (AS), (b1-b2) sucrose, and (c1-c2) bovine serum albumin. The left three panels show the un-normalized data and the right three panels show the normalized data. Reprinted with permission from ref 385. Copyright 2015 Copernicus Publications.

Coating of SiO_2 particles with more hygroscopic materials can increase their CCN activities. Dalirian et al.[385] generated SiO_2 particles mixed with different amounts of ammonia sulfate (AS), sucrose, and bovine serum albumin (BSA). As shown in Figure 26, mixing SiO_2 with compounds with higher CCN activities (compared to SiO_2) can decrease the critical super-saturation ratios and increase their CCN activity, when compared to pure SiO_2 particles.[385] The extent of decrease in critical super-saturation ratios depends on the mass fraction of SiO_2, i.e. the less SiO_2 the mixed particles contain, the more CCN active these particles are. In addition, different materials have different effects even when their mass fractions are the same. For the three compounds investigated

83

1561   by Dalirian et al.,[385] ammonia sulfate has the most significant effect because it is most CCN activity

1562   with a κ value of 0.61, while BSA has a smaller effect because its κ value is ~0.13 (and the κ value

1563   is 0.084 for sucrose).[385]

1564   **4.7 Metal oxides (TiO_2, Al_2O_3, and Fe_2O_3)**

1565   Previous studies which have investigated water adsorption on fresh and/or reacted TiO_2, Al_2O_3,

1566   and Fe_2O_3 particles are summarized in Table 10.

1567   **4.7.1 TiO_2**

1568   Goodman et al.[250] investigated water adsorption on P25 TiO_2 particles (BET surface area: 50 m^2 g^{-1}

1569   ) at different RH using transmission FTIR. It was found that [250] the surface coverage of adsorbed

1570   water can be fitted by the modified three-parameter BET equation, i.e. Eq. (5), with n equal to 8

1571   and c equal to 74.8. Ma et al.[269] used DRIFTS to study the water adsorption on P25 TiO_2 particles,

1572   and suggested that surface coverage of adsorbed water can be fitted with the modified three-

1573   parameter BET equation with n equal to 6.2 and c equal to 5.5. The results reported by these two

1574   studies are plotted in Figure 27, suggesting that the surface coverage of adsorbed water measured

1575   by Goodman et al.[250] is slightly higher than that determined by Ma et al.[269]
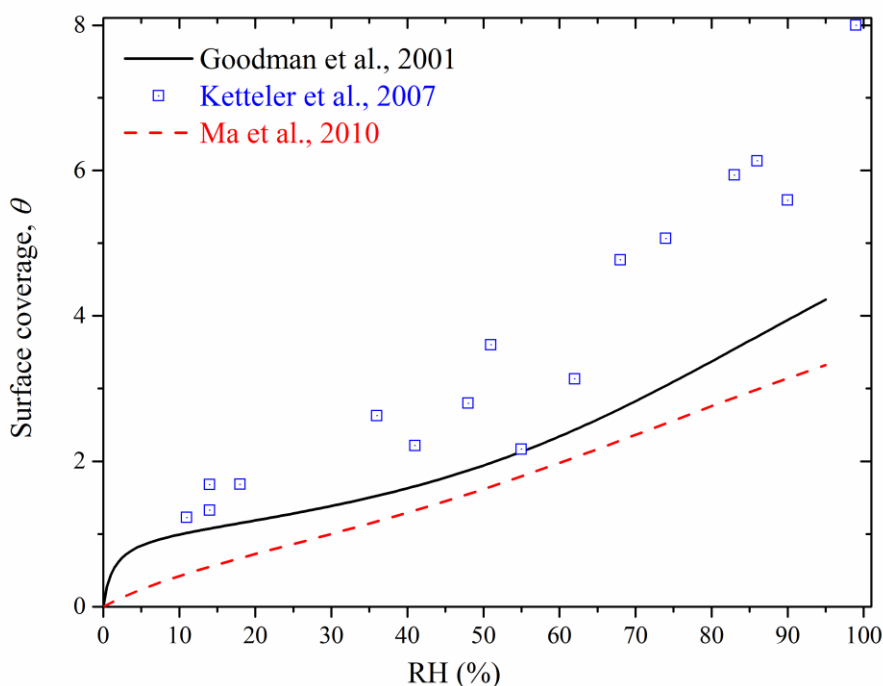
Figure 27. Surface coverage of adsorbed water on TiO_2 particles reported by previous studies. Solid curve: Goodman et al.;[250] squares: Ketteler et al.;[241] dashed curve: Ma et al.[269]

In addition, AP-XPS was also used to study water adsorption on the rutile single crystal surface(110).[241] The AP-XPS measurement suggested that 2 and 3 monolayers of adsorbed water are found at 12% and 25%,[241] and the surface coverage is higher than those reported Goodman et al.[250] and Ma et al.[269] However, it may not be directly comparable because Ketteler et al.[241] used single crystals while P25 TiO_2 particles were used by the other two studies.[250,269] Many previous studies have investigated water adsorption on rutile and anatase singles crystals, as summarized by Chen et al.[155] Since those studies are not of direct atmospheric relevance, they are not further discussed.

4.7.2 Al$_2$O$_3$

Transmission FTIR was used to study water adsorption on α-Al_2O_3 particles,[250] and it was suggested that the surface coverage of adsorbed water can be fitted with the modified three-

parameter BET equation with n equal to 8 and c equal to 25.2. Transmission FTIR was also used to investigate water adsorption on α-Al$_2$O$_3$ single crystals;[240] this work is of less atmospheric relevance and thus not further discussed. Water adsorption on α-Al$_2$O$_3$ particles was further investigated by Schuttlefield et al.[249] using ATR-FTIR and QCM, and the amount of adsorbed water at different RH was reported. Ma et al.[269] used DRIFTS to measure the amount of water adsorbed on α-Al$_2$O$_3$ particles, and suggested that its surface coverage can be described by a modified three-parameter BET equation, with n equal to 15.4 and c equal to 9.66. In addition, PSA was used by Ma et al.[212] to measure water adsorbed on α-Al$_2$O$_3$, and it was shown that one monolayer adsorbed water is formed at ~20% RH.
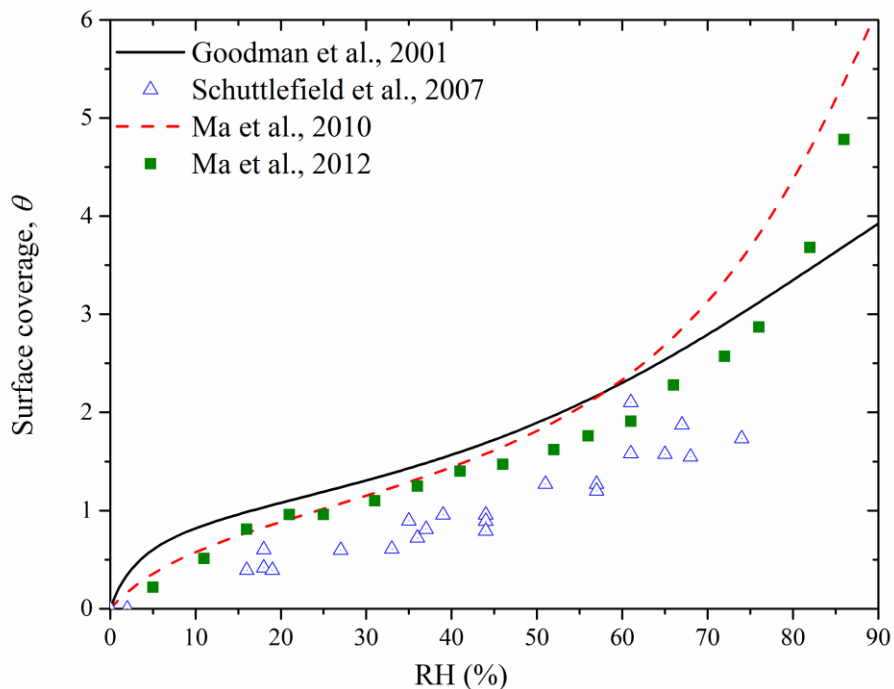
Figure 28. Comparison of surface coverage of adsorbed water on α-Al$_2$O$_3$ at different RH, as reported in previous studies. Solid curve: Goodman et al.;[250] dashed curve: Ma et al.;[269] squares: Ma et al.;[212] triangles: chuttlefield et al.[249]

Surface coverages of adsorbed water on α-Al$_2$O$_3$, as measured by these four different studies, are displayed together in Figure 28 as a function of RH. As evident in Figure 28, in general different

1607   studies show good agreement, though different methods have been used to quantify the amount of

1608   water adsorbed on the particle surface. A close inspection also reveals that for RH > 80%, the

1609   discrepancy between Goodman et al.[250] and Ma et al.[212,269] may increase. This may suggest that

1610   experimental uncertainties increase with RH.
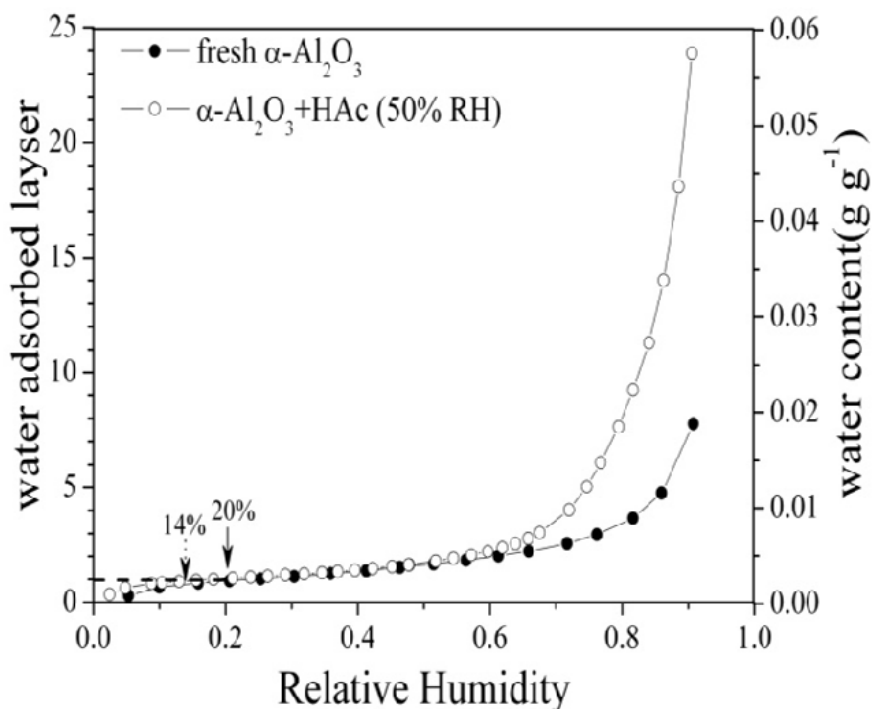
1611

1612   **Figure 29**. Amounts of water adsorbed on α-Al$_2$O$_3$ particles before and after heterogeneous reaction with

1613   gaseous acetic acid. Reprinted with permission from ref 212. Copyright 2012 the PCCP Owner Societies.

1614

1615   Heterogeneous reactions can change the hygroscopicity of α-Al$_2$O$_3$. For example, Ma et al.[212]

1616   measured the amount of water adsorbed on α-Al$_2$O$_3$ before and after reaction with acetic acid. As

1617   shown in Figure 29, it was found that the RH required to form one monolayer of adsorbed water

1618   decreased from ~20% to 14% after the reaction with acetic acid.[212] In addition, at 90% RH the

1619   amount of water adsorbed on the surface increased from 1.7% (by mass) for fresh particles to 5.2%

1620   (by mass) for reacted particles.[212] The study by Ma et al.[212] suggests that heterogeneous reaction

1621 with acetic acid increases the hygroscopicity of α-Al_2O_3 particles. In contract, another study by

1622 Rubasinghege et al.[386] found that exposure to formic acid could largely reduce the amount of water

1623 adsorbed by γ-Al_2O_3.

1624 **4.7.3 Fe₂O₃**

1625 Water adsorption on Fe_2O_3 was investigated by transmission FTIR [250] and DRIFTS [269] respectively.

1626 Both studies suggest that the surface coverage of adsorbed water can be described by a modified

1627 three-parameter BET equation, with n and c equal to 4 and 51.1 reported by Goodman et al.[250] and

1628 11.3 and 4.68 derived by Ma et al.[269] As shown in Figure 30, the surface coverage of adsorbed

1629 water measured by Goodman et al.[250] is higher for RH $<$ ~55% and lower for RH $>$ ~55% than that

1630 measured by Ma et al.[269] In addition, the discrepancy between the two studies seems to increase

1631 with RH for RH $>$ ~55%.
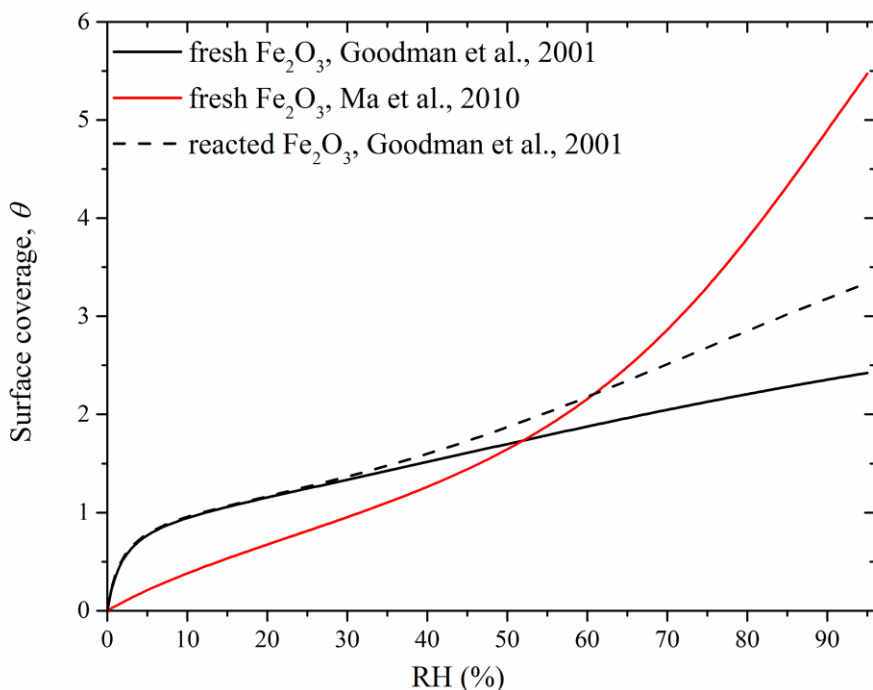
Figure 30. Surface coverages of adsorbed water on Fe_2O_3. Solid black curve: fresh particles measured by Goodman et al.;[250] dashed black curve: reacted particles measured by Goodman et al.;[250] solid red curve: fresh particles measured by Ma et al.[269]

In addition, Goodman et al.[250] found that the exposure to HNO_3 significantly increased the amount of water adsorbed by Fe_2O_3 particles, with n and c equal 6 and 55.3 for aged Fe_2O_3, compared to 4 and 51.1, respectively, for fresh Fe_2O_3.

4.8 Authentic complex dust mixture

Water adsorption properties, hygroscopicity, and CCN activity of a variety of authentic dust samples have been investigated in the last two decades, and Table 11 provides a quick overview of these studies. Arizona Test Dust is also an authentic dust sample; however, it has been separately discussed in Section 4.2 because it has been extensively studied and is often used as a dust standard. A direct comparison between different studies is difficult, because dust particles, even if they have

1646 the same name (for examples, Saharan dust), may be collected from different locations and thus

1647 their compositions may show large variations.

1648

1649 **Table 11.** Water adsorption, hygroscopicity, and CCN activity of authentic dust particles: summary of

1650 previous studies.

reference	techniques	dust
Seisel et al., 2004 [298]	Knudsen cell	Saharan dust
Seisel et al., 2005 [299]	Knudsen cell	Saharan dust
Koehler et al., 2007 [387]	H-TDMA and CCNc	Owens (dry) Lake dust
Koehler et al., 2009 [46]	H-TDMA and CCNc	Canary Islands dust, Cairo dust
Herich et al., 2009 [49]	H-TDMA and CCNc	Saharan dust, Chinese dust
Navea et al., 2010 [246]	ATR-FTIR and QCM	Saharan dust, China loess
Yamashita et al., 2011 [376]	CCNc	Asian mineral dust
Kumar et al., 2011 [262]	CCNc	Niger dust, and five different East Asian dust
Kumar et al., 2011 [263]	CCNc	Niger dust, and five different East Asian dust
Ma et al., 2012 [182]	DRIFTS	Asian dust

1651

1652 Using a Knudsen cell reactor coupled to a mass spectrometer, Seisel et al.[298,299] measured the

1653 uptake of water vapor by Saharan dust particles over 203-298 K, and the initial uptake coefficient

1654 was determined to be $(6.3\pm0.7)\times10^{-2}$, independent of temperature. Yamashita et al.[376] studied the

1655 CCN activity of dry-generated Asian mineral dust particles, and reported an average κ of 0.014.

1656 Ma et al.[182] collected Asian dust particles in Beijing during a dust storm event, and measured the

1657 water adsorption by these dust particles at different RH before and after heterogeneous reaction

1658 with SO_2. They [182] found that ~8 monolayers of adsorbed water were found at 90% RH, and that

1659 the reaction with SO_2 did not significantly change the hygroscopicity of Asian dust particles they

1660 collected.

1661

1662   Koehler et al.[387] measured the hygroscopicity and CCN activity of dust particles collected from

1663   Owens Lake region (California, USA), using H-TDMA and CCNc. They [387] found that 35% of the

1664   dry-generated particles are very hygroscopic with an average κ of 0.69 and the other 65% are much

1665   less hygroscopic with an average κ of ~0.05. Koehler et al.[46] also investigated the hygroscopicity

1666   and CCN activity of two North African dust samples: one from the Canary Islands and the other

1667   one from outside Cairo. It is suggested that the CCN activity of these dust particles can be

1668   represented using the single hygroscopicity parameter of $0.01 < \kappa < 0.08$.[46] In addition, wet-

1669   generated Canary Islands dust and Cairo dust were found to be much more hygroscopic, with κ

1670   equal to 0.26 and 0.7,[46] suggesting that wet-generation may artificially enhance the hygroscopicity

1671   and CCN activity of dust particles.

1672

1673   Using H-TDMA and CCNc, Herich et al.[49] investigated the hygroscopicity and CCN activity of

1674   Saharan dust and Chinese dust. Dust aerosol particles were produced by both dry- and wet-

1675   generation, and it was found that wet generation could significantly increase the CCN activity of

1676   dust particles.[49] The single hygroscopicity parameter, κ, was found to be 0.023 for dry-generated

1677   Saharan dust and 0.007 for dry-generated Chinese dust.[49] In addition, Herich et al.[49] found that κ

1678   derived from H-TDMA measurement may be smaller than those derived from CCNc measurement;

1679   nevertheless, the difference may be within the experimental uncertainties.

1680

1681   QCM was used to study water adsorption on Saharan dust and China Loess at room temperature

1682   and at different RH.[246] The results are displayed in Figure 31, suggesting that both Saharan dust

1683   and China loess can adsorb substantial amount of water.[246] In addition, it appears that the two

1684   samples show somewhat similar water uptake capacities on a per mass basis, although their

1685   chemical compositions based on the XPS, SEM-EDX, and ATR-FTIR analyses show large

1686   differences.[246]
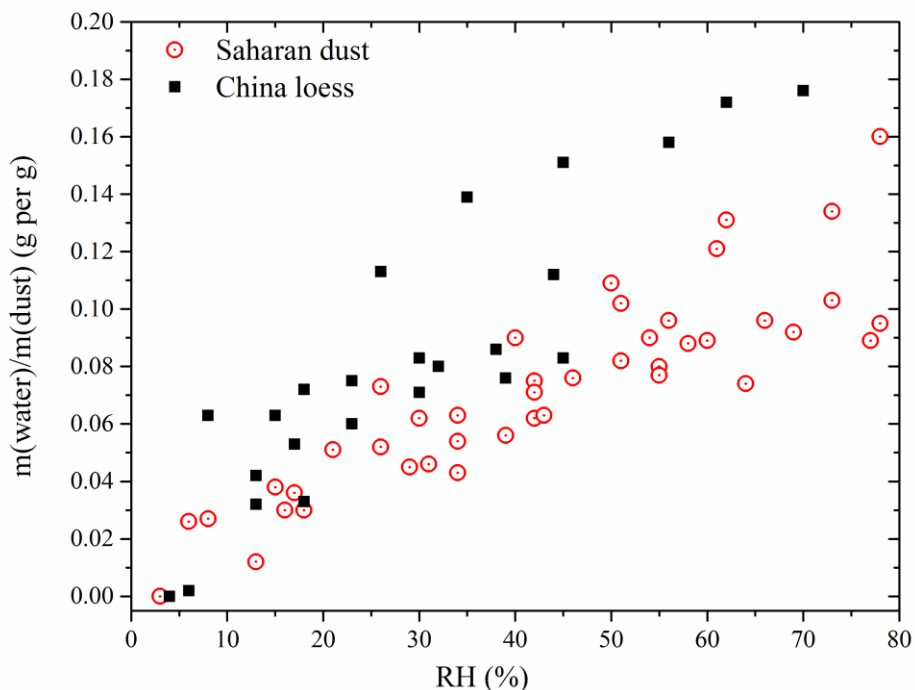
Figure 31. The amounts of water adsorbed by Saharan dust (red circles) and China loess (black squares) at room temperature and at different RH, as measured by Navea et al.[246]

Kumar et al.[262] investigated the CCN activity of six different types of dust particles, one collected from Niger (Sahel) and the other five collected from different locations in East Asian deserts. It was suggested that the FHH adsorption activation theory could better describe the CCN activation of these dry-generated dust aerosol particles,[262] compared to the κ-Köhler activation theory. The measured CCN activity of all the dust particles can be represented by one set of FHH parameters with A_{FHH} equal to ~2.25±0.75 and B_{FHH} equal to ~1.20±0.10.[262] Kumar et al.[263] also measured the CCN activity of wet-generated aerosol particles for these six types of dust, and found that κ for these wet-generated dust aerosol particles varies in the range of 0.14-0.44.[263] It was also suggested that wet-generation can lead to enhancement of the measured CCN activity of dust particles, compared to dry generation.[262,263]

4.9 Theoretical studies on water adsorption on mineral dust surface

There have been several theoretical studies focused on adsorption of gas phase water on mineral surfaces. These studies include but are not limited to calcite,[388-390] kaolinite,[391-395] montmorillonite,[377,396,397] quartz,[398,399] titanium dioxide,[400-402] and FeOOH.[275,403,404] In this review we do not provide a comprehensive review of these studies, but instead we highlight a few these. In particular, we highlight several theoretical studies which have significantly improved our understanding of water adsorption on mineral dust particles of atmospheric relevance at a fundamental level. This discussion is limited to four representative components contained by mineral dust aerosol particles in the troposphere. These components are representative of carbonate minerals (calcite), clay minerals (kaolinite and montmorillonite), and oxide minerals (quartz). A recent review paper [155] summarized some theoretical work for water adsorption on $TiO_2(110)$ surface. In general, it appears that it is non-trivial for theoretical studies to quantitatively predict the amount of water adsorbed by mineral surfaces as a function of RH. However, insights into fundamental processes involved in water-mineral interactions can be gained from these theoretical studies. Recently Gerber et al.[405] provided several excellent examples to illustrate how theoretical studies could help us understand atmospherically relevant chemical reactions at various interfaces/surfaces.

4.9.1 Calcium carbonate

Using molecular dynamics simulations, de Leeuw and Parker [388] investigated the effect of water adsorption on the surface structures and energetics for several different planar calcite surfaces. They found that physisorption of water is energetically favourable for all the planar surfaces, among which the (1014) surface is most stable.[388] Kerist and Parker [406] calculated the free energy of water adsorption on the (1014) calcite surface using molecular dynamics simulations. Their simulations [406] suggested that the free energy of water adsorption is smaller than the enthalpy, indicating that there is a large change in entropy associated with water adsorption on the surface.

93

1726 Additionally, ab-initio calculations by Kerisit et al.[389] were used to predict the surface phase

1727 diagram for the (1014) calcite surface, and they [389] suggested that nonstoichiometric surfaces can

1728 be important in determining the chemistry of calcite at high RH.

1729

1730 Rahaman et al.[390] developed a molecular dynamics scheme to study the dynamics of water

1731 adsorption on the (1014) calcite surface at different RH. They [390] found that the timescale for the

1732 surface to become in equilibrium with the environment is of several nanoseconds, and predicted

1733 that water adsorption on the surface would follow a BET-like isotherm. They [390] also suggested

1734 that mobility of adsorbed water is enhanced at higher RH, and that at lower RH adsorbed water is

1735 more tightly bound to the surface.

1736 **4.9.2 Kaolinite**

1737 Previous theoretical studies on water adsorption on kaolinite, for example, by Hu and

1738 Michaelides,[407-409] mostly focused on the Al-terminated(001) and Si-terminated(001) surfaces.

1739 Croteau et al.[392-395] used grand canonical Monte Carlo simulations to investigate adsorption and

1740 structure of water on kaolinite surfaces. They [392] found that at 235 K, the Si-surface is hydrophobic

1741 and does not display potential to adsorb water when RH is less than 100%, and adsorption on the

1742 Al-surface exhibits first-order characteristics. More importantly, they [392] suggested that adsorption

1743 on edges, dominated by strong water-surface interactions, is much more continuous and

1744 contributes significantly to water uptake by kaolinite.

1745

1746 In a following study, Croteau et al.[393] further investigated water adsorbed on four different surfaces

1747 (the Al-terminated surface, the Si-terminated surface, and two edge-like surfaces) of kaolinite at

1748 different RH and at two different temperatures (235 and 298 K), using Monte Carlo simulations.

1749 Several conclusions have been drawn from their simulations:[393] i) the Si-terminated surface does

1750 not uptake significant amount of water, and the Al-terminated surface and the two edge-like

1751   surfaces can adsorb monolayers of water for RH below 100%; ii) the edge-like surfaces have the

1752   largest affinity for water; iii) water adsorption on the edge-like surfaces grows continuously until

1753   one monolayer is reached, while on the Al-surface the formation of one monolayer adsorbed water

1754   appears as a sharp transition (this also indicates that collective behavior occurs among water

1755   molecules on the Al-surface but not on the edges) and practically there is no submonolayer

1756   adsorption. This suggests that mechanisms of water adsorption on the Al-surface and the edge-

1757   like surfaces are distinctively different.[393]

1758

1759   The two previous studies carried out by Croteau et al.[392,393] used atomistically smooth kaolinite

1760   surfaces in these simulations, and their predicted surface coverages of adsorbed water are much

1761   lower than those experimentally measured by Schuttlefield et al.[249] In an effort to explain the

1762   experimental results, Croteau et al.[395] further performed water adsorption simulations at 296 K on

1763   kaolinite surfaces which contain trenchlike structures. The structures of different trenches

1764   considered by Croteau et al.[395] are shown in Figure 32.
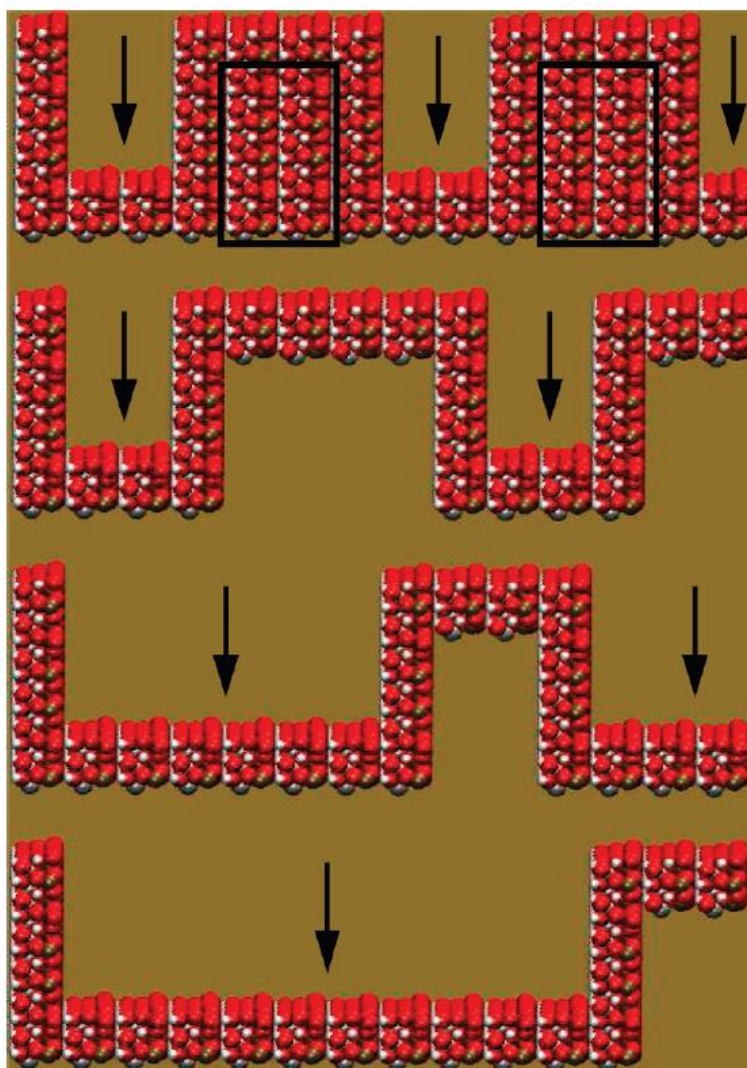
Figure 32. The structures of different trenches on kaolinite surfaces considered by Croteau et al.[395] in their simulations. O, H, Al, and Si atoms are in red, white, gray, and brown. From top to bottom, the trenches are refered as 1, 2, 3, and 4, with trend widths of 14.78, 14.78, 44.34, and 73.91 Å, respectively. Simulations were carried out for trench 1 without (1A) and with (1B) intertrench spacing filled (atoms inside the black rectangle). Black arrows indicate where the trenches are. Reprinted from permission from ref 395. Copyright 2010 American Chemical Society.

Simulated water adsorption on kaolinite surfaces with different trenches at 298 K are shown in Figure 33 as a function of RH. Compared to that for an atomistically smooth edge-like surface, it was found that the amount of adsorbed water is largely increased for surfaces with all the different

1776   trenches.[395] The study by Croteau et al.[395] suggests that surface trenches (and very likely other

1777   surface defects) may have strong affinity for water and thus can adsorb multilayers of water. The

1778   amounts of adsorbed water on kaolinite predicted by Croteau et al.[395] as a function of RH are on

1779   the same order of magnitude as those measured by Hung et al.,[270] but appear to be significantly

1780   smaller than those measured by Schuttlefield et al.[249] and Hatch et al.[348]
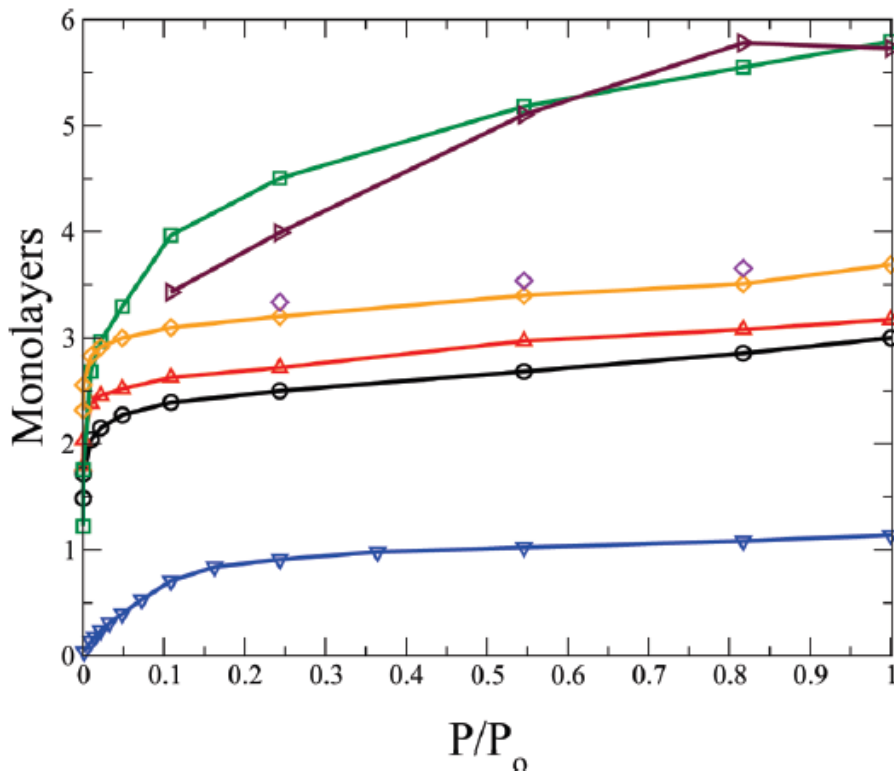
1781

1782   **Figure 33.** Simulated surface coverages of adsorbed water on an atomistically smooth edge kaolinite

1783   surface (blue triangles) and kaolinite surfaces containing different types of trenches as a function of RH

1784   (P/P_0, defined as the ratio of partial pressure of water vapor to the saturated vapor pressure of water) at 298

1785   K. Blue triangles: atomistically smooth edge-like surface; red triangles: trenches 1A; orange diamonds:

1786   trenches 1B; black circles: trenches 2; green squares: trenches 3; maroon triangles: trenches 4. Trench

1787   structures are given in Figure 32. Reprinted from permission from ref 395. Copyright 2010 American

1788   Chemical Society.

4.9.3 Montmorillonite

1789

1790 Hensen et al.[396] combined molecular dynamics and Monte Carlo simulations to investigate water

1791 adsorption by Li-, Na-, and K-montmorillonite. It is found that water adsorption by these

1792 montmorillonite occurs via two mechanism:[396] 1) at low RH, water adsorption is driven by

1793 hydration of interlayer counterions, and the extent of water adsorption increases with cation-H_2O

1794 hydration energy ($Li^+ > Na^+ > K^+$); 2) at high RH, water molecules are adsorbed near mineral

1795 surface, coordinating to the structural OH groups. This enables the formation of an extensive

1796 hydrogen bonding network and therefore leads to a sharp increase of adsorbed water with RH.[396]

1797

1798 In a following theoretical study, Hensen and Smit [377] was able to quantitatively predict the amount

1799 of water adsorbed by Na-montmorillonite as a function of RH. In addition, their simulations [377]

1800 suggested that montmorillonite swelling occurs by migration of counterions (which are initially

1801 strongly bound to clay surface) to positions in the clay interlayers where these ions can be fully

1802 hydrated.

4.9.4 Quartz

1803

1804 Several review articles [410,411] and books [412,413] have summarized theoretical studies on the

1805 interaction of water with silica surfaces, especially for liquid water-quartz interactions. Interested

1806 readers are referred to these publications for more information. Density functional theory based

1807 molecular dynamics simulations were used by Sulpiz et al.[414] to understand the molecular behavior

1808 of quartz-water interface. They [414] suggested that two types of silanol groups exist at the quartz

1809 surface: i) out-of-plane silanols with a pKa of 5.6, forming strong and short H-bonds with

1810 interfacial water molecules, giving rise to highly correlated hydrogen-bonding network and thus

1811 exhibiting a band at ~3200 cm^{-1} in the sum frequency generation (SFG) spectroscopy.[415-417] For

1812 simplicity, these water molecules are also referred to as the "ice-like" water because of their

1813 similarity in structure to water molecules in bulk ice;[418] ii) in-plane silanols with a pKa of 8.5,

1814   forming weak hydrogen bonds with interfacial water molecules and showing a broad band at ~3400

1815   cm^{-1} in the SFG spectrum.[415-417] Intensity in this region corresponds with OH stretch intensities of

1816   bulk liquid water, and therefore for simplicity these water molecules are sometimes referred to as

1817   "liquid-like" water.[418]

1818

1819   Recently Murdachaew et al.[399] used initio molecular dynamics to study the adsorption of HCl on

1820   the hydroxylated α-quartz (0001) surface, and observed that adsorbed HCl is rapidly dissociated

1821   and ionized on wetted surface at temperatures between 250 and 300 K. Ionization of adsorbed HCl

1822   seems to be enhanced by lattice mismatch between the silica and water layer.[399] The dissociation

1823   and ionization of HCl on SiO$_2$ surface has several important implications for atmospheric

1824   chemistry. For example, it lowers the pH for silica surface and leads to the charging and

1825   disordering of adsorbed water.[399] These changes could significantly impact chemical processes on

1826   silica surfaces.[399]

1827   **4.10 Chemical aging modifies the interaction of water vapor with mineral dust**

1828   **particles: results from field measurements**

1829   As summarized in previous sections, numerous laboratory studies have suggested that atmospheric

1830   heterogeneous reactions could substantially increase the water adsorption ability, hygroscopicity,

1831   and CCN activity of mineral dust particles. Very frequently tropospheric dust aerosol particles

1832   have been observed to be internally mixed with nitrate, sulfate, chloride, and organic

1833   compounds.[158,159,162,202,206,419-425] [158,159,162,202,206,419-425] More importantly, the effect of atmospheric

1834   aging processes has also been supported by increasing evidence from field measurements. Instead

1835   of providing an exhaustive literature survey, here we highlight some important findings from field

1836   measurements to provide evidence if atmospheric chemical transformation could influence the

1837   interaction of mineral dust particles with water vapor. Tables 12 summarizes the major findings of

1838   field studies which are discussed in the section. A recent review paper by Li et al.[426] summarized

1839 single particle studies on the changes in chemical compositions, morphology, and hygroscopicity

1840 of aerosol particles (including mineral dust) collected in East Asia.

Table 12. Field measurements of water adsorption, hygrsoscopicity, and CCN activity of mineral dust aerosol particles: summary of major findings

from previous studied included in this review.

reference	Location	major findings
Perry et al., 2004 [427]	Trinidad Head, California, USA	Elemental (Al, Si, and Fe) mass distributions all shifted toward smaller sizes as RH was reduced, indicating that mineral dust particles transported from Asia to the west coast of the United States is somewhat more hygroscopic upon its arrival.
Laskin et al., 2005 [245]	Shoresh, Israel	In agreement with laboratory studies, it was shown that solid nonspherical calcium carbonate particles were converted to spherical liquid droplets which contain $Ca(NO_3)_2$, due to heterogeneous reactions with HNO_3.
Matsuki et al., 2005 [159]	Beijing, China	Some Ca-rich dust particle are spherical under humid conditions, due to the formation of nitrate and sulfate on these particles.
Massling et al. 2007 [428]	off the coasts of Japan, Korea, and China	For all continentally influenced air masses, 1 μm particles can be classified as two groups according to their hygroscopic growth factors at 90% RH: one with growth factors of around 1.0 (representative of dust particles) and the other one with a growth factors of ~2(representative of sea spray particles).
Shi et al., 2008 [429]	southwestern Japan	Nitrate free dust particle, even though they may contain sulfate, did not change their morphology when RH was increased from 15% to 90%; however, dust particles containing nitrate became aqueous droplets even at 15% RH.
Crumeyrolle et al., 2008 [430]	Banizoumbou, Niger	Cloud processing during a mesoscale convective system may enhance the formation of soluble materials associated with dust particles and therefore enhance their CCN activity.
Tobo et al., 2009,[431] Tobo et al., 2010 [432]	Kanazawa, Japan	Some Ca-rich particles contain substantial amount of chloride, and they existed in an amorphous state and were nearly spherical even under high vacuum.

Kim and Park, 2012 [433]	Gwangju, Korea	Dust aerosol particles transported to Korea exhibited enhanced hygroscopicity, compared to fresh aluminum silicate and calcium carbonate.
Begue et al., 2015 [267]	Cabauw, Netherlands	CCN activities of Saharan dust aerosol particles transported to Netherlands were significantly increased due to heterogeneous reactions with anthropogenic pollutants.
Denjean et al., 2015 [434]	Fajardo, Puerto Rico	Supermicron African dust particles, after being transported across the Atlantic in summertime, were largely unprocessed and did not show significant change in hygroscopic properties.

1843

1844

1845   Laskin et al.[245] collected mineral dust particles at Shoresh, Israel, and analyzed the morphology

1846   and composition of individual dust particles using scanning electron microscopy with energy

1847   dispersive analysis of X-ray (SEM-EDX). For the first time, they [245] provided field evidence that

1848   due to heterogeneous reactions with HNO_3, solid nonspherical calcium carbonate particles were

1849   converted to spherical liquid droplets which contain $Ca(NO_3)_2$. This important finding has been

1850   supported by a number of following studies. For example, Matsuki et al.[159] collected Asian dust

1851   particles (>1 μm) in Beijing and analysed them using electron microscopy. As shown in Figure 34,

1852   Matsuki et al.[159] found that some Ca-rich dust particle are spherical under humid conditions, due

1853   to the formation of nitrate and sulfate on these particles.
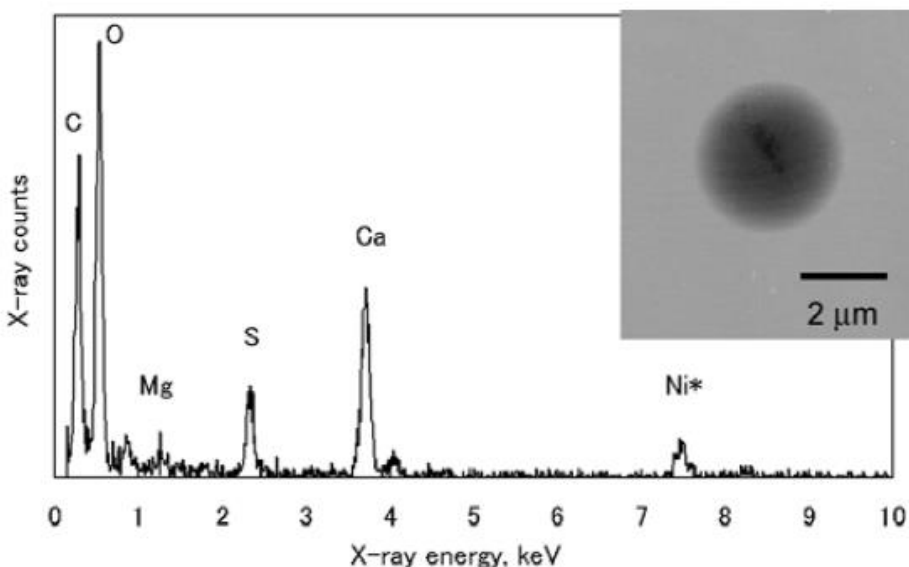
1854

1855   **Figure 34.** Electron micrograph and X-ray spectrum of a typical Ca-rich spherical particle collected in the

1856   boundary layer in Beijing. The signal of Ni in the X-ray spectrum was caused by the Ni-containing grids

1857   used to support the films on which particles were collected. Reprinted with permission from ref 159.

1858   Copyright 2005 John Wiley & Sons, Inc.

1859

1860   Asian dust particles (>1 μm) were also collected in Southwestern Japan after long-range transport

1861   and analyzed with environmental scanning electron microscopy.[429] It was found that nitrate free

103

1862   dust particle, even though they may contain sulfate, did not change their morphology when RH

1863   was increased from 15% to 90%;[429] in contract, dust particles containing nitrate became aqueous

1864   droplets even at 15% RH.[429] This suggested that the formation of nitrate coating could substantially

1865   increase the hygroscopicity of dust particles, whereas the formation of sulfate did not.[429] This

1866   observation can be explained by the fact that $Ca(NO_3)_2$ is more hygroscopic than $CaSO_4$.[217,357]

1867

1868   Tobo et al.[431,432] collected Asian dust particles around Japan Islands and analyzed them by SEM-

1869   EDX. They [432] found that substantial amount of chloride was found on Ca-rich particles, and these

1870   particles existed in an amorphous state and were nearly spherical even under high vacuum.

1871   Consequently, Tobo et al.[432] proposed that in remote marine troposphere where the concentrations

1872   of reactive nitrogen species are typically very low, heterogeneous reactions with HCl can also

1873   significantly change the composition and thus hygroscopicity of dust particles.

1874

1875   In another study, Asian dust particles were collected in Trinidad Head (California, USA) after

1876   long-range transport during three significant dust episodes.[427] Two impactors were used in parallel,

1877   one maintained at ambient RH and the other one maintained at a lower RH of 55%.[427] Elemental

1878   analysis of collected samples using synchrotron X-ray fluorescence suggested that the elemental

1879   (Al, Si, and Fe) mass distributions all shifted toward smaller sizes as the RH was reduced.[427] This

1880   may indicate that mineral dust particles transported from Asia to the west coast of the United States

1881   is somewhat more hygroscopic upon its arrival, and it was tentatively attributed to the formation

1882   of sulfate coatings on dust particles.[427]

1883

1884   Most of studies which investigated the hygroscopicity of ambient dust particles require collection

1885   of dust particles followed by offline analysis. In an airborne field campaign in West African,

1886   aerosol properties in a layer between 1300 and 3000 m were measured during the passage of a

104

1887 mesoscale convective system (MCS).[430] After passage of the MCS, a significant increase in CCN

1888 fraction was observed together with higher contribution of sulfate, nitrate, and chloride to the total

1889 aerosol mass.[430] A mesoscale model was used to interpret the results, and it was concluded that

1890 cloud processing during the MCS could enhance the formation of soluble materials associated with

1891 dust particles and therefore enhance their CCN activity.[430] In another study, Kim and Park [433]

1892 measured the hygroscopicity of Asian dust aerosol particles using a system similar to H-TDMA.

1893 They [433] found that dust aerosol particles transported to Korea exhibited enhanced hygroscopicity

1894 compared to fresh aluminum silicate and calcium carbonate, due to heterogeneous reactions and

1895 cloud processing. More recently, it is suggested that the CCN activity of Saharan dust aerosol

1896 particles transported to Netherlands were significantly increased due to heterogeneous reactions

1897 with anthropogenic pollutants.[267]

1898

1899 However, not all the field measurements conclude that after long-range transport in the troposphere,

1900 the hygroscopicity of mineral dust aerosol particles will be significantly enhanced. Massling et

1901 al.[428] measured the hygroscopic growth of 1 μm (dry diameter) particles off the coats of Japan,

1902 Korea, and China in spring 2001 during the ACE-Asia study. It is found that for all continentally

1903 influenced air masses, 1 μm particles can be classified as two groups according to their hygroscopic

1904 growth factors at 90% RH: one with growth factors of around 1.0 and the other one with a growth

1905 factors of ~2.[19,428] [435,436]The first one was suggested to be representative of dust particles, and the

1906 second one appears to be similar to sea spray particles.[437] This study may indicate that the change

1907 in hygroscopicity of Asian dust particles after long-range transport can be very small, though lack

1908 of particle composition measurements makes it difficult to draw more convincing conclusions. A

1909 recent field campaign in Fajardo, Puerto Rico found that supermicron African dust particles, after

1910 being transported across the Atlantic in summertime, did not show significant change in

1911 hygroscopic properties.[434] Measurements of chemical composition suggest that most of mineral

1912 dust was chemically unprocessed and externally mixed, and only a minor portion of mineral dust

1913 was internally mixed with sulfate and/and chloride.[434] In addition, Kaaden et al.[438] measured the

1914 hygroscopic growth of aerosol particles at Tinfou, Morocco, and found that particles larger than

1915 720 nm were completely hydrophobic. The hygroscopic growth of aerosol particles at Cape Verde

1916 was investigated by Schladitz et al.,[439] who found that the κ value was almost 0 for particles with

1917 volume equivalent diameters of >250 nm. Both studies [438,439] seem to suggest that Saharan dust

1918 particles they detected are largely hydrophobic; nevertheless, both measurements are very close to

1919 source regions and therefore it is highly likely that those dust particles have not aged much in the

1920 atmosphere and my not have been exposed very much to acidic gases.

1921

1922 Discrepancies reported by the aforementioned field measurements of hygroscopicity of mineral

1923 dust particles may due to their different exposure histories (and thus the effective aging extents)

1924 and their variations in mineralogy. Several single particle studies [159,245,429,432,440] seem to indicate

1925 that the major components of hygroscopic aged dust particles could be carbonates (e.g., calcite and

1926 dolomite), which can undergo rapid reactions with acidic trace gases, leading to the formation of

1927 very hygroscopic salts, such as $Ca(NO_3)_2$ and $CaCl_2$. The only solid conclusion which can be

1928 drawn up to now is that some dust particles can be converted to aqueous droplets after long-range

1929 transport, but it is still unclear to which extent the hygroscopicity distribution of mineral dust

1930 aerosol particles will change during their residence time in the troposphere. In addition, there will

1931 be a very strong dependence on the mineralogy as noted above.

1932 **4.11 Summary**

1933 **4.11.1 Fresh dust particles**

1934 Table 13 summarizes CCN activity, as represented by κ, of $CaCO_3$, ATD, illite, kaolinite,

1935 montmorillonite, and African and Asian dust particles reported in previous studies. Only studies

1936 using dry-generated aerosol particles are included, because wet-generation may enhance the CCN

activity of dust particles.[49,256,259,262,263] In order for simple and direct comparison, CCN activity measurements interpreted using the FHH adsorption activation theory are not included, but they have been discussed in previous subsections. Garimella et al.[259] provided an intercomparison of measured critical super-saturations as a function of particles diameter for several types of dry-generated mineral dust particles. H-TDMA measurements have also been used to derive κ; however, these measurements can be significantly influenced by the non-sphericity of dust particles. Therefore, Table 13 does not include H-TDMA measurements.

Table 13. Summary of single hygroscopicity parameter (κ) of $CaCO_3$, ATD, illite, kaolinite, montmorillonite, and African and Asian dust particles reported in previous studies. Only studies in which the CCN activity of dry-generated mineral aerosol particles were measured are included.

mineral	reported κ	reference
$CaCO_3$	0.0008-0.0018	Sullivan et al., 2010 [256]
	0.0019±0.0007	Zhao et al., 2010 [264]
	0.0013-0.0033	Tang et al., 2015 [357]
ATD	~0.025	Koehler et al., 2009 [46]
	~0.003	Herich et al., 2009 [49]
	0.002	Sullivan et al., 2010 [261]
	0.0042	Sullivan et al., 2010 [375]
	0.017	Yamashita et al., 2011 [376]
	0.0041	Garimella et al., 2014 [259]
illite	0.002-0.003	Herich et al., 2009 [49]
	0.0072	Garimella et al., 2014 [259]
kaolinite	~0.001	Herich et al., 2009 [49]
montmorillonite	~0.003	Herich et al., 2009 [49]
	0.0088	Garimella et al., 2014 [259]
North African dust	0.01-0.08	Koehler et al., 2009 [46]

Saharan dust	0.023	Herich et al., 2009 [49]	
Chinese dust	0.007	Herich et al., 2009 [49]	
Asian dust	0.014	Yamashita et al., 2011 [376]	

1948

1949 κ values given in Table 13 reveal that there is fairly good agreement between previous studies. It

1950 appears that the CCN activity of $CaCO_3$, ATD, illite, kaolinite, and montmorillonite particles is

1951 very low and can be described with a κ value of less than 0.01. Authentic dust samples collected

1952 in Africa and Asia show somehow slightly higher κ value, probably because those samples contain

1953 more soluble components which increase their CCN activity.

1954

1955 In this section, we have compared measurements carried out under sub-saturation conditions using

1956 particles supported on substrates and those using aerosol particles performed under sub- and super-

1957 saturations conditions. Despite experimental and theoretical issues which can make such

1958 comparisons difficult (as discussed in Sections 2-3), reasonably good agreement has been found

1959 for $CaCO_3$, SiO_2, TiO_2 , Al_2O_3, and Fe_2O_3. On the other hand, as discussed in Sections 4.2-4.5,

1960 large discrepancies exist between studies using aerosol particles and those using particles

1961 supported on substrates for ATD, illite, kaolinite, and montmorillonite, and surface coverages of

1962 adsorbed water interpreted from measurements using aerosol particles are much lower. Even

1963 among studies which used very similar sample preparation methods and experimental techniques,

1964 significant disagreement are also observed for some clay minerals, with illite as an example shown

1965 in Figure 18b.

1966

1967 In experiments in which particles were supported on substrates, normally a slurry of dust particles

1968 in a solvent (e.g., water, methanol, or ethanol) was deposited on the supporting substrates to form

1969 a film. We speculate that though this type of sample preparation methods may not lead to

1970   substantial change in physicochemical properties for relative simple minerals such as Al_2O_3 and

1971 SiO_2, it has the potential to cause some artifacts for clays and authentic dust samples. The effects

1972   of different sample preparation menthods needs to be carefully and systematically examined in

1973   future studies.

1974

1975   The interactions of mineral dust particles with water vapor at temperatures above the onset of ice

1976   nucleation can influence their heterogeneous reactivity, hygroscopic growth, and CCN activity;

1977   therefore, a better understanding of these interactions is very important. Efforts are required to

1978   reduce the existing large discrepancies among different studies. In a well-coordinated

1979   collaboration, same mineral dust samples can be distributed to different groups which may use a

1980   variety of experimental techniques to study their interactions with water vapor, and reported results

1981   can be directly compared in order to find out the advantages and limitations of different experiment

1982   techniques. Very recently a similar campaign has been successfully carried out to investigate the

1983   ice nucleation activity of illite particles,[441] and similar actions will also definitely be beneficial for

1984   investigation of water adsorption, hygroscopicity, and CCN activity of mineral dust particles.

1985

1986   Compared to the κ-Köhler theory, the FHH theory is less used to interpret the hygroscopic growth

1987   and CCN activity of mineral dust particles. The two FHH parameters (A_{FHH} and B_{FHH}) reported for

1988   mineral dust particles, are compiled in Table 14. Direct comparison of hygroscopicity or CCN

1989   activity from the two FHH parameters is difficult, and interested readers can calculate the surface

1990   coverage of adsorbed water as a function of RH, using Eqs. (10) or (20).

1991   **Table 14.** Summary of A_{FHH} and B_{FHH} parameteres of mineral dust particles reported in the literature.

mineral	sample preparation method	A_{FHH}	B_{FHH}	reference
CaCO$_3$	dry-generated aerosol particles	3.00±0.04	1.30±0.03	Kumar et al., 2011 [262]
	wet-generated aerosol particles	1.74	1.22	Kumar et al., 2011 [263]
ATD	dry-generated aerosol particles	2.96±0.03	1.28±0.03	Kumar et al., 2011 [262]
illite	dry-generated aerosol particles	1.02±0.38	1.12±0.04	Kumar et al., 2011 [262]
	wet-generated aerosol particles	3.00	1.27	Kumar et al., 2011 [263]
	particles supported on substrates	75±17	1.77±0.11	Hatch et al., 2014 [348]
kaolinite	particles supported on substrates	1.70	2.25	Hung et al., 2015 [270]
montmorillonite	dry-generated aerosol particles [a]	2.06±0.72	1.23±0.04	Kumar et al., 2011 [262]
	dry-generated aerosol particles [b]	1.23±0.31	1.08±0.03	Kumar et al., 2011 [262]
	wet-generated aerosol particles [a]	1.09	1.04	Kumar et al., 2011 [263]
	wet-generated aerosol particles [b]	0.87	1.00	Kumar et al., 2011 [263]
	particles supported on substrates	98±22	1.79±0.11	Hatch et al., 2014 [348]
	particles supported on substrates	1.25	1.33	Hung et al., 2015 [270]
SiO$_2$	dry-generated aerosol particles	2.95±0.05	1.36±0.03	Kumar et al., 2011 [262]

1992

1993   [a]: Ca-montmorillonite; [b]: Na-montmorillonite

1994   It is noteworthy that most of the previous measurements have only been performed at around room

1995   temperature, near 295 K. However, the relevant temperatures in the troposphere range

1996   approximately from 200 to 300 K, and mineral dust particles mainly exist in the free troposphere

1997   where the temperature is much lower than room temperature. Therefore, the effects of temperature

1998   on the water adsorption, hygroscopicity, and CCN activity of mineral dust particles, which have

1999   been seldom examined, deserve further investigation.

2000   **4.11.2 Aged dust particles**

2001   Due to numerous studies over the last 1-2 decades, it is widely recognized that heterogeneous

2002   reactions, mostly through the formation of more soluble materials (although sometimes insoluble

2003   compounds can also be formed), can lead to significant enhancement of water adsorption,

2004   hygroscopicity, and CCN activity of mineral dust particles. Nevertheless, most of previous studies

2005   are either rather qualitative or their direct atmospheric relevance is lacking. Further research, which

2006   are carried out at atmospherically relevant conditions to quantitatively understand the effects of

2007   atmospheric chemical transformation, will be very helpful.

2008

2009   Most of previous studies on the atmospheric aging effects focuses on $CaCO_3$, probably the most

2010   reactive mineral contained by tropospheric dust aerosol particles. It is recommended that future

2011   studies should also examine the effect of aging processes for more abundant clay minerals and

2012   authentic dust samples which have more direct relevance for tropospheric dust aerosol particles.

2013   **5 Effects of chemical aging on ice nucleation activity of mineral dust particles**

2014   The formation of ice crystals in clouds is of particular scientific interest, because more than 50%

2015   of the global precipitation is initiated via the ice phase.[442] Ice formation may occur in clouds

2016   through both homogeneous and heterogeneous ice nucleation. Different ice nucleation

2017   mechanisms are depicted in Figure 35.[443] Homogeneous ice nucleation requires the temperature to

2018   be lower than -36 °C,[167,444] while heterogeneous ice nucleation can occur at higher

temperature.[167,445,446] Heterogeneous ice nucleation can be classified into four modes:[167] 1) deposition nucleation, which occurs on particles in the absence of the formation of liquid water (below water saturation); 2 and 3) condensation freezing and immersion freezing: ice formation occurs either during the simultaneous action of IN as CCN (condensation freezing) or during the subsequent lifting and cooling of cloud droplets containing insoluble particles (immersion freezing), 4) contact freezing, which occurs via collisions of particles with supercooled cloud droplets.
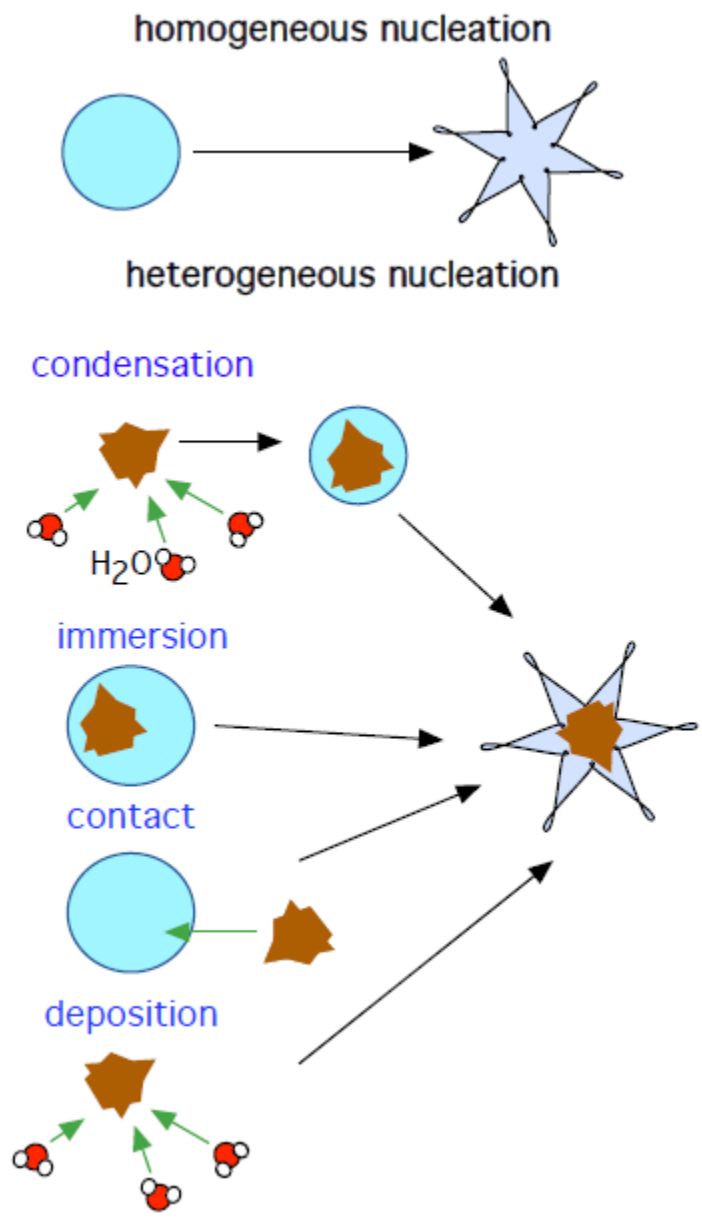
2028   **Figure 35.** Illustration of homogeneous nucleation and heterogeneous nucleation mechanisms.

2029   Heterogeneous nucleation can occur via deposition nucleation, concensation freezing, immeriosn freezing,

2030   and contact freezing.Reprinted with permission from ref 443 by Freedman. Copyright 2011 American

2031   Chemical Society.

2032

2033   Mineral dust particles may be the most abundant IN in the troposphere,[58,74,75] and the ice nucleation

2034   activity of fresh mineral dust particles (and also other types of aerosol particles) has been recently

2035   discussed in several excellent review papers.[140,167,237,238,447,448] In the last several years, numerous

2036   laboratory studies have suggested that atmospheric aging processes can substantially change the

2037   ice nucleation activity of mineral dust particles, as will be discussed here. Hoose and Möhler [238]

2038   briefly summarized the effect of atmospheric chemical reactions on the IN activity of mineral dust

2039   particles and below we expand on this discussion.

2040

2041   The impacts of change in IN activity due to atmospheric aging processes have been supported by

2042   several modeling studies. For example, using parameterizations based on their laboratory

2043   measurements, Kulkarni et al.[449] simulated the influence of particle coatings on the ice crystal

2044   number concentration and the ice water content in clouds over the Southern Great Plain (SGP) site

2045   near Lamont, Oklahoma, USA. As shown in Figure 36a, under water sub-saturation conditions

2046   where only deposition nucleation is possible, the modeled monthly mean ice crystal number for

2047   the coated case (aged dust particles) was about one order of magnitude lower than the uncoated

2048   case (fresh dust particles).[449] Under water super-saturation conditions (Figure 36b), both the

2049   simulated ice crystal number and ice water content are higher in the uncoated case than in the

2050   coated case;[449] the difference between them in regions with pressure <600 hPa is significantly

2051   smaller,[449] and this is partly due to that the difference between the IN activity of uncoated and

2052   coated dust particles (illite in this case) is smaller at lower temperatures.[449] Girard et al.[450] used the

2053   Global Multiscale Environmental Model to assess the potential influence of acid coatings on cloud

2054   and radiation processes in the Arctic during January and February 2007. Their modeling results [450]

2055   suggest that acid coating on dust particles may have significant impacts on cloud microphysics

2056   and radiation over the Central Arctic. More specifically, modification in the cloud microstructures,

2057   due to acid coating, could change the radiation at the top of the atmosphere by 0 and -6 W m^{-2} over

2058   the region which is covered by the Arctic air masses.[450]
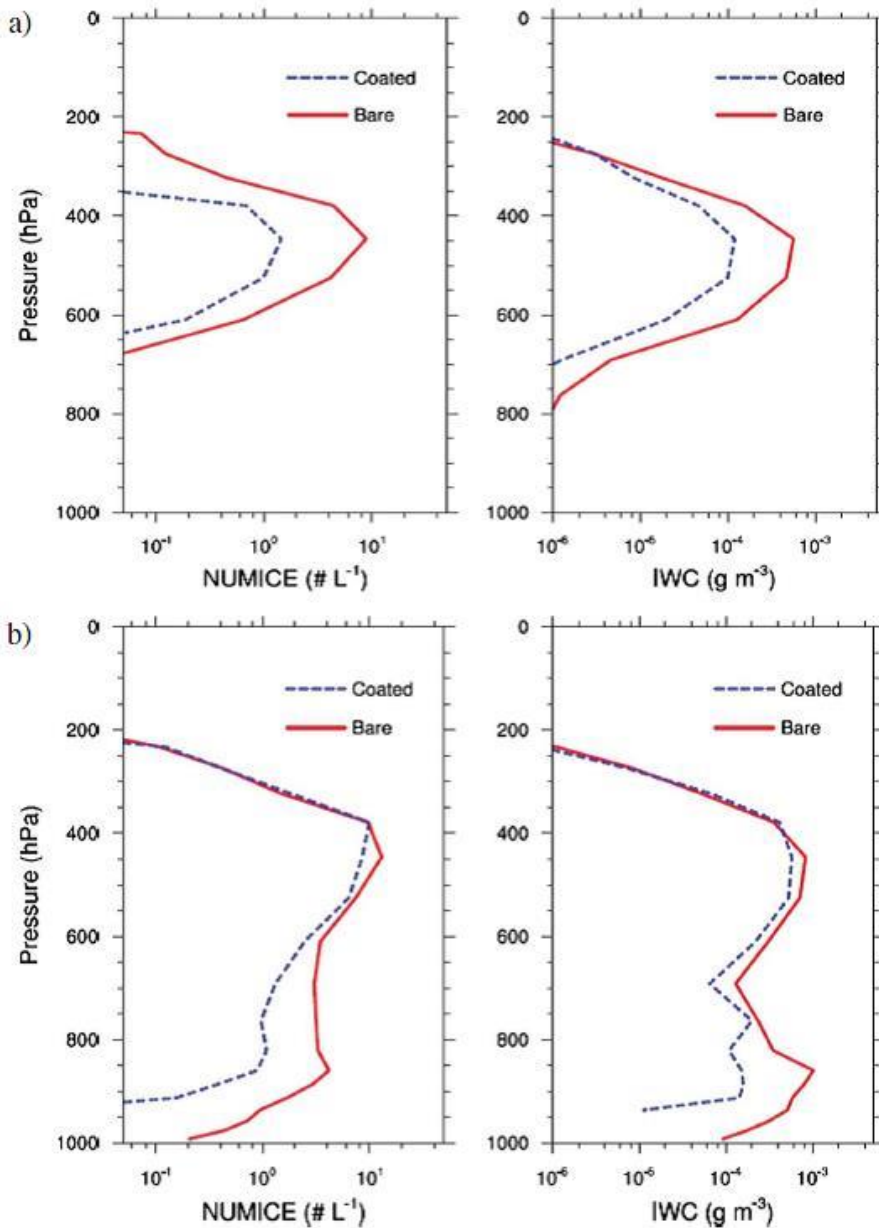
2059

Figure 36. Modeled monthly mean profiles of the ice crystal number concentration (NUMICE) and ice water content (IWC) over the SGP site in (a) deposition ice nucleation mode and (b) condensation/immersion freezing mode. Reprinted with permission from ref 449. Copyright 2014 John Wiley & Sons, Inc.

In this section, we have taken a comprehensive approach to review laboratory studies on the potential effects of atmospheric aging processes on the IN activity of mineral dust particles. This section is divided into several subsections, according to the types of coatings formed on dust particles and/or the trace gases used to react with dust particles to form these coatings.

5.1 Sulfate coating and exposure to SO_2

Table 15 summarizes previous laboratory studies which investigated the efffects of sulfate coating and reaction with SO_2 on the IN activity of mineral dust particles. Previous studies were mainly focused the influence of H_2SO_4 and $(NH_4)_2SO_4$ coating on the IN activity of mineral dust particles, and only one study [451] explored the impact due to the heterogeneous reaction with SO_2.

2075 **Table 15.** Summary of laboratory studies on the effects of chemical aging processes on the IN activity of mineral dust particles: sulfate coatings and

2076 reaction with SO_2

coating or trace gases used to form coating	mineral dust	ice nucleation mode	references	major finding
H_2SO_4	aluminum oxide, alumina-silicate, iron oxide	deposition	Archuleta et al. [452]	H_2SO_4 coating largely reduced the IN activity of alumina-silicate particles, had no significant impact for aluminium oxide particles, and may increase the IN activity of iron oxides.
	ATD	deposition	Knopf and Koop [453]	No significant difference in IN activity was observed between fresh and H_2SO_4-coated ATD particles in the deposition nucleation mode.
	ATD, illite	deposition, immersion, condensation	Cziczo et al.[219]	H_2SO_4 coating reduced the IN activity of ATD and illite particles, and the extent of reduction depended on the coating thickness.
	kaolinite	deposition	Eastwood et al.[454]	H_2SO_4 coating reduced the IN activity of kaolinite particles in the deposition nucleation mode.
	illite, kaolinite, montmorillonite, quartz	deposition	Chernoff and Bertram [455]	H_2SO_4 coating substantially reduced the IN activity of illite, kaolinite, montmorillonite, and quartz particles.

ATD	immersion	Niedermeier et al.[456]	H$_2$SO$_4$ coatings could substantially reduce the IN activity of ATD particles in the immersion freezing mode.
ATD	deposition, immersion, condensation	Sullivan et al.[261]	H$_2$SO$_4$ coatings always reduced the IN activity of ATD particles, and the extent of decrease was much larger in the deposition nucleation mode than in the immersion/condensation freezing modes.
ATD	immersion	Niedermeier et al.[221]	Expsoure of H$_2$SO$_4$-coated ATD particles to water vapor resulted in further decrease in the IN activity.
kaolinite	deposition, immersion, condensation	Tobo et al.[440]	H$_2$SO$_4$ coating reduced the IN activity of kaolinite particles in both deposition nucleation and immersion/condensation freezing modes.
kaolinite	deposition, immersion	Wex et al.[457]	For immersion freezing, H$_2$SO$_4$ coating (with a thickness of a few nm or less) largely reduced the IN activity of Fluka kaolinite but did not lead to a significant change for CMS kaolinite. In the deposition nucleation mode, for both types of kaolinite particles, H$_2$SO$_4$ coating led to a decrease in IN activity at RH <95% but an increase in IN activity for RH >95%.

	ATD, illite, montmorillonite, K-feldspar, quartz	deposition, immersion, condensation	Kulkarni et al.[449]	H_2SO_4 coating reduced the IN actitivity of all the dust particles in the deposition nucleation modes, but its effects were not observable in the immersion/condensation freezing modes.
	kaolinite, montmorillonite	deposition	Sihvonen et al.[458]	Treatments of kaolinite and montmorillonite with H_2SO_4 led to compositional and structural changes of the surfaces, causing reduction in IN activity in the deposition nucleation modes.
	feldspar, ATD, illite, kaolinite	immersion	Augustin-Bauditz et al.[459]	H_2SO_4 coating could reduce the IN activity (in the immersion freezing mode) of all the dust particles under investigation, and the largest effect was obserevd for feldspar.
$(NH_4)_2SO_4$	ATD, illite	deposition, immersion, condensation	Cziczo et al.[219]	$(NH_4)_2SO_4$ coatings could reduce the IN activity of ATD and illite particles, and the extent of reduction depended on the coating thickness.
	kaolinite	deposition	Eastwood et al.[454]	$(NH_4)_2SO_4$ coating reduced the IN activity of kaolinite particles in the deposition nucleation mode, though the effects appeared to be less significant compared to H_2SO_4.
	ATD	immersion	Niedermeier et al.[456]	$(NH_4)_2SO_4$ coatings could substantially reduce the IN activity of ATD particles in the immersion freezing mode. Compared to H_2SO_4, the effects of $(NH_4)_2SO_4$ were more significant.

	ATD	deposition, immersion, condensation	Sullivan et al.[261]	In the immersion/condensation freezing modes, exposure of H_2SO_4-coated ATD particles to NH_3 would further suppress the IN activity.
	ATD	immersion	Niedermeier et al.[221]	Expsoure of ATD particles to H_2SO_4 followed by NH_3 led to a signficant reduction in IN activity, compared to fresh particles.
NH_4HSO_4	illite, kaolinite, montmorillonite, quartz	deposition	Chernoff and Bertram [455]	NH_4HSO_4 coatings substantially reduced the IN activity of illite, kaolinite, montmorillonite, and quartz particles, and the effects varied with temperature.
SO_2	montmorillonite	deposition	Salam et al.[451]	After exposure to pure SO_2 for 2.5 h or 45 ppmv SO2 for 70 h at ~0% RH, no significant change in IN activity in the deposition nucleation mode was observed for montmorillonite.

2077

5.1.1 Sulfate coating

Archuleta et al.[452] measured the ice nucleation activity of fresh and H_2SO_4-coated submicron aluminium oxides, alumina-silicate, and iron oxide particles under deposition nucleation mode conditions between -60 and -45 $^{\circ}$C, and found that H_2SO_4 coating influenced the IN activity of different minerals in different ways. For example, although the coating had no significant impact for aluminium oxide particles, it largely reduced the IN activity of alumina-silicate particles.[452] For iron oxides, H_2SO_4 coatings statistically reduced the required RHi (relative humidity with respect to ice) to freeze for iron oxides;[452] in other words, the H_2SO_4 coating may increase the IN activity of iron oxides.

IN activity of fresh and coated ATD and illite aerosol particles were investigated in deposition nucleation, immersion freezing, and condensation freezing modes by Cziczo et al.,[219] using the Aerosol Interactions and Dynamics in the Atmosphere (AIDA) chamber in Karlsruhe, Germany. It was found [219] that coating with H_2SO_4 or $(NH_4)_2SO_4$ would largely reduce the IN activity of ATD particles, and that the super-saturations required by freezing coated ATD particles often approached those for homogeneous freezing of aqueous H_2SO_4 and $(NH_4)_2SO_4$ solution alone. Inhibition of ice nucleation by H_2SO_4 and $(NH_4)_2SO_4$ coatings was also observed for illite particles, though the effect was smaller compared to ATD particles.[219] In addition, they [219] observed that dust particles coated with less material were activated earlier than those coated with more material, suggesting that the amount of coating determines to which extent the IN activity of dust particles is reduced. Another study by Niedermeier et al.[456] suggested that H_2SO_4 and $(NH_4)_2SO_4$ both could significantly reduce the IN activity of ATD particles in the immersion freezing mode (233.15-239.15 K), and the effect of $(NH_4)_2SO_4$ coating is more significant than H_2SO_4. In contrast, an earlier study by Knopf and Koop [453] did not observe significant difference in the ice nucleation ability between fresh and H_2SO_4-coated ATD particles in the deposition nucleation mode.

2103

2104 Eastwood et al.[454] investigated the deposition nucleation properties (represented by ice nucleation

2105 onset conditions, defined as the RHi and temperature at which the first ice nucleation event was

2106 observed) of fresh and coated kaolinite particles over 233-246 K. As shown in Figure 37, it was

2107 found that H_2SO_4 coatings drastically reduced the ice nucleating ability of kaolinite particles,

2108 increasing the RH*i* required for ice nucleation by approximately 30% across the entire temperature

2109 range they investigated.[454] On the other hand, the decease of ice nucleation activity due to

2110 $(NH_4)_2SO_4$ coating was much smaller at 245 K compared to that at 236 K.[454] Tobo et al.[440] also

2111 suggested that H_2SO_4 coating reduced the IN activity of kaolinite aerosol particles for both

2112 deposition nucleation and immersion/condensation freezing modes for temperature between -34

2113 to -26 °C.
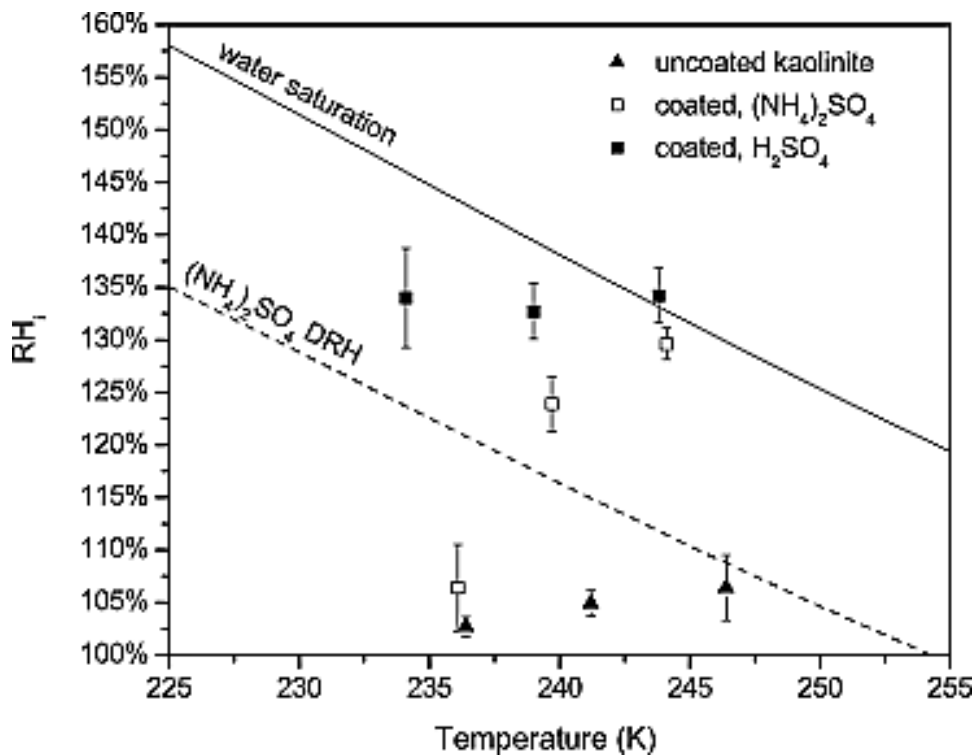
2114

2115 **Figure 37.** Summary of ice nucleation onset conditions for uncoated, H_2SO_4-, and $(NH_4)_2SO_4$-coated

2116 kaolinite particles. The error bars represent 95% confidence intervals based on at least six measurements

2117 per data point. Reprinted with permission from ref 454. Copyright 2009 John Wiley & Sons, Inc.

2118

2119   The effects of H_2SO_4 and NH_4HSO_4 coatings on the IN activity of several mineral dust particles

2120   in the deposition nucleation mode from 234-247 K were examined by Chernoff and Bertram.[455]

2121   They [455] found that H_2SO_4 coatings increased the onset RH*i* (and thus reduced the IN activity) by

2122   ~30% for kaolinite and illite and ~20% for montmorillonite and quartz. Additionally, it was found

2123   by Chernoff and Bertram [455] that NH_4HSO_4 coatings also impair the IN activity of kaolinite

2124   particles, increasing the onset RH*i* by 18-26%, depending on the temperature under which the ice

2125   nucleation occurred.

2126

2127   Sullivan et al.[261] investigated the change in ice nucleation properties of 300 nm ATD particles (in

2128   both deposition nucleation and immersion/condensation freezing modes) after being exposure to

2129 H_2SO_4 alone or H_2SO_4 followed by NH_3, and some representative results are shown in Figure 38.

2130   Several conclusions have been drawn by this study:[261] i) heating of ATD particles in a thermal

2131   denuder up to 200 ^oC did not lead to significant change in their IN activity; ii) H_2SO_4 coating

2132   always reduced the IN activity of ATD, compared to fresh particles, and the extent of decrease is

2133   much larger in the deposition nucleation mode than the immersion/condensation freezing modes;

2134   iii) heating the H_2SO_4-coated ATD particles further decreased IN activity in the

2135   immersion/condensation freezing mode, probably because heating may accelerate the reaction of

2136   coated H_2SO_4 with ATD particle surface; and iv) in the immersion/condensation freezing modes,

2137   subsequent exposure of H_2SO_4-coated ATD particles to NH_3 would further suppress the IN activity.
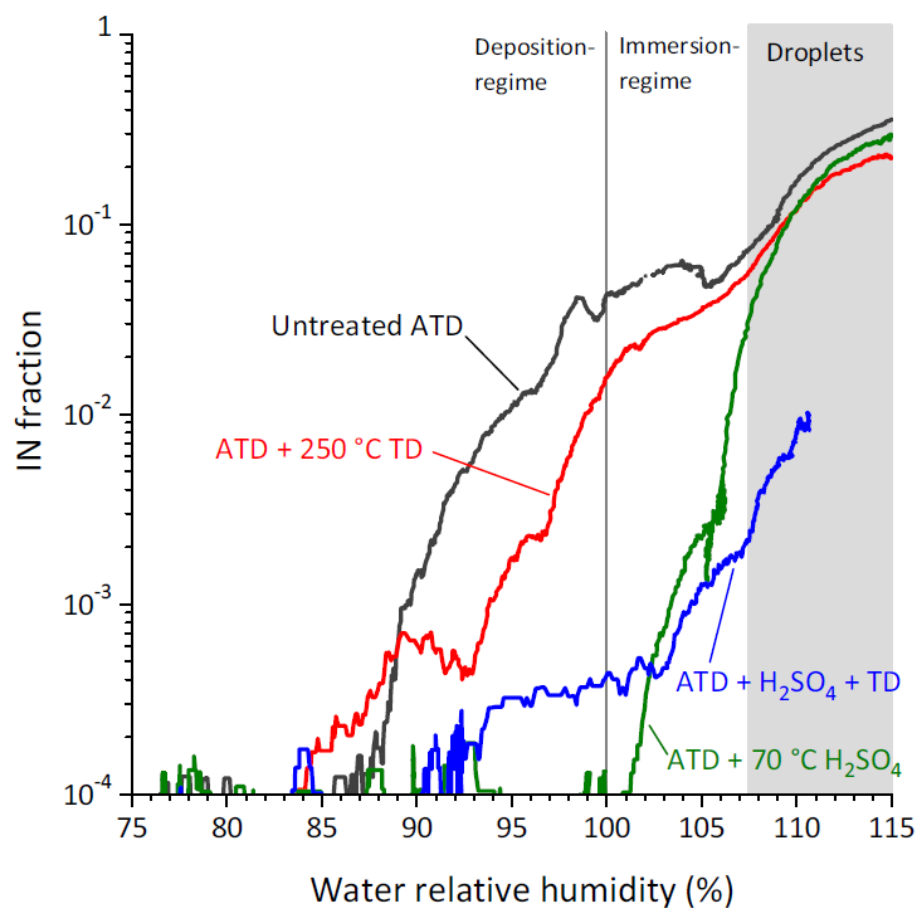
Figure 38. Measured fractions of 300 nm fresh and aged ATD particles which were activated to ice crystals at -30 °C as a function of RH. Black curve: untreated ATD; red curve: ATD heated in the thermodenuder (TD) at 250 °C; green curve: ATD coated with sulphuric acid; blue curve: ATD coated with sulfuric acid and then heated in the TD at 250 °C. In the region (RH >107%) covered by the grey box, measurements were not reliable because droplets could survive in the evaporation region (of the ice nuclei counter) and therefore could not be distinguished from ice crystals. Reprinted with permission from ref 261. Copyright 2010 Copernicus Publications.

Using an Aerosol Mass Spectrometer and an Aerosol Time of Flight Mass Spectrometer, Reitz et al.[220] simultaneously measured the composition of H_2SO_4-coated ATD particles (the IN activity of which were studied by Sullivan et al.[261]), and found that condensation of H_2SO_4 vapor onto ATD particles not only resulted in the formation of a H_2SO_4 coating on the particle surface but also led

2151   to reactions which produced metal (including Na, K, Mg, Al, and etc.) sulfate, ammonium metal

2152   sulfate, and ammonia sulfate on the surface. These surface modifications may be responsible for

2153   that observed decrease in IN activity of ATD particles.[220] In the same campaign as Sullivan et al.[261]

2154   and Reitz et al.,[220] Niedermeier et al.[221] found that additional exposure of H_2SO_4-coated ATD

2155   particles to water vapor could further strongly reduce their IN activity, and this may be caused by

2156   that the presence of water could accelerate the chemical reaction of H_2SO_4 coating with particle

2157   surface, leading to further depletion of ice nucleation active sites on the surface.

2158

2159   Using the Leipzig Aerosol Cloud Interaction Simulator, Augustin-Bauditz et al.[459] measured the

2160   IN activity of fresh (with mobility diameters of 300 nm) and H_2SO_4-coated dust particles in the

2161   immersion freezing mode. As shown in Figure 39, H_2SO_4 coating could reduce the IN activity of

2162   all the dust particles (including feldspar, ATD, illite, and kaolinite) from around -38 ^{o}C to -32 ^{o}C,

2163   and the largest suppression in IN activity was observed for feldspar particles.[459]

2164
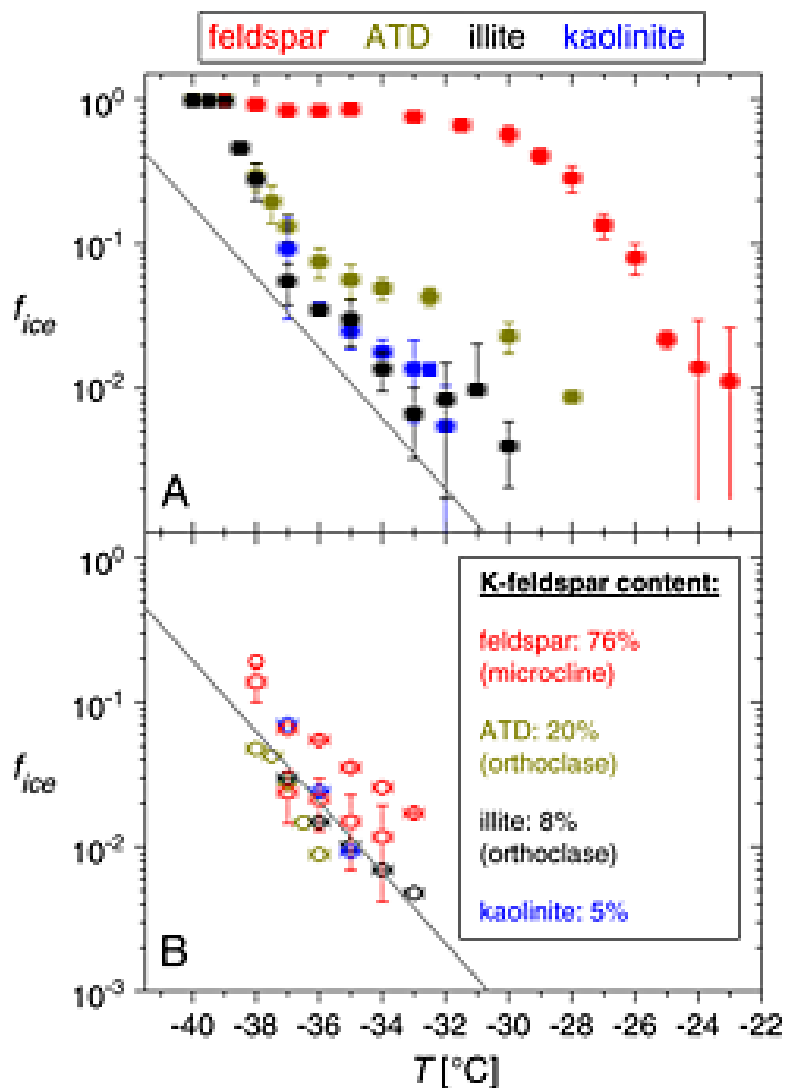
Figure 39. Measured ice nucleation fractions of (a) uncoated particles and (b) particles coated with sulfuric acid (circles: coating at 70 °C; squares: coating at 80 °C). Reprinted with permission from ref 459. Copyright 2014 John Wiley & Sons, Inc.

Sihvonen et al.[458] found that the treatment with H_2SO_4 could cause reduction in IN activity for kaolinite and illite particles in the deposition nucleation mode. They [458] also used X-ray diffraction, TEM, and inductively coupled plasma-atomic emission spectroscopy to measure the physical and chemical changes of dust particle treated with H_2SO_4. Formation of new products and structural change of the surface were observed, both probably explaining the suppression of IN activities

2175 after treatment with H_2SO_4.[458] This study [458] shows the importance of post-analysis of modified

2176 dust particles to better understand the impact of chemical processing on IN activity.

2177

2178 Kulkarni et al.[449] studied the IN activity of 200 nm fresh and H_2SO_4-coated ATD, illite,

2179 montmorillonite, K-feldspar, and quartz particles as a function of temperature (-35 to -25 ^{o}C) and

2180 RH (75-110%). It was found [449] that H_2SO_4 coating led to reduction in IN activity of all five

2181 different types of dust particles in the deposition nucleation mode; nevertheless, its effect under

2182 water-super-saturation conditions (i.e. in immersion/condensation freezing modes) was not

2183 observable for any type of dust particles.[449] X-ray diffraction measurements showed that coating

2184 dust particles with H_2SO_4 changed the surface crystalline nature and resulted in surface structural

2185 disorders.[449] Therefore, it was further concluded that the suppression of IN activity of dust particles

2186 in the deposition freezing mode due to H_2SO_4 coating was caused by the lack of structured order

2187 of the surface after treatment with H_2SO_4.[449]

2188

2189 The effect of H_2SO_4 (with a thickness of a few nm or less) on the IN activity of two different types

2190 of kaolinite particles was investigated by Wex et al.[457] in the deposition nucleation and immersion

2191 freezing mode. For immersion freezing, while H_2SO_4 substantially reduced the IN activity of Fluka

2192 kaolinite particles, it did not lead to significant change to Clay Mineral Society kaolinite.[457] The

2193 following explanation was provided:[457] Fluka kaolinite contained K-feldspar which is very IN

2194 active [141] but the other type of kaolinite did not, and H_2SO_4 coating could efficiently react with K-

2195 feldspar and thus largely reduce its IN activity. Under water sub-saturation conditions, H_2SO_4

2196 coating suppressed the ice nucleation of kaolinite particles for RH <95% while a significant

2197 increase in ice nucleation activity was observed for RH >95%.[457] For RH in the range of 95-100 %,

2198 H_2SO_4 coating kaolinite particles may become aqueous droplets with solid inclusion, and therefore

2199 immersion freezing actually dominated over deposition freezing.[457]

2200

2201   Though many studies have shown that sulfate coating could significantly modify the IN activity

2202   of mineral dust particles, fundamental understanding of deactivation mechanisms on the molecular

2203   level is lacking. Yang et al.[460] explored why sulfuric acid coatings influence the IN activity of

2204   mineral dust particles. They [460] probed the structure of water at the interface between mica (used

2205   as a surrogate as dust particles) and aqueous D_2SO_4 solutions of different concentrations using sum

2206   frequency generation vibrational spectroscopy. In this study [460] deuterated water and sulfuric acid

2207   were used to avoid the overlap with the IR absorption peak of mica at 3620 cm^{-1}.[461] The spectra of

2208   interfacial D_2O molecules show two peaks at around 2375 and 2550 cm^{-1}. These two peaks are

2209   sometimes called the "ice-like" and the "liquid-like" peaks, because their peak positions are similar

2210   to those of bulk ice and liquid water, respectively.[286,462] It is usually believed that the interfacial

2211   water molecules observed by SFG are more ordered than those in the bulk because SFG is largely

2212   depressed in a disordered medium.[463] As shown in Figure 40, Yang et al.[460] found that when the

2213   concentration of D_2SO_4 in the aqueous solution increased from 0 to 5 M, the two peaks at 2375

2214   and 2550 cm^{-1} both gradually disappeared.
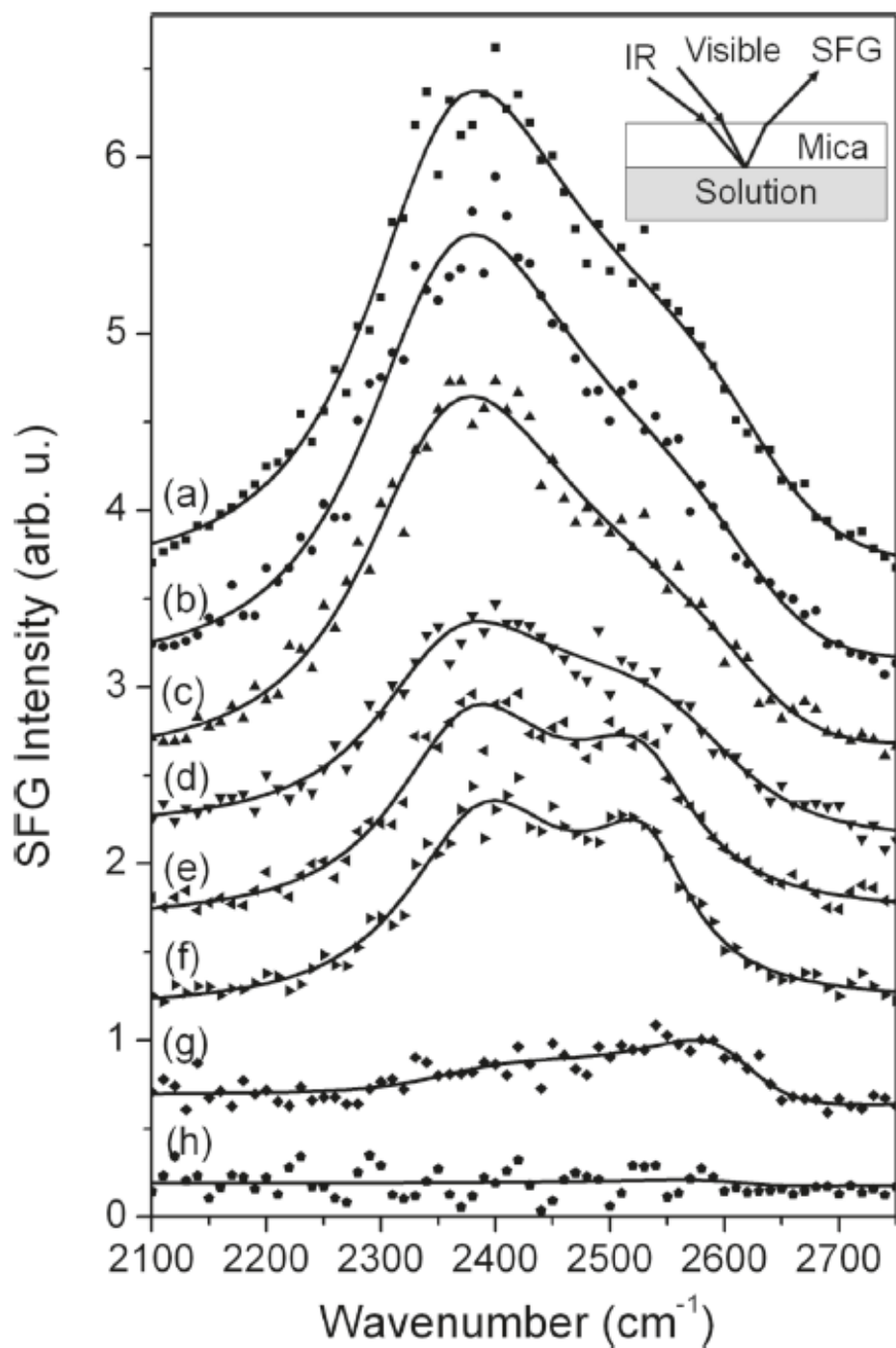
2215

Figure 40. SFG spectra of D_2O/mica interfaces with D_2SO_4 concentrations of (a) 0, (b) 5×10^{-6}, (c) 5×10^{-5}, (d) 5×10^{-4}, (e) 0.005, (f) 0.05, (g) 0.5, and (h) 5 M. The inset shows the schematic layout of the spectroscopic setup. Reprinted with permission from ref 460. Copyright 2011 American Chemical Society.

2216

2217

2218

2219

2220   The observation shown in Figure 40 is interpreted as the reduction of ordered water structures at

2221   the interface with increasing D_2SO_4 concentrations.[460] It was further suggested by Yang et al.[460]

2222   that IN activity is correlated with the presence of structured water at the interface. The reduction

2223   in ordered water structure was due to the combination of several factors,[460] including i) reduced

2224   mica surface potential at low pH, ii) adsorption of sulfate on mica surface, iii) decrease of free

2225   water molecules at higher H_2SO_4 in the aqueous solution. Though it has provided fundamental

2226   insights into the structure of the mineral-aqueous solution interface, the study by Yang et al.[460] was

2227   carried at room temperature instead of those at which ice nucleation may occur.

2228

2229   Very recently second harmonic generation spectroscopy has been used to monitor the mineral-

2230   water interface during the occurrence of immersion freezing in an in-situ and online manner.[464]

2231   Local ordering of water on the mica (which provides a good ice nucleating surface) was observed

2232   by SFG during cooling down to the freezing point;[464] in contract, no significant change in water

2233   structure at sapphire (which is a poor ice nucleator) surface was observed during cooling.[464] This

2234   is supported by a recent molecular dynamics simulation study,[465] suggesting that layering and

2235   ordering of interfacial liquid water are critical to heterogeneous nucleation of ice. This novel

2236   application developed by Abdelmonem et al.[464] has a great potential to help understand how

2237   heterogeneous ice nucleation occurs in general and more specifically how chemical aging alters

2238   the IN activity at the molecular level.

2239   **5.1.2 Exposure to SO₂**

2240   To our knowledge only one previous study [451] explored the effect of SO_2 exposure on the IN

2241   activity of mineral dust particles. No significant change in deposition ice nucleation efficiency was

2242   observed for montmorillonite particles after being exposed to pure SO_2 for 2.5 h or 45 ppmv SO_2

2243   for 70 h at room temperature and ~0% RH.[451]

5.2 Organic coatings

Several previous studies have investigated how organic coatings can alter the IN activities of mineral dust particles, and an overview of these studies is provided in Table 16.

2249   **Table 16.** Summary of laboratory studies on the effects of chemical aging processes on the IN activity of mineral dust particles: organic coatings,

2250   and reactions with HNO_3, NH_3, and O_3.

coating or trace gases used to form coating	mineral dust	ice nucleation mode	references	major finding
organic coating	ATD, kaolinite	deposition, immersion, condensation	Möhler et al.[466]	Organic coating formed by ozonolysis of α-pinene could substantially reduced the IN activity of ATD and illite particles, and the extent of decrease depended on the coating thickness.
	ATD	immersion	Niedermeier et al.[456]	ATD particles coated with succinic acid had lower IN activity in the immersion freezing mode, compared to fresh ATD particles
	kaolinite	deposition, immersion, condensation	Tobo et al.,[440]	Levoglusocan coating significantly reduced the IN activity of kaolinite particles in the deposition nucleation mode, while its impact was not observable in the immersion/condensation freezing modes.
	kaolinite	deposition, immersion	Wex et al.,[457]	In the immersion freezing mode, neither succinic acid or levoglusocan changed the IN activity of kaolinite particles. In the deposition nucleation mode, both organic coatings suppressed the IN activity of kaolinite particles for RH below 95%, while a significant increase in IN activity was observed for RH >95%.

131

HNO₃	ATD	deposition, immersion, condensation	Sullivan et al.[375]	In the immersion/condensation freezing modes, exposure to HNO₃(g) has no significant impact on IN activity. For RH <97%, heterogeneous reaction with HNO₃(g) significantly reduced the IN activity of ATD particles; while around the RH of 97-100 % no significant difference in IN activity was observed between fresh and aged particles
	kaolinite and montmorillonite	deposition	Sihvonen et al.[458]	In the deposition nucleation mode, treatment with HNO₃ reduced the IN activity of kaolinite but did not significantly affect the ice nucleation properties of montmorillonite.
	ATD, illite, K-feldspar, and quartz	deposition, immersion, condensation	Kulkarni et al.[467]	In deposition nucleation mode, aged dust particles, except quartz, showed reduced IN activity compared to fresh particles. In the immersion/condensation freezing modes, fresh and aged dust particles exhibited equivalent IN activity.
NH₃	montmorillonite	deposition	Salam et al.[468]	Exposure to pure and 25 ppmv NH₃ could enhance the IN activity of montmorillonite particles in the deposition nucleation mode.
	montmorillonite	deposition	Salam et al.[451]	Exposure to ~100 pptv NH₃ for 70 h increased the ice nucleation efficiency of montmorillonite by a factor of ~2.

| O$_3$ | montmorillonite | deposition | Salam et al.[451] | Exposure of montmorillonite to 200 ppbv O$_3$ for 70 h at room temperature and at 0% RH did not significantly change the IN activity in the deposition nucleation mode. |
| | ATD and kaolinite | deposition, immersion | Kanji et al.,[469] | The change in IN activity after exposure to O$_3$ was found to be complex, depending on O$_3$ concentrations, ice nucleation modes, and minerals. |

2251

2252   The ice nucleation activity (in deposition and immersion/condensation freezing modes) of ATD

2253   and kaolinite aerosol particles with and without secondary organic matter (SOM) coating formed

2254   by the ozonolysis of α-pinene was investigated using the AIDA chamber at 205-210 K.[466] It was

2255   found that the SOM coating could substantially suppress the IN activity of both ATD and illite

2256   particles, and the suppression extent depended on the thickness of the coating.[466] Almost all the

2257   fresh ATD and illite particles with diameters of 0.1-1.0 μm were efficient deposition mode IN at

2258   RHi between 105 and 120%.[466] However, if coated with 17 wt% SOM, only ~20% of ATD

2259   particles were activated to ice crystals at RHi between 115 and 130%;[466] and only 10% of illite

2260   particles were ice-active at RHi between 160 and 170%, if coated with 41 wt% SOM.[466] In another

2261   study by Niedermeier et al.,[456] ATD particles coated with succinic acid were found to have lower

2262   IN activity in the immersion freezing mode (233.15-239.15 K), compared to fresh ATD particles.
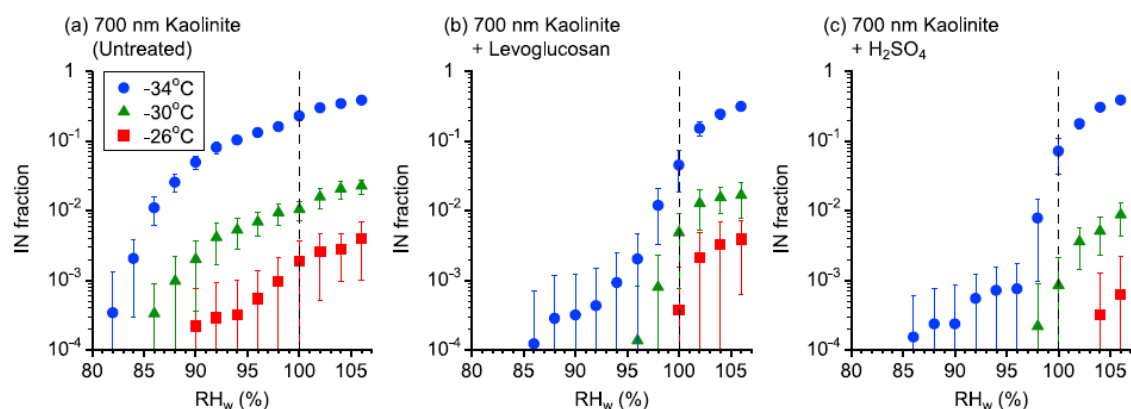
2263

2264   **Figure 41.** Fractions of 700 nm kaolinite particles which were activated to ice particles at -34 (circles), -

2265   30 (triangles), and -26 °C (squares) as a function of RH. (a) fresh kaolinite particles, (b) kaolinite particles

2266   treated with levoglucosan at 93 °C, and (c) kaolinite particles treated with H_2SO_4 at 70 °C. Dashed lines

2267   indicate liquid water saturated conditions. Error bars indicate the standard deviation from multiple

2268   measurements. Reprinted with permission from ref 440. Copyright 2014 John Wiley & Sons, Inc.

2269

2270   Tobo et al.[440] investigated the effects of levoglusocan coating on the IN activity of kaolinite

2271   particles. As shown in Figure 41, they [440] found that for temperature ranging from -34 to -26 °C,

134

2272 levoglusocan coating significantly reduced the IN activity of kaolinite particles for the deposition

2273 nucleation mode while its impact was not observable for immersion/condensation freezing modes.

2274 Wex et al.[457] systematically examined how succinic acid and levoglusocan coatings with a

2275 thickness of a few nm or less could change the IN activity of kaolinite particles in deposition

2276 nucleation and immersion freezing modes. In the immersion freezing mode, neither organic

2277 compounds changed the IN activity of kaolinite particles.[457] Under water sub-saturation conditions,

2278 the effect of organic coatings were more complicated:[457] i) for RH below 95%, both organic

2279 coatings were found to suppress the ice nucleation of kaolinite particles; ii) on the other hand, a

2280 significant increase in ice nucleation activity was observed for RH >95%, probably because in this

2281 RH range mainly immersion freezing instead of deposition nucleation took place (i.e. coated

2282 kaolinite particles at RH >95% may become aqueous particles with solid inclusion).

2283 **5.3 Exposure to HNO$_3$**

2284 Nitrate has been frequently observed to internally mixed with mineral dust particles in the

2285 troposphere by field measurements [158-160,202,429] due to the heterogeneous reactions with

2286 HNO$_3$,[199,227,365,470-473] N$_2$O$_5$,[131-134,136,139] NO$_2$,[474-478] and NO$_3$ radicals.[177,479] Nevertheless, only a

2287 few studies [375,458,467] have investigated whether and how nitrate coatings could alter the IN activity

2288 of mineral dust particles, as summarized in Table 16.

2289

2290 The effects of HNO$_3$ exposure on the IN activity of ATD aerosol particles were investigated by

2291 Sullivan et al.,[375] who reacted 200 nm ATD particles with HNO$_3$(g) in an aerosol flow tube at room

2292 temperature and at different RH and then measured their ice nucleation properties at -30 ºC as a

2293 function of RH. As shown in Figure 42, for RH <97% under which deposition nucleation occurred,

2294 heterogeneous reaction with HNO$_3$(g) significantly reduced the IN activity of ATD particles;[375]

2295 however, for RH>100% where immersion/condensation freezing dominated, the effect of exposure

2296 to HNO$_3$(g) was insignificant.[375] In addition, around the RH of 97-100 % no significant difference

2297   in IN activity was observed between fresh and coated particles.[375] At 97-100 % RH deposition

2298   nucleation dominated for fresh particles; however, at this RH range aged particles may become

2299   aqueous particles (due to the formation of nitrate coating) and thus immersion/condensation

2300   freezing can become the main ice nucleation mechanism. The change in ice nucleation modes

2301   could cause fresh and aged particles to be activated under similar conditions, though their

2302   compositions differ.
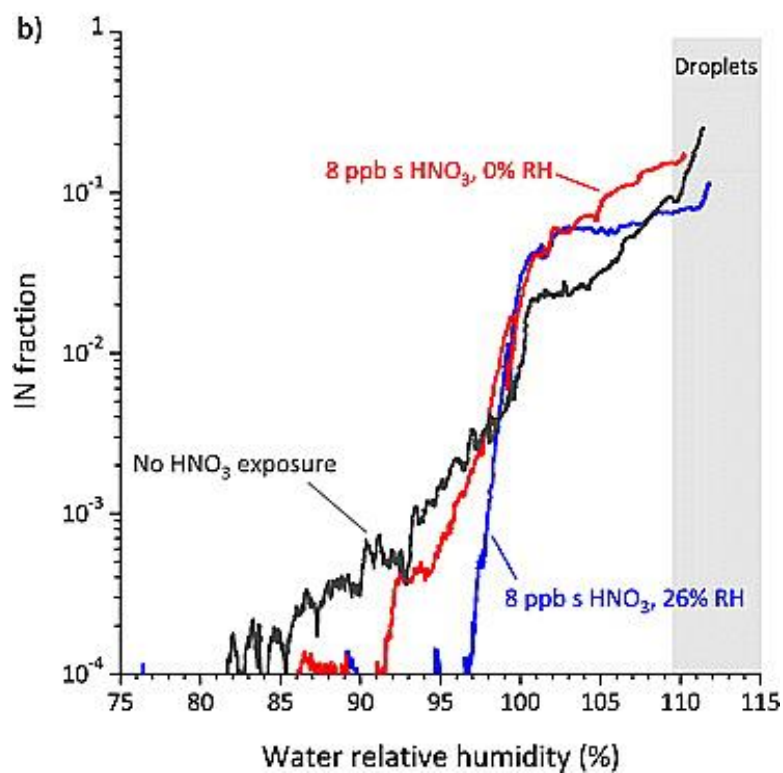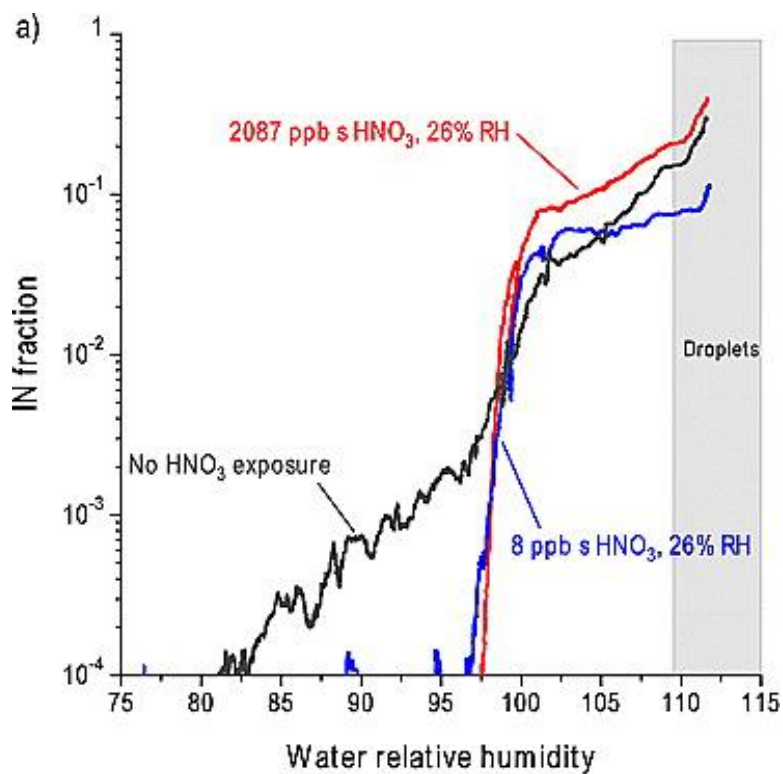
Figure 42. Fractions of 200 nm fresh and HNO$_3$-exposed ATD aerosol particles that were activated to ice crystals at -30 ºC as a function of RH. (a) black curve: no HNO$_3$ exposure; blue curve: HNO$_3$ exposure of 8 ppbv·s at 26% RH; red curve: HNO$_3$ exposure of 2087 ppbv·s at 26% RH. (b) Black curve: no HNO$_3$

2307 exposure; blue curve: HNO$_3$ exposure of 8 ppbv·s at 26% RH; red curve: HNO$_3$ exposure of 8 ppbv·s at 0%

2308 RH. In the region covered by the grey box, droplets may interfere with IN measurements and therefore

2309 these measurement may not be reliable. Reprinted with permission from ref 375. Copyright 2010 John

2310 Wiley & Sons, Inc.

2311

2312 In addition, exposure to HNO$_3$ at 26% RH, compared to that at 0%, will more significantly reduce

2313 the deposition nucleation activity of ATD particles for RH<97%,[375] as shown in Figure 42. This

2314 may be explained by the fact that heterogeneous reaction of HNO$_3$ with ATD particles is

2315 accelerated and thus more particulate nitrate is formed at higher RH.[213]

2316

2317 Sihvonen et al.[458] showed that in the deposition nucleation mode, while treatment with HNO$_3$

2318 decreased the IN activity of kaolinite, it did not significantly affect the ice nucleation properties of

2319 montmorillonite. In another study, Kulkarni et al.[467] investigated the ice nucleation activity of ATD,

2320 illite, K-feldspar, and quartz as a function of temperature and RH before and after reaction with

2321 HNO$_3$. They [467] found that at subsaturated conditions (i.e. in deposition nucleation mode), aged

2322 dust particles, except quartz, showed reduced IN activity compared to fresh particles. In contract,

2323 at super-saturation conditions (i.e. in immersion/condensation freezing modes), fresh and aged

2324 dust particles exhibited equivalent IN activity.[467]

2325 **5.4 Exposure to NH$_3$**

2326 As summarized in Table 16, the impacts of heterogeneous reaction with NH$_3$ have been

2327 investigated by two previous studies.[451,468] Salam et al.[468] studied the ice nucleation activity of

2328 NH$_3$-exposed montmorillonite particles under the deposition nucleation mode and provided the

2329 first experimental evidence that exposure to NH$_3$ could enhance the IN activity of mineral dust

2330 particles. They [468] suggested that ice nucleation activity of montmorillonite particles increased

2331 with exposure time to NH$_3$. It was further observed by Salam et al.[468] that compared to fresh

138

montmorillonite particles, the activation temperature (defined as the highest temperature at which >1% particles were activated to ice crystals) at RH of 100% and 90% was 15 $^{\circ}$C higher for particles exposed to pure NH$_3$, and was 5 $^{\circ}$C higher for particles exposed to 25 ppmv NH$_3$. In a following study, Salam et al.[451] further measured the deposition ice nucleation activity of montmorillonite particles after exposed to NH$_3$ of ~100 pptv (a typical atmospheric concentration) for 70 h, and found that this exposure increased the ice nucleation efficiency of montmorillonite by a factor of around two.

5.5 Exposure to O$_3$

The influence of heterogeneous reaction with O$_3$ on the IN activity of mineral dust particles have also been explored,[451,469] as shown in Table 16. Salam et al.[451] exposed montmorillonite particles to 200 ppbv O$_3$ for 70 h at room temperature and ~0% RH. No clear change in deposition nucleation efficiency was observed after exposure, compared to fresh particles.[451] Kanji et al.[469] systematically investigated the IN activity of ATD and kaolinite aerosol particles in deposition and immersion modes (between 233 and 263 K) before and after exposure to 0.4-4.3 ppmv O$_3$ at room temperature and 0% RH in a stainless steel aerosol chamber. Complex response of IN activity to O$_3$ exposure was reported:[469] 1) after exposure to 430 ppbv O$_3$ for ~130 min, kaolinite particles showed enhanced ice nucleation activity in both deposition and immersion modes over the temperature range (233-263 K) they studied, whereas the change of IN activity was insignificant for ATD particles in either deposition or immersion nucleation modes; 2) compared to fresh particles, kaolinite particles exposed to 1.4 ppmv O$_3$ for ~130 min showed a lower ice nucleation activity over 232-240 K in the deposition mode, and only slight suppression of IN activity was observed for the immersion over 233-263 K; 3) additionally, ATD particles exposed to 4.3 ppmv O$_3$ for ~130 min, compared to unexposed particles, showed significantly lower IN activity in both deposition and immersion modes over 233-263 K.

5.6 Summary

Increasing numbers of laboratory studies have shown that chemical aging processes can substantially change the IN activity of mineral dust particles. Furthermore, several modeling studies have suggested that these changes can have important impacts on cloud microphysics, radiation, and thus the climate. In the last two decades significant progress has been made in this field, and a comprehensive and systematic picture is emerging. Nevertheless, our understanding in the effects of atmospheric aging processes on the IN activity of mineral dust particles is still not comprehensive or quantitative.

The same coating formed on dust particles may influence on the IN activity for different minerals and different ice nucleation modes in different ways. In addition, it is not unusual that inconsistent results have been reported by different studies for the same coating on the same type of dust in the same ice nucleation mode. For example, most studies suggest that sulfuric acid coating typically reduces the IN activity, while the effect of HNO_3 coating is largely unclear. This may be partly due to the fact that it is still nontrivial or even challenging to measure the IN activity of aerosol particles. What makes it more complicated is that the formation of coating could change the mode in which dust particles are activated to ice crystals (e.g., from deposition nucleation to condensation/immersion freezing, due to the increase in CCN activity of aged dust particles).[375] Several studies have revealed that the extent of IN activity changes depends on the thickness of coatings;[219,375,466] however, a quantitative understanding of effects of chemical aging processes on IN activity of mineral dust particles is still lacking.

Furthermore, it is still not clear at the molecular level why and how chemical processes with acids usually turn to reduce the IN activity of mineral dust particles. It may be largely due to the fact that we still do not understand why some minerals are more ice nucleation active than others and

2381 the nature of ice nucleation active sites on the surface.[443,480] Five factors have been empirically

2382 proposed to promote heterogeneous ice nucleation.[167] 1) It is typically assumed that the number of

2383 ice nucleation active sites is proportional to the particle surface area.[238,481-484] 2) Heterogeneous

2384 ice nucleation is preferentially initiated by surfaces of insoluble materials. 3) The ability of a

2385 surface to form hydrogen bonds usually promotes water adsorption and ice nucleation. 4) Surfaces

2386 which have similar crystallographic structures to that of ice will promote ice nucleation. 5)

2387 Morphological, chemical, and electrical heterogeneities on the surface can also promote ice

2388 nucleation. Several hypotheses have been suggested to explain why exposure to acid gases (e.g.,

2389 H_2SO_4 and HNO_3) may suppress the IN activity of mineral dust particles. Laboratory studies

2390 [220,261,458] have shown that reaction products which are more soluble (and thus less IN active) can

2391 lead to the loss of or cover the active sites. Chemical aging processes can also lead to structural

2392 changes of surfaces, alter their crystalline nature, and cause structural disorders,[443,449,458] therefore

2393 reducing their ice nucleation activity. The patterns in which surfaces interact with water can also

2394 be changed due to chemical processes, resulting in changes in heterogeneous ice formation.[460] In

2395 addition, a few recent studies [457,459] also suggest that the loss/deactivation of feldspar (which is

2396 very IN active) heterogeneities may be responsible for the decrease in IN activity of clay minerals.

2397 **6 Concluding remarks and recommendations for future studies**

2398 Interactions of mineral dust particles with water vapor influence their heterogeneous reactivity

2399 towards reactive trace gases, their hygroscopicity and hence their ability to directly scatter and

2400 absorb solar and terrestrial radiation, and their activity to serve as CCN and IN and therefore their

2401 roles in indirect radiative forcing. Additionally, atmospheric heterogeneous and multiphase

2402 reactions will change their chemical compositions after mineral dust particles are lifted into the

2403 troposphere, as a result modifying the interactions of mineral dust particles with water vapor. A

2404 complete and in-depth understanding of the interactions of fresh and aged dust particles with water

2405 vapor will help us assess the roles of mineral dust aerosols in many aspects of atmosphere

2406 chemistry and climate change.

2407

2408 In this article we provide a comprehensive review of water adsorption, hygroscopicity, and CCN

2409 activity of fresh and aged mineral dust particles, and the effects of chemical aging on the IN activity

2410 of mineral dust particles. As shown in this review, previous studies have largely improved our

2411 understanding of the interactions of mineral dust particles with water vapor. Brief summaries are

2412 provided in Section 4.11 for water adsorption, hygroscopicity, and CCN activities of fresh and

2413 aged mineral dust particles and in Section 5.6 for the IN activity of aged mineral dust particles.

2414 However, there still remain many open questions which can only be satisfactorily answered

2415 through a close collaboration among laboratory studies, field measurements, modeling work, and

2416 theoretical analysis. Several future directions are recommended here in order to address these

2417 challenges:

2418

2419 (1) Large discrepancies still exist for water adsorption and hygroscopicity of fresh mineral dust

2420 particles reported by different studies, especially for clay minerals. Reasons for these discrepancies

2421 are largely unclear. Further measurements are recommended to solve these discrepancies, and

2422 well-coordinated collaborations in which same dust samples are distributed to different groups and

2423 experimental results are intercompared will be very helpful. Most experimental data are only

2424 presented in graphical forms, yet numerical tabulation of the data can enhance their accessibility

2425 and usability.

2426

2427 (2) Previous studies which measured water adsorption and hygroscopicity of fresh mineral dust

2428 particles were mainly carried out at RH lower than 80%. It is recommended that future

2429 measurements should be extended to RH above 90% or even 99%. Nevertheless, it is non-trivial

2430   to do these measurements at RH very close to 100%. In addition, most previous studies have been

2431   performed at or near room temperature, but temperature varies from ~200 to ~300 K in the

2432   troposphere, and profound effects of temperature on the hygroscopicity have been reported for

2433   some materials of atmospheric relevance.[485-487] Therefore, the effects of temperature on the water

2434   adsorption and hygroscopicity of mineral dust particles need to be systematically investigated by

2435   future studies.

2436

2437   (3) Large numbers of previous laboratory studies have suggested that chemical aging could

2438   substantially increase the water adsorption ability, hygroscopicity, and CCN activity of mineral

2439   dust particles. However, most of these studies focused on $CaCO_3$, and the effect of chemical aging

2440   should also been examined for more abundant minerals and real dust samples. It is also

2441   recommended that future laboratory work should be carried out at atmospherically relevant

2442   conditions (e.g., concentrations of reactive trace gases, reaction time, and RH etc.). Studies of this

2443   type can help to answer how rapidly water adsorption, hygroscopicity, and CCN activity of mineral

2444   dust particles will be changed during their residence in the atmosphere.

2445

2446   (4) The interactions of mineral dust particles with water vapor influences, and is influenced by,

2447   interactions with reactive trace gases. Such complex interactions are likely to involve mass transfer

2448   [306,488-492] and chemical reactions in and between all three different phases (gas, liquid, and solid)

2449   in nonlinear manners.[172,173,493-499] Multiphase models have been developed in order to integrate

2450   these processes and have been applied to study chemical reactions and phase transition of organic

2451   particles.[499-502] If developed for and applied to mineral dust chemistry, they can be very helpful for

2452   a better understanding of the complex interactions between mineral dust particles, water, and

2453   reactive trace gases.

2454

2455 (5) Many field measurements have shown that coated dust particles in the troposphere have

2456 different phase transition properties when compared to uncoated dust particles. However, most of

2457 these studies are of a qualitative nature. It will be useful for future field measurements to

2458 quantitatively and simultaneously determine 1) the amount and type of coating formed on ambient

2459 mineral dust particles, and 2) the change of water adsorption, hygroscopicity, or CCN activity of

2460 these coated mineral dust particles. Measurements of this type, though very challenging, will

2461 largely improve our understanding of the effects of chemical aging processes in the atmosphere.

2462

2463 (6) The impacts of heterogeneous reactions on trace gases and compositions of mineral dust

2464 particles have been assessed by many regional and global models in the last 2-3 decades. However,

2465 their effects on the hygroscopicity and CCN activity of mineral dust particles have seldom been

2466 investigated by modeling studies. Modeling analyses will give a better understanding, on a much

2467 larger spatial and temporal scale, of the atmospheric relevance of change in hygroscopicity and

2468 CCN activity of mineral dust particles due to chemical aging processes.

2469

2470 (7) Compared to the effects of atmospheric aging processes on hygroscopicity and CCN activity,

2471 the impact on IN activity has been much less widely investigated. While sulfate coatings have

2472 received some attention, much less has been paid to the effects of nitrate and organic species on

2473 the IN activity of mineral dust particles. In order for a more comprehensive understanding, further

2474 studies are needed on the effect of different coatings, especially nitrate and organic, on the IN

2475 activity of mineral dust particles. It is also highly desirable to carry out aging experiments at

2476 atmospheric relevant conditions, and to control the amount of coatings and/or exposure conditions

2477 in more quantitative and atmospherically relevent ways. One of the current limitations on our

2478 ability to understand how chemical aging changes the IN activity of mineral dust particles is to

2479 correctly mimic atmospheric processing of aerosol particles in the laboratory. For example, it is

2480   critical that surface coating composition and thickness realistically mimic what is present in the

2481   atmosphere. Since coatings, in particular, appear to effectively deactivate effective mineral dust

2482   ice nuclei,[74,219] future studies will need to consider how to properly compare laboratory particles

2483   to atmospheric measurements.

2484

2485   (8) Mechanisms that change IN activity of dust particles due to atmospheric aging processes are

2486   largely unknown on a molecular level, and a collaborative effort from experts in aerosol/cloud

2487   chemistry microphysics, surface science and surface chemistry, and theoretical chemistry will be

2488   very beneficial.

2489

2490   (9) Field measurements are required to understand if and to which extent the IN activity of mineral

2491   dust particles in the troposphere is influenced by a variety of aging processes during transport.

2492   Modeling studies are encouraged to include more laboratory-derived and realistic

2493   parameterizations for the effects of aging processes on IN activity in their simulations, in order to

2494   better evaluate the effects of atmospheric aging processes on IN activity, cloud microphysics, and

2495   climate impacts.

2496

2497   **Author information**

2498   **Corresponding author**

2499   *Phone: (319)335-1392. Fax: (319)353-1115. E-mail: vicki-grassian@uiowa.edu.

2500   **Notes**

2501   The authors declare no competing financial interest.

Biographies

Mingjin Tang is currently a postdoctoral fellow in Professor Grassian's group, Department of Chemistry, University of Iowa, USA. Before arriving in the USA in the beginning of 2015, he received his BSc (in 2005) and MSc (in 2008) from Peking University (China) under the supervision of Professor Tong Zhu, and then received his PhD (in 2011) in Max Planck Institute for Chemistry and Johannes Gutenberg-Universität Mainz (Germany), advised by Drs. John N Crowley, Ulrich Pöschl, and Thorsten Hoffmann. After a short postdoc in Max Planck Institute for Chemistry, he joined Dr. Markus Kalberer's group at Department of Chemistry, University of Cambridge (UK) as a postdoctoral fellow. His research interest focuses on the fundamental physical chemistry of atmospheric aerosol particles and how physicochemical changes of aerosol particles influence air quality, clouds, and climate. He would like to thank Professor Tong Zhu for bringing him into atmospheric heterogeneous and multiphase chemistry studies as a young scientist in Peking University.

Daniel J. Cziczo is currently the Victor P. Starr Professor of Atmospheric Chemistry in the Department of Earth, Atmospheric and Planetary Sciences and Civil and Environmental Engineering at the Massachusetts Institute of Technology, USA. His research revolves around the interrelationship of particulate matter and cloud formation. His group utilizes laboratory and field studies to elucidate how small particles interact with water vapor to form droplets and ice crystals which are important players in the Earth's climate system. Experiments include using small cloud chambers in the laboratory to mimic atmospheric conditions that lead to cloud formation and observing clouds in situ from remote mountaintop sites or through the use of research aircraft.

As of January 2016, Vicki H. Grassian is a Distinguished Professor at the University of California San Diego (UCSD) with appointments in Chemistry and Biochemistry, Nanoengineering and

Scripps Institution of Oceanography. She is also Distinguished Chair of Physical Chemistry and currently serves as co-director at the Center for Aerosol Impacts on Climate and the Environment centered at UCSD. Prior to her move to UCSD, she was the F. Wendell Miller Professor in Chemistry at the University of Iowa. Her research area focuses on environmental molecular surface science, heterogeneous and multiphase chemistry of atmospheric aerosol particles, the impact of atmospheric aerosol on air quality and climate, and environmental and health aspects of nanoscience and nanotechnology.

Acknowledgement

References

(1)   Seinfeld, J. H.; Pandis, S. N. *Atmospheric Chemistry and Physics: From air pollution to climate change*; Wiley Interscience: New York, 2006.
(2)   Finlayson-Pitts, B. J.; Pitts, J. N. *Chemistry of the Upper and Lower Atmosphere: Theory, Experiments, and Applications*; Academic Press: San Diego, 2000.
(3)   Stevens, B.; Feingold, G. Untangling aerosol effects on clouds and precipitation in a buffered system. *Nature* **2009**, *461*, 607-613.
(4)   Carslaw, K. S.; Lee, L. A.; Reddington, C. L.; Pringle, K. J.; Rap, A.; Forster, P. M.; Mann, G. W.; Spracklen, D. V.; Woodhouse, M. T.; Regayre, L. A. *et al.* Large contribution of natural aerosols to uncertainty in indirect forcing. *Nature* **2013**, *503*, 67-71.

2556 (5)   IPCC *Climate Change 2013: The Physical Science Basis*; Cambridge University Press:
2557   Cambridge, UK, 2013.
2558 (6)   Laurent, B.; Marticorena, B.; Bergametti, G.; Léon, J. F.; Mahowald, N. M. Modeling
2559   mineral dust emissions from the Sahara desert using new surface properties and soil
2560   database. *J. Geophys. Res.-Atmos* **2008**, *113*, D14218, doi:
2561   14210.11029/12007JD009484.
2562 (7)   Laurent, B.; Marticorena, B.; Bergametti, G.; Mei, F. Modeling mineral dust emissions
2563   from Chinese and Mongolian deserts. *Glob. Planet. Change* **2006**, *52*, 121-141.
2564 (8)   Textor, C.; Schulz, M.; Guibert, S.; Kinne, S.; Balkanski, Y.; Bauer, S.; Berntsen, T.;
2565   Berglen, T.; Boucher, O.; Chin, M. *et al.* Analysis and quantification of the diversities of
2566   aerosol life cycles within AeroCom. *Atmos. Chem. Phys.* **2006**, *6*, 1777-1813.
2567 (9)   Huneeus, N.; Schulz, M.; Balkanski, Y.; Griesfeller, J.; Prospero, J.; Kinne, S.; Bauer, S.;
2568   Boucher, O.; Chin, M.; Dentener, F. *et al.* Global dust model intercomparison in
2569   AeroCom phase I. *Atmos. Chem. Phys.* **2011**, *11*, 7781-7816.
2570 (10) Ginoux, P.; Prospero, J. M.; Gill, T. E.; Hsu, N. C.; Zhao, M. Global-scale attribution of
2571   anthropogenic and natural dust sources and their emission rates based on MODIS Deep
2572   Blue aerosol products. *Rev. Geophys.* **2012**, *50*, RG3005, doi:
2573   3010.1029/2012RG000388.
2574 (11) Forster, P.; Ramaswamy, V.; Artaxo, P.; Berntsen, T.; Betts, R.; Fahey, D. W.; Haywood,
2575   J.; Lean, J.; Lowe, D. C.; Myhre, G. *et al.* In *Climate Change 2007: The Physical Science
2576   Basis. Contribution of Working Group I to the Fourth Assessment Report of the
2577   Intergovernmental Panel on Climate Change*; Solomon, S., Qin, D., Manning, M., Chen,
2578   Z., Marquis, M., Averyt, K. B., Tignor, M., Miller, H. L., Eds.; Cambridge University
2579   Press: Cambridge, United Kingdom, 2007.
2580 (12) Prospero, J. M. Long-range transport of mineral dust in the global atmosphere: Impact of
2581   African dust on the environment of the southeastern United States. *Proc. Natl. Acad. Sci.
2582   U. S. A.* **1999**, *96*, 3396-3403.
2583 (13) Uno, I.; Eguchi, K.; Yumimoto, K.; Takemura, T.; Shimizu, A.; Uematsu, M.; Liu, Z.;
2584   Wang, Z.; Hara, Y.; Sugimoto, N. Asian dust transported one full circuit around the
2585   globe. *Nature Geosci.* **2009**, *2*, 557-560.
2586 (14) Schepanski, K.; Tegen, I.; Macke, A. Saharan dust transport and deposition towards the
2587   tropical northern Atlantic. *Atmos. Chem. Phys.* **2009**, *9*, 1173-1189.
2588 (15) Hande, L. B.; Engler, C.; Hoose, C.; Tegen, I. Seasonal variability of Saharan desert dust
2589   and ice nucleating particles over Europe. *Atmos. Chem. Phys.* **2015**, *15*, 4389-4397.
2590 (16) Fairlie, T. D.; Jacob, D. J.; Dibb, J. E.; Alexander, B.; Avery, M. A.; van Donkelaar, A.;
2591   Zhang, L. Impact of mineral dust on nitrate, sulfate, and ozone in transpacific Asian
2592   pollution plumes. *Atmos. Chem. Phys.* **2010**, *10*, 3999-4012.
2593 (17) Fairlie, T. D.; Jacob, D. J.; Park, R. J. The impact of transpacific transport of mineral dust
2594   in the United States. *Atmos. Environ.* **2007**, *41*, 1251-1266.
2595 (18) Prospero, J. M.; Mayol-Bracero, O. L. Understanding the Transport and Impact of
2596   African Dust on the Caribbean Basin. *Bull. Amer. Meteorol. Soc.* **2013**, *94*, 1329-1337.
2597 (19) Quinn, P. K.; Collins, D. B.; Grassian, V. H.; Prather, K. A.; Bates, T. S. Chemistry and
2598   Related Properties of Freshly Emitted Sea Spray Aerosol. *Chem. Rev.* **2015**, *115*, 4383-
2599   4399.
2600 (20) Prospero, J. M.; Lamb, P. J. African droughts and dust transport to the Caribbean:
2601   Climate change implications. *Science* **2003**, *302*, 1024-1027.
2602 (21) Mahowald, N. M.; Kloster, S.; Engelstaedter, S.; Moore, J. K.; Mukhopadhyay, S.;
2603   McConnell, J. R.; Albani, S.; Doney, S. C.; Bhattacharya, A.; Curran, M. A. J. *et al.*

2604   Observed 20th century desert dust variability: impact on climate and biogeochemistry.
2605   *Atmos. Chem. Phys.* **2010**, *10*, 10875-10893.
2606   (22) Tegen, I.; Lacis, A. A.; Fung, I. The influence on climate forcing of mineral aerosols
2607   from disturbed soils. *Nature* **1996**, *380*, 419-422.
2608   (23) Tegen, I.; Harrison, S. P.; Kohfeld, K.; Prentice, I. C.; Coe, M.; Heimann, M. Impact of
2609   vegetation and preferential source areas on global dust aerosol: Results from a model
2610   study. *J. Geophys. Res.-Atmos.* **2002**, *107*, 4576, DOI: 4510.1029/2001JD000963.
2611   (24) Tegen, I.; Werner, M.; Harrison, S. P.; Kohfeld, K. E. Relative importance of climate and
2612   land use in determining present and future global soil dust emission. *Geophys. Res. Lett.*
2613   **2004**, *31*, L05105, doi: 05110.01029/02003GL019216.
2614   (25) Muhs, D. R. The geologic records of dust in the Quaternary. *Aeolian Res.* **2013**, *9*, 3-48.
2615   (26) Muhs, D.; Prospero, J.; Baddock, M.; Gill, T. In *Mineral Dust*; Knippertz, P., Stuut, J.-B.
2616   W., Eds.; Springer: Netherlands, 2014.
2617   (27) Mahowald, N. Aerosol Indirect Effect on Biogeochemical Cycles and Climate. *Science*
2618   **2011**, *334*, 794-796.
2619   (28) Choobari, O. A.; Zawar-Reza, P.; Sturman, A. The global distribution of mineral dust and
2620   its impacts on the climate system: A review. *Atmos. Res.* **2014**, *138*, 152-165.
2621   (29) Li, X.; Maring, H.; Savoie, D.; Voss, K.; Prospero, J. M. Dominance of mineral dust in
2622   aerosol light-scattering in the North Atlantic trade winds. *Nature* **1996**, *380*, 416-419.
2623   (30) Balkanski, Y.; Schulz, M.; Claquin, T.; Guibert, S. Reevaluation of Mineral aerosol
2624   radiative forcings suggests a better agreement with satellite and AERONET data. *Atmos.*
2625   *Chem. Phys.* **2007**, *7*, 81-95.
2626   (31) Sokolik, I. N.; Toon, O. B. Direct radiative forcing by anthropogenic airborne mineral
2627   aerosols. *Nature* **1996**, *381*, 681-683.
2628   (32) Linke, C.; Möhler, O.; Veres, A.; Mohácsi, Á.; Bozóki, Z.; Szabó, G.; Schnaiter, M.
2629   Optical properties and mineralogical composition of different Saharan mineral dust
2630   samples: a laboratory study. *Atmos. Chem. Phys.* **2006**, *6*, 3315-3323.
2631   (33) Sokolik, I. N.; Winker, D. M.; Bergametti, G.; Gillette, D. A.; Carmichael, G.; Kaufman,
2632   Y. J.; Gomes, L.; Schuetz, L.; Penner, J. E. Introduction to special section: Outstanding
2633   problems in quantifying the radiative impacts of mineral dust. *J. Geophys. Res.-Atmos.*
2634   **2001**, *106*, 18015-18027.
2635   (34) Huang, X.; Song, Y.; Zhao, C.; Cai, X.; Zhang, H.; Zhu, T. Direct Radiative Effect by
2636   Multicomponent Aerosol over China. *J. Climate* **2015**, *28*, 3472-3495.
2637   (35) Wu, Z. J.; Cheng, Y. F.; Hu, M.; Wehner, B.; Sugimoto, N.; Wiedensohler, A. Dust
2638   events in Beijing, China (2004–2006): comparison of ground-based measurements with
2639   columnar integrated observations. *Atmos. Chem. Phys.* **2009**, *9*, 6915-6932.
2640   (36) Di Biagio, C.; Boucher, H.; Caquineau, S.; Chevaillier, S.; Cuesta, J.; Formenti, P.
2641   Variability of the infrared complex refractive index of African mineral dust: experimental
2642   estimation and implications for radiative transfer and satellite remote sensing. *Atmos.*
2643   *Chem. Phys.* **2014**, *14*, 11093-11116.
2644   (37) McConnell, C. L.; Formenti, P.; Highwood, E. J.; Harrison, M. A. J. Using aircraft
2645   measurements to determine the refractive index of Saharan dust during the DODO
2646   Experiments. *Atmos. Chem. Phys.* **2010**, *10*, 3081-3098.
2647   (38) Lemaitre, C.; Flamant, C.; Cuesta, J.; Raut, J. C.; Chazette, P.; Formenti, P.; Pelon, J.
2648   Radiative heating rates profiles associated with a springtime case of Bodele and Sudan
2649   dust transport over West Africa. *Atmos. Chem. Phys.* **2010**, *10*, 8131-8150.
2650   (39) Tanre, D.; Haywood, J.; Pelon, J.; Leon, J. F.; Chatenet, B.; Formenti, P.; Francis, P.;
2651   Goloub, P.; Highwood, E. J.; Myhre, G. Measurement and modeling of the Saharan dust

2652   radiative impact: Overview of the Saharan Dust Experiment (SHADE). *J. Geophys. Res.-*
2653   *Atmos.* **2003**, *108*, 8574, doi: 8510.1029/2002jd003273.

2654 (40) Highwood, E.; Ryder, C. In *Mineral Dust*; Knippertz, P., Stuut, J.-B. W., Eds.; Springer:
2655   Netherlands, 2014.

2656 (41) Kim, K. W.; He, Z.; Kim, Y. J. Physicochemical characteristics and radiative properties
2657   of Asian dust particles observed at Kwangju, Korea, during the 2001 ACE-Asia intensive
2658   observation period. *J. Geophys. Res.-Atmos* **2004**, *109*, D19S02, doi:
2659   10.1029/2003JD003693.

2660 (42) Jung, J.; Kim, Y. J.; Lee, K. Y.; Cayetano, M. G.; Batmunkh, T.; Koo, J. H.; Kim, J.
2661   Spectral optical properties of long-range transport Asian dust and pollution aerosols over
2662   Northeast Asia in 2007 and 2008. *Atmos. Chem. Phys.* **2010**, *10*, 5391-5408.

2663 (43) Miller, R.; Knippertz, P.; Pérez García-Pando, C.; Perlwitz, J.; Tegen, I. In *Mineral Dust*;
2664   Knippertz, P., Stuut, J.-B. W., Eds.; Springer: Netherlands, 2014.

2665 (44) Schladitz, A.; Müller, T.; Nordmann, S.; Tesche, M.; Groß, S.; Freudenthaler, V.;
2666   Gasteiger, J.; Wiedensohler, A. In situ aerosol characterization at Cape Verde Part 2:
2667   Parametrization of relative humidity- and wavelength-dependent aerosol optical
2668   properties. *Tellus B* **2011**, *63*.

2669 (45) Jeong, G. R.; Sokolik, I. N. Effect of mineral dust aerosols on the photolysis rates in the
2670   clean and polluted marine environments. *J. Geophys. Res.-Atmos.* **2007**, *112*, D21308,
2671   doi: 21310.21029/22007jd008442.

2672 (46) Koehler, K. A.; Kreidenweis, S. M.; DeMott, P. J.; Petters, M. D.; Prenni, A. J.; Carrico,
2673   C. M. Hygroscopicity and cloud droplet activation of mineral dust aerosol. *Geophys. Res.*
2674   *Lett.* **2009**, *36*, L08805, doi: 08810.01029/02009gl037348.

2675 (47) Kumar, P.; Sokolik, I. N.; Nenes, A. Parameterization of cloud droplet formation for
2676   global and regional models: including adsorption activation from insoluble CCN. *Atmos.*
2677   *Chem. Phys.* **2009**, *9*, 2517-2532.

2678 (48) Twohy, C. H.; Kreidenweis, S. M.; Eidhammer, T.; Browell, E. V.; Heymsfield, A. J.;
2679   Bansemer, A. R.; Anderson, B. E.; Chen, G.; Ismail, S.; DeMott, P. J. *et al.* Saharan dust
2680   particles nucleate droplets in eastern Atlantic clouds. *Geophys. Res. Lett.* **2009**, *36*,
2681   L01807, doi: 01810.01029/02008gl035846.

2682 (49) Herich, H.; Tritscher, T.; Wiacek, A.; Gysel, M.; Weingartner, E.; Lohmann, U.;
2683   Baltensperger, U.; Cziczo, D. J. Water uptake of clay and desert dust aerosol particles at
2684   sub- and supersaturated water vapor conditions. *Phys. Chem. Chem. Phys.* **2009**, *11*,
2685   7804-7809.

2686 (50) Manktelow, P. T.; Carslaw, K. S.; Mann, G. W.; Spracklen, D. V. The impact of dust on
2687   sulfate aerosol, CN and CCN during an East Asian dust storm. *Atmos. Chem. Phys.* **2010**,
2688   *10*, 365-382.

2689 (51) Karydis, V. A.; Kumar, P.; Barahona, D.; Sokolik, I. N.; Nenes, A. On the effect of dust
2690   particles on global cloud condensation nuclei and cloud droplet number. *J. Geophys.*
2691   *Res.-Atmos.* **2011**, *116*, D23204, doi: 23210.21029/22011jd016283.

2692 (52) Kumar, P.; Nenes, A.; Sokolik, I. N. Importance of adsorption for CCN activity and
2693   hygroscopic properties of mineral dust aerosol. *Geophys. Res. Lett.* **2009**, *36*, L24804,
2694   doi: 24810.21029/22009gl040827.

2695 (53) Solomos, S.; Kallos, G.; Kushta, J.; Astitha, M.; Tremback, C.; Nenes, A.; Levin, Z. An
2696   integrated modelling study on the effects of mineral dust and sea salt particles on clouds
2697   and precipitation. *Atmos. Chem. Phys.* **2011**, *11*, 873-892.

2698 (54) Nenes, A.; Murray, B.; Bougiatioti, A. In *Mineral Dust*; Knippertz, P., Stuut, J.-B. W.,
2699   Eds.; Springer: Netherlands, 2014.

2700 (55) Zhang, H.; McFarquhar, G. M.; Cotton, W. R.; Deng, Y. Direct and indirect impacts of
2701 Saharan dust acting as cloud condensation nuclei on tropical cyclone eyewall
2702 development. *Geophys. Res. Lett.* **2009**, *36*, L06802, doi: 06810.01029/02009GL037276.
2703 (56) DeMott, P. J.; Sassen, K.; Poellot, M. R.; Baumgardner, D.; Rogers, D. C.; Brooks, S. D.;
2704 Prenni, A. J.; Kreidenweis, S. M. African dust aerosols as atmospheric ice nuclei.
2705 *Geophys. Res. Lett.* **2003**, *30*, 1732, doi: 1710.1029/2003gl017410.
2706 (57) Klein, H.; Nickovic, S.; Haunold, W.; Bundke, U.; Nillius, B.; Ebert, M.; Weinbruch, S.;
2707 Schuetz, L.; Levin, Z.; Barrie, L. A. *et al.* Saharan dust and ice nuclei over Central
2708 Europe. *Atmos. Chem. Phys.* **2010**, *10*, 10211-10221.
2709 (58) Creamean, J. M.; Suski, K. J.; Rosenfeld, D.; Cazorla, A.; DeMott, P. J.; Sullivan, R. C.;
2710 White, A. B.; Ralph, F. M.; Minnis, P.; Comstock, J. M. *et al.* Dust and Biological
2711 Aerosols from the Sahara and Asia Influence Precipitation in the Western U.S. *Science*
2712 **2013**, *339*, 1572-1578.
2713 (59) Hoose, C.; Lohmann, U.; Erdin, R.; Tegen, I. The global influence of dust mineralogical
2714 composition on heterogeneous ice nucleation in mixed-phase clouds. *Environ. Res. Lett.*
2715 **2008**, *3*, 025003.
2716 (60) Field, P. R.; Mohler, O.; Connolly, P.; Kramer, M.; Cotton, R.; Heymsfield, A. J.;
2717 Saathoff, H.; Schnaiter, M. Some ice nucleation characteristics of Asian and Saharan
2718 desert dust. *Atmos. Chem. Phys.* **2006**, *6*, 2991-3006.
2719 (61) DeMott, P. J.; Cziczo, D. J.; Prenni, A. J.; Murphy, D. M.; Kreidenweis, S. M.; Thomson,
2720 D. S.; Borys, R.; Rogers, D. C. Measurements of the concentration and composition of
2721 nuclei for cirrus formation. *Proc. Natl. Acad. Sci. U. S. A.* **2003**, *100*, 14655-14660.
2722 (62) DeMott, P. J.; Prenni, A. J.; Liu, X.; Kreidenweis, S. M.; Petters, M. D.; Twohy, C. H.;
2723 Richardson, M. S.; Eidhammer, T.; Rogers, D. C. Predicting global atmospheric ice
2724 nuclei distributions and their impacts on climate. *Proc. Natl. Acad. Sci. U. S. A.* **2010**,
2725 *107*, 11217-11222.
2726 (63) Zimmermann, F.; Weinbruch, S.; Schutz, L.; Hofmann, H.; Ebert, M.; Kandler, K.;
2727 Worringen, A. Ice nucleation properties of the most abundant mineral dust phases. *J.*
2728 *Geophys. Res.-Atmos.* **2008**, *113*, D23204, doi: 23210.21029/22008jd010655.
2729 (64) Stith, J. L.; Ramanathan, V.; Cooper, W. A.; Roberts, G. C.; DeMott, P. J.; Carmichael,
2730 G.; Hatch, C. D.; Adhikary, B.; Twohy, C. H.; Rogers, D. C. *et al.* An overview of
2731 aircraft observations from the Pacific Dust Experiment campaign. *J. Geophys. Res.-*
2732 *Atmos.* **2009**, *114*, D05207, doi: 05210.01029/02008jd010924.
2733 (65) Ryder, C. L.; McQuaid, J. B.; Flamant, C.; Rosenberg, P. D.; Washington, R.; Brindley,
2734 H. E.; Highwood, E. J.; Marsham, J. H.; Parker, D. J.; Todd, M. C. *et al.* Advances in
2735 understanding mineral dust and boundary layer processes over the Sahara from Fennec
2736 aircraft observations. *Atmos. Chem. Phys.* **2015**, *15*, 8479-8520.
2737 (66) Burrows, S. M.; Hoose, C.; Pöschl, U.; Lawrence, M. G. Ice nuclei in marine air:
2738 biogenic particles or dust? *Atmos. Chem. Phys.* **2013**, *13*, 245-267.
2739 (67) Pratt, K. A.; DeMott, P. J.; French, J. R.; Wang, Z.; Westphal, D. L.; Heymsfield, A. J.;
2740 Twohy, C. H.; Prenni, A. J.; Prather, K. A. In situ detection of biological particles in
2741 cloud ice-crystals. *Nature Geoscience* **2009**, *2*, 397-400.
2742 (68) Baustian, K. J.; Cziczo, D. J.; Wise, M. E.; Pratt, K. A.; Kulkarni, G.; Hallar, A. G.;
2743 Tolbert, M. A. Importance of aerosol composition, mixing state, and morphology for
2744 heterogeneous ice nucleation: A combined field and laboratory approach. *J. Geophys.*
2745 *Res.-Atmos.* **2012**, *117*, D06217, doi: 06210.01029/02011jd016784.
2746 (69) Cziczo, D. J.; Froyd, K. D. Sampling the composition of cirrus ice residuals. *Atmos. Res.*
2747 **2014**, *142*, 15-31.

2748   (70)   Ebert, M.; Worringen, A.; Benker, N.; Mertes, S.; Weingartner, E.; Weinbruch, S.
2749   Chemical composition and mixing-state of ice residuals sampled within mixed phase
2750   clouds. *Atmos. Chem. Phys.* **2011**, *11*, 2805-2816.
2751   (71)   Kamphus, M.; Ettner-Mahl, M.; Klimach, T.; Drewnick, F.; Keller, L.; Cziczo, D. J.;
2752   Mertes, S.; Borrmann, S.; Curtius, J. Chemical composition of ambient aerosol, ice
2753   residues and cloud droplet residues in mixed-phase clouds: single particle analysis during
2754   the Cloud and Aerosol Characterization Experiment (CLACE 6). *Atmos. Chem. Phys.*
2755   **2010**, *10*, 8077-8095.
2756   (72)   DeMott, P. J.; Prenni, A. J.; McMeeking, G. R.; Sullivan, R. C.; Petters, M. D.; Tobo, Y.;
2757   Niemand, M.; Möhler, O.; Snider, J. R.; Wang, Z. *et al.* Integrating laboratory and field
2758   data to quantify the immersion freezing ice nucleation activity of mineral dust particles.
2759   *Atmos. Chem. Phys.* **2015**, *15*, 393-409.
2760   (73)   Prenni, A. J.; Petters, M. D.; Kreidenweis, S. M.; Heald, C. L.; Martin, S. T.; Artaxo, P.;
2761   Garland, R. M.; Wollny, A. G.; Poschl, U. Relative roles of biogenic emissions and
2762   Saharan dust as ice nuclei in the Amazon basin. *Nat. Geosci.* **2009**, *2*, 401-404.
2763   (74)   Cziczo, D. J.; Froyd, K. D.; Hoose, C.; Jensen, E. J.; Diao, M.; Zondlo, M. A.; Smith, J.
2764   B.; Twohy, C. H.; Murphy, D. M. Clarifying the Dominant Sources and Mechanisms of
2765   Cirrus Cloud Formation. *Science* **2013**, *340*, 1320-1324.
2766   (75)   Hoose, C.; Kristjansson, J. E.; Burrows, S. M. How important is biological ice nucleation
2767   in clouds on a global scale? *Environ. Res. Lett.* **2010**, *5*, 024009.
2768   (76)   Lohmann, U.; Feichter, J. Global indirect aerosol effects: a review. *Atmos. Chem. Phys.*
2769   **2005**, *5*, 715-737.
2770   (77)   Baker, M. B. Cloud microphysics and climate. *Science* **1997**, *276*, 1072-1078.
2771   (78)   Gettelman, A.; Liu, X.; Barahona, D.; Lohmann, U.; Chen, C. Climate impacts of ice
2772   nucleation. *J. Geophys. Res.-Atmos.* **2012**, *117*.
2773   (79)   Wiacek, A.; Peter, T. On the availability of uncoated mineral dust ice nuclei in cold cloud
2774   regions. *Geophys. Res. Lett.* **2009**, *36*.
2775   (80)   Rosenfeld, D.; Lohmann, U.; Raga, G. B.; O'Dowd, C. D.; Kulmala, M.; Fuzzi, S.;
2776   Reissell, A.; Andreae, M. O. Flood or drought: How do aerosols affect precipitation?
2777   *Science* **2008**, *321*, 1309-1313.
2778   (81)   Yin, Y.; Wurzler, S.; Levin, Z.; Reisin, T. G. Interactions of mineral dust particles and
2779   clouds: Effects on precipitation and cloud optical properties. *J. Geophys. Res.-Atmos.*
2780   **2002**, *107*, 4724, doi: 4710.1029/2001jd001544.
2781   (82)   Ramanathan, V.; Crutzen, P. J.; Kiehl, J. T.; Rosenfeld, D. Atmosphere - Aerosols,
2782   climate, and the hydrological cycle. *Science* **2001**, *294*, 2119-2124.
2783   (83)   Rosenfeld, D.; Rudich, Y.; Lahav, R. Desert dust suppressing precipitation: A possible
2784   desertification feedback loop. *Proc. Natl. Acad. Sci. U. S. A.* **2001**, *98*, 5975-5980.
2785   (84)   Shi, Z. B.; Krom, M. D.; Jickells, T. D.; Bonneville, S.; Carslaw, K. S.; Mihalopoulos,
2786   N.; Baker, A. R.; Benning, L. G. Impacts on iron solubility in the mineral dust by
2787   processes in the source region and the atmosphere: A review. *Aeolian Res.* **2012**, *5*, 21-
2788   42.
2789   (85)   Boyd, P. W.; Ellwood, M. J. The biogeochemical cycle of iron in the ocean. *Nature
2790   Geosci* **2010**, *3*, 675-682.
2791   (86)   Boyd, P. W.; Jickells, T.; Law, C. S.; Blain, S.; Boyle, E. A.; Buesseler, K. O.; Coale, K.
2792   H.; Cullen, J. J.; de Baar, H. J. W.; Follows, M. *et al.* Mesoscale Iron Enrichment
2793   Experiments 1993-2005: Synthesis and Future Directions. *Science* **2007**, *315*, 612-617.
2794   (87)   Moore, J. K.; Braucher, O. Sedimentary and mineral dust sources of dissolved iron to the
2795   world ocean. *Biogeosciences* **2008**, *5*, 631-656.

(88) Nenes, A.; Krom, M. D.; Mihalopoulos, N.; Van Cappellen, P.; Shi, Z.; Bougiatioti, A.; Zarmpas, P.; Herut, B. Atmospheric acidification of mineral aerosols: a source of bioavailable phosphorus for the oceans. *Atmos. Chem. Phys.* **2011**, *11*, 6265-6272.

(89) Okin, G. S.; Baker, A. R.; Tegen, I.; Mahowald, N. M.; Dentener, F. J.; Duce, R. A.; Galloway, J. N.; Hunter, K.; Kanakidou, M.; Kubilay, N. *et al.* Impacts of atmospheric nutrient deposition on marine productivity: Roles of nitrogen, phosphorus, and iron. *Glob. Biogeochem. Cycle* **2011**, *25*, GB2022, doi: 2010.1029/2010GB003858.

(90) Okin, G. S.; Mahowald, N.; Chadwick, O. A.; Artaxo, P. Impact of desert dust on the biogeochemistry of phosphorus in terrestrial ecosystems. *Glob. Biogeochem. Cycle* **2004**, *18*, GB2005, doi: 2010.1029/2003GB002145.

(91) Mahowald, N.; Jickells, T. D.; Baker, A. R.; Artaxo, P.; Benitez-Nelson, C. R.; Bergametti, G.; Bond, T. C.; Chen, Y.; Cohen, D. D.; Herut, B. *et al.* Global distribution of atmospheric phosphorus sources, concentrations and deposition rates, and anthropogenic impacts. *Glob. Biogeochem. Cycle* **2008**, *22*, GB4026, doi: 4010.1029/2008GB003240.

(92) Jordi, A.; Basterretxea, G.; Tovar-Sánchez, A.; Alastuey, A.; Querol, X. Copper aerosols inhibit phytoplankton growth in the Mediterranean Sea. *Proc. Natl. Acad. Sci. U.S.A.* **2012**, *109*, 21246-21249.

(93) Paytan, A.; Mackey, K. R. M.; Chen, Y.; Lima, I. D.; Doney, S. C.; Mahowald, N.; Labiosa, R.; Post, A. F. Toxicity of atmospheric aerosols on marine phytoplankton. *Proc. Natl. Acad. Sci. U.S.A.* **2009**, *106*, 4601-4605.

(94) Mahowald, N. M.; Baker, A. R.; Bergametti, G.; Brooks, N.; Duce, R. A.; Jickells, T. D.; Kubilay, N.; Prospero, J. M.; Tegen, I. Atmospheric global dust cycle and iron inputs to the ocean. *Glob. Biogeochem. Cycle* **2005**, *19*, GB4025, doi:4010.1029/2004GB002402.

(95) Schulz, M.; Prospero, J. M.; Baker, A. R.; Dentener, F.; Ickes, L.; Liss, P. S.; Mahowald, N. M.; Nickovic, S.; García-Pando, C. P.; Rodríguez, S. *et al.* Atmospheric Transport and Deposition of Mineral Dust to the Ocean: Implications for Research Needs. *Environ. Sci. Technol.* **2012**, *46*, 10390-10404.

(96) Meskhidze, N.; Chameides, W. L.; Nenes, A. Dust and pollution: A recipe for enhanced ocean fertilization? *J. Geophys. Res.-Atmos.* **2005**, *110*, D03301, doi: 03310.01029/02004jd005082.

(97) Paytan, A.; McLaughlin, K. The Oceanic Phosphorus Cycle. *Chem. Rev.* **2007**, *107*, 563-576.

(98) Bristow, C. S.; Hudson-Edwards, K. A.; Chappell, A. Fertilizing the Amazon and equatorial Atlantic with West African dust. *Geophys. Res. Lett.* **2010**, *37*, L14807, doi: 14810.11029/12010GL043486.

(99) Yu, H.; Chin, M.; Yuan, T.; Bian, H.; Remer, L. A.; Prospero, J. M.; Omar, A.; Winker, D.; Yang, Y.; Zhang, Y. *et al.* The Fertilizing Role of African Dust in the Amazon Rainforest: A First Multiyear Assessment Based on CALIPSO Lidar Observations. *Geophys. Res. Lett.* **2015**, *42*, GL063040, doi: 063010.061002/062015GL063040.

(100) Mahowald, N.; Ward, D. S.; Kloster, S.; Flanner, M. G.; Heald, C. L.; Heavens, N. G.; Hess, P. G.; Lamarque, J.-F.; Chuang, P. Y. Aerosol Impacts on Climate and Biogeochemistry. *Annu. Rev. Environ. Resour.* **2011**, *36*, 45-74.

(101) Jickells, T. D.; An, Z. S.; Andersen, K. K.; Baker, A. R.; Bergametti, G.; Brooks, N.; Cao, J. J.; Boyd, P. W.; Duce, R. A.; Hunter, K. A. *et al.* Global iron connections between desert dust, ocean biogeochemistry, and climate. *Science* **2005**, *308*, 67-71.

(102) Garrison, V. H.; Shinn, E. A.; Foreman, W. T.; Griffin, D. W.; Holmes, C. W.; Kellogg, C. A.; Majewski, M. S.; Richardson, L. L.; Ritchie, K. B.; Smith, G. W. African and Asian Dust: From Desert Soils to Coral Reefs. *BioScience* **2003**, *53*, 469-480.

2845 (103) Jickells, T.; Boyd, P.; Hunter, K. In *Mineral Dust*; Knippertz, P., Stuut, J.-B. W., Eds.;
2846   Springer: Netherlands, 2014.
2847 (104) Zhu, T.; Shang, J.; Zhao, D. F. The roles of heterogeneous chemical processes in the
2848   formation of an air pollution complex and gray haze. *Sci. China-Chem.* **2011**, *54*, 145-
2849   153.
2850 (105) Lelieveld, J.; Evans, J. S.; Fnais, M.; Giannadaki, D.; Pozzer, A. The contribution of
2851   outdoor air pollution sources to premature mortality on a global scale. *Nature* **2015**, *525*,
2852   367-371.
2853 (106) Morman, S.; Plumlee, G. In *Mineral Dust*; Knippertz, P., Stuut, J.-B. W., Eds.; Springer:
2854   Netherlands, 2014.
2855 (107) Mahowald, N. M.; Ballantine, J. A.; Feddema, J.; Ramankutty, N. Global trends in
2856   visibility: implications for dust sources. *Atmos. Chem. Phys.* **2007**, *7*, 3309-3339.
2857 (108) Giannadaki, D.; Pozzer, A.; Lelieveld, J. Modeled global effects of airborne desert dust
2858   on air quality and premature mortality. *Atmos. Chem. Phys.* **2014**, *14*, 957-968.
2859 (109) De Longueville, F.; Hountondji, Y.-C.; Henry, S.; Ozer, P. What do we know about
2860   effects of desert dust on air quality and human health in West Africa compared to other
2861   regions? *Sci. Total Environ.* **2010**, *409*, 1-8.
2862 (110) de Longueville, F.; Ozer, P.; Doumbia, S.; Henry, S. Desert dust impacts on human
2863   health: an alarming worldwide reality and a need for studies in West Africa. *Int. J.*
2864   *Biometeorol.* **2013**, *57*, 1-19.
2865 (111) Perez, L.; Tobias, A.; Querol, X.; Künzli, N.; Pey, J.; Alastuey, A.; Viana, M.; Valero,
2866   N.; González-Cabré, M.; Sunyer, J. Coarse Particles From Saharan Dust and Daily
2867   Mortality. *Epidemiology* **2008**, *19*, 800-807.
2868 (112) Karanasiou, A.; Moreno, N.; Moreno, T.; Viana, M.; de Leeuw, F.; Querol, X. Health
2869   effects from Sahara dust episodes in Europe: Literature review and research gaps.
2870   *Environ. Int.* **2012**, *47*, 107-114.
2871 (113) Meng, Z.; Lu, B. Dust events as a risk factor for daily hospitalization for respiratory and
2872   cardiovascular diseases in Minqin, China. *Atmos. Environ.* **2007**, *41*, 7048-7058.
2873 (114) Kwon, H.-J.; Cho, S.-H.; Chun, Y.; Lagarde, F.; Pershagen, G. Effects of the Asian Dust
2874   Events on Daily Mortality in Seoul, Korea. *Environ. Res.* **2002**, *90*, 1-5.
2875 (115) Fubini, B.; Otero Arean, C. Chemical aspects of the toxicity of inhaled mineral dusts.
2876   *Chem. Soc. Rev.* **1999**, *28*, 373-381.
2877 (116) Thalib, L.; Al-Taiar, A. Dust storms and the risk of asthma admissions to hospitals in
2878   Kuwait. *Sci. Total Environ.* **2012**, *433*, 347-351.
2879 (117) Yang, C.-Y.; Chen, Y.-S.; Chiu, H.-F.; Goggins, W. B. Effects of Asian dust storm events
2880   on daily stroke admissions in Taipei, Taiwan. *Environ. Res.* **2005**, *99*, 79-84.
2881 (118) Tobías, A.; Pérez, L.; Díaz, J.; Linares, C.; Pey, J.; Alastruey, A.; Querol, X. Short-term
2882   effects of particulate matter on total mortality during Saharan dust outbreaks: A case-
2883   crossover analysis in Madrid (Spain). *Sci. Total Environ.* **2011**, *412–413*, 386-389.
2884 (119) Chen, Y.-S.; Sheen, P.-C.; Chen, E.-R.; Liu, Y.-K.; Wu, T.-N.; Yang, C.-Y. Effects of
2885   Asian dust storm events on daily mortality in Taipei, Taiwan. *Environ. Res.* **2004**, *95*,
2886   151-155.
2887 (120) Alessandrini, E. R.; Stafoggia, M.; Faustini, A.; Gobbi, G. P.; Forastiere, F. Saharan dust
2888   and the association between particulate matter and daily hospitalisations in Rome, Italy.
2889   *Occup. Environ. Med.* **2013**, *70*, 432-434.
2890 (121) Claquin, T.; Schulz, M.; Balkanski, Y. J. Modeling the mineralogy of atmospheric dust
2891   sources. *J. Geophys. Res.-Atmos.* **1999**, *104*, 22243-22256.

2892 (122) Nickovic, S.; Vukovic, A.; Vujadinovic, M.; Djurdjevic, V.; Pejanovic, G. Technical
2893   Note: High-resolution mineralogical database of dust-productive soils for atmospheric
2894   dust modeling. *Atmos. Chem. Phys.* **2012**, *12*, 845-855.

2895 (123) Journet, E.; Balkanski, Y.; Harrison, S. P. A new data set of soil mineralogy for dust-
2896   cycle modeling. *Atmos. Chem. Phys.* **2014**, *14*, 3801-3816.

2897 (124) Formenti, P.; Schutz, L.; Balkanski, Y.; Desboeufs, K.; Ebert, M.; Kandler, K.; Petzold,
2898   A.; Scheuvens, D.; Weinbruch, S.; Zhang, D. Recent progress in understanding physical
2899   and chemical properties of African and Asian mineral dust. *Atmos. Chem. Phys.* **2011**, *11*,
2900   8231-8256.

2901 (125) Klaver, A.; Formenti, P.; Caquineau, S.; Chevaillier, S.; Ausset, P.; Calzolai, G.;
2902   Osborne, S.; Johnson, B.; Harrisone, M.; Dubovik, O. Physico-chemical and optical
2903   properties of Sahelian and Saharan mineral dust: in situ measurements during the
2904   GERBILS campaign. *Q. J. R. Meteorol. Soc.* **2011**, *137*, 1193-1210.

2905 (126) Fitzgerald, E.; Ault, A. P.; Zauscher, M. D.; Mayol-Bracero, O. L.; Prather, K. A.
2906   Comparison of the mixing state of long-range transported Asian and African mineral
2907   dust. *Atmos. Environ.* **2015**, *115*, 19-25.

2908 (127) Scheuvens, D.; Schütz, L.; Kandler, K.; Ebert, M.; Weinbruch, S. Bulk composition of
2909   northern African dust and its source sediments - A compilation. *Earth-Sci. Rev.* **2013**,
2910   *116*, 170-194.

2911 (128) Scheuvens, D.; Kandler, K. In *Mineral Dust*; Knippertz, P., Stuut, J.-B. W., Eds.;
2912   Springer: Netherlands, 2014.

2913 (129) Perlwitz, J. P.; Pérez García-Pando, C.; Miller, R. L. Predicting the mineral composition
2914   of dust aerosols – Part 1: Representing key processes. *Atmos. Chem. Phys.* **2015**, *15*,
2915   11593-11627.

2916 (130) Perlwitz, J. P.; Pérez García-Pando, C.; Miller, R. L. Predicting the mineral composition
2917   of dust aerosols – Part 2: Model evaluation and identification of key processes with
2918   observations. *Atmos. Chem. Phys.* **2015**, *15*, 11629-11652.

2919 (131) Seisel, S.; Borensen, C.; Vogt, R.; Zellner, R. Kinetics and mechanism of the uptake of
2920 N_2O_5 on mineral dust at 298 K. *Atmos. Chem. Phys.* **2005**, *5*, 3423-3432.

2921 (132) Karagulian, F.; Santschi, C.; Rossi, M. J. The heterogeneous chemical kinetics of N_2O_5
2922   on $CaCO_3$ and other atmospheric mineral dust surrogates. *Atmos. Chem. Phys.* **2006**, *6*,
2923   1373-1388.

2924 (133) Mogili, P. K.; Kleiber, P. D.; Young, M. A.; Grassian, V. H. N_2O_5 hydrolysis on the
2925   components of mineral dust and sea salt aerosol: Comparison study in an environmental
2926   aerosol reaction chamber. *Atmos. Environ.* **2006**, *40*, 7401-7408.

2927 (134) Wagner, C.; Hanisch, F.; Holmes, N.; de Coninck, H.; Schuster, G.; Crowley, J. N. The
2928   interaction of N_2O_5 with mineral dust: aerosol flow tube and Knudsen reactor studies.
2929   *Atmos. Chem. Phys.* **2008**, *8*, 91-109.

2930 (135) Wagner, C.; Schuster, G.; Crowley, J. N. An aerosol flow tube study of the interaction of
2931 N_2O_5 with calcite, Arizona dust and quartz. *Atmos. Environ.* **2009**, *43*, 5001-5008.

2932 (136) Tang, M. J.; Thieser, J.; Schuster, G.; Crowley, J. N. Kinetics and mechanism of the
2933   heterogeneous reaction of N2O5 with mineral dust particles. *Phys. Chem. Chem. Phys.*
2934   **2012**, *14*, 8551-8561.

2935 (137) Tang, M. J.; Schuster, G.; Crowley, J. N. Heterogeneous reaction of N2O5 with illite and
2936   Arizona test dust particles. *Atmos. Chem. Phys.* **2014**, *14*, 245-254.

2937 (138) Tang, M. J.; Telford, P. J.; Pope, F. D.; Rkiouak, L.; Abraham, N. L.; Archibald, A. T.;
2938   Braesicke, P.; Pyle, J. A.; McGregor, J.; Watson, I. M. *et al.* Heterogeneous reaction of
2939   N2O5 with airborne TiO2 particles and its implication for stratospheric particle injection.
2940   *Atmos. Chem. Phys.* **2014**, *14*, 6035-6048.

2941 (139) Tang, M. J.; Camp, J. C. J.; Rkiouak, L.; McGregor, J.; Watson, I. M.; Cox, R. A.;
2942   Kalberer, M.; Ward, A. D.; Pope, F. D. Heterogeneous Interaction of SiO2 with N2O5:
2943   Aerosol Flow Tube and Single Particle Optical Levitation-Raman Spectroscopy Studies.
2944   *J. Phys. Chem. A* **2014**, *118*, 8817-8827.
2945 (140) Murray, B. J.; O'Sullivan, D.; Atkinson, J. D.; Webb, M. E. Ice nucleation by particles
2946   immersed in supercooled cloud droplets. *Chem. Soc. Rev.* **2012**, *41*, 6519-6554.
2947 (141) Atkinson, J. D.; Murray, B. J.; Woodhouse, M. T.; Whale, T. F.; Baustian, K. J.; Carslaw,
2948   K. S.; Dobbie, S.; O/'Sullivan, D.; Malkin, T. L. The importance of feldspar for ice
2949   nucleation by mineral dust in mixed-phase clouds. *Nature* **2013**, *498*, 355-358.
2950 (142) Journet, E.; Desboeufs, K. V.; Caquineau, S.; Colin, J.-L. Mineralogy as a critical factor
2951   of dust iron solubility. *Geophys. Res. Lett.* **2008**, *35*, L07805, doi:
2952   07810.01029/02007GL031589.
2953 (143) Cwiertny, D. M.; Baltrusaitis, J.; Hunter, G. J.; Laskin, A.; Scherer, M. M.; Grassian, V.
2954   H. Characterization and acid-mobilization study of iron-containing mineral dust source
2955   materials. *J. Geophys. Res.-Atmos.* **2008**, *113*, D05202, doi:
2956   05210.01029/02007JD009332.
2957 (144) Fu, H. B.; Cwiertny, D. M.; Carmichael, G. R.; Scherer, M. M.; Grassian, V. H.
2958   Photoreductive dissolution of Fe-containing mineral dust particles in acidic media. *J.*
2959   *Geophys. Res.-Atmos.* **2010**, *115*, D11304, doi: 11310.11029/12009JD012702.
2960 (145) Formenti, P.; Caquineau, S.; Desboeufs, K.; Klaver, A.; Chevaillier, S.; Journet, E.;
2961   Rajot, J. L. Mapping the physico-chemical properties of mineral dust in western Africa:
2962   mineralogical composition. *Atmos. Chem. Phys.* **2014**, *14*, 10663-10686.
2963 (146) Jeong, G. Y. Bulk and single-particle mineralogy of Asian dust and a comparison with its
2964   source soils. *J. Geophys. Res.-Atmos.* **2008**, *113*, D02208, doi:
2965   02210.01029/02007jd008606.
2966 (147) Avila, A.; QueraltMitjans, I.; Alarcon, M. Mineralogical composition of African dust
2967   delivered by red rains over northeastern Spain. *J. Geophys. Res.-Atmos.* **1997**, *102*,
2968   21977-21996.
2969 (148) Caquineau, S.; Gaudichet, A.; Gomes, L.; Legrand, M. Mineralogy of Saharan dust
2970   transported over northwestern tropical Atlantic Ocean in relation to source regions. *J.*
2971   *Geophys. Res.-Atmos.* **2002**, *107*, 4251, doi: 4210.1029/2000jd000247.
2972 (149) Kandler, K.; Schutz, L.; Deutscher, C.; Ebert, M.; Hofmann, H.; Jackel, S.; Jaenicke, R.;
2973   Knippertz, P.; Lieke, K.; Massling, A. *et al.* Size distribution, mass concentration,
2974   chemical and mineralogical composition and derived optical parameters of the boundary
2975   layer aerosol at Tinfou, Morocco, during SAMUM 2006. *Tellus Ser. B-Chem. Phys.*
2976   *Meteorol.* **2009**, *61*, 32-50.
2977 (150) Scanza, R. A.; Mahowald, N.; Ghan, S.; Zender, C. S.; Kok, J. F.; Liu, X.; Zhang, Y.;
2978   Albani, S. Modeling dust as component minerals in the Community Atmosphere Model:
2979   development of framework and impact on radiative forcing. *Atmos. Chem. Phys.* **2015**,
2980   *15*, 537-561.
2981 (151) Hanisch, F.; Crowley, J. N. Ozone decomposition on Saharan dust: an experimental
2982   investigation. *Atmos. Chem. Phys.* **2003**, *3*, 119-130.
2983 (152) Adedokun, J. A.; Emofurieta, W. O.; Adedeji, O. A. Physical, mineralogical and
2984   chemical properties of harmattan dust at Ile-Ife, Nigeria. *Theor. Appl. Climatol.* **1989**, *40*,
2985   161-169.
2986 (153) Hsu, S.-C.; Liu, S. C.; Huang, Y.-T.; Chou, C. C. K.; Lung, S. C. C.; Liu, T.-H.; Tu, J.-
2987   Y.; Tsai, F. Long-range southeastward transport of Asian biosmoke pollution: Signature
2988   detected by aerosol potassium in Northern Taiwan. *J. Geophys. Res.-Atmos* **2009**, *114*,
2989   D14301, doi: 14310.11029/12009JD011725.

2990   (154)   George, C.; D'Anna, B.; Herrmann, H.; Weller, C.; Vaida, V.; Donaldson, D. J.; Bartels-
2991   Rausch, T.; Ammann, M. In *Atmospheric and Aerosol Chemistry*; McNeill, V. F., Ariya,
2992   P. A., Eds.; Springer Berlin Heidelberg, 2014; Vol. 339.
2993   (155)   Chen, H. H.; Nanayakkara, C. E.; Grassian, V. H. Titanium Dioxide Photocatalysis in
2994   Atmospheric Chemistry. *Chem. Rev.* **2012**, *112*, 5919-5948.
2995   (156)   George, C.; Ammann, M.; D'Anna, B.; Donaldson, D. J.; Nizkorodov, S. A.
2996   Heterogeneous Photochemistry in the Atmosphere. *Chem. Rev.* **2015**, *115*, 4218-4258.
2997   (157)   Harris, E.; Sinha, B.; van Pinxteren, D.; Tilgner, A.; Fomba, K. W.; Schneider, J.; Roth,
2998   A.; Gnauk, T.; Fahlbusch, B.; Mertes, S. *et al.* Enhanced Role of Transition Metal Ion
2999   Catalysis During In-Cloud Oxidation of SO2. *Science* **2013**, *340*, 727-730.
3000   (158)   Sullivan, R. C.; Guazzotti, S. A.; Sodeman, D. A.; Prather, K. A. Direct observations of
3001   the atmospheric processing of Asian mineral dust. *Atmos. Chem. Phys.* **2007**, *7*, 1213-
3002   1236.
3003   (159)   Matsuki, A.; Iwasaka, Y.; Shi, G. Y.; Zhang, D. Z.; Trochkine, D.; Yamada, M.; Kim, Y.
3004   S.; Chen, B.; Nagatani, T.; Miyazawa, T. *et al.* Morphological and chemical modification
3005   of mineral dust: Observational insight into the heterogeneous uptake of acidic gases.
3006   *Geophys. Res. Lett.* **2005**, *32*, L22806, doi: 22810.21029/22005gl024176.
3007   (160)   Mori, I.; Nishikawa, M.; Tanimura, T.; Quan, H. Change in size distribution and
3008   chemical composition of kosa (Asian dust) aerosol during long-range transport. *Atmos.*
3009   *Environ.* **2003**, *37*, 4253-4263.
3010   (161)   Usher, C. R.; Michel, A. E.; Grassian, V. H. Reactions on mineral dust. *Chem. Rev.* **2003**,
3011   *103*, 4883-4939.
3012   (162)   Matsuki, A.; Schwarzenboeck, A.; Venzac, H.; Laj, P.; Crumeyrolle, S.; Gomes, L. Cloud
3013   processing of mineral dust: direct comparison of cloud residual and clear sky particles
3014   during AMMA aircraft campaign in summer 2006. *Atmos. Chem. Phys.* **2010**, *10*, 1057-
3015   1069.
3016   (163)   Pope, F. D.; Braesicke, P.; Grainger, R. G.; Kalberer, M.; Watson, I. M.; Davidson, P. J.;
3017   Cox, R. A. Stratospheric aerosol particles and solar-radiation management. *Nature Clim.*
3018   *Change* **2012**, *2*, 713-719.
3019   (164)   Ferraro, A. J.; Highwood, E. J.; Charlton-Perez, A. J. Stratospheric heating by potential
3020   geoengineering aerosols. *Geophys. Res. Lett.* **2011**, *38*, L24706, doi:
3021   24710.21029/22011gl049761.
3022   (165)   Weisenstein, D. K.; Keith, D. W. Solar geoengineering using solid aerosol in the
3023   stratosphere. *Atmos. Chem. Phys. Discuss.* **2015**, *15*, 11799-11851.
3024   (166)   Crutzen, P. J. Albedo enhancement by stratospheric sulfur injections: A contribution to
3025   resolve a policy dilemma? *Clim. Change* **2006**, *77*, 211-219.
3026   (167)   Pruppacher, H. R.; Klett, J. D. *Microphysics of Clouds and Precipitation* Kluwer
3027   Academic Publishers: Dordrecht, Netherlands 1994.
3028   (168)   Dusek, U.; Frank, G. P.; Hildebrandt, L.; Curtius, J.; Schneider, J.; Walter, S.; Chand, D.;
3029   Drewnick, F.; Hings, S.; Jung, D. *et al.* Size Matters More Than Chemistry for Cloud-
3030   Nucleating Ability of Aerosol Particles. *Science* **2006**, *312*, 1375-1378.
3031   (169)   Petters, M. D.; Kreidenweis, S. M. A single parameter representation of hygroscopic
3032   growth and cloud condensation nucleus activity. *Atmos. Chem. Phys.* **2007**, *7*, 1961-1971.
3033   (170)   McFiggans, G.; Artaxo, P.; Baltensperger, U.; Coe, H.; Facchini, M. C.; Feingold, G.;
3034   Fuzzi, S.; Gysel, M.; Laaksonen, A.; Lohmann, U. *et al.* The effect of physical and
3035   chemical aerosol properties on warm cloud droplet activation. *Atmos. Chem. Phys.* **2006**,
3036   *6*, 2593-2649.
3037   (171)   Cwiertny, D. M.; Young, M. A.; Grassian, V. H. Chemistry and photochemistry of
3038   mineral dust aerosol. *Annu. Rev. Phys. Chem.* **2008**, *59*, 27-51.

3039   (172)   Crowley, J. N.; Ammann, M.; Cox, R. A.; Hynes, R. G.; Jenkin, M. E.; Mellouki, A.;
3040   Rossi, M. J.; Troe, J.; Wallington, T. J. Evaluated kinetic and photochemical data for
3041   atmospheric chemistry: Volume V - heterogeneous reactions on solid substrates. *Atmos.*
3042   *Chem. Phys.* **2010**, *10*, 9059-9223.
3043   (173)   Kolb, C. E.; Cox, R. A.; Abbatt, J. P. D.; Ammann, M.; Davis, E. J.; Donaldson, D. J.;
3044   Garrett, B. C.; George, C.; Griffiths, P. T.; Hanson, D. R. *et al.* An overview of current
3045   issues in the uptake of atmospheric trace gases by aerosols and clouds. *Atmos. Chem.*
3046   *Phys.* **2010**, *10*, 10561-10605.
3047   (174)   Tong, S. R.; Wu, L. Y.; Ge, M. F.; Wang, W. G.; Pu, Z. F. Heterogeneous chemistry of
3048   monocarboxylic acids on α-Al$_2$O$_3$ at different relative humidities. *Atmos. Chem. Phys.*
3049   **2010**, *10*, 7561-7574.
3050   (175)   Wu, L. Y.; Tong, S. R.; Wang, W. G.; Ge, M. F. Effects of temperature on the
3051   heterogeneous oxidation of sulfur dioxide by ozone on calcium carbonate. *Atmos. Chem.*
3052   *Phys.* **2011**, *11*, 6593-6605.
3053   (176)   Tang, M. J.; Li, M. Q.; Zhu, T. Heterogeneous reactions of gaseous methanesulfonic acid
3054   with calcium carbonate and kaolinite particles. *Sci. China-Chem.* **2010**, *53*, 2657-2662.
3055   (177)   Tang, M. J.; Thieser, J.; Schuster, G.; Crowley, J. N. Uptake of NO$_3$ and N$_2$O$_5$ to Saharan
3056   dust, ambient urban aerosol and soot: a relative rate study. *Atmos. Chem. Phys.* **2010**, *10*,
3057   2965-2974.
3058   (178)   Fu, H. B.; Wang, X.; Wu, H. B.; Yin, Y.; Chen, J. M. Heterogeneous uptake and
3059   oxidation of SO2 on iron oxides. *J. Phys. Chem. C* **2007**, *111*, 6077-6085.
3060   (179)   Kong, L. D.; Zhao, X.; Sun, Z. Y.; Yang, Y. W.; Fu, H. B.; Zhang, S. C.; Cheng, T. T.;
3061   Yang, X.; Wang, L.; Chen, J. M. The effects of nitrate on the heterogeneous uptake of
3062   sulfur dioxide on hematite. *Atmos. Chem. Phys.* **2014**, *14*, 9451-9467.
3063   (180)   Zhao, X.; Kong, L. D.; Sun, Z. Y.; Ding, X. X.; Cheng, T. T.; Yang, X.; Chen, J. M.
3064   Interactions between Heterogeneous Uptake and Adsorption of Sulfur Dioxide and
3065   Acetaldehyde on Hematite. *J. Phys. Chem. A* **2015**, *119*, 4001-4008.
3066   (181)   He, H.; Wang, Y.; Ma, Q.; Ma, J.; Chu, B.; Ji, D.; Tang, G.; Liu, C.; Zhang, H.; Hao, J.
3067   Mineral dust and NOx promote the conversion of SO2 to sulfate in heavy pollution days.
3068   *Sci. Rep.* **2014**, *4*, 4172, doi: 4110.1038/srep04172.
3069   (182)   Ma, Q.; Liu, Y.; Liu, C.; Ma, J.; He, H. A case study of Asian dust storm particles:
3070   Chemical composition, reactivity to SO2 and hygroscopic properties. *J. Environ. Sci.*
3071   **2012**, *24*, 62-71.
3072   (183)   Wu, L.-Y.; Tong, S.-R.; Zhou, L.; Wang, W.-G.; Ge, M.-F. Synergistic Effects between
3073   SO2 and HCOOH on α-Fe2O3. *J. Phys. Chem. A* **2013**, *117*, 3972-3979.
3074   (184)   Zhou, L.; Wang, W. G.; Gai, Y. B.; Ge, M. F. Knudsen cell and smog chamber study of
3075   the heterogeneous uptake of sulfur dioxide on Chinese mineral dust. *J. Environ. Sci.*
3076   **2014**, *26*, 2423-2433.
3077   (185)   Zhao, Y.; Chen, Z. M.; Shen, X. L.; Huang, D. Heterogeneous reactions of gaseous
3078   hydrogen peroxide on pristine and acidic gas-processed calcium carbonate particles:
3079   Effects of relative humidity and surface coverage of coating. *Atmos. Environ.* **2013**, *67*,
3080   63-72.
3081   (186)   Zhao, Y.; Chen, Z. M.; Shen, X. L.; Zhang, X. A. Kinetics and Mechanisms of
3082   Heterogeneous Reaction of Gaseous Hydrogen Peroxide on Mineral Oxide Particles.
3083   *Environ. Sci. Technol.* **2011**, *45*, 3317-3324.
3084   (187)   Arimoto, R.; Kim, Y. J.; Kim, Y. P.; Quinn, P. K.; Bates, T. S.; Anderson, T. L.; Gong,
3085   S.; Uno, I.; Chin, M.; Huebert, B. J. *et al.* Characterization of Asian Dust during ACE-
3086   Asia. *Glob. Planet. Change* **2006**, *52*, 23-56.

3087 (188) Deguillaume, L.; Leriche, M.; Desboeufs, K.; Mailhot, G.; George, C.; Chaumerliac, N.
3088   Transition metals in atmospheric liquid phases: Sources, reactivity, and sensitive
3089   parameters. *Chem. Rev.* **2005**, *105*, 3388-3431.
3090 (189) Jacob, D. J. Heterogeneous chemistry and tropospheric ozone. *Atmos. Environ.* **2000**, *34*,
3091   2131-2159.
3092 (190) Hoose, C.; Lohmann, U.; Bennartz, R.; Croft, B.; Lesins, G. Global simulations of
3093   aerosol processing in clouds. *Atmos. Chem. Phys.* **2008**, *8*, 6939-6963.
3094 (191) Desboeufs, K.; Journet, E.; Rajot, J. L.; Chevaillier, S.; Triquet, S.; Formenti, P.; Zakou,
3095   A. Chemistry of rain events in West Africa: evidence of dust and biogenic influence in
3096   convective systems. *Atmos. Chem. Phys.* **2010**, *10*, 9283-9293.
3097 (192) Dentener, F. J.; Carmichael, G. R.; Zhang, Y.; Lelieveld, J.; Crutzen, P. J. Role of
3098   mineral aerosol as a reactive surface in the global troposphere. *J. Geophys. Res.-Atmos.*
3099   **1996**, *101*, 22869-22889.
3100 (193) de Reus, M.; Fischer, H.; Sander, R.; Gros, V.; Kormann, R.; Salisbury, G.; Van
3101   Dingenen, R.; Williams, J.; Zollner, M.; Lelieveld, J. Observations and model
3102   calculations of trace gas scavenging in a dense Saharan dust plume during MINATROC.
3103   *Atmos. Chem. Phys.* **2005**, *5*, 1787-1803.
3104 (194) Bauer, S. E.; Balkanski, Y.; Schulz, M.; Hauglustaine, D. A.; Dentener, F. Global
3105   modeling of heterogeneous chemistry on mineral aerosol surfaces: Influence on
3106   tropospheric ozone chemistry and comparison to observations. *J. Geophys. Res.-Atmos.*
3107   **2004**, *109*, D02304, doi: 02310.01029/02003JD003868.
3108 (195) Matthews, P. S. J.; Baeza-Romero, M. T.; Whalley, L. K.; Heard, D. E. Uptake of HO2
3109   radicals onto Arizona test dust particles using an aerosol flow tube. *Atmos. Chem. Phys.*
3110   **2014**, *14*, 7397-7408.
3111 (196) Romanias, M. N.; El Zein, A.; Bedjanian, Y. Heterogeneous Interaction of H2O2 with
3112   TiO2 Surface under Dark and UV Light Irradiation Conditions. *J. Phys. Chem. A* **2012**,
3113   *116*, 8191-8200.
3114 (197) El Zein, A.; Romanias, M. N.; Bedjanian, Y. Heterogeneous Interaction of H2O2 with
3115   Arizona Test Dust. *J. Phys. Chem. A* **2014**, *118*, 441-448.
3116 (198) Sullivan, R. C.; Guazzotti, S. A.; Sodeman, D. A.; Tang, Y. H.; Carmichael, G. R.;
3117   Prather, K. A. Mineral dust is a sink for chlorine in the marine boundary layer. *Atmos.*
3118   *Environ.* **2007**, *41*, 7166-7179.
3119 (199) Goodman, A. L.; Underwood, G. M.; Grassian, V. H. A laboratory study of the
3120   heterogeneous reaction of nitric acid on calcium carbonate particles. *J. Geophys. Res.-*
3121   *Atmos.* **2000**, *105*, 29053-29064.
3122 (200) Prince, A. P.; Kleiber, P. D.; Grassian, V. H.; Young, M. A. Reactive uptake of acetic
3123   acid on calcite and nitric acid reacted calcite aerosol in an environmental reaction
3124   chamber. *Phys. Chem. Chem. Phys.* **2008**, *10*, 142-152.
3125 (201) Li, H. J.; Zhu, T.; Zhao, D. F.; Zhang, Z. F.; Chen, Z. M. Kinetics and mechanisms of
3126   heterogeneous reaction of NO2 on CaCO3 surfaces under dry and wet conditions. *Atmos.*
3127   *Chem. Phys.* **2010**, *10*, 463-474.
3128 (202) Li, W. J.; Shao, L. Y. Observation of nitrate coatings on atmospheric mineral dust
3129   particles. *Atmos. Chem. Phys.* **2009**, *9*, 1863-1871.
3130 (203) Li, W. J.; Shao, L. Y. Transmission electron microscopy study of aerosol particles from
3131   the brown hazes in northern China. *J. Geophys. Res.-Atmos.* **2009**, *114*, D09302, doi:
3132   09310.01029/02008jd011285.
3133 (204) Huang, X.; Song, Y.; Zhao, C.; Li, M.; Zhu, T.; Zhang, Q.; Zhang, X. Pathways of sulfate
3134   enhancement by natural and anthropogenic mineral aerosols in China. *J. Geophys. Res.-*
3135   *Atmos* **2014**, *119*, 14165-14179.

3136 (205) Tang, Y. H.; Carmichael, G. R.; Seinfeld, J. H.; Dabdub, D.; Weber, R. J.; Huebert, B.;
3137   Clarke, A. D.; Guazzotti, S. A.; Sodeman, D. A.; Prather, K. A. *et al.* Three-dimensional
3138   simulations of inorganic aerosol distributions in east Asia during spring 2001. *J.*
3139   *Geophys. Res.-Atmos.* **2004**, *109*, D19s23, doi: 10.1029/2003jd004201.
3140 (206) Hand, V. L.; Capes, G.; Vaughan, D. J.; Formenti, P.; Haywood, J. M.; Coe, H. Evidence
3141   of internal mixing of African dust and biomass burning particles by individual particle
3142   analysis using electron beam techniques. *J. Geophys. Res.-Atmos.* **2010**, *115*, D13301,
3143   doi: 13310.11029/12009jd012938.
3144 (207) Formenti, P.; Elbert, W.; Maenhaut, W.; Haywood, J.; Andreae, M. O. Chemical
3145   composition of mineral dust aerosol during the Saharan Dust Experiment (SHADE)
3146   airborne campaign in the Cape Verde region, September 2000. *J. Geophys. Res.-Atmos.*
3147   **2003**, *108*, 8576, doi: 8510.1029/2002jd002648.
3148 (208) Sullivan, R. C.; Prather, K. A. Investigations of the diurnal cycle and mixing state of
3149   oxalic acid in individual particles in Asian aerosol outflow. *Environ. Sci. Technol.* **2007**,
3150   *41*, 8062-8069.
3151 (209) Trochkine, D.; Iwasaka, Y.; Matsuki, A.; Yamada, M.; Kim, Y. S.; Nagatani, T.; Zhang,
3152   D.; Shi, G. Y.; Shen, Z. Mineral aerosol particles collected in Dunhuang, China, and their
3153   comparison with chemically modified particles collected over Japan. *J. Geophys. Res.-*
3154   *Atmos* **2003**, *108*.
3155 (210) Matsuki, A.; Iwasaka, Y.; Shi, G. Y.; Chen, H. B.; Osada, K.; Zhang, D.; Kido, M.;
3156   Inomata, Y.; Kim, Y. S.; Trochkine, D. *et al.* Heterogeneous Sulfate Formation on Dust
3157   Surface and Its Dependence on Mineralogy: Balloon-Borne Observations from Balloon-
3158   Borne Measurements in The Surface Atmosphere of Beijing, China. *Water Air Soil*
3159   *Pollut: Focus* **2005**, *5*, 101-132.
3160 (211) Al-Abadleh, H. A.; Krueger, B. J.; Ross, J. L.; Grassian, V. H. Phase transitions in
3161   calcium nitrate thin films. *Chem. Commun.* **2003**, 2796-2797.
3162 (212) Ma, Q. X.; Liu, Y. C.; Liu, C.; He, H. Heterogeneous reaction of acetic acid on MgO, α-
3163   Al2O3, and CaCO3 and the effect on the hygroscopic behavior of these particles. *Phys.*
3164   *Chem. Chem. Phys.* **2012**, *14*, 8403-8409.
3165 (213) Vlasenko, A.; Sjogren, S.; Weingartner, E.; Stemmler, K.; Gaggeler, H. W.; Ammann, M.
3166   Effect of humidity on nitric acid uptake to mineral dust aerosol particles. *Atmos. Chem.*
3167   *Phys.* **2006**, *6*, 2147-2160.
3168 (214) Krueger, B. J.; Grassian, V. H.; Laskin, A.; Cowin, J. P. The transformation of solid
3169   atmospheric particles into liquid droplets through heterogeneous chemistry: Laboratory
3170   insights into the processing of calcium containing mineral dust aerosol in the troposphere.
3171   *Geophys. Res. Lett.* **2003**, *30*, 1148, doi: 1110.1029/2002gl016563.
3172 (215) Liu, Y. J.; Zhu, T.; Zhao, D. F.; Zhang, Z. F. Investigation of the hygroscopic properties
3173   of $Ca(NO_3)_2$ and internally mixed $Ca(NO_3)_2/CaCO_3$ particles by micro-Raman
3174   spectrometry. *Atmos. Chem. Phys.* **2008**, *8*, 7205-7215.
3175 (216) Hatch, C. D.; Gierlus, K. M.; Schuttlefield, J. D.; Grassian, V. H. Water adsorption and
3176   cloud condensation nuclei activity of calcite and calcite coated with model humic and
3177   fulvic acids. *Atmos. Environ.* **2008**, *42*, 5672-5684.
3178 (217) Sullivan, R. C.; Moore, M. J. K.; Petters, M. D.; Kreidenweis, S. M.; Roberts, G. C.;
3179   Prather, K. A. Effect of chemical mixing state on the hygroscopicity and cloud nucleation
3180   properties of calcium mineral dust particles. *Atmos. Chem. Phys.* **2009**, *9*, 3303-3316.
3181 (218) Gierlus, K. M.; Laskina, O.; Abernathy, T. L.; Grassian, V. H. Laboratory study of the
3182   effect of oxalic acid on the cloud condensation nuclei activity of mineral dust aerosol.
3183   *Atmos. Environ.* **2012**, *46*, 125-130.

3184   (219)   Cziczo, D. J.; Froyd, K. D.; Gallavardin, S. J.; Moehler, O.; Benz, S.; Saathoff, H.;
3185   Murphy, D. M. Deactivation of ice nuclei due to atmospherically relevant surface
3186   coatings. *Environ. Res. Lett.* **2009**, *4*, 044013.
3187   (220)   Reitz, P.; Spindler, C.; Mentel, T. F.; Poulain, L.; Wex, H.; Mildenberger, K.;
3188   Niedermeier, D.; Hartmann, S.; Clauss, T.; Stratmann, F. *et al.* Surface modification of
3189   mineral dust particles by sulphuric acid processing: implications for ice nucleation
3190   abilities. *Atmos. Chem. Phys.* **2011**, *11*, 7839-7858.
3191   (221)   Niedermeier, D.; Hartmann, S.; Clauss, T.; Wex, H.; Kiselev, A.; Sullivan, R. C.;
3192   DeMott, P. J.; Petters, M. D.; Reitz, P.; Schneider, J. *et al.* Experimental study of the role
3193   of physicochemical surface processing on the IN ability of mineral dust particles. *Atmos.*
3194   *Chem. Phys.* **2011**, *11*, 11131-11144.
3195   (222)   Laskina, O.; Young, M. A.; Kleiber, P. D.; Grassian, V. H. Infrared extinction
3196   spectroscopy and micro-Raman spectroscopy of select components of mineral dust mixed
3197   with organic compounds. *J. Geophys. Res.-Atmos.* **2013**, *118*, 6593-6606.
3198   (223)   Abdelkader, M.; Metzger, S.; Mamouri, R. E.; Astitha, M.; Barrie, L.; Levin, Z.;
3199   Lelieveld, J. Dust–air pollution dynamics over the eastern Mediterranean. *Atmos. Chem.*
3200   *Phys.* **2015**, *15*, 9173-9189.
3201   (224)   Fan, S. M.; Horowitz, L. W.; Levy, H.; Moxim, W. J. Impact of air pollution on wet
3202   deposition of mineral dust aerosols. *Geophys. Res. Lett.* **2004**, *31*, 4.
3203   (225)   Meskhidze, N.; Chameides, W. L.; Nenes, A.; Chen, G. Iron mobilization in mineral dust:
3204   Can anthropogenic SO_2 emissions affect ocean productivity? *Geophys. Res. Lett.* **2003**,
3205   *30*, 2085, doi: 2010.1029/2003GL018035.
3206   (226)   Pradhan, M.; Kalberer, M.; Griffiths, P. T.; Braban, C. F.; Pope, F. D.; Cox, R. A.;
3207   Lambert, R. M. Uptake of Gaseous Hydrogen Peroxide by Submicrometer Titanium
3208   Dioxide Aerosol as a Function of Relative Humidity. *Environ. Sci. Technol.* **2010**, *44*,
3209   1360-1365.
3210   (227)   Liu, Y.; Gibson, E. R.; Cain, J. P.; Wang, H.; Grassian, V. H.; Laskin, A. Kinetics of
3211   heterogeneous reaction of $CaCO_3$ particles with gaseous HNO_3 over a wide range of
3212   humidity. *J. Phys. Chem. A* **2008**, *112*, 1561-1571.
3213   (228)   Nicolas, M.; Ndour, M.; Ka, O.; D'anna, B.; George, C. Photochemistry of atmospheric
3214   dust: ozone decomposition on illuminatd titanium dioxide. *Environ. Sci. Technol.* **2009**,
3215   *43*, 7347-7442.
3216   (229)   Rubasinghege, G.; Grassian, V. H. Role(s) of adsorbed water in the surface chemistry of
3217   environmental interfaces. *Chem. Commun.* **2013**, *49*, 3071-3094.
3218   (230)   Ewing, G. E. Ambient Thin Film Water on Insulator Surfaces. *Chem. Rev.* **2006**, *106*,
3219   1511-1526.
3220   (231)   Henderson, M. A. Structural Sensitivity in the Dissociation of Water on TiO2 Single-
3221   Crystal Surfaces. *Langmuir* **1996**, *12*, 5093-5098.
3222   (232)   Schaub, R.; Thostrup, P.; Lopez, N.; Lægsgaard, E.; Stensgaard, I.; Nørskov, J. K.;
3223   Besenbacher, F. Oxygen Vacancies as Active Sites for Water Dissociation on Rutile
3224 TiO_2(110). *Phys. Rev. Lett.* **2001**, *87*, 266104.
3225   (233)   Beaglehole, D.; Radlinska, E. Z.; Ninham, B. W.; Christenson, H. K. Inadequacy of
3226   Lifshitz theory for thin liquid films. *Phys. Rev. Lett.* **1991**, *66*, 2084-2087.
3227   (234)   Miranda, P. B.; Xu, L.; Shen, Y. R.; Salmeron, M. Icelike Water Monolayer Adsorbed on
3228   Mica at Room Temperature. *Phys. Rev. Lett.* **1998**, *81*, 5876-5879.
3229   (235)   Zhang, Z.; Bondarchuk, O.; Kay, B. D.; White, J. M.; Dohnálek, Z. Imaging Water
3230   Dissociation on TiO2(110): Evidence for Inequivalent Geminate OH Groups. *J. Phys.*
3231   *Chem. B* **2006**, *110*, 21840-21845.

(236) Smith, R. S.; Li, Z.; Chen, L.; Dohnálek, Z.; Kay, B. D. Adsorption, Desorption, and Displacement Kinetics of H2O and CO2 on TiO2(110). *J. Phys. Chem. B* **2014**, *118*, 8054-8061.

(237) Cantrell, W.; Heymsfield, A. Production of ice in tropospheric clouds - A review. *Bull. Amer. Meteorol. Soc.* **2005**, *86*, 795-807.

(238) Hoose, C.; Moehler, O. Heterogeneous ice nucleation on atmospheric aerosols: a review of results from laboratory experiments. *Atmos. Chem. Phys.* **2012**, *12*, 9817–9854.

(239) Ladino, L. A.; Stetzer, O.; Lohmann, U. Contact freezing: a review of experimental studies. *Atmos. Chem. Phys.* **2013**, *13*, 9745-9769.

(240) Al-Abadleh, H. A.; Grassian, V. H. FT-IR study of water adsorption on aluminum oxide surfaces. *Langmuir* **2003**, *19*, 341-347.

(241) Ketteler, G.; Yamamoto, S.; Bluhm, H.; Andersson, K.; Starr, D. E.; Ogletree, D. F.; Ogasawara, H.; Nilsson, A.; Salmeron, M. The Nature of Water Nucleation Sites on TiO2(110) Surfaces Revealed by Ambient Pressure X-ray Photoelectron Spectroscopy. *J. Phys. Chem. C* **2007**, *111*, 8278-8282.

(242) Yamamoto, S.; Kendelewicz, T.; Newberg, J. T.; Ketteler, G.; Starr, D. E.; Mysak, E. R.; Andersson, K. J.; Ogasawara, H.; Bluhm, H.; Salmeron, M. *et al.* Water Adsorption on α-Fe2O3(0001) at near Ambient Conditions. *J. Phys. Chem. C* **2010**, *114*, 2256-2266.

(243) Murphy, D. M.; Thomson, D. S.; Mahoney, T. M. J. In situ measurements of organics, meteoritic material, mercury, and other elements in aerosols at 5 to 19 kilometers. *Science* **1998**, *282*, 1664-1669.

(244) Cziczo, D. J.; Murphy, D. M.; Hudson, P. K.; Thomson, D. S. Single particle measurements of the chemical composition of cirrus ice residue during CRYSTAL-FACE. *J. Geophys. Res.-Atmos.* **2004**, *109*, D04201, doi: 04210.01029/02003jd004032.

(245) Laskin, A.; Iedema, M. J.; Ichkovich, A.; Graber, E. R.; Taraniuk, I.; Rudich, Y. Direct observation of completely processed calcium carbonate dust particles. *Faraday Discuss.* **2005**, *130*, 453-468.

(246) Navea, J. G.; Chen, H. H.; Huang, M.; Carmichael, G. R.; Grassian, V. H. A comparative evaluation of water uptake on several mineral dust sources. *Environ. Chem.* **2010**, *7*, 162-170.

(247) Gustafsson, R. J.; Orlov, A.; Badger, C. L.; Griffiths, P. T.; Cox, R. A.; Lambert, R. M. A comprehensive evaluation of water uptake on atmospherically relevant mineral surfaces: DRIFT spectroscopy, thermogravimetric analysis and aerosol growth measurements. *Atmos. Chem. Phys.* **2005**, *5*, 3415-3421.

(248) Ma, Q. X.; Liu, Y. C.; He, H. The Utilization of Physisorption Analyzer for Studying the Hygroscopic Properties of Atmospheric Relevant Particles. *J. Phys. Chem. A* **2010**, *114*, 4232-4237.

(249) Schuttlefield, J. D.; Cox, D.; Grassian, V. H. An investigation of water uptake on clays minerals using ATR-FTIR spectroscopy coupled with quartz crystal microbalance measurements. *J. Geophys. Res.-Atmos.* **2007**, *112*, D21303, doi: 21310.21029/22007JD008973.

(250) Goodman, A. L.; Bernard, E. T.; Grassian, V. H. Spectroscopic study of nitric acid and water adsorption on oxide particles: Enhanced nitric acid uptake kinetics in the presence of adsorbed water. *J. Phys. Chem. A* **2001**, *105*, 6443-6457.

(251) Pope, F. D.; Dennis-Smither, B. J.; Griffiths, P. T.; Clegg, S. L.; Cox, R. A. Studies of Single Aerosol Particles Containing Malonic Acid, Glutaric Acid, and Their Mixtures with Sodium Chloride. I. Hygroscopic Growth. *J. Phys. Chem. A* **2010**, *114*, 5335-5341.

3279 (252) Tong, H. J.; Reid, J. P.; Bones, D. L.; Luo, B. P.; Krieger, U. K. Measurements of the
3280   timescales for the mass transfer of water in glassy aerosol at low relative humidity and
3281   ambient temperature. *Atmos. Chem. Phys.* **2011**, *11*, 4739-4754.
3282 (253) Attwood, A. R.; Greenslade, M. E. Optical Properties and Associated Hygroscopicity of
3283   Clay Aerosols. *Aerosol Sci. Technol.* **2011**, *45*, 1350-1359.
3284 (254) Li-Jones, X.; Maring, H. B.; Prospero, J. M. Effect of relative humidity on light scattering
3285   by mineral dust aerosol as measured in the marine boundary layer over the tropical
3286   Atlantic Ocean. *J. Geophys. Res.-Atmos* **1998**, *103*, 31113-31121.
3287 (255) Utry, N.; Ajtai, T.; Pintér, M.; Tombácz, E.; Illés, E.; Bozóki, Z.; Szabó, G. Mass-specific
3288   optical absorption coefficients and imaginary part of the complex refractive indices of
3289   mineral dust components measured by a multi-wavelength photoacoustic spectrometer.
3290   *Atmos. Meas. Tech.* **2015**, *8*, 401-410.
3291 (256) Sullivan, R. C.; Moore, M. J. K.; Petters, M. D.; Kreidenweis, S. M.; Qafoku, O.; Laskin,
3292   A.; Roberts, G. C.; Prather, K. A. Impact of Particle Generation Method on the Apparent
3293   Hygroscopicity of Insoluble Mineral Particles. *Aerosol Sci. Technol.* **2010**, *44*, 830-846.
3294 (257) Gibson, E. R.; Gierlus, K. M.; Hudson, P. K.; Grassian, V. H. Generation of internally
3295   mixed insoluble and soluble aerosol particles to investigate the impact of atmospheric
3296   aging and heterogeneous processing on the CCN activity of mineral dust aerosol. *Aerosol*
3297   *Sci. Technol.* **2007**, *41*, 914-924.
3298 (258) Sullivan, R. C.; Moore, M. J. K.; Petters, M. D.; Kreidenweis, S. M.; Roberts, G. C.;
3299   Prather, K. A. Timescale for hygroscopic conversion of calcite mineral particles through
3300   heterogeneous reaction with nitric acid. *Phys. Chem. Chem. Phys.* **2009**, *11*, 7826-7837.
3301 (259) Garimella, S.; Huang, Y. W.; Seewald, J. S.; Cziczo, D. J. Cloud condensation nucleus
3302   activity comparison of dry- and wet-generated mineral dust aerosol: the significance of
3303   soluble material. *Atmos. Chem. Phys.* **2014**, *14*, 6003-6019.
3304 (260) Vlasenko, A.; Sjogren, S.; Weingartner, E.; Gaggeler, H. W.; Ammann, M. Generation of
3305   submicron Arizona test dust aerosol: Chemical and hygroscopic properties. *Aerosol Sci.*
3306   *Technol.* **2005**, *39*, 452-460.
3307 (261) Sullivan, R. C.; Petters, M. D.; DeMott, P. J.; Kreidenweis, S. M.; Wex, H.; Niedermeier,
3308   D.; Hartmann, S.; Clauss, T.; Stratmann, F.; Reitz, P. *et al.* Irreversible loss of ice
3309   nucleation active sites in mineral dust particles caused by sulphuric acid condensation.
3310   *Atmos. Chem. Phys.* **2010**, *10*, 11471-11487.
3311 (262) Kumar, P.; Sokolik, I. N.; Nenes, A. Measurements of cloud condensation nuclei activity
3312   and droplet activation kinetics of fresh unprocessed regional dust samples and minerals.
3313   *Atmos. Chem. Phys.* **2011**, *11*, 3527-3541.
3314 (263) Kumar, P.; Sokolik, I. N.; Nenes, A. Cloud condensation nuclei activity and droplet
3315   activation kinetics of wet processed regional dust samples and minerals. *Atmos. Chem.*
3316   *Phys.* **2011**, *11*, 8661-8676.
3317 (264) Zhao, D. F.; Buchholz, A.; Mentel, T. F.; Müller, K. P.; Borchardt, J.; Kiendler-Scharr,
3318   A.; Spindler, C.; Tillmann, R.; Trimborn, A.; Zhu, T. *et al.* Novel method of generation
3319   of Ca(HCO3)2 and CaCO3 aerosols and first determination of hygroscopic and cloud
3320   condensation nuclei activation properties. *Atmos. Chem. Phys.* **2010**, *10*, 8601-8616.
3321 (265) Wurzler, S.; Reisin, T. G.; Levin, Z. Modification of mineral dust particles by cloud
3322   processing and subsequent effects on drop size distributions. *J. Geophys. Res.-Atmos*
3323   **2000**, *105*, 4501-4512.
3324 (266) Smoydzin, L.; Teller, A.; Tost, H.; Fnais, M.; Lelieveld, J. Impact of mineral dust on
3325   cloud formation in a Saharan outflow region. *Atmos. Chem. Phys.* **2012**, *12*, 11383-
3326   11393.

3327 (267) Begue, N.; Tulet, P.; Pelon, J.; Aouizerats, B.; Berger, A.; Schwarzenboeck, A. Aerosol
3328   processing and CCN formation of an intense Saharan dust plume during the EUCAARI
3329   2008 campaign. *Atmos. Chem. Phys.* **2015**, *15*, 3497-3516.
3330 (268) Hatch, C. D.; Wiese, J. S.; Crane, C. C.; Harris, K. J.; Kloss, H. G.; Baltrusaitis, J. Water
3331   Adsorption on Clay Minerals As a Function of Relative Humidity: Application of BET
3332   and Freundlich Adsorption Models. *Langmuir* **2011**, *28*, 1790-1803.
3333 (269) Ma, Q. X.; He, H.; Liu, Y. C. In situ DRIFTS study of hygroscopic behavior of mineral
3334   aerosol. *J. Environ. Sci.* **2010**, *22*, 555-560.
3335 (270) Hung, H. M.; Wang, K. C.; Chen, J. P. Adsorption of nitrogen and water vapor by
3336   insoluble particles and the implication on cloud condensation nuclei activity. *J. Aerosol.*
3337   *Sci.* **2015**, *86*, 24-31.
3338 (271) Arenas, K. J. L.; Schill, S. R.; Malla, A.; Hudson, P. K. Deliquescence Phase Transition
3339   Measurements by Quartz Crystal Microbalance Frequency Shifts. *J. Phys. Chem. A* **2012**,
3340   *116*, 7658-7667.
3341 (272) Lu, C. S.; Lewis, O. Investigation of film‐thickness determination by oscillating quartz
3342   resonators with large mass load. *J. Appl. Phys.* **1972**, *43*, 4385-4390.
3343 (273) Schuttlefield, J.; Al-Hosney, H.; Zachariah, A.; Grassian, V. H. Attenuated total
3344   reflection Fourier transform infrared spectroscopy to investigate water uptake and phase
3345   transitions in atmospherically relevant particles. *Appl. Spectrosc.* **2007**, *61*, 283-292.
3346 (274) Wijenayaka, L. A.; Rubasinghege, G.; Baltrusaitis, J.; Grassian, V. H. Surface Chemistry
3347   of alpha-FeOOH Nanorods and Microrods with Gas-Phase Nitric Acid and Water Vapor:
3348   Insights into the Role of Particle Size, Surface Structure, and Surface Hydroxyl Groups in
3349   the Adsorption and Reactivity of alpha-FeOOH with Atmospheric Gases. *J. Phys. Chem.*
3350   *C* **2012**, *116*, 12566-12577.
3351 (275) Song, X. W.; Boily, J. F. Water Vapor Adsorption on Goethite. *Environ. Sci. Technol.*
3352   **2013**, *47*, 7171-7177.
3353 (276) Wendt, S.; Schaub, R.; Matthiesen, J.; Vestergaard, E. K.; Wahlström, E.; Rasmussen, M.
3354   D.; Thostrup, P.; Molina, L. M.; Lægsgaard, E.; Stensgaard, I. *et al.* Oxygen vacancies on
3355   TiO2(1 1 0) and their interaction with H2O and O2: A combined high-resolution STM
3356   and DFT study. *Surf. Sci.* **2005**, *598*, 226-245.
3357 (277) Wendt, S.; Matthiesen, J.; Schaub, R.; Vestergaard, E. K.; Lægsgaard, E.; Besenbacher,
3358   F.; Hammer, B. Formation and Splitting of Paired Hydroxyl Groups on Reduced
3359   TiO2(110). *Phys. Rev. Lett.* **2006**, *96*, 066107.
3360 (278) He, Y.; Tilocca, A.; Dulub, O.; Selloni, A.; Diebold, U. Local ordering and electronic
3361   signatures of submonolayer water on anatase TiO2(101). *Nat Mater* **2009**, *8*, 585-589.
3362 (279) Krueger, B. J.; Grassian, V. H.; Iedema, M. J.; Cowin, J. P.; Laskin, A. Probing
3363   heterogeneous chemistry of individual atmospheric particles using scanning electron
3364   microscopy and energy-dispersive X-ray analysis. *Anal. Chem.* **2003**, *75*, 5170-5179.
3365 (280) Salmeron, M.; Schlogl, R. Ambient pressure photoelectron spectroscopy: A new tool for
3366   surface science and nanotechnology. *Surf. Sci. Rep.* **2008**, *63*, 169-199.
3367 (281) Lampimäki, M.; Schreiber, S.; Zelenay, V.; Křepelová, A.; Birrer, M.; Axnanda, S.; Mao,
3368   B.; Liu, Z.; Bluhm, H.; Ammann, M. Exploring the Environmental Photochemistry on the
3369   TiO2(110) Surface in Situ by Near Ambient Pressure X-ray Photoelectron Spectroscopy.
3370   *J. Phys. Chem. C* **2015**, *119*, 7076-7085.
3371 (282) Lampimaki, M.; Zelenay, V.; Krepelova, A.; Liu, Z.; Chang, R.; Bluhm, H.; Ammann,
3372   M. Ozone-Induced Band Bending on Metal-Oxide Surfaces Studied under Environmental
3373   Conditions. *ChemPhysChem* **2013**, *14*, 2419 – 2425.
3374 (283) Rosseler, O.; Sleiman, M.; Montesinos, V. N.; Shavorskiy, A.; Keller, V.; Keller, N.;
3375   Litter, M. I.; Bluhm, H.; Salmeron, M.; Destaillats, H. Chemistry of NOx on TiO2

3376   Surfaces Studied by Ambient Pressure XPS: Products, Effect of UV Irradiation, Water,
3377   and Coadsorbed K+. *J. Phys. Chem. Lett.* **2013**, *4*, 536-541.
3378   (284)   Starr, D. E.; Liu, Z.; Havecker, M.; Knop-Gericke, A.; Bluhm, H. Investigation of
3379   solid/vapor interfaces using ambient pressure X-ray photoelectron spectroscopy. *Chem.*
3380   *Soc. Rev.* **2013**, *42*, 5833-5857.
3381   (285)   Perry, A.; Neipert, C.; Space, B.; Moore, P. B. Theoretical modeling of interface specific
3382   vibrational spectroscopy: Methods and applications to aqueous interfaces. *Chem. Rev.*
3383   **2006**, *106*, 1234-1258.
3384   (286)   Shen, Y. R.; Ostroverkhov, V. Sum-frequency vibrational spectroscopy on water
3385   interfaces: Polar orientation of water molecules at interfaces. *Chem. Rev.* **2006**, *106*,
3386   1140-1154.
3387   (287)   Ebben, C. J.; Ault, A. P.; Ruppel, M. J.; Ryder, O. S.; Bertram, T. H.; Grassian, V. H.;
3388   Prather, K. A.; Geiger, F. M. Size-Resolved Sea Spray Aerosol Particles Studied by
3389   Vibrational Sum Frequency Generation. *J. Phys. Chem. A* **2013**, *117*, 6589-6601.
3390   (288)   Jubb, A. M.; Hua, W.; Allen, H. C. Environmental Chemistry at Vapor/Water Interfaces:
3391   Insights from Vibrational Sum Frequency Generation Spectroscopy. *Annu. Rev. Phys.*
3392   *Chem.* **2012**, *63*, 107-130.
3393   (289)   Ma, G.; Liu, D. F.; Allen, H. C. Piperidine adsorption on hydrated alpha-alumina (0001)
3394   surface studied by vibrational sum frequency generation spectroscopy. *Langmuir* **2004**,
3395   *20*, 11620-11629.
3396   (290)   Liu, D. F.; Ma, G.; Xu, M.; Allen, H. C. Adsorption of ethylene glycol vapor on α-
3397   Al2O3(0001) and amorphous SiO2 surfaces: Observation of molecular orientation and
3398   surface hydroxyl groups as sorption sites. *Environ. Sci. Technol.* **2005**, *39*, 206-212.
3399   (291)   Baltrusaitis, J.; Grassian, V. H. Calcite (1014) surface in humid environments. *Surf. Sci.*
3400   **2009**, *603*, L99-L104.
3401   (292)   Stipp, S. L. S.; Konnerup-Madsen, J.; Franzreb, K.; Kulik, A.; Mathieu, H. J.
3402   Spontaneous movement of ions through calcite at standard temperature and pressure.
3403   *Nature* **1998**, *396*, 356-359.
3404   (293)   Carpick, R. W.; Salmeron, M. Scratching the Surface: Fundamental Investigations of
3405   Tribology with Atomic Force Microscopy. *Chem. Rev.* **1997**, *97*, 1163-1194.
3406   (294)   Xu, L.; Lio, A.; Hu, J.; Ogletree, D. F.; Salmeron, M. Wetting and Capillary Phenomena
3407   of Water on Mica. *J. Phys. Chem. B* **1998**, *102*, 540-548.
3408   (295)   Caloz, F.; Fenter, F. F.; Tabor, K. D.; Rossi, M. J. Paper I: Design and construction of a
3409   Knudsen-cell reactor for the study of heterogeneous reactions over the temperature range
3410   130-750 K: Performances and limitations. *Rev. Sci. Instrum.* **1997**, *68*, 3172-3179.
3411   (296)   Underwood, G. M.; Miller, T. M.; Grassian, V. H. Transmission FT-IR and Knudsen cell
3412   study of the heterogeneous reactivity of gaseous nitrogen dioxide on mineral oxide
3413   particles. *J. Phys. Chem. A* **1999**, *103*, 6184-6190.
3414   (297)   Liu, Y.; Ma, J.; Liu, C.; He, H. Heterogeneous uptake of carbonyl sulfide onto kaolinite
3415   within a temperature range of 220–330 K. *J. Geophys. Res.-Atmos* **2010**, *115*, D24311,
3416   doi: 24310.21029/22010JD014778.
3417   (298)   Seisel, S.; Lian, Y.; Keil, T.; Trukhin, M. E.; Zellner, R. Kinetics of the interaction of
3418   water vapour with mineral dust and soot surfaces at T=298 K. *Phys. Chem. Chem. Phys.*
3419   **2004**, *6*, 1926-1932.
3420   (299)   Seisel, S.; Pashkova, A.; Lian, Y.; Zellner, R. Water uptake on mineral dust and soot: A
3421   fundamental view of the hydrophilicity of atmospheric particles? *Faraday Discuss.* **2005**,
3422   *130*, 437-451.
3423   (300)   Nathanson, G. M.; Davidovits, P.; Worsnop, D. R.; Kolb, C. E. Dynamics and kinetics at
3424   the gas-liquid interface. *J. Phys. Chem.* **1996**, *100*, 13007-13020.

3425   (301)   Kong, X.; Thomson, E. S.; Papagiannakopoulos, P.; Johansson, S. M.; Pettersson, J. B. C.
3426   Water Accommodation on Ice and Organic Surfaces: Insights from Environmental
3427   Molecular Beam Experiments. *J. Phys. Chem. B* **2014**, *118*, 13378-13386.
3428   (302)   Nathanson, G. M. Molecular beam studies of gas-liquid interfaces. *Annu. Rev. Phys.*
3429   *Chem.* **2004**, *55*, 231-255.
3430   (303)   Burden, D. K.; Johnson, A. M.; Nathanson, G. M. HCl Uptake through Films of
3431   Pentanoic Acid and Pentanoic Acid/Hexanol Mixtures at the Surface of Sulfuric Acid. *J.*
3432   *Phys. Chem. A* **2009**, *113*, 14131-14140.
3433   (304)   Kong, X.; Papagiannakopoulos, P.; Thomson, E. S.; Marković, N.; Pettersson, J. B. C.
3434   Water Accommodation and Desorption Kinetics on Ice. *J. Phys. Chem. A* **2014**, *118*,
3435   3973-3979.
3436   (305)   Thomson, E. S.; Kong, X.; Papagiannakopoulos, P.; Pettersson, J. B. C. Deposition-mode
3437   ice nucleation reexamined at temperatures below 200 K. *Atmos. Chem. Phys.* **2015**, *15*,
3438   1621-1632.
3439   (306)   Krieger, U. K.; Marcolli, C.; Reid, J. P. Exploring the complexity of aerosol particle
3440   properties and processes using single particle techniques. *Chem. Soc. Rev.* **2012**, *41*,
3441   6631-6662.
3442   (307)   Peng, C.; Chan, C. K. The water cycles of water-soluble organic salts of atmospheric
3443   importance. *Atmos. Environ.* **2001**, *35*, 1183-1192.
3444   (308)   Reid, J. P.; Sayer, R. M. Heterogeneous atmospheric aerosol chemistry: laboratory
3445   studies of chemistry on water droplets. *Chem. Soc. Rev.* **2003**, *32*, 70-79.
3446   (309)   King, M. D.; Thompson, K. C.; Ward, A. D. Laser Tweezers Raman Study of Optically
3447   Trapped Aerosol Droplets of Seawater and Oleic Acid Reacting with Ozone:
3448   Implications for Cloud-Droplet Properties. *J. Am. Chem. Soc.* **2004**, *126*, 16710-16711.
3449   (310)   Hunt, O. R.; Ward, A. D.; King, M. D. Heterogeneous oxidation of nitrite anion by gas-
3450   phase ozone in an aqueous droplet levitated by laser tweezers (optical trap): is there any
3451   evidence for enhanced surface reaction? *Phys. Chem. Chem. Phys.* **2015**, *17*, 2734-2741.
3452   (311)   Rkiouak, L.; Tang, M. J.; Camp, J. C. J.; McGregor, J.; Watson, I. M.; Cox, R. A.;
3453   Kalberer, M.; Ward, A. D.; Pope, F. D. Optical trapping and Raman Spectroscopy of
3454   solid aerosol particles. *Phys. Chem. Chem. Phys.* **2014**, *16*, 11426-11434.
3455   (312)   Miles, R. E. H.; Walker, J. S.; Burnham, D. R.; Reid, J. P. Retrieval of the complex
3456   refractive index of aerosol droplets from optical tweezers measurements. *Phys. Chem.*
3457   *Chem. Phys.* **2012**, *14*, 3037-3047.
3458   (313)   Power, R. M.; Burnham, D. R.; Reid, J. P. Toward optical-tweezers-based force
3459   microscopy for airborne microparticles. *Appl. Optics* **2014**, *53*, 8522-8534.
3460   (314)   Lee, A. K. Y.; Ling, T. Y.; Chan, C. K. Understanding hygroscopic growth and phase
3461   transformation of aerosols using single particle Raman spectroscopy in an electrodynamic
3462   balance. *Faraday Discuss.* **2008**, *137*, 245-263.
3463   (315)   Choi, M. Y.; Chan, C. K. Investigation of Efflorescence of Inorganic Aerosols Using
3464   Fluorescence Spectroscopy. *J. Phys. Chem. A* **2005**, *109*, 1042-1048.
3465   (316)   Swietlicki, E.; Hansson, H. C.; Hameri, K.; Svenningsson, B.; Massling, A.; McFiggans,
3466   G.; McMurry, P. H.; Petaja, T.; Tunved, P.; Gysel, M. *et al.* Hygroscopic properties of
3467   submicrometer atmospheric aerosol particles measured with H-TDMA instruments in
3468   various environments - a review. *Tellus Ser. B-Chem. Phys. Meteorol.* **2008**, *60*, 432-469.
3469   (317)   Weingartner, E.; Gysel, M.; Baltensperger, U. Hygroscopicity of Aerosol Particles at
3470   Low Temperatures. 1. New Low-Temperature H-TDMA Instrument: Setup and First
3471   Applications. *Environ. Sci. Technol.* **2002**, *36*, 55-62.

3472   (318) Duplissy, J.; Gysel, M.; Sjogren, S.; Meyer, N.; Good, N.; Kammermann, L.; Michaud,
3473   V.; Weigel, R.; Martins dos Santos, S.; Gruening, C. *et al.* Intercomparison study of six
3474   HTDMAs: results and recommendations. *Atmos. Meas. Tech.* **2009**, *2*, 363-378.
3475   (319) Wex, H.; Petters, M. D.; Carrico, C. M.; Hallbauer, E.; Massling, A.; McMeeking, G. R.;
3476   Poulain, L.; Wu, Z.; Kreidenweis, S. M.; Stratmann, F. Towards closing the gap between
3477   hygroscopic growth and activation for secondary organic aerosol: Part 1 – Evidence from
3478   measurements. *Atmos. Chem. Phys.* **2009**, *9*, 3987-3997.
3479   (320) Keskinen, H.; Romakkaniemi, S.; Jaatinen, A.; Miettinen, P.; Saukko, E.; Jorma, J.;
3480   Mäkelä, J. M.; Virtanen, A.; Smith, J. N.; Laaksonen, A. On-Line Characterization of
3481   Morphology and Water Adsorption on Fumed Silica Nanoparticles. *Aerosol Sci. Technol.*
3482   **2011**, *45*, 1441-1447.
3483   (321) Ardon-Dryer, K.; Garimella, S.; Huang, Y. W.; Christopoulos, C.; Cziczo, D. J.
3484   Evaluation of DMA Size Selection of Dry Dispersed Mineral Dust Particles. *Aerosol Sci.*
3485   *Technol.* **2015**, *49*, 828-841.
3486   (322) Veghte, D. P.; Freedman, M. A. The Necessity of Microscopy to Characterize the Optical
3487   Properties of Size-Selected, Nonspherical Aerosol Particles. *Anal. Chem.* **2012**, *84*, 9101-
3488   9108.
3489   (323) Garland, R. M.; Ravishankara, A. R.; Lovejoy, E. R.; Tolbert, M. A.; Baynard, T.
3490   Parameterization for the relative humidity dependence of light extinction: Organic-
3491   ammonium sulfate aerosol. *J. Geophys. Res.-Atmos.* **2007**, *112*, D19303, doi:
3492   19310.11029/12006JD008179.
3493   (324) Langridge, J. M.; Richardson, M. S.; Lack, D.; Law, D.; Murphy, D. M. Aircraft
3494   Instrument for Comprehensive Characterization of Aerosol Optical Properties, Part I:
3495   Wavelength-Dependent Optical Extinction and Its Relative Humidity Dependence
3496   Measured Using Cavity Ringdown Spectroscopy. *Aerosol Sci. Technol.* **2011**, *45*, 1305-
3497   1318.
3498   (325) Washenfelder, R. A.; Flores, J. M.; Brock, C. A.; Brown, S. S.; Rudich, Y. Broadband
3499   measurements of aerosol extinction in the ultraviolet spectral region. *Atmos. Meas. Tech.*
3500   **2013**, *6*, 861-877.
3501   (326) Baynard, T.; Garland, R. M.; Ravishankara, A. R.; Tolbert, M. A.; Lovejoy, E. R. Key
3502   factors influencing the relative humidity dependence of aerosol light scattering. *Geophys.*
3503   *Res. Lett.* **2006**, *33*, L06813, doi: 06810.01029/02005GL024898.
3504   (327) Meland, B.; Kleiber, P. D.; Grassian, V. H.; Young, M. A. Visible light scattering study
3505   at 470, 550, and 660 nm of components of mineral dust aerosol: Hematite and goethite. *J.*
3506   *Quant. Spectrosc. Radiat. Transf.* **2011**, *112*, 1108-1118.
3507   (328) Malm, W. C.; Day, D. E.; Kreidenweis, S. M. Light Scattering Characteristics of
3508   Aerosols as a Function of Relative Humidity: Part I—A Comparison of Measured
3509   Scattering and Aerosol Concentrations Using the Theoretical Models. *J. Air Waste*
3510   *Manage. Assoc.* **2000**, *50*, 686-700.
3511   (329) Lack, D. A.; Lovejoy, E. R.; Baynard, T.; Pettersson, A.; Ravishankara, A. R. Aerosol
3512   absorption measurement using photoacoustic spectroscopy: Sensitivity, calibration, and
3513   uncertainty developments. *Aerosol Sci. Technol.* **2006**, *40*, 697-708.
3514   (330) Roberts, G. C.; Nenes, A. A continuous-flow streamwise thermal-gradient CCN chamber
3515   for atmospheric measurements. *Aerosol Sci. Technol.* **2005**, *39*, 206-221.
3516   (331) Lance, S.; Medina, J.; Smith, J. N.; Nenes, A. Mapping the operation of the DMT
3517   Continuous Flow CCN counter. *Aerosol Sci. Technol.* **2006**, *40*, 242-254.
3518   (332) Good, N.; Coe, H.; McFiggans, G. Instrumentational operation and analytical
3519   methodology for the reconciliation of aerosol water uptake under sub- and supersaturated
3520   conditions. *Atmos. Meas. Tech.* **2010**, *3*, 1241-1254.

3521   (333)   Lathem, T. L.; Nenes, A. Water Vapor Depletion in the DMT Continuous-Flow CCN
3522   Chamber: Effects on Supersaturation and Droplet Growth. *Aerosol Sci. Technol.* **2011**,
3523   *45*, 604-615.
3524   (334)   Ehara, K.; Hagwood, C.; Coakley, K. J. Novel method to classify aerosol particles
3525   according to their mass-to-charge ratio—Aerosol particle mass analyser. *J. Aerosol. Sci.*
3526   **1996**, *27*, 217-234.
3527   (335)   Park, K.; Cao, F.; Kittelson, D. B.; McMurry, P. H. Relationship between Particle Mass
3528   and Mobility for Diesel Exhaust Particles. *Environ. Sci. Technol.* **2003**, *37*, 577-583.
3529   (336)   Khalizov, A. F.; Zhang, R. Y.; Zhang, D.; Xue, H. X.; Pagels, J.; McMurry, P. H.
3530   Formation of highly hygroscopic soot aerosols upon internal mixing with sulfuric acid
3531   vapor. *J. Geophys. Res.-Atmos.* **2009**, *114*, D05208, doi: 05210.01029/02008JD010595.
3532   (337)   Abegglen, M.; Durdina, L.; Brem, B. T.; Wang, J.; Rindlisbacher, T.; Corbin, J. C.;
3533   Lohmann, U.; Sierau, B. Effective density and mass–mobility exponents of particulate
3534   matter in aircraft turbine exhaust: Dependence on engine thrust and particle size. *J.*
3535   *Aerosol. Sci.* **2015**, *88*, 135-147.
3536   (338)   Amaral, S. S.; de Carvalho, J. A.; Costa, M. A. M.; Pinheiro, C. An Overview of
3537   Particulate Matter Measurement Instruments. *Atmosphere* **2015**, *6*, 1327-1345.
3538   (339)   Pope, F. D. Pollen grains are efficient cloud condensation nuclei. *Environ. Res. Lett.*
3539   **2010**, *5*, 044015.
3540   (340)   Atkins, P. W. *Physical Chemistry (Sixith Edition)*; Oxford University Press: Oxford, UK,
3541   1998.
3542   (341)   Lowell, S.; Shields, J. E.; Thomas, M. A.; Thommes, M. *Characterization of Porous*
3543   *Solids and Powders: Surface Area, Pore Size and Density*; Springer: Netherlands, 2010.
3544   (342)   Crittenden, B.; Thomas, W. J. *Adsorption Technology & Design*; Butterworth-
3545   Heinemann: Oxford, UK, 1998.
3546   (343)   Langmuir, I. The consitution and fundmental properties of solids and liquids. Part I.
3547   Solids. *J. Am. Chem. Soc.* **1916**, *38*, 2221-2295.
3548   (344)   Brunauer, S.; Emmett, P. H.; Teller, E. Adsorption of Gases in Multimolecular Layers. *J.*
3549   *Am. Chem. Soc.* **1938**, *60*, 309-319.
3550   (345)   Joyner, L. G.; Weinberger, E. B.; Montgomery, C. W. Surface Area Measurements of
3551   Activated Carbons, Silica Gel and other Adsorbents. *J. Am. Chem. Soc.* **1945**, *67*, 2182-
3552   2188.
3553   (346)   Sips, R. On the Structure of a Catalyst Surface. *J. Chem. Phys.* **1948**, *16*, 490-495.
3554   (347)   Skopp, J. Derivation of the Freundlich Adsorption Isotherm from Kinetics. *J. Chem.*
3555   *Educ.* **2009**, *86*, 1341.
3556   (348)   Hatch, C. D.; Greenaway, A. L.; Christie, M. J.; Baltrusaitis, J. Water adsorption
3557   constrained Frenkel–Halsey–Hill adsorption activation theory: Montmorillonite and illite.
3558   *Atmos. Environ.* **2014**, *87*, 26-33.
3559   (349)   Sorjamaa, R.; Laaksonen, A. The effect of H_2O adsorption on cloud drop activation of
3560   insoluble particles: a theoretical framework. *Atmos. Chem. Phys.* **2007**, *7*, 6175-6180.
3561   (350)   Kohler, H. The nucleus in and the growth of hygroscopic droplets. *Trans. Faraday Soc.*
3562   **1936**, *32*, 1152-1161.
3563   (351)   Farmer, D. K.; Cappa, C. D.; Kreidenweis, S. M. Atmospheric Processes and Their
3564   Controlling Influence on Cloud Condensation Nuclei Activity. *Chem. Rev.* **2015**, *115*,
3565   4199-4217.
3566   (352)   Henson, B. F. An adsorption model of insoluble particle activation: Application to black
3567   carbon. *J. Geophys. Res.-Atmos* **2007**, *112*, D24S16, doi: 10.1029/2007JD008549.

3568   (353)   DeCarlo, P. F.; Slowik, J. G.; Worsnop, D. R.; Davidovits, P.; Jimenez, J. L. Particle
3569   morphology and density characterization by combined mobility and aerodynamic
3570   diameter measurements. Part 1: Theory. *Aerosol Sci. Technol.* **2004**, *38*, 1185-1205.
3571   (354)   Al-Hosney, H. A.; Grassian, V. H. Water, sulfur dioxide and nitric acid adsorption on
3572   calcium carbonate: A transmission and ATR-FTIR study. *Phys. Chem. Chem. Phys.*
3573   **2005**, *7*, 1266-1276.
3574   (355)   Gibson, E. R.; Hudson, P. K.; Grassian, V. H. Aerosol chemistry and climate: Laboratory
3575   studies of the carbonate component of mineral dust and its reaction products. *Geophys.*
3576   *Res. Lett.* **2006**, *33*, L13811, doi: 13810.11029/12006GL026386.
3577   (356)   Schuttlefield, J. D. *Laboratory studies of reactions of atmospheric gases with components*
3578   *of mineral dust aerosol and research in chemical education, PhD Dissertation*; The
3579   University of Iowa, Iowa City, USA, 2008.
3580   (357)   Tang, M. J.; Whitehead, J.; Davidson, N. M.; Pope, F. D.; Alfarra, M. R.; McFiggans, G.;
3581   Kalberer, M. Cloud condensation nucleation activities of calcium carbonate and its
3582   atmospheric ageing products. *Phys. Chem. Chem. Phys.* **2015**, *17*, 32194-32203.
3583   (358)   Neagle, W.; Rochester, C. H. Infrared study of the adsorption of water and ammonia on
3584   calcium carbonate. *J. Chem. Soc., Faraday Trans.* **1990**, *86*, 181-183.
3585   (359)   Bohr, J.; Wogelius, R. A.; Morris, P. M.; Stipp, S. L. S. Thickness and structure of the
3586   water film deposited from vapour on calcite surfaces. *Geochim. Cosmochim. Acta* **2010**,
3587   *74*, 5985-5999.
3588   (360)   Stipp, S. L. S.; Eggleston, C. M.; Nielsen, B. S. Calcite Surface-Structure Observed at
3589   Microtopographic and Molecular Scales with Atomic-Force Microscopy (Afm).
3590   *Geochim. Cosmochim. Acta* **1994**, *58*, 3023-3033.
3591   (361)   Stipp, S. L. S. Toward a conceptual model of the calcite surface: Hydration, hydrolysis,
3592   and surface potential. *Geochim. Cosmochim. Acta* **1999**, *63*, 3121-3131.
3593   (362)   Hausner, D. B.; Reeder, R. J.; Strongin, D. R. Humidity-induced restructuring of the
3594   calcite surface and the effect of divalent heavy metals. *J. Colloid Interface Sci.* **2007**,
3595   *305*, 101-110.
3596   (363)   Al-Abadleh, H. A.; Grassian, V. H. Phase transitions in magnesium nitrate thin films: A
3597   transmission FT-IR study of the deliquescence and efflorescence of nitric acid reacted
3598   magnesium oxide interfaces. *J. Phys. Chem. B* **2003**, *107*, 10829-10839.
3599   (364)   Tang, I. N.; Fung, K. H. Hydration and Raman scattering studies of levitated
3600   microparticles: $Ba(NO_3)_2$, $Sr(NO_3)_2$, and $Ca(NO_3)_2$. *J. Chem. Phys.* **1997**, *106*, 1653-
3601   1660.
3602   (365)   Seisel, S.; Borensen, C.; Vogt, R.; Zellner, R. The heterogeneous reaction of HNO_3 on
3603   mineral dust and gamma-alumina surfaces: a combined Knudsen cell and DRIFTS study.
3604   *Phys. Chem. Chem. Phys.* **2004**, *6*, 5498-5508.
3605   (366)   Kelly, J. T.; Wexler, A. S. Thermodynamics of carbonates and hydrates related to
3606   heterogeneous reactions involving mineral aerosol. *J. Geophys. Res.-Atmos* **2005**, *110*,
3607   D11201, doi: 11210.11029/12004jd005583.
3608   (367)   Kelly, J. T.; Chuang, C. C.; Wexler, A. S. Influence of dust composition on cloud droplet
3609   formation. *Atmos. Environ.* **2007**, *41*, 2904-2916.
3610   (368)   Huey, L. G.; Dunlea, E. J.; Lovejoy, E. R.; Hanson, D. R.; Norton, R. B.; Fehsenfeld, F.
3611   C.; Howard, C. J. Fast time response measurements of HNO_3 in air with a chemical
3612   ionization mass spectrometer. *J. Geophys. Res.-Atmos.* **1998**, *103*, 3355-3360.
3613   (369)   Hanke, M.; Umann, B.; Uecker, J.; Arnold, F.; Bunz, H. Atmospheric measurements of
3614   gas-phase HNO_3 and SO_2 using chemical ionization mass spectrometry during the
3615   MINATROC field campaign 2000 on Monte Cimone. *Atmos. Chem. Phys.* **2003**, *3*, 417-
3616   436.

3617   (370)   Bey, I.; Jacob, D. J.; Logan, J. A.; Yantosca, R. M. Asian chemical outflow to the Pacific
3618   in spring: Origins, pathways, and budgets. *J. Geophys. Res.-Atmos* **2001**, *106*, 23097-
3619   23113.
3620   (371)   Brown, S. S.; Stark, H.; Ryerson, T. B.; Williams, E. J.; Nicks, D. K.; Trainer, M.;
3621   Fehsenfeld, F. C.; Ravishankara, A. R. Nitrogen oxides in the nocturnal boundary layer:
3622   Simultaneous in situ measurements of NO3, N2O5, NO2, NO, and O3. *J. Geophys. Res.-*
3623   *Atmos* **2003**, *108*, 4299.
3624   (372)   Osthoff, H. D.; Roberts, J. M.; Ravishankara, A. R.; Williams, E. J.; Lerner, B. M.;
3625   Sommariva, R.; Bates, T. S.; Coffman, D.; Quinn, P. K.; Dibb, J. E. *et al.* High levels of
3626   nitryl chloride in the polluted subtropical marine boundary layer. *Nature Geosci.* **2008**, *1*,
3627   324-328.
3628   (373)   Thornton, J. A.; Kercher, J. P.; Riedel, T. P.; Wagner, N. L.; Cozic, J.; Holloway, J., S.;
3629   Dube, W. P.; Wolfe, G. M.; Quinn, P. K.; Middlebrook, A. M. *et al.* A large atomic
3630   chlorine source inferred from mid-continental reactive nitrogen chemistry. *Nature* **2010**,
3631   *464*, 271-174.
3632   (374)   Crowley, J. N.; Thieser, J.; Tang, M. J.; Schuster, G.; Bozem, H.; Beygi, Z. H.; Fischer,
3633   H.; Diesch, J. M.; Drewnick, F.; Borrmann, S. *et al.* Variable lifetimes and loss
3634   mechanisms for NO3 and N2O5 during the DOMINO campaign: contrasts between
3635   marine, urban and continental air. *Atmos. Chem. Phys.* **2011**, *11*, 10853-10870.
3636   (375)   Sullivan, R. C.; Minambres, L.; DeMott, P. J.; Prenni, A. J.; Carrico, C. M.; Levin, E. J.
3637   T.; Kreidenweis, S. M. Chemical processing does not always impair heterogeneous ice
3638   nucleation of mineral dust particles. *Geophys. Res. Lett.* **2010**, *37*, L24805, doi:
3639   24810.21029/22010GL045540.
3640   (376)   Yamashita, K.; Murakami, M.; Hashimoto, A.; Tajiri, T. CCN Ability of Asian Mineral
3641   Dust Particles and Their Effects on Cloud Droplet Formation. *J. Meteorol. Soc. Jpn.*
3642   **2011**, *89*, 581-587.
3643   (377)   Hensen, E. J. M.; Smit, B. Why clays swell. *J. Phys. Chem. B* **2002**, *106*, 12664-12667.
3644   (378)   Keskinen, H.; Kortelainen, A. M.; Jaatinen, A.; Yli-Pirila, P.; Joutsensaari, J.;
3645   Romakkaniemi, S.; Hao, L. Q.; Torvela, T.; Miettinen, P.; Virtanen, A. *et al.* Increased
3646   hygroscopicity of Arizona Test Dust seeds by secondary organic aerosol coating from
3647   alpha-pinene ozonolysis. *Boreal Environ. Res.* **2014**, *19*, 182-190.
3648   (379)   Hall, P. L.; Astill, D. M. Adsorption of water by homoionic exchange forms of Wyoming
3649   montmorillonite (SWY-1). *Clays Clay Miner.* **1989**, *37*, 355-363.
3650   (380)   Cases, J. M.; Berend, I.; Besson, G.; Francois, M.; Uriot, J. P.; Thomas, F.; Poirier, J. E.
3651   Mechanism of adsorption and desorption of water vapor by homoionic montmorillonite.
3652   1. The sodium-exchanged form. *Langmuir* **1992**, *8*, 2730-2739.
3653   (381)   Xu, W. Z.; Johnston, C. T.; Parker, P.; Agnew, S. F. Infrared study of water sorption on
3654   Na-, Li-, Ca-, and Mg-exchanged (SWy-1 and SAz-1) montmorillonite. *Clays Clay*
3655   *Miner.* **2000**, *48*, 120-131.
3656   (382)   Zent, A. P.; Howard, D. J.; Quinn, R. C. H2O adsorption on smectites: Application to the
3657   diurnal variation of H2O in the Martian atmosphere. *J. Geophys. Res.-Planets* **2001**, *106*,
3658   14667-14674.
3659   (383)   Frinak, E. K.; Mashburn, C. D.; Tolbert, M. A.; Toon, O. B. Infrared characterization of
3660   water uptake by low-temperature Na-montmorillonite: Implications for Earth and Mars.
3661   *J. Geophys. Res.-Atmos.* **2005**, *110*, D09308, doi: 09310.01029/02004JD005647.
3662   (384)   Attwood, A. R.; Greenslade, M. E. Deliquescence Behavior of Internally Mixed Clay and
3663   Salt Aerosols by Optical Extinction Measurements. *J. Phys. Chem. A* **2012**, *116*, 4518-
3664   4527.

3665 (385) Dalirian, M.; Keskinen, H.; Ahlm, L.; Ylisirniö, A.; Romakkaniemi, S.; Laaksonen, A.;
3666 Virtanen, A.; Riipinen, I. CCN activation of fumed silica aerosols mixed with soluble
3667 pollutants. *Atmos. Chem. Phys.* **2015**, *15*, 3815-3829.
3668 (386) Rubasinghege, G.; Ogden, S.; Baltrusaitis, J.; Grassian, V. H. Heterogeneous Uptake and
3669 Adsorption of Gas-Phase Formic Acid on Oxide and Clay Particle Surfaces: The Roles of
3670 Surface Hydroxyl Groups and Adsorbed Water in Formic Acid Adsorption and the
3671 Impact of Formic Acid Adsorption on Water Uptake. *J. Phys. Chem. A* **2013**, *117*, 11316-
3672 11327.
3673 (387) Koehler, K. A.; Kreidenweis, S. M.; DeMott, P. J.; Prenni, A. J.; Petters, M. D. Potential
3674 impact of Owens (dry) Lake dust on warm and cold cloud formation. *J. Geophys. Res.-*
3675 *Atmos.* **2007**, *112*, D12210, doi: 12210.11029/12007jd008413.
3676 (388) deLeeuw, N. H.; Parker, S. C. Atomistic simulation of the effect of molecular adsorption
3677 of water on the surface structure and energies of calcite surfaces. *J. Chem. Soc.-Faraday*
3678 *Trans.* **1997**, *93*, 467-475.
3679 (389) Kerisit, S.; Marmier, A.; Parker, S. C. Ab initio surface phase diagram of the {10(1)over-
3680 bar4} calcite surface. *J. Phys. Chem. B* **2005**, *109*, 18211-18213.
3681 (390) Rahaman, A.; Grassian, V. H.; Margulis, C. J. Dynamics of water adsorption onto a
3682 calcite surface as a function of relative humidity. *J. Phys. Chem. C* **2008**, *112*, 2109-
3683 2115.
3684 (391) Tunega, D.; Gerzabek, M. H.; Lischka, H. Ab initio molecular dynamics study of a
3685 monomolecular water layer on octahedral and tetrahedral kaolinite surfaces. *J. Phys.*
3686 *Chem. B* **2004**, *108*, 5930-5936.
3687 (392) Croteau, T.; Bertram, A. K.; Patey, G. N. Adsorption and Structure of Water on Kaolinite
3688 Surfaces: Possible Insight into Ice Nucleation from Grand Canonical Monte Carlo
3689 Calculations. *J. Phys. Chem. A* **2008**, *112*, 10708-10712.
3690 (393) Croteau, T.; Bertram, A. K.; Patey, G. N. Simulation of Water Adsorption on Kaolinite
3691 under Atmospheric Conditions. *J. Phys. Chem. A* **2009**, *113*, 7826-7833.
3692 (394) Croteau, T.; Bertram, A. K.; Patey, G. N. Observations of High-Density Ferroelectric
3693 Ordered Water in Kaolinite Trenches using Monte Carlo Simulations. *J. Phys. Chem. A*
3694 **2010**, *114*, 8396-8405.
3695 (395) Crotean, T.; Bertram, A. K.; Patey, G. N. Water adsorption on kaolinite surfaces
3696 containing trenches. *J. Phys. Chem. A* **2010**, *114*, 2171-2178.
3697 (396) Hensen, E. J. M.; Tambach, T. J.; Bliek, A.; Smit, B. Adsorption isotherms of water in
3698 Li-, Na-, and K-montmorillonite by molecular simulation. *J. Chem. Phys.* **2001**, *115*,
3699 3322-3329.
3700 (397) Tambach, T. J.; Hensen, E. J. M.; Smit, B. Molecular simulations of swelling clay
3701 minerals. *J. Phys. Chem. B* **2004**, *108*, 7586-7596.
3702 (398) Argyris, D.; Tummala, N. R.; Striolo, A.; Cole, D. R. Molecular structure and dynamics
3703 in thin water films at the silica and graphite surfaces. *J. Phys. Chem. C* **2008**, *112*, 13587-
3704 13599.
3705 (399) Murdachaew, G.; Gaigeot, M.-P.; Halonen, L.; Gerber, R. B. Dissociation of HCl into
3706 Ions on Wet Hydroxylated (0001) α-Quartz. *J. Phys. Chem. Lett.* **2013**, *4*, 3500-3507.
3707 (400) Lindan, P. J. D.; Harrison, N. M.; Gillan, M. J. Mixed dissociative and molecular
3708 adsorption of water on the rutile (110) surface. *Phys. Rev. Lett.* **1998**, *80*, 762-765.
3709 (401) Jug, K.; Nair, N. N.; Bredow, T. Molecular dynamics investigation of water adsorption
3710 on rutile surfaces. *Surf. Sci.* **2005**, *590*, 9-20.
3711 (402) Harris, L. A.; Quong, A. A. Molecular chemisorption as the theoretically preferred
3712 pathway for water adsorption on ideal rutile TiO2(110). *Phys. Rev. Lett.* **2004**, *93*,
3713 086105.

3714 (403) Rustad, J. R.; Boily, J. F. Density functional calculation of the infrared spectrum of
3715   surface hydroxyl groups on goethite (α-FeOOH). *Am. Mineral.* **2010**, *95*, 414-417.
3716 (404) Song, X. W.; Boily, J. F. Water vapor interactions with FeOOH particle surfaces. *Chem.*
3717   *Phys. Lett.* **2013**, *560*, 1-9.
3718 (405) Gerber, R. B.; Varner, M. E.; Hammerich, A. D.; Riikonen, S.; Murdachaew, G.;
3719   Shemesh, D.; Finlayson-Pitts, B. J. Computational Studies of Atmospherically-Relevant
3720   Chemical Reactions in Water Clusters and on Liquid Water and Ice Surfaces. *Accounts*
3721   *Chem. Res.* **2015**, *48*, 399-406.
3722 (406) Kerisit, S.; Parker, S. C. Free energy of adsorption of water and metal ions on the {1014}
3723   calcite surface. *J. Am. Chem. Soc.* **2004**, *126*, 10152-10161.
3724 (407) Hu, X. L.; Michaelides, A. Water on the hydroxylated (001) surface of kaolinite: From
3725   monomer adsorption to a flat 2D wetting layer. *Surf. Sci.* **2008**, *602*, 960-974.
3726 (408) Hu, X. L.; Michaelides, A. Ice formation on kaolinite: Lattice match or amphoterism?
3727   *Surf. Sci.* **2007**, *601*, 5378-5381.
3728 (409) Hu, X. L.; Michaelides, A. The kaolinite (001) polar basal plane. *Surf. Sci.* **2010**, *604*,
3729   111-117.
3730 (410) Yang, J.; Wang, E. G. Reaction of water on silica surfaces. *Curr. Opin. Solid State Mater.*
3731   *Sci.* **2006**, *10*, 33-39.
3732 (411) Rimola, A.; Costa, D.; Sodupe, M.; Lambert, J. F.; Ugliengo, P. Silica Surface Features
3733   and Their Role in the Adsorption of Biomolecules: Computational Modeling and
3734   Experiments. *Chem. Rev.* **2013**, *113*, 4216-4313.
3735 (412) Legrand, A. P. *The Surface Properties of Silicas*; Wiley: Chichester, U.K., 1998.
3736 (413) Papirer, E. *Adsorption on Silica Surfaces*; CRC Press: Boca Raton, USA, 2000.
3737 (414) Sulpizi, M.; Gaigeot, M. P.; Sprik, M. The Silica-Water Interface: How the Silanols
3738   Determine the Surface Acidity and Modulate the Water Properties. *J. Chem. Theory*
3739   *Comput.* **2012**, *8*, 1037-1047.
3740 (415) Du, Q.; Freysz, E.; Shen, Y. R. Vibrational spectra of water molecules at quartz/water
3741   interfaces. *Phys. Rev. Lett.* **1994**, *72*, 238-241.
3742 (416) Ostroverkhov, V.; Waychunas, G. A.; Shen, Y. R. Vibrational spectra of water at
3743   water/α-quartz (0001) interface. *Chem. Phys. Lett.* **2004**, *386*, 144-148.
3744 (417) Ostroverkhov, V.; Waychunas, G. A.; Shen, Y. R. New information on water interfacial
3745   structure revealed by phase-sensitive surface spectroscopy. *Phys. Rev. Lett.* **2005**, *94*,
3746   046102.
3747 (418) Richmond, G. L. Molecular bonding and interactions at aqueous surfaces as probed by
3748   vibrational sum frequency spectroscopy. *Chem. Rev.* **2002**, *102*, 2693-2724.
3749 (419) Falkovich, A. H.; Ganor, E.; Levin, Z.; Formenti, P.; Rudich, Y. Chemical and
3750   mineralogical analysis of individual mineral dust particles. *J. Geophys. Res.-Atmos* **2001**,
3751   *106*, 18029-18036.
3752 (420) Falkovich, A. H.; Schkolnik, G.; Ganor, E.; Rudich, Y. Adsorption of organic compounds
3753   pertinent to urban environments onto mineral dust particles. *J. Geophys. Res.-Atmos.*
3754   **2004**, *109*, D02208, doi: 02210.01029/02003JD003919.
3755 (421) Maxwell-Meier, K.; Weber, R.; Song, C.; Orsini, D.; Ma, Y.; Carmichael, G. R.; Streets,
3756   D. G. Inorganic composition of fine particles in mixed mineral dust-pollution plumes
3757   observed from airborne measurements during ACE-Asia. *J. Geophys. Res.-Atmos.* **2004**,
3758   *109*, D19s07, doi: 10.1029/2003jd004464.
3759 (422) Ro, C. U.; Hwang, H.; Chun, Y.; Van Grieken, R. Single-particle characterization of four
3760   "Asian Dust" samples collected in Korea, using low-Z particle electron probe X-ray
3761   microanalysis. *Environ. Sci. Technol.* **2005**, *39*, 1409-1419.

3762 (423) Shi, Z. B.; Shao, L. T.; Jones, T. P.; Lu, S. L. Microscopy and mineralogy of airborne
3763 particles collected during severe dust storm episodes in Beijing, China. *J. Geophys. Res.-*
3764 *Atmos.* **2005**, *110*, D01303, doi: 01310.01029/02004jd005073.
3765 (424) Geng, H.; Park, Y.; Hwang, H.; Kang, S.; Ro, C. U. Elevated nitrogen-containing
3766 particles observed in Asian dust aerosol samples collected at the marine boundary layer
3767 of the Bohai Sea and the Yellow Sea. *Atmos. Chem. Phys.* **2009**, *9*, 6933-6947.
3768 (425) Li, W. J.; Shao, L. Y.; Shi, Z. B.; Chen, J. M.; Yang, L. X.; Yuan, Q.; Yan, C.; Zhang, X.
3769 Y.; Wang, Y. Q.; Sun, J. Y. *et al.* Mixing state and hygroscopicity of dust and haze
3770 particles before leaving Asian continent. *J. Geophys. Res.-Atmos* **2014**, *119*, 1044-1059.
3771 (426) Li, W.; Shao, L.; Zhang, D.; Ro, C.-U.; Hu, M.; Bi, X.; Geng, H.; Matsuki, A.; Niu, H.;
3772 Chen, J. A review of single aerosol particle studies in the atmosphere of East Asia:
3773 morphology, mixing state, source, and heterogeneous reactions. *J. Clean. Prod.* **2015**,
3774 *112*, 1330-1349.
3775 (427) Perry, K. D.; Cliff, S. S.; Jimenez-Cruz, M. P. Evidence for hygroscopic mineral dust
3776 particles from the Intercontinental Transport and Chemical Transformation Experiment.
3777 *J. Geophys. Res.-Atmos* **2004**, *109*, D23S28, doi: 10.1029/2004JD004979.
3778 (428) Massling, A.; Leinert, S.; Wiedensohler, A.; Covert, D. Hygroscopic growth of sub-
3779 micrometer and one-micrometer aerosol particles measured during ACE-Asia. *Atmos.*
3780 *Chem. Phys.* **2007**, *7*, 3249-3259.
3781 (429) Shi, Z.; Zhang, D.; Hayashi, M.; Ogata, H.; Ji, H.; Fujiie, W. Influences of sulfate and
3782 nitrate on the hygroscopic behaviour of coarse dust particles. *Atmos. Environ.* **2008**, *42*,
3783 822-827.
3784 (430) Crumeyrolle, S.; Gomes, L.; Tulet, P.; Matsuki, A.; Schwarzenboeck, A.; Crahan, K.
3785 Increase of the aerosol hygroscopicity by cloud processing in a mesoscale convective
3786 system: a case study from the AMMA campaign. *Atmos. Chem. Phys.* **2008**, *8*, 6907-
3787 6924.
3788 (431) Tobo, Y.; Zhang, D. Z.; Nakata, N.; Yamada, M.; Ogata, H.; Hara, K.; Iwasaka, Y.
3789 Hygroscopic mineral dust particles as influenced by chlorine chemistry in the marine
3790 atmosphere. *Geophys. Res. Lett.* **2009**, *36*, L05817, doi: 05810.01029/02008gl036883.
3791 (432) Tobo, Y.; Zhang, D.; Matsuki, A.; Iwasaka, Y. Asian dust particles converted into
3792 aqueous droplets under remote marine atmospheric conditions. *Proc. Natl. Acad. Sci. U.*
3793 *S. A.* **2010**, *107*, 17905-17910.
3794 (433) Kim, J. S.; Park, K. Atmospheric Aging of Asian Dust Particles During Long Range
3795 Transport. *Aerosol Sci. Technol.* **2012**, *46*, 913-924.
3796 (434) Denjean, C.; Caquineau, S.; Desboeufs, K.; Laurent, B.; Maille, M.; Quiñones Rosado,
3797 M.; Vallejo, P.; Mayol-Bracero, O. L.; Formenti, P. Long-range transport across the
3798 Atlantic in summertime does not enhance the hygroscopicity of African mineral dust.
3799 *Geophys. Res. Lett.* **2015**, *42*, 7835-7843.
3800 (435) Bates, T. S.; Quinn, P. K.; Frossard, A. A.; Russell, L. M.; Hakala, J.; Petaja, T.;
3801 Kulmala, M.; Covert, D. S.; Cappa, C. D.; Li, S. M. *et al.* Measurements of ocean derived
3802 aerosol off the coast of California. *J. Geophys. Res.-Atmos.* **2012**, *117*, D00V15, doi:
3803 10.1029/2012jd017588.
3804 (436) Fuentes, E.; Coe, H.; Green, D.; McFiggans, G. On the impacts of phytoplankton-derived
3805 organic matter on the properties of the primary marine aerosol - Part 2: Composition,
3806 hygroscopicity and cloud condensation activity. *Atmos. Chem. Phys.* **2011**, *11*, 2585-
3807 2602.
3808 (437) Laskina, O.; Morris, H. S.; Grandquist, J. R.; Qin, Z.; Stone, E. A.; Tivanski, A. V.;
3809 Grassian, V. H. Size Matters in the Water Uptake and Hygroscopic Growth of

3810   Atmospherically Relevant Multicomponent Aerosol Particles. *J. Phys. Chem. A* **2015**,
3811   *119*, 4489-4497.
3812 (438) Kaaden, N.; Massling, A.; Schladitz, A.; Müller, T.; Kandler, K.; SchüTz, L.; Weinzierl,
3813   B.; Petzold, A.; Tesche, M.; Leinert, S. *et al.* State of mixing, shape factor, number size
3814   distribution, and hygroscopic growth of the Saharan anthropogenic and mineral dust
3815   aerosol at Tinfou, Morocco. *Tellus B* **2009**, *61*, 51-63.
3816 (439) Schladitz, A.; Müller, Thomas; Nowak, A.; Kandler, K.; Lieke, K.; Massling, A.;
3817   Wiedensohler, A. In situ aerosol characterization at Cape Verde. Part 1: particle number
3818   size distributions, hygroscopic growth and state of mixing of the marine and Saharan dust
3819   aerosol. *Tellus B* **2011**, *63*, 531-548.
3820 (440) Tobo, Y.; DeMott, P. J.; Raddatz, M.; Niedermeier, D.; Hartmann, S.; Kreidenweis, S.
3821   M.; Stratmann, F.; Wex, H. Impacts of chemical reactivity on ice nucleation of kaolinite
3822   particles: A case study of levoglucosan and sulfuric acid. *Geophys. Res. Lett.* **2012**, *39*,
3823   L19803, doi: 19810.11029/12012gl053007.
3824 (441) Hiranuma, N.; Augustin-Bauditz, S.; Bingemer, H.; Budke, C.; Curtius, J.; Danielczok,
3825   A.; Diehl, K.; Dreischmeier, K.; Ebert, M.; Frank, F. *et al.* A comprehensive laboratory
3826   study on the immersion freezing behavior of illite NX particles: a comparison of 17 ice
3827   nucleation measurement techniques. *Atmos. Chem. Phys.* **2015**, *15*, 2489-2518.
3828 (442) Lau, K. M.; Wu, H. T. Warm rain processes over tropical oceans and climate
3829   implications. *Geophys. Res. Lett.* **2003**, *30*, 2290, doi: 2210.1029/2003gl018567.
3830 (443) Freedman, M. A. Potential Sites for Ice Nucleation on Aluminosilicate Clay Minerals and
3831   Related Materials. *J. Phys. Chem. Lett.* **2015**, *6*, 3850-3858.
3832 (444) DeMott, P. J.; Möhler, O.; Stetzer, O.; Vali, G.; Levin, Z.; Petters, M. D.; Murakami, M.;
3833   Leisner, T.; Bundke, U.; Klein, H. *et al.* Resurgence in Ice Nuclei Measurement
3834   Research. *Bull. Amer. Meteorol. Soc.* **2011**, *92*, 1623-1635.
3835 (445) Vali, G. Nucleation terminology. *Bull. Amer. Meteorol. Soc.* **1985**, *66*, 1426-1427.
3836 (446) Vali, G.; DeMott, P. J.; Möhler, O.; Whale, T. F. Technical Note: A proposal for ice
3837   nucleation terminology. *Atmos. Chem. Phys.* **2015**, *15*, 10263-10270.
3838 (447) Martin, S. T. Phase transitions of aqueous atmospheric particles. *Chem. Rev.* **2000**, *100*,
3839   3403-3453.
3840 (448) Szyrmer, W.; Zawadzki, I. Biogenic and Anthropogenic Sources of Ice-Forming Nuclei:
3841   A Review. *Bull. Amer. Meteorol. Soc.* **1997**, *78*, 209-228.
3842 (449) Kulkarni, G.; Sanders, C.; Zhang, K.; Liu, X.; Zhao, C. Ice nucleation of bare and
3843   sulfuric acid-coated mineral dust particles and implication for cloud properties. *J.
3844   Geophys. Res.-Atmos* **2014**, *119*, 9993-10011.
3845 (450) Girard, E.; Dueymes, G.; Du, P.; Bertram, A. K. Assessment of the effects of acid-coated
3846   ice nuclei on the Arctic cloud microstructure, atmospheric dehydration, radiation and
3847   temperature during winter. *Int. J. Climatol.* **2013**, *33*, 599-614.
3848 (451) Salam, A.; Lesins, G.; Lohmann, U. Laboratory study of heterogeneous ice nucleation in
3849   deposition mode of montmorillonite mineral dust particles aged with ammonia, sulfur
3850   dioxide, and ozone at polluted atmospheric concentrations. *Air Qual. Atmos. Health*
3851   **2008**, *1*, 135-142.
3852 (452) Archuleta, C. M.; DeMott, P. J.; Kreidenweis, S. M. Ice nucleation by surrogates for
3853   atmospheric mineral dust and mineral dust/sulfate particles at cirrus temperatures. *Atmos.
3854   Chem. Phys.* **2005**, *5*, 2617-2634.
3855 (453) Knopf, D. A.; Koop, T. Heterogeneous nucleation of ice on surrogates of mineral dust. *J.
3856   Geophys. Res.-Atmos.* **2006**, *111*, D12201, doi: 12210.11029/12005jd006894.
3857 (454) Eastwood, M. L.; Cremel, S.; Wheeler, M.; Murray, B. J.; Girard, E.; Bertram, A. K.
3858   Effects of sulfuric acid and ammonium sulfate coatings on the ice nucleation properties

3859   of kaolinite particles. *Geophys. Res. Lett.* **2009**, *36*, L02811, doi:
3860   02810.01029/02008gl035997.
3861 (455) Chernoff, D. I.; Bertram, A. K. Effects of sulfate coatings on the ice nucleation properties
3862   of a biological ice nucleus and several typs of minerals. *J. Geophys. Res.-Atmos.* **2010**,
3863   *115*, D20205, doi: 20210.21029/22010JD014254.
3864 (456) Niedermeier, D.; Hartmann, S.; Shaw, R. A.; Covert, D.; Mentel, T. F.; Schneider, J.;
3865   Poulain, L.; Reitz, P.; Spindler, C.; Clauss, T. *et al.* Heterogeneous freezing of droplets
3866   with immersed mineral dust particles – measurements and parameterization. *Atmos.*
3867   *Chem. Phys.* **2010**, *10*, 3601-3614.
3868 (457) Wex, H.; DeMott, P. J.; Tobo, Y.; Hartmann, S.; Rösch, M.; Clauss, T.; Tomsche, L.;
3869   Niedermeier, D.; Stratmann, F. Kaolinite particles as ice nuclei: learning from the use of
3870   different kaolinite samples and different coatings. *Atmos. Chem. Phys.* **2014**, *14*, 5529-
3871   5546.
3872 (458) Sihvonen, S. K.; Schill, G. P.; Lyktey, N. A.; Veghte, D. P.; Tolbert, M. A.; Freedman,
3873   M. A. Chemical and Physical Transformations of Aluminosilicate Clay Minerals Due to
3874   Acid Treatment and Consequences for Heterogeneous Ice Nucleation. *J. Phys. Chem. A*
3875   **2014**, *118*, 8787-8796.
3876 (459) Augustin-Bauditz, S.; Wex, H.; Kanter, S.; Ebert, M.; Niedermeier, D.; Stolz, F.; Prager,
3877   A.; Stratmann, F. The immersion mode ice nucleation behavior of mineral dusts: A
3878   comparison of different pure and surface modified dusts. *Geophys. Res. Lett.* **2014**, *41*,
3879   7375-7382.
3880 (460) Yang, Z.; Bertram, A. K.; Chou, K. C. Why Do Sulfuric Acid Coatings Influence the Ice
3881   Nucleation Properties of Mineral Dust Particles in the Atmosphere? *J. Phys. Chem. Lett.*
3882   **2011**, *2*, 1232-1236.
3883 (461) Serratosa, J. M.; Bradley, W. F. Infra-Red Absorption of OH Bonds in Micas. *Nature*
3884   **1958**, *181*, 111-111.
3885 (462) Du, Q.; Freysz, E.; Shen, Y. R. Surface Vibrational Spectroscopic Studies of Hydrogen
3886   Bonding and Hydrophobicity. *Science* **1994**, *264*, 826-828.
3887 (463) Sovago, M.; Campen, R. K.; Wurpel, G. W. H.; Müller, M.; Bakker, H. J.; Bonn, M.
3888   Vibrational Response of Hydrogen-Bonded Interfacial Water is Dominated by
3889   Intramolecular Coupling. *Phys. Rev. Lett.* **2008**, *100*, 173901.
3890 (464) Abdelmonem, A.; Lützenkirchen, J.; Leisner, T. Probing ice-nucleation processes on the
3891   molecular level using second harmonic generation spectroscopy. *Atmos. Meas. Tech.*
3892   **2015**, *8*, 3519-3526.
3893 (465) Lupi, L.; Molinero, V. Does Hydrophilicity of Carbon Particles Improve Their Ice
3894   Nucleation Ability? *J. Phys. Chem. A* **2014**, *118*, 7330-7337.
3895 (466) Möhler, O.; Benz, S.; Saathoff, H.; Schnaiter, M.; Wagner, R.; Schneider, J.; Walter, S.;
3896   Ebert, V.; Wagner, S. The effect of organic coating on the heterogeneous ice nucleation
3897   efficiency of mineral dust aerosols. *Environ. Res. Lett.* **2008**, *3*, 025007.
3898 (467) Kulkarni, G.; Zhang, K.; Zhao, C.; Nandasiri, M.; Shutthanandan, V.; Liu, X.; Fast, J.;
3899   Berg, L. Ice formation on nitric acid coated dust particles: Laboratory and modeling
3900   studies. *J. Geophys. Res.-Atmos* **2015**, *120*, 7682-7698.
3901 (468) Salam, A.; Lohmann, U.; Lesins, G. Ice nucleation of ammonia gas exposed
3902   montmorillonite mineral dust particles. *Atmos. Chem. Phys.* **2007**, *7*, 3923-3931.
3903 (469) Kanji, Z. A.; Welti, A.; Chou, C.; Stetzer, O.; Lohmann, U. Laboratory studies of
3904   immersion and deposition mode ice nucleation of ozone aged mineral dust particles.
3905   *Atmos. Chem. Phys.* **2013**, *13*, 9097-9118.
3906 (470) Fenter, F. F.; Caloz, F.; Rossi, M. J. Experimental-Evidence for the Efficient Dry
3907   Deposition of Nitric-Acid on Calcite. *Atmos. Environ.* **1995**, *29*, 3365-3372.

3908 (471) Hanisch, F.; Crowley, J. N. Heterogeneous reactivity of gaseous nitric acid on Al_2O_3,
3909 $CaCO_3$, and atmospheric dust samples: A Knudsen cell study. *J. Phys. Chem. A* **2001**,
3910   *105*, 3096-3106.
3911 (472) Mashburn, C. D.; Frinak, E. K.; Tolbert, M. A. Heterogeneous uptake of nitric acid on
3912   Na-montmorillonite clay as a function of relative humidity. *J. Geophys. Res.-Atmos.*
3913   **2006**, *111*, D15213, doi: 15210.11029/12005JD006525.
3914 (473) Vlasenko, A.; Huthwelker, T.; Gaggeler, H. W.; Ammann, M. Kinetics of the
3915   heterogeneous reaction of nitric acid with mineral dust particles: an aerosol flow tube
3916   study. *Phys. Chem. Chem. Phys.* **2009**, *11*, 7921-7930.
3917 (474) Underwood, G. M.; Li, P.; Al-Abadleh, H.; Grassian, V. H. A Knudsen cell study of the
3918   heterogeneous reactivity of nitric acid on oxide and mineral dust particles. *J. Phys. Chem.*
3919   *A* **2001**, *105*, 6609-6620.
3920 (475) Gustafsson, R. J.; Orlov, A.; Griffiths, P. T.; Cox, R. A.; Lambert, R. M. Reduction of
3921 NO_2 to nitrous acid on illuminated titanium dioxide aerosol surfaces: implications for
3922   photocatalysis and atmospheric chemistry. *Chem. Commun.* **2006**, 3936-3938.
3923 (476) Angelini, M. M.; Garrard, R. J.; Rosen, S. J.; Hinrichs, R. Z. Heterogeneous reactions of
3924   gaseous HNO_3 and NO_2 on the clay minerals kaolinite and pyrophyllite. *J. Phys. Chem. A*
3925   **2007**, *111*, 3326-3335.
3926 (477) Ndour, M.; D'Anna, B.; George, C.; Ka, O.; Balkanski, Y.; Kleffmann, J.; Stemmler, K.;
3927   Ammann, M. Photoenhanced uptake of NO_2 on mineral dust: Laboratory experiments
3928   and model simulations. *Geophys. Res. Lett.* **2008**, *35*, L05812, doi:
3929   05810.01029/02007gl032006.
3930 (478) Ndour, M.; Nicolas, M.; D'Anna, B.; Ka, O.; George, C. Photoreactivity of NO_2 on
3931   mineral dusts originating from different locations of the Sahara desert. *Phys. Chem.*
3932   *Chem. Phys.* **2009**, *11*, 1312-1319.
3933 (479) Karagulian, F.; Rossi, M. J. The heterogeneous chemical kinetics of NO_3 on atmospheric
3934   mineral dust surrogates. *Phys. Chem. Chem. Phys.* **2005**, *7*, 3150-3162.
3935 (480) Zolles, T.; Burkart, J.; Häusler, T.; Pummer, B.; Hitzenberger, R.; Grothe, H.
3936   Identification of Ice Nucleation Active Sites on Feldspar Dust Particles. *J. Phys. Chem. A*
3937   **2015**, *119*, 2692-2700.
3938 (481) Steinke, I.; Hoose, C.; Möhler, O.; Connolly, P.; Leisner, T. A new temperature- and
3939   humidity-dependent surface site density approach for deposition ice nucleation. *Atmos.*
3940   *Chem. Phys.* **2015**, *15*, 3703-3717.
3941 (482) Connolly, P. J.; Moehler, O.; Field, P. R.; Saathoff, H.; Burgess, R.; Choularton, T.;
3942   Gallagher, M. Studies of heterogeneous freezing by three different desert dust samples.
3943   *Atmos. Chem. Phys.* **2009**, *9*, 2805-2824.
3944 (483) Niemand, M.; Möhler, O.; Vogel, B.; Vogel, H.; Hoose, C.; Connolly, P.; Klein, H.;
3945   Bingemer, H.; DeMott, P.; Skrotzki, J. *et al.* A Particle-Surface-Area-Based
3946   Parameterization of Immersion Freezing on Desert Dust Particles. *J. Atmos. Sci.* **2012**,
3947   *69*, 3077-3092.
3948 (484) Phillips, V. T. J.; DeMott, P. J.; Andronache, C. An empirical parameterization of
3949   heterogeneous ice nucleation for multiple chemical species of aerosol. *J. Atmos. Sci.*
3950   **2008**, *65*, 2757-2783.
3951 (485) Gysel, M.; Weingartner, E.; Baltensperger, U. Hygroscopicity of Aerosol Particles at
3952   Low Temperatures. 2. Theoretical and Experimental Hygroscopic Properties of
3953   Laboratory Generated Aerosols. *Environ. Sci. Technol.* **2002**, *36*, 63-68.
3954 (486) Zeng, G.; Kelley, J.; Kish, J. D.; Liu, Y. Temperature-Dependent Deliquescent and
3955   Efflorescent Properties of Methanesulfonate Sodium Studied by ATR-FTIR
3956   Spectroscopy. *J. Phys. Chem. A* **2014**, *118*, 583-591.

3957 (487) Christensen, S. I.; Petters, M. D. The Role of Temperature in Cloud Droplet Activation.
3958   *J. Phys. Chem. A* **2012**, *116*, 9706-9717.

3959 (488) Tang, M. J.; Cox, R. A.; Kalberer, M. Compilation and evaluation of gas phase diffusion
3960   coefficients of reactive trace gases in the atmosphere: volume 1. Inorganic compounds.
3961   *Atmos. Chem. Phys.* **2014**, *14*, 9233-9247.

3962 (489) Tang, M. J.; Shiraiwa, M.; Pöschl, U.; Cox, R. A.; Kalberer, M. Compilation and
3963   evaluation of gas phase diffusion coefficients of reactive trace gases in the atmosphere:
3964   Volume 2. Diffusivities of organic compounds, pressure-normalised mean free paths, and
3965   average Knudsen numbers for gas uptake calculations. *Atmos. Chem. Phys.* **2015**, *15*,
3966   5585-5598.

3967 (490) Shiraiwa, M.; Ammann, M.; Koop, T.; Poschl, U. Gas uptake and chemical aging of
3968   semisolid organic aerosol particles. *Proc. Natl. Acad. Sci. U. S. A.* **2011**, *108*, 11003-
3969   11008.

3970 (491) Zobrist, B.; Soonsin, V.; Luo, B. P.; Krieger, U. K.; Marcolli, C.; Peter, T.; Koop, T.
3971   Ultra-slow water diffusion in aqueous sucrose glasses. *Phys. Chem. Chem. Phys.* **2011**,
3972   *13*, 3514-3526.

3973 (492) Vaden, T. D.; Imre, D.; Beranek, J.; Shrivastava, M.; Zelenyuk, A. Evaporation kinectis
3974   and phase of laboratory and ambient secondary organic aerosol. *Proc. Natl. Acad. Sci. U.
3975   S. A.* **2011**, *108*, 2190-2195.

3976 (493) Davidovits, P.; Hu, J. H.; Worsnop, D. R.; Zahniser, M. S.; Kolb, C. E. Entry of gas
3977   molecules into liquids. *Faraday Discuss.* **1995**, *100*, 65-81.

3978 (494) Pöschl, U. Atmospheric aerosols: Composition, transformation, climate and health
3979   effects. *Angew. Chem.-Int. Edit.* **2005**, *44*, 7520-7540.

3980 (495) Davidovits, P.; Kolb, C. E.; Williams, L. R.; Jayne, J. T.; Worsnop, D. R. Update 1 of:
3981   Mass Accommodation and Chemical Reactions at Gas-Liquid Interfaces. *Chem. Rev.*
3982   **2011**, *111*, PR76-PR109.

3983 (496) Pöschl, U. Gas–particle interactions of tropospheric aerosols: Kinetic and thermodynamic
3984   perspectives of multiphase chemical reactions, amorphous organic substances, and the
3985   activation of cloud condensation nuclei. *Atmos. Res.* **2011**, *101*, 562-573.

3986 (497) Ammann, M.; Cox, R. A.; Crowley, J. N.; Jenkin, M. E.; Mellouki, A.; Rossi, M. J.;
3987   Troe, J.; Wallington, T. J. Evaluated kinetic and photochemical data for atmospheric
3988   chemistry: Volume VI - heterogeneous reactions with liquid substrates. *Atmos. Chem.
3989   Phys.* **2013**, *12*, 8045-8228.

3990 (498) Sander, S. P.; Abbatt, J. P. D.; Barker, J. R.; Burkholder, J. B.; Friedl, R. R.; Golden, D.
3991   M.; Huie, R. E.; Kolb, C. E.; Kurylo, M. J.; Moortgat, G. K. *et al.* "Chemical Kinetics
3992   and Photochemical Data for Use in Atmospheric Studies, Evaluation No. 17, JPL
3993   Publication 10-6," Jet Propulsion Lab., 2011.

3994 (499) Pöschl, U.; Shiraiwa, M. Multiphase Chemistry at the Atmosphere–Biosphere Interface
3995   Influencing Climate and Public Health in the Anthropocene. *Chem. Rev.* **2015**, *115*,
3996   4440-4475.

3997 (500) Pöschl, U.; Rudich, Y.; Ammann, M. Kinetic model framework for aerosol and cloud
3998   surface chemistry and gas-phase interaction-Part 1: General equation, parameters, and
3999   terminology. *Atmos. Chem. Phys.* **2007**, *7*, 5989-6023.

4000 (501) Shiraiwa, M.; Pfrang, C.; Koop, T.; Poschl, U. Kinetic multi-layer model of gas-particle
4001   interactions in aerosols and clouds (KM-GAP): linking condensation, evaporation and
4002   chemical reactions of organics, oxidants and water. *Atmos. Chem. Phys.* **2012**, *12*, 2777-
4003   2794.

4004 (502) Berkemeier, T.; Huisman, A. J.; Ammann, M.; Shiraiwa, M.; Koop, T.; Pöschl, U.
4005   Kinetic regimes and limiting cases of gas uptake and heterogeneous reactions in

4006   atmospheric aerosols and clouds: a general classification scheme. *Atmos. Chem. Phys.*
4007   **2013**, *13*, 6663-6686.
4008